Phenotypic and transcriptomic characterisation of *Pseudomonas aeruginosa* biofilm infection in an *ex vivo* model of the Cystic Fibrosis lung

Niamh Ellen Harrington

A thesis submitted in partial fulfillment of the requirements for the degree of

Doctor of Philosophy in Life Sciences.

University of Warwick, School of Life Sciences

January 2022

Contents

List of Figures

List of Tables

Acknowledgements

I would first like to thank my supervisor, Dr Freya Harrison, for all your support and guidance. Thank you for giving me the confidence to believe in myself and for listening to all my crazy ideas – even letting me run with some of them! I really appreciate all the time and opportunities that you have given me, it has been a privilege to watch your lab grow. The last few years would also not have been the same without the other members of the Harrison lab, who are an amazing group of people that I have been so lucky to get the opportunity to work, and laugh, alongside. You have all made this experience far more enjoyable and kept me going. In particular, I would like to thank Esther for all her help, patience, kindness, and the laughter and advice during the many hours we spent together dissecting lungs and staining tissue samples. I also express my thanks to John for always being willing to listen and help, it was a pleasure to work alongside you. As well as this, a special thanks to Freya Allen – you were a joy to supervise in the lab, thank you for all your hard work. I can't wait to see you have a successful career!

I would also like to thank Jess, Jenny, and Ramón, I would not have got this far without all your support and suggestions. You have all made me a better scientist and I now cannot imagine how I got through life without you all. Thank you for sharing advice when needed and always being willing to help, you are all amazing scientists with great things ahead of you. Jess and Jenny, you have lifted me up on the days when I needed it and have made my life so much richer, I am so grateful to have met you. Jess we have come so far since our first day in the lab and I hope you know you are stuck with me forever! Who else am I going to FaceTime from the side of the road when a bird drives into my car?! Thank you also to all the amazing people I have met throughout this PhD, in particular Holly, Rohini, and Jeff. My PhD experience would not have been the same without you all.

I would also like to thank my family for their love and support. Shaun, I truly could not have done this without you – not just showing me that 12 commas is too much for one sentence - but also the laughter, love, and cooking me dinner when I disappear to the lab for 15 hours at a time! You are a wonderful person that I am so lucky to have in my life. I would also like to thank my Auntie Emma and Uncle Craig for all their support, and Uncle Craig for the many years transporting all my stuff back and forth from different

Declaration

This thesis is submitted to the University of Warwick in support of my application for the degree of Doctor of Philosophy. It has been composed by myself and has not been submitted in any previous application for any degree apart from the data in Table 4.7 in chapter 4, which was previously submitted in Freya Allen's dissertation in partial fulfilment of the requirements for her undergraduate MBio degree in Biomedical Sciences at the University of Warwick in 2021. The work presented (including data generated and data analysis) was carried out by the author except in the cases outlined below:

- The samples used to in the quorum sensing assays in chapter 4 were prepared in collaboration with Jenny Littler, who prepared the *in vitro* SCFM samples. This is made clear in the relevant figure legends (Figure 4.12, Figure 4.12, and Appendix A: Figure A.3). The experiment was designed by the author, all other samples used were prepared by the author, and data analysis was performed by the author.

- The MIC assay results reported in chapter 4 were performed by Freya Allen. This is made clear in the table legend (Table 4.7). This work was designed by the author and performed under the author's supervision as part of an undergraduate Master's project supervised by the author.

- The confocal microscopy images shown in the discussion chapter (chapter 7) were taken and processed by Dr. John MJ Lapage, this is made clear in the Figure legend (Figure 7.1). The samples used were prepared by the author.

Parts of this thesis have been published by the author:

Chapter 3: Harrington, N. E., Sweeney, E., and Harrison, F. (2020). Building a better biofilm - Formation of *in vivo*-like biofilm structures by *Pseudomonas aeruginosa* in a porcine model of cystic fibrosis lung infection. *Biofilm*, 2:100024.

Chapter 4: Harrington, N. E., Littler, J. L., and Harrison, F. (2021). Transcriptome analysis of *Pseudomonas aeruginosa* biofilm infection in an *ex vivo* pig model of the cystic fibrosis lung. *Applied and Environmental Microbiology*, In Press: https://doi.org/10.1128/AEM.01789-21.

Abstract

The high mortality rate amongst people with cystic fibrosis (CF) is associated with the incidence of lung disease. *Pseudomonas aeruginosa* is the most common pathogen isolated from the CF lung, and the environmental conditions drive adaptations leading to a chronic, biofilm infection that is highly resistant to antibiotics. Research is limited by the lack of a laboratory model that accurately recapitulates all aspects of human infection. This thesis has focused on development of an *ex vivo* pig lung (EVPL) model to further understand *P. aeruginosa* infection in the CF lung, using pig bronchiolar tissue and synthetic cystic fibrosis sputum media (SCFM).

Virulence factor assays demonstrated that *P. aeruginosa* virulence was at low levels in the EVPL model. Histological staining showed the *P. aeruginosa* biofilm on the surface of the tissue had an architecture comparable to patient biopsies, not observed in *in vitro* models. RNA-sequencing was then performed, and a distinction in *P. aeruginosa* gene expression in SCFM compared with the EVPL model was found. *P. aeruginosa* expression of quorum sensing genes was reduced in the EVPL biofilm, also observed in studies comparing CF sputum with *in vitro* growth. These findings demonstrated that the EVPL model facilitated a chronic-like *P. aeruginosa* infection. Investigation of the *P. aeruginosa* transcriptome over time in the EVPL biofilm provided further insight into infection dynamics and future optimisation for long term infection. *Burkholderia cenocepacia* and *Burkholderia multivorans* were then introduced and it was shown that the EVPL model is also suitable for their growth, and to explore interactions during mixed infection with *P. aeruginosa*.

The EVPL model has been shown to capture key aspects of *P. aeruginosa* chronic biofilm infection in the CF lung. It can now be used to better understand these infections, and as a diagnostic and drug testing platform to improve treatment outcomes.

Abbreviations

3-oxo-C12-HSL 3-oxo-dodecanoyl homoserine lactone.

ABC ATP-binding cassette.

AHL Acyl Homoserine Lactone.

AMR Antimicrobial resistance.

ANOVA Analysis of variance.

ASL Airway surface liquid.

BR Broad Range.

BWA Burrows-Wheeler Aligner.

C4-HSL N-butanoyl-L-homoserine lactone.

C6-HSL N-hexanoyl homoserine lactone.

C8-HSL N-octanoyl homoserine lactone.

CAMHB Cation-adjusted Mueller Hinton broth.

CAMP Cationic antimicrobial peptide.

cAMP Cyclic adenosine monophosphate.

CARD Comprehensive Antibiotic Resistance Database.

CF Cystic Fibrosis.

CFTR Cystic fibrosis transmembrane conductance regulator.

CFU Colony Forming Units.

CLIMB Cloud Infrastructure for Big Data Microbial Bioinformatics.

DEGs Differentially Expressed Genes.

dH$_2$O Distilled water.

DMEM Dulbecco's Modified Eagle Medium.

DNA Deoxyribonucleic Acid.

ELISA Enzyme-Linked Immunosorbent Assay.

EVPL *Ex vivo* Pig Lung.

FISH Fluorescence *in situ* hybridisation.

GAC Global activator of antibiotic and cyanide synthesis.

GO Gene Ontology.

H & E Hematoxylin and Eosin.

HHQ 2-heptyl-4-quinolone.

IL-10 Interleukin-10.

IL-8 Interleukin-8.

KEGG Kyoto encyclopedia of genes and genomes.

LB Luria-Bertani.

Log$_2$FC Log$_2$ Fold Change.

MEM Maximal Exact Match.

MIC Minimum Inhibitory Concentration.

mRNA Messenger RNA.

PBS Phosphate-Buffered Saline.

PCA Principal Component Analysis.

PCH Pyochelin.

PCR Polymerase Chain Reaction.

PQS *Pseudomonas* quinolone signal.

PVD Pyoverdine.

qPCR Quantitative real time PCR.

QS Quorum sensing.

RNA Ribonucleic Acid.

RNA-seq RNA sequencing.

RND Resistance-nodulation-division.

RPMI 1640 Roswell Park Memorial Insitute 1640.

rRNA Ribosomal ribonucleic acid.

RT-PCR Reverse transcription-polymerase chain reaction.

SCFM Synthetic Cystic Fibrosis sputum Media.

T1SS Type 1 secretion systems.

TCA Trichloroacetic Acid.

UV Ultraviolet.

WT Wild Type.

Chapter 1

Introduction

1.1 Cystic Fibrosis

1.1.1 Overview

The autosomal recessive genetic condition cystic fibrosis (CF) has been extensively studied since it was first described in 1938 as a disease of the pancreas. It was originally characterised by mucus plugs found in the glandular ducts of young children during post mortems (Davis, 2012). It is now known to affect ~70,000 people around the world, predominantly amongst Caucasian people, although the known prevalence is increasing in other populations as diagnostics and reporting improve (Elborn, 2016). In 2017, there were more than 10,000 people in the UK alone registered with CF (Charman et al., 2018). There are a number of clinical presentations now known to be associated including cirrhosis, pancreatic exocrine dysfunction and diabetes, intestinal obstructions, increased sweat chloride concentration, and arguably the most important: infection and inflammation of the lungs and sinuses (Cutting, 2015). The associated morbidities and mortalities are predominantly caused by CF lung disease due to the progressive bronchiectasis, increased inflammation, and high incidence of chronic bacterial infections (Stoltz et al., 2015). CF has the highest mortality rate of all human genetic conditions (Aali et al., 2017), thus the associated lung disease is an important research focus.

CF is caused by mutations in the cystic fibrosis transmembrane conductance regulator (CFTR) gene that have been divided into six categories based on the type of mutation (Table 1.1). There has been around 2,000 different CFTR variants reported, however not all have been associated with the presentation of disease. The clinical and functional

translation of CFTR project identified 127 variants as pathogenic, and showed that the severity of disease depended on the variant (Sosnay et al., 2013). Hence, not all CFTR mutations result in the same clinical presentation, and there are differences between each mutation category. Briefly, the mutations cause a loss of the chloride and bicarbonate transport mediated by CFTR. There have been other effects found, including loss of inhibition of epithelial Na+ channel-mediated sodium absorption (Stoltz et al., 2015).

Table 1.1: **The six categories of cystic fibrosis (CF) mutations**. The mutations in the cystic fibrosis transmembrane conductance regulator (CFTR) gene that cause CF are divided into six different categories, listed in the table. The defect caused by each CFTR mutation type is shown, as well as the effect of each defect. Information was sourced from Elborn (2016) and Hine et al. (2020).

Category	CFTR defect	Effect
I	Non-functional	CFTR protein is no longer produced (*caused by stop codons in the gene*).
II	Trafficking	Mutations affect CFTR processing in the endoplasmic reticulum.
III	Channel regulation	The opening of the CTFR protein is impaired.
IV	Channel function	Reduction of chloride ions passing through the CFTR protein channel.
V	Synthesis	A reduced production of CFTR protein.
VI	Stability	Poor stability of CFTR, so there is less of the protein at the cell surface.

The ongoing research into the mutations that cause CF, and their effects, has led to massive advancements in treatment options, improved quality of life, and an overall better outlook for people with CF. When first reported in the 1930s, many individuals with CF did not survive past 6 months (Davis, 2012). However, the median age of survival amongst Caucasian populations is now between 44 to 52 (McBennett et al., 2021). Although drastically increased, this is still much lower than the life expectancy for people without CF; people in the UK are now expected to live to an average age of between 79 to 83 (Buxton, 2021). Therefore, there are still improvements to treatment options to be made.

Typically treatments for CF and the associated symptoms have included genetic screening, antibiotics for the chronic lung infections, and often lung transplants.

However in recent years CFTR modulators have become a predominant focus of research. They target the underlying cause of CF, the CFTR protein, and restore the loss of chloride transport, which has dramatically improved patient outcomes (Hine et al., 2020). There have been different modulators developed for the different categories of CFTR mutation, such as tezacaftor, elexacaftor, lumacaftor, and ivacaftor (Laselva et al., 2021). Most notable is the recently approved elexacaftor-tezacaftor-ivacaftor combination therapy, known as Kaftrio. It is suitable for the mutations in ~90% of people with CF and has been associated with improved lung function (Ridley and Condren, 2020). However, there are still ~10% of people with CF for which this treatment is not effective, thus there is ongoing research into other molecular targets (Laselva et al., 2021).

Despite the promising results, there are a number of concerns with these treatments; they are expensive and there have been restrictions on access. In the UK, there was a significant delay in gaining access to Kaftrio caused by extensive negotiations. The health implications of taking these drugs long term has also not been fully elucidated as they are so new (Hine et al., 2020). This also means that the effect of CFTR modulators on the CF lung and the associated infections is not clear. Initial studies indicated that taking ivacaftor, suitable for the G551D mutation (category III: see Table 1.1), improved lung function and reduced denisty of the most prevalent CF lung pathogen: *Pseudomonas aeruginosa*, in CF sputum. However, there is evidence to suggest that this may not be a long term effect and may be reversed over time (Kidd, 2017). There are also some people for which these treatments are not suitable (Laselva et al., 2021), or people with CF who have extensive lung damage and chronic infection established prior to suitable modulator availability. Alongside this, the increasing life expectancy for people with CF brings with it increased therapeutic challenges from the further complications that arise with ageing (McBennett et al., 2021). Taking all of this into account, further understanding of the lung infections of people with CF, and the development of new treatments, is still essential to improve quality of life and overall outcomes.

1.1.2   Pathogenesis of the CF lung

The CF lung environment is affected by the CFTR mutations; they cause a reduction in sodium chloride in the airway surface liquid (ASL). This results in dehydration of the airway surface and defective mucociliary clearance, which leads to an accumulation

of mucus (Clunes and Boucher, 2007). The mucus produced in the respiratory tract of someone with CF is thick, sticky, and salty compared with a non-CF lung (Riordan et al., 1986; Welsh et al., 2001; Stoltz et al., 2015; Bhagirath et al., 2016). There is increased adhesion of this mucus to the surface of the airways, leading to the formation of mucus 'plugs' (Boucher, 2007). These mucus plugs are ideal environments for microbial infection, known to reduce quality of life and increase mortalities (Cutting, 2015; Aali et al., 2017; Moore and Mastoridis, 2017). The mucus build up initiates pathogenesis of the CF lung, and likely drives inflammation and the subsequent microbial infections (Boucher, 2007).

There have been observations of inflammation in the lungs of infants with CF prior to any established microbial infection, likely caused by the condition itself (Boucher, 2007; Bragonzi et al., 2018). Chronic inflammation induces damage to the airway epithelium, which increases the risk of respiratory infections (Henderson et al., 2014). Airway epithelium damage is linked to remodelling of the airway, regulated by the airway epitehlial cells following regeneration. Remodelling worsens the defective mucocillary clearence, thus increasing mucus build up (Adam et al., 2015). The incidence of infection further increases inflammation. Following establishment of chronic infection with *P. aeruginosa*, there is an increase in pro-inflammatory cytokine production and reduced production of interleukin-10 (IL-10), an anti-inflammatory cytokine. This leads to heightened, persistant inflammation of the airways and thus accelerated lung function decline (Heijerman, 2005). Therefore, whilst the decline in lung function supports bacterial growth, it is also further caused by it.

One of the key distinctions between the CF lung and a non-CF lung is the density of microbes in the lower respiratory tract. The innate immune response ensures the lower respiratory tract of non-CF individuals remains relatively sterile (Bhagirath et al., 2016). It has recently been shown that the lower respiratory tract of people with CF is colonised by a number of pathogens and the lung microbiota, including species of the genera *Streptococcus*, *Prevotella*, and *Neisseria* (Surette, 2014). Following pathogen infection, often regarded as inevitable, progressive bronchiectasis occurs in the CF lung. This is the widening of the bronchi, and it is a key symptom of CF (Stoltz et al., 2015). As shown in Figure 1.1, widening of the bronchi is seen in young children and becomes established over time. Once established, it is considered to be the endpoint of CF lung disease and

increases the risk of periods of exacerbation, where worsened symptoms are experienced (Stick et al., 2013).
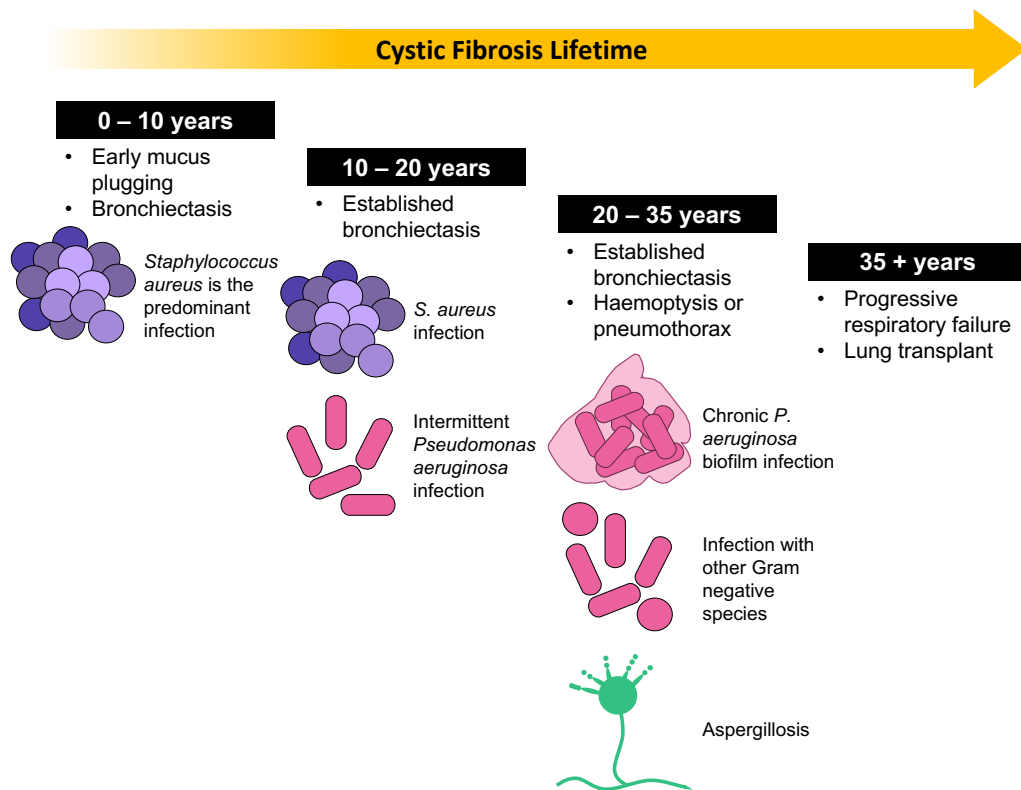
Figure 1.1: **The timeline of progression of Cystic Fibrosis (CF) lung disease and microbial infection.** The diagram outlines the airway symptoms observed at each stage of life for people with CF, and the predominant infections at each of these stages. Other Gram negative infections from 20 years old include the *Burkholderia cepacia* complex (Bcc). The figure was created using information from Elborn (2016).

There is also a change in the most common pathogens found in the CF lung over time (Figure 1.1). Children with CF are most likely to experience stable *Staphylococcus aureus* and *Haemophilus influenzae* infections, then become intermittently infected with *P. aeruginosa* later in life (Elborn, 2016). Eventually *P. aeruginosa* becomes the dominant pathogen in the lungs of more than 50% of people with CF, alongside infection with other Gram negative pathogens such as the *Burkholderia cepacia* complex (Bcc) (O'Brien and Fothergill, 2017). The cause of this change in microbial community composition, and its association with the CF lung environment, is not fully understood.

1.2 *Pseudomonas aeruginosa* and cystic fibrosis

1.2.1 Overview

P. aeruginosa is an opportunistic pathogen that predominantly affects individuals with existing health concerns. It is amongst the most common causes of hospital-acquired infections including wound and burn infections, urinary tract infections, sepsis, and hospital-acquiried pneumonia (Berube et al., 2016). *P. aeruginosa* also poses a significant risk to those who are immunocompromised, such as individuals with cancer, AIDS, people with indwelling medical devices, and those with the genetic condition CF (Diggle and Whiteley, 2020). The species are Gram negative, facultative aerobes that have been isolated from a diverse range of environments. *P. aeruginosa* uses nitrate and arginine to survive in anoxic conditions, and can use more than 100 organic molecules as sources of energy, as well as being able to survive at temperatures as low as 4 °C and up to 42 °C (Diggle and Whiteley, 2020). This versatility means *P. aeruginosa* is able to survive in different environmental conditions.

As mentioned, *P. aeruginosa* is the most prevalent pathogen of the CF lung. In fact, three quarters of adults with CF will be infected with *P. aeruginosa* during their lifetime, either transiently or as a chronic infection (Surette, 2014; Sanders and Fink, 2016). Chronic *P. aeruginosa* infections persist for years and are the stage of infection associated with the rapid lung function decline observed, worsened disease outcomes, and increased mortality rates (Nixon et al., 2001; Konstan et al., 2007; Lund-Palau et al., 2016). The conditions in the CF lung are largely responsible for these outcomes and drive *P. aeruginosa* evolutionary adaptations that make it almost impossible to eradicate. These include biofilm formation, increased antimicrobial resistance, and high intraspecies diversity (Winstanley et al., 2016). Hence, the infection environment is key to understanding chronic *P. aeruginosa* infections of the CF lung.

Upon initial colonisation, *P. aeruginosa* infection of the CF lung is comparable to acute infections; it is highly motile, and produces a range of virulence factors (Broder et al., 2016). There is a transition to chronic infection over time; although the exact mechanisms involved in this switch in lifestyle are not fully understood, there are a number of pathways that have been associated (Figure 1.2). The global regulatory gene

gacA regulates virulence factor production including lipases, pyocyanin, and cyanide, and has been linked to the switch from acute to chronic infection and the reduction in virulence factor production observed (Reimmann et al., 1997). The GacA-GacS regulatory system is also associated the RsmA/RsmZ system; the small ribonucleic acid (RNA)-binding protein RsmA is essential for the production of lipases, swarming motility, and rhamnolipid biosynthesis during acute infection and thus loss of this protein results in a loss of virulence (Heurlier et al., 2004). The gene *retS* is also an important regulator, which represses expression of genes encoding biofilm exopolysaccharide production and promotes virulence factors including the Type III secretion system, thus associated with the initial acute infection (Goodman et al., 2004). The adaptations conferring loss of virulence are likely due to the numerous environmental pressures including osmotic stress, the host inflammatory response, and antibiotic treatments (Winstanley et al., 2016). As shown in Figure 1.2, the conditions in the CF lung result in downregulation of acute infection phenotypes and upregulation of chronic infection characteristics, involving the two-component systems and regulators shown. The establishment of a chronic *P. aeruginosa* infection, particularly the formation of a biofilm, mean many antibiotics become ineffective (Mah and O'Toole, 2001).

Cystic Fibrosis Lung

Acute-Chronic Switch

GacA-GacS system
RetS-LadS system
RsmA small regulatory protein
Small RNAs **RsmZ** & **RsmY**
AmpR regulator

ACUTE INFECTION

CHRONIC INFECTION

- Type III secretion **(exotoxins – *ExoS, ExoU, ExoT* & *ExoY*)**
- Quorum sensing
- Lipases
- Elastase
- Rhamnolipids
- Motility **(swimming, swarming & twitching)**

- Hydrogen cyanide
- Pyocyanin

- Biofilm formation
- Overproduction of alginate
- Auxotrophic mutations
- Hypermutators
- Antibiotic resistance
- Type VI secretion

- Osmotic stress **(mucus)**
- Oxidative stress **(host immune response)**
- Nitrosative stress **(host immune response)**
- Sub-inhibitory antibiotic exposure
- Presence of other microorganisms **(lung microbiota & co-infecting pathogens)**

Figure 1.2: ***Pseudomonas aeruginosa* switch from acute infection to chronic infection in the cystic fibrosis (CF) lung.** The conditions in the CF lung that drive the switch in *P. aeruginosa* infection lifestyle are shown with the cause in brackets and bold font, as well as the genes known to cause this change listed in the acute-chronic switch box. The virulence factors and phenotypes associated with each infection type are shown; the characteristics of acute infection are downregulated in the CF lung and the characteristics of chronic infection upregulated. The two virulence factors in the yellow bubble (pyocyanin and hydrogen cyanide production) are likely to be produced during both stages of infection. The figure was created using information from Winstanley et al. (2016).

People with CF experience acute pulmonary exacerbations where symptoms are worsened, including increased sputum production, reduced energy, and a decline in lung function. There is also an increase in the concentration of *P. aeruginosa* in the CF lung during exacerbation (Goss and Burns, 2007). The cause is not known, however acute exacerbations result in increased mortality and morbidity, and *P. aeruginosa* exhibits increased virulence reminiscent of acute infection (Langan et al., 2015). Interestingly, it has been shown that there is no change in *P. aeruginosa* antibiotic susceptibility, and there is no significant association with the acquisition of new *P. aeruginosa* strains (Aaron et al., 2003). Thus, there is a change in *P. aeruginosa* virulence-associated gene expression rather than increased virulence caused by newly colonising strains. There has also been identification of sub-populations amongst chronic *P. aeruginosa* infection communities that exhibit high virulence (O'Brien et al., 2017). Therefore, the expression of virulence factors is complex in the CF lung and may not be downregulated across the whole infection population. It has been suggested that rather than a complete drive to reduced virulence, there may be alterations in virulence strategies (Bragonzi et al., 2009).

As shown in Figure 1.2 *P. aeruginosa* possess multiple virulence strategies, a number of which have been investigated in this thesis and will thus be further discussed.

1.2.2 Extracellular proteases

P. aeruginosa produces a number of exoproducts during early, acute infection of the CF lung such as extracellular proteases. These include type VI protease, the *P. aeruginosa* small protease, MucD, alkaline protease, large exoprotease A, and the elastases LasA and LasB (Jurado-Martín et al., 2021). During acute infection, extracellular proteases damage the host lung tissue and modulate the inflammatory response, hence protease inhibitors have been developed to reduce lung inflammation (Sandri et al., 2018). The LasB elastase is regarded as the principal extracellular virulence factor due to its ability to disrupt host mechanisms of bacterial clearance, facilitate *P. aeruginosa* modifications for immune evasion, and its involvement in biofilm formation (Jurado-Martín et al., 2021). Many of these functions are important for initial infection of the CF lung, however it has been shown that there is a loss of secreted proteases over time caused by the accumulation of mutations during adaptation to the CF lung (Smith et al., 2006).

There is high diversity within a chronic *P. aeruginosa* biofilm population in the lungs of people with CF, and this includes protease production. O'Brien et al. (2017) found that although overall *P. aeruginosa* chronic isolates produced less protease, specifically LasA, than the laboratory strain *P. aeruginosa* LESB58, loss of production was not ubiquitous among *P. aerugonisa* isolates in an individual. LasA is a zinc metalloendopeptidase, and is involved in disruption of the host epithelial barrier, which enhances colonisation and promotes survival (Winstanley and Fothergill, 2009). It has been associated with increased antibiotic resistance, and is also known as staphylolysin as it lyses *S. aureus* cells (Jurado-Martín et al., 2021). The role of proteases in multispecies interactions may also be important for colonisation. As shown in Figure 1.1, *P. aeruginosa* infection typically follows *S. aureus* infection. Therefore, lysis of *S. aureus* may further facilitate infection. Hence, the production of extracellular proteases is a key infection characteristic of *P. aeruginosa*.

1.2.3 Siderophores

Iron uptake and the production of siderophores is another key factor of *P. aeruginosa* infection in the CF lung. *P. aeruginosa* requires iron for growth, and iron-sequestering

behaviour has been linked to its ability to survive in different ecological niches. There is an abundance of extracellular iron in CF sputum, which is positively correlated with the incidence of chronic *P. aeruginosa* infection (Reid et al., 2007). *P. aeruginosa* iron uptake systems include production of the iron-chelating siderophores pyoverdine (PVD) and pyochelin (PCH), TonB-dependent receptors that uptake ferrisiderophores, heme uptake, and using siderophores produced by other bacterial species (xenosiderophores) (Cornelis and Dingemans, 2013). The different iron uptake strategies have been associated with each stage of *P. aeruginosa* infection in the CF lung. Konings et al. (2013) showed that there is reduced expression of *P. aeruginosa* siderophore and heme uptake genes in CF sputum compared with *in vitro* growth. More specifically, PVD and PCH -associated gene expression was either not detectable or at very low levels in sputum samples. It was concluded that *P. aeruginosa* changes its iron uptake mechanism depending on iron availability over time in the CF lung, and whether it is present as ferric iron, ferrous iron, or heme (Konings et al., 2013). Consistent with these findings, a lack of PVD production has been suggested to be indicative of chronic infection, likely due to high iron availability (Hogardt and Heesemann, 2010). The iron source has also been linked to CF lung disease progression; ferritin-bound iron as a predominant iron source in the CF lung has been linked to increased lung damage and bacterial growth (Stites et al., 1998).

Iron scavenging is not the only function of *P. aeruginosa* siderophores; PVD is also involved in the regulation of prouction of other virulence factors and is the predominant iron source required for biofilm formation (Kang and Kirienko, 2018). In a mouse model for burn wounds, PVD-deficient *P. aeruginosa* mutants exhibited reduced virulence, which was restored upon supplementation with PVD (Meyer et al., 1996). More recently, a mouse model for pulmonary infection was used to demonstrate that defective PVD production negatively impacts pathogenecity via both iron uptake activity and the induction of other virulence factors, although PCH had less of an effect (Minandri et al., 2016). PVD is able to regulate its own production, acting as a signalling molecule, but also production of the proteases exotoxin A and PrpL (Lamont et al., 2002). This is a result of its role as a determinant for PvdS activity, which is an alternate sigma factor involved in the regulation of gene expression for a number of secreted virulence factors (Kang and Kirienko, 2018). Hence *P. aeruginosa* siderophores, particularly PVD, play an integral role in the formation of a chronic, biofilm infection.

1.2.4 Biofilm formation

A biofilm consists of aggregates of microbial cells surrounded by a self-produced matrix that is composed of lipids, proteins, nucelic acids, and polysaccharides (Flemming and Wingender, 2010). The establishment of a chronic *P. aeruginosa* infection in the CF lung is predominantly characterised by the formation of a biofilm. The biofilm becomes embedded in mucus plugs in the airways and persists for years, often for an individuals entire lifetime (Bjarnsholt et al., 2009). *P. aeruginosa* biofilm formation is largely affected by the ecological niche in which it exists, for example the presence of immune cells has been indicated to play a pivotal role in *P. aeruginosa* entering a biofilm lifestyle in the CF lung (Roberts et al., 2015). Thus many aspects of *in vivo* biofilms are not captured by *in vitro* models, such as the biofilm architecture which will be explored later in the introduction (section 1.3.1). *In vitro* models suggested that a *P. aeruginosa* biofilm is homogenous (Kragh et al., 2019), however *in vivo* this is not the case (Bjarnsholt et al., 2009). This is important for the development of novel treatments and determination of antibiotic susceptibility profiles. The biofilm is involved in antibiotic resistance and there has been different resistance phenotypes observed for *in vitro* biofilms compared with human infection (Müsken et al., 2017). This has resulted in poor correlation between the clinical outcomes following antibiotic treatment, and the results of *in vitro* antibiotic susceptibility testing (Smith et al., 2003; Hurley et al., 2012).

The main structural components of the *P. aeruginosa* biofilm are extracellular deoxyribonucleic acid (DNA), and the three exopolysaccharides: alginate, Psl, and Pel. Production of alginate results in a mucoid phenotype; it is typically overproduced by *P. aeruginosa* CF isolates and contributes to increased antibiotic tolerance (Ghafoor et al., 2011). It also acts to protect *P. aeruginosa* cells from the conditions in the CF lung (Wozniak et al., 2003), and has been implicated in increased airway inflammation by inhibiting apoptotic cell clearance by macrophages in the alveoli (McCaslin et al., 2015). Alginate overproduction has also been linked to the ability of *P. aeruginosa* and *S. aureus* to co-exist in the CF lung. The mucoid phenotype causes a decline in rhamnolipid and siderophore production, both involved in *S. aureus* killing (Limoli et al., 2017). However, non-mucoid isolates are associated with initial colonisation of the CF lung, and in the laboratory strains *P. aeruginosa* PAO1 and PA14 alginate is not required for biofilm formation (Wozniak et al., 2003). Psl has a protective role against the host immune

response, and has been associated with adherence to epithelial cells. It is also associated with the mature architecture of a chronic *P. aeruginosa* biofilm (Mann and Wozniak, 2012). However the strain *P. aeruginosa* PA14 is deficient in Psl, thus biofilm formation is dependent on Pel production (Colvin et al., 2011; Xu et al., 2016). As *P. aeruginosa* PA14 was the main strain studied in this thesis, Pel was the exopolysaccharide of most interest.

The exopolysaccharide Pel cross-links the extracellular DNA in the biofilm, and its positive charge gives it a distinct ability to interact with components of the biofilm matrix (Jennings et al., 2015). Hence, it is an integral component of the biofilm structure. Pel biosynthesis is encoded by an operon made up of seven genes (*pelA-F*) (Friedman and Kolter, 2004). As well as being involved in the structure of a *P. aeruginosa* biofilm, Pel has been implicated in the protective functions of the biofilm. It has been shown to be involved in the maintenance of cell-to-cell interactions, to provide the biofilm structural scaffold, and enhance resistance to aminoglycoside antibiotics (Colvin et al., 2011).

1.2.5 Quorum sensing

Quorum sensing (QS) regulates ~10% of *P. aeruginosa* genes and is involved in the regulation of many of the infection traits discussed so far (Diggle and Whiteley, 2020). QS systems use signalling molecules to regulate gene expression and for cell-to-cell communication in a cell density-dependent manner, affected by the growth environment conditions (Chugani et al., 2012). Extracellular signal molecules are produced and either repress or activate target genes once a threshold of production is reached. This is a positive feedback loop, with high cell densities causing increased signalling molecule production and thus increased target gene expression (Williams and Cámara, 2009). *P. aeruginosa* uses multiple QS systems and signals to regulate the production of virulence factors, swarming motility, the expression of efflux pumps, and maturation of the biofilm (Williams and Cámara, 2009). There are three well described *P. aeruginosa* QS sytems. Two of these systems are regulated by acyl homoserine lactones (AHLs): the LasI-LasR system and RhlI-RhlR (Figure 1.3), and the third is regulated by the *Pseudomonas* quinolone signal (PQS) (2-heptyl-3-hydroxy-4-quinolone) and its precursor 2-heptyl-4-quinolone (HHQ) (Kostylev et al., 2019). Each *P. aeruginosa* QS system, and how they interact, is further detailed in Figure 1.3.
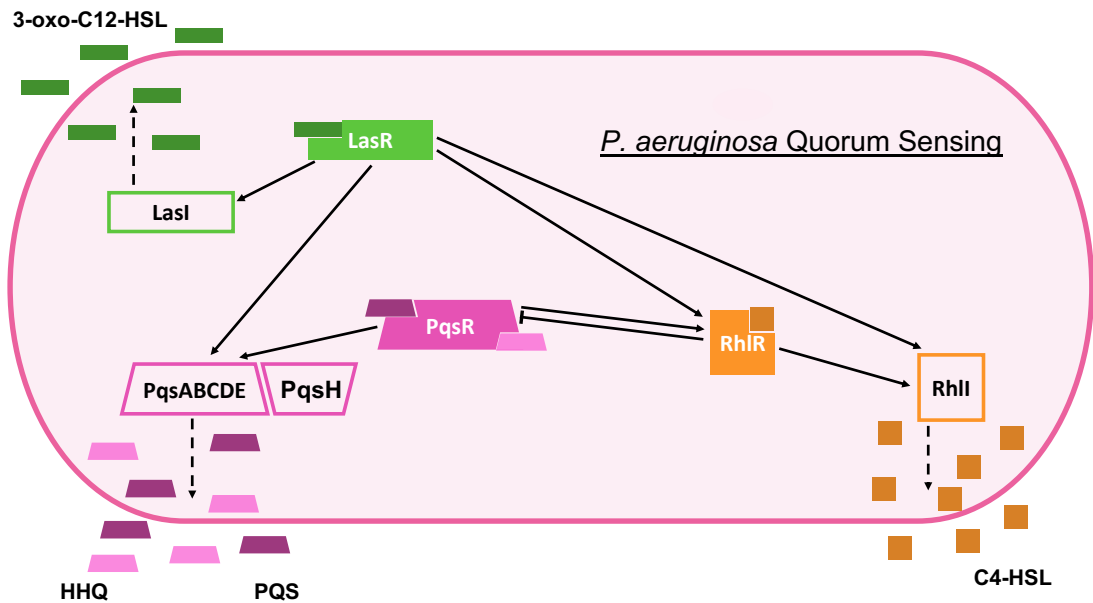
Figure 1.3: **The three *Pseudomonas aeruginosa* quorum sensing (QS) systems.** Each system is represented by a different colour; the response regulators are shown by the full size, filled shapes and the QS signalling molecule synthases shown by the full size, unfilled shapes. For the *Pseudomonas* quinolone signal (PQS) system, the gene clusters shown are involved in synthesis. The dashed arrows represent where the synthase catalyses each signalling molecule, the solid arrows show gene expression activation, and the blocked lines represent inhibition. Each signalling molecule binds to the corresponding response regulator as shown. The LasI-LasR and RhlI-RhlR systems use acyl-homoserine lactone signalling molecules: 3-oxo-dodecanoyl homoserine lactone (3-oxo-C12-HSL) and N-butanoyl-L-homoserine lactone (C4-HSL) respectively. The PQS system involves the signal 2-heptyl-3-hydroxy-4-quinolone (PQS) and its biosynthetic precursor 2-heptyl-4-quinolone (HHQ). An adaptation of Figure 3 by Lee and Zhang (2015), incorporating information from Kostylev et al. (2019).

Although QS facilitates growth in diverse environments, it has a metabolic cost. It has been indicated that some *P. aeruginosa* strains in the CF lung chronic infection population may behave as QS cheats, which are signal-blind so cannot respond to the QS signalling molecules. These cheats do not incur the metabolic cost of producing the signals or producing exoproducts in response to signals (Diggle et al., 2007). QS is most important during the initial stages of infection where virulence factor production is high, however its role in infection is thought to be reduced over time (Winstanley and Fothergill, 2009). There is an overall loss of QS in *P. aeruginosa* biofilms in the CF lung as chronic infection establishes, caused by mutations and associated with the loss of virulence (Hogardt and Heesemann, 2011). More specifically, there is an accumulation of mutations in the LasR gene which lead to reduced or no production of the *las* signalling molecule 3-oxo-dodecanoyl homoserine lactone (3-oxo-C12-HSL), and the associated virulence factors (Jiricny et al., 2014). QS has been identified as a target for anti-virulence drugs (Diggle and Whiteley, 2020), as interruption of these systems is likely to reduce virulence

during early infection and may prevent chronic infection. However as QS is affected by the environmental conditions in the CF lung (Chugani et al., 2012), development of effective drugs requires a model that accurately captures this and the resultant gene expression.

1.2.6 Antimicrobial resistance

One of the main challenges of *P. aeruginosa* infection is the high incidence of antimicrobial resistance. *P. aeruginosa* is one of the World Health Organisation's ESKAPE pathogens: *Enterococcus faecium*, *S. aureus*, *Klebsiella pneumoniae*, *Acinetobacter baumannii*, *P. aeruginosa*, and *Enterobacter* species, which are priority pathogens for which new antimicrobial treatments are urgently required. They have acquired resistance to most antibiotics in use, including those considered to be last resort options such as carbapenems and polymyxins, through mutations and acquisition of mobile genetic elements (De Oliveira et al., 2020). *P. aeruginosa* possesses a diverse range of resistance mechanisms that are either adaptive, innate, or acquired, which make it resistant to most conventional antibiotics (Pang et al., 2019). This also means *P. aeruginosa* often becomes resistant to novel antibiotics, so alternative treatments are being developed. These include phage therapy and QS inhibitors, however they are rarely brought to market due to the associated cost, safety concerns, and the high incidence of side effects (Pang et al., 2019).

The evolutionary adaptations undergone by *P. aeruginosa* to form a chronic infection in the CF lung, driven by the environment, result in increased antibiotic resistance (Winstanley et al., 2016). The formation of a biofilm is arguably the primary mechanism. Although it has been shown that the biofilm is unable to completely block antibiotics, the biofilm matrix can interact with antimicrobial compounds and reduce, or slow, penetration of the biofilm (Mah and O'Toole, 2001). The proteins, exopolysaccharides, and extracellular DNA that form the matrix are able to limit diffusion and in some cases sequester antibiotics, which significantly reduces the dosage that *P. aeruginosa* cells are exposed to (Varadarajan et al., 2020). This can result in exposure to sub-inihibitory concentrations of antibiotics, which leads to positive selection for resistance mutations. Overall, the rate of mutation in *P. aeruginosa* cells is at least 100 times higher during growth as a biofilm compared with planktonic growth anyway, and many of these mutations are associated with increased antibiotic tolerance (Conibear et al.,

2009). Therefore, the mutations conferring resistance that are caused by the CF lung environment and formation of a biofilm may be further driven by ineffective antibiotic treatments, rather than the antibiotics combating infection. This highlights the importance of accurate prescribing.

The conditions within the biofilm also have an effect on resistance. A *P. aeruginosa* biofilm is typically anoxic within the deeper cell layers, and there is oxygen limitation in the region of the CF lung where chronic infection forms. There are antibiotics that target aerobic metabolism and require reactive oxygen species generation for action, hence these are not effective against all *P. aeruginosa* cells in the CF lung biofilm (Varadarajan et al., 2020). There are also phenotypic variants within the population, including persistor cells, which exhibit different resistance profiles. Persistor cells are able to tolerate multidrug treatments, and are associated with the recurrent infections observed in people with CF (Pang et al., 2019). These cells are largely expressed under nutritent-limiting conditions caused by co-colonising microbes and conditions in the CF lung (Varadarajan et al., 2020). The general stress response causes these physiological changes to protect the *P. aeruginosa* cells from pH changes, temperature shock, and exposure to chemical agents, regulated by the σ factor RpoS. This is induced when cell density is high, such as in biofilms (Mah and O'Toole, 2001). Often referred to as dormant, persistor cells are distinct from metabolically active cells, and those in stationary phase, as they are alive but inactive. This means that persistor cells are tolerant to antibiotics rather than resistant; they survive high antibiotic doses due to many of the drug targets not being expressed in these cells (Mulcahy et al., 2010).

Metabolically active *P. aeruginosa* cells possess intrinsic resistance mechanisms, including reduced outer membrane permeability to limit antibiotic penetration, the production of enzymes that inactivate antibiotics, and efflux pumps which remove antibiotics from the cell (Pang et al., 2019). In particular, resistance-nodulation-division (RND) efflux pumps have been shown to be responsible for *P. aeruginosa* multidrug resistance, and have been extensively researched (Poole, 2009). There are 12 RND efflux pump systems in *P. aeruginosa* that have been described, including the MexAB-OprM pump which increases β-lactam resistance, and the MexXY-OprM pump which confers aminoglycoside resistance (Poole, 2009). Investigation of *P. aeruginosa* clinical isolates has shown that there is a significant positive relationship between resistance to

the majority of anti-pseudomonal antibiotics and expression of RND efflux pumps (Zahedi bialvaei et al., 2021). This indicated that these pumps play an integral role in the antibiotic resistance exhibited by *P. aeruginosa in vivo*.

The majority of *P. aeruginosa* antibiotic resistance mechanisms are regulated by two-component regulatory systems such as the PhoP-PhoQ system. PhoQ detects when there is a low extracellular Mg^{2+} concentration, which then leads to the response regulator PhoP upregulating expression of the *arn* locus (Gooderham and Hancock, 2009). The *arn* locus encodes a lipid A modification which reduces the charge of lipopolysaccharides, and thus negatively effects membrane interactions with polycationic antimicrobials such as polymyxin B, reducing their effect (Gooderham and Hancock, 2009). This evidences the role of environmental conditions on the antibiotic resistance mechanisms of *P. aeruginosa*.

The other bacterial species present in the CF lung, both pathogens and the microbiota, the host immune response, and nutrient availability affect *P. aeruginosa* antibiotic resistance. The review by Van den Bossche et al. (2021) detailed how the different factors of the CF lung microenvironment affect the activity of antibiotics against *P. aeruginosa*, summarised in Figure 1.4. For example, components of the CF mucus reduce activity of Tobramycin, β-lactams, and aminoglycosides. They induce expression of antimicrobial resistance genes, increase biofilm formation, and cause changes in hydrophobicity and cell surface charge. Conversely, the CF lung environment can also increase antibiotic activity. The low *P. aeruginosa* metabolic activity that is driven by the anoxic conditions, associated with the incidence of persistor cells, can cause increased activity of colistin through inactivation of *P. aeruginosa* adaptive mechanisms of resistance (Kolpen et al., 2016). This is mediated by expression of the *pmr* operon and MexAB-OprM efflux pump. When metabolically active, *P. aeruginosa* induces an adaptive resistance mechanism involving *pmr* modification of lipopolysaccharides and the MexAB-OprM pump, which makes cells tolerant to colistin treatment (Pamp et al., 2008). This action is not observed in non-metabolically active cells. All of this evidences the influence of the CF lung environment on the success of antibiotic treatments for *P. aeruginosa* chronic biofilm infection. Thus for rapid development of novel drugs, a laboratory model that captures the key characteristics of the CF lung that influence *P. aeruginosa* antibiotic tolerance and resistance is required.
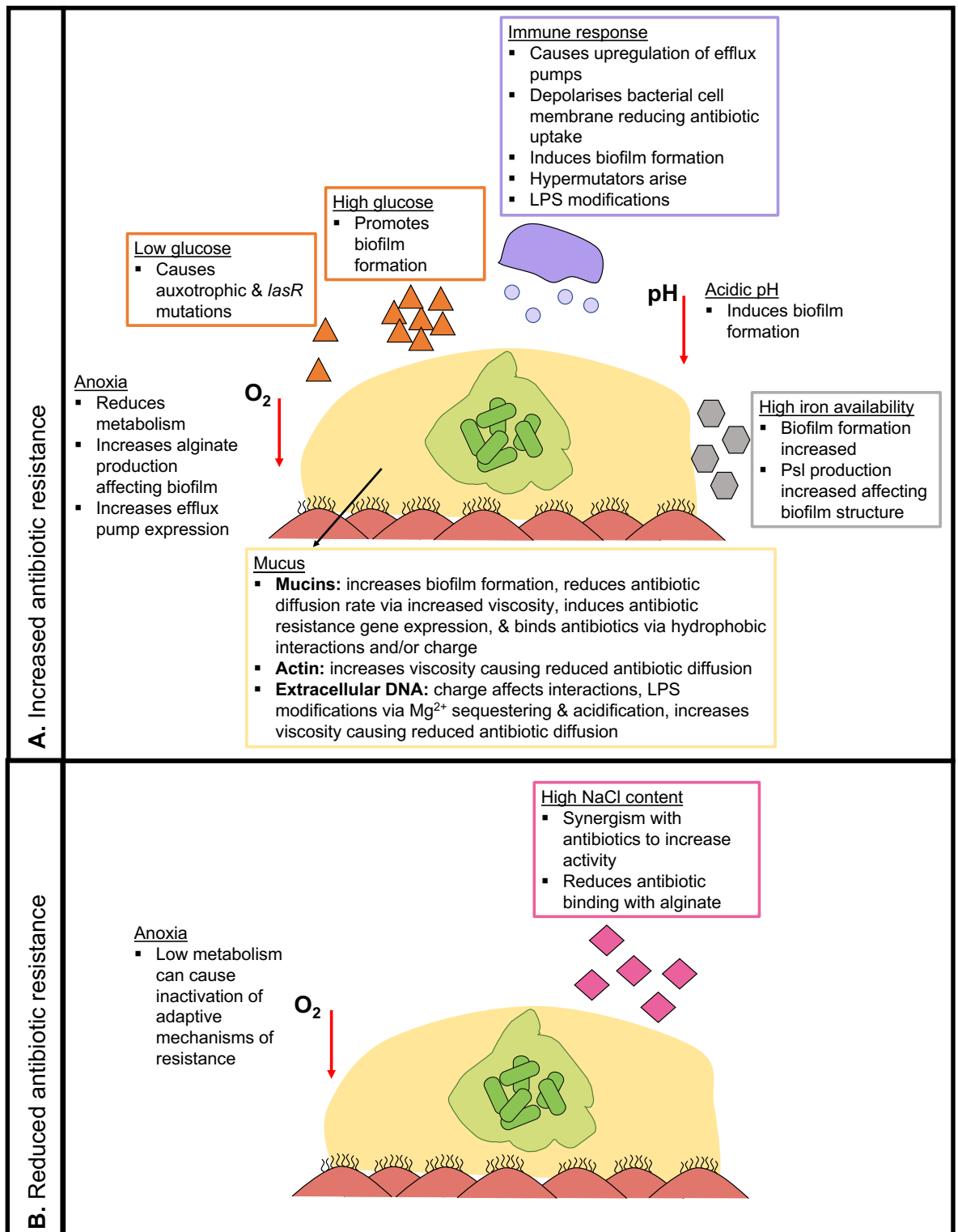
Figure 1.4: **Host factors in the cystic fibrosis (CF) lung that affect *Pseudomonas aeruginosa* susceptibilty to antibiotics.** Each host factor is shown on the diagrams and the corresponding boxes describe how each factor affects *P. aeruginosa* interaction/response to antibiotic treatment. The central diagram shows lung epithelial cells with cilia (dark pink), the CF sputum (yellow) and a *P. aeruginosa* biofilm with individual cells (green). **(A)** How host factors can increase *P. aeruginosa* resistance to antibiotics. **(B)** How host factors can reduce *P. aeruginosa* antibiotic resistance. The diagram is an adaptation of Figure 1 from Van den Bossche et al. (2021), incorporating information from Table 1 (Van den Bossche et al., 2021).

1.3   Infection models for the cystic fibrosis lung

There have been a number of different laboratory models developed to recapitulate *P. aeruginosa* biofilm infection in the CF lung. These include media to mimic CF sputum, continuous flow models, bead models, *ex vivo* models using animal and human tissue, human cell models, and live animal models. Although each of these capture aspects of infection in the CF lung, there are limitations associated with each. This has led to a focus on the development of an optimal model for the CF lung to address key research questions: how to target and solve the growing incidence of antimicrobial resistance, and what is the effect of polymicrobial interactions on pathogenesis (O'Toole et al., 2021)?

1.3.1   Current models

One of the main challenges for laboratory models of *P. aeruginosa* chronic infection in the CF lung is the formation of a mature, structured biofilm reminiscent of patient biopsies. There have been clear qualitative differences observed in biofilm structure when *P. aeruginosa* is grown in different *in vitro* systems. In flow cell models, a *P. aeruginosa* biofilm typically has a 'mushroom'-like structure with open channels (Roberts et al., 2015). Whereas microtitre plate models for biofilm infection lead to a homogenous mass of *P. aeruginosa* cells, which are densely packed (Kragh et al., 2019). Both are a contrast with the *in vivo P. aeruginosa* biofilm structure seen in the lungs of people with CF. Biopsies taken from the CF lung show *P. aeruginosa* biofilms that have a 'sponge'-like structure, composed of aggregates of *P. aeruginosa* cells with gaps potentially filled with lung fluid, mucus, or alginate (Baltimore et al., 1989; Bjarnsholt et al., 2009; Henderson et al., 2014). This means it is unlikely that *in vitro* models are capturing all biofilm-associated phenotypes, such as increased antibiotic resistance.

There is a distinction in *P. aeruginosa* antibiotic resistance phenotypes from biofilm cells grown *in vitro* compared with *in vivo* (Müsken et al., 2017). To improve *in vitro* antibiotic susceptibility testing accuracy, Calgary biofilm devices have been used where biofilms are grown on pegs in microplates. However, it has been shown that this does not improve the accuracy of results from planktonic growth, and there is still increased resistance observed *in vivo* in comparison (Smith et al., 2020; Harrington et al., 2021b). This is a key driver for the development of clinically relevant *P. aeruginosa* biofilm models for the CF lung, to accurately prescribe treatment plans and identify novel, effective drug targets.

Artificial sputum media have been developed to replicate the composition of CF sputum. In CF, the sputum induces key *P. aeruginosa* physiological adaptations that drive its pathogenesis and the development of chronic infection, involving QS regulation (Palmer et al., 2005). There have been nine different recipes for artificial sputum media widely used in the literature, either derived from the initial Ghani and Soothill (1997) protocol which uses egg yolk emulsion, DNA, mucin, potassium, sodium, chloride, and amino acids, or a synthetic cystic fibrosis sputum media (SCFM) that has been chemically derived (Palmer et al., 2007). The different formulations cause differences in *P. aeruginosa* growth and virulence. Distinct secondary metabolite production has been observed, driven by iron availability, presence of mucin, and the aromatic amino acid concentrations (Neve et al., 2021). It has been shown that aromatic amino acids are essential for *P. aeruginosa* QS signalling (Palmer et al., 2007).

The SCFM recipe has been used for the work in this thesis. The original recipe (see Table 2.3) was defined in 2007 and was shown to cue *P. aeruginosa* gene expression, QS, and resultant phenotypes comparable to growth in CF sputum (Palmer et al., 2007). However, a study by Turner et al. (2015) that used transposon sequencing to investigate the *P. aeruginosa* essential genome in CF identified a number of adaptations required to improve the clinical relevance of SCFM. This led to the refinement of the original SCFM to produce SCFM2, which incorporated mucin, DNA, dioleoylphosphatidylcholine, and N-acetylglucosamine. These additions resulted in only 0.7% of *P. aeruginosa* PA14 and PAO1 genes being differentially essential compared with CF sputum (Turner et al., 2015). This medium has since been used in a number of studies of CF lung infection, including investigation of co-infection with *S. aureus* (Barraza and Whiteley, 2021). Despite this, a key aspect of CF lung infection is missing from sputum media: the presence of a tissue structure.

Animal models for CF lung infection exist, which better replicate the spatial structure of the CF lung. A number of different animals have a CFTR ortholog with amino acid identity above 50% similar to humans: pigs (93%), ferrets (92%), sheep (91%), mice (78%), rats (75.5%), and zebrafish (55%) (Semaniakou et al., 2018). However, none are able to fully replicate chronic *P. aeruginosa* infections in the CF lung. Pigs and ferrets have the most similarity to human infection and show the most promise, but they are

yet to be fully developed as model organisms. There are limitations on the reagents available for use with these model organisms, specifically for studying the immunology (Bayes et al., 2016). Mice are frequently used to study these infections, and do exhibit pulmonary symptoms. However, they are unable to fully replicate the *P. aeruginosa* infections observed in people (Davidson and Rolfe, 2001). Adaptations have been made to address this, including an agar bead murine model where *P. aeruginosa* beads are inserted into the mice surgically. However, this did not fully capture *in vivo* pathogenesis (Bayes et al., 2016). Mice with CFTR mutations are also used to replicate CF, however the airway secretions are distinct from those in people with CF (Benahmed et al., 2014). This may contribute to the differences observed; there are significant differences in *P. aeruginosa* gene expression when grown in CFTR mice compared with humans with CF (Cornforth et al., 2018). It is also known that in murine models with CFTR mutations, *P. aeruginosa* is unable to develop a chronic infection (Bayes et al., 2016). Hence, animal models have not solved the disparity between laboratory research and *in vivo* infection. It also raises the ethical debate of using live animal models if they do not truly replicate *in vivo* infection. Therefore, there is still a gap in research for an accurate model for *P. aeruginosa* CF lung infection.

1.3.2 Model evaluations

To determine the validity of different infection models, *P. aeruginosa* RNA sequencing (RNA-seq) data has been studied. Cornforth et al. (2018) evaluated RNA-seq data from a diverse range of laboratory growth conditions, including SCFM2 and Luria-Bertani (LB) media, and compared it with *P. aeruginosa* gene expression in CF patient sputum samples. The transcriptome from *in vitro* growth and mouse model infections were compared with soft-tissue wound infections and CF exporated sputum. It was shown that *P. aeruginosa* gene expression was distinct in each environment, and the *P. aeruginosa* transcriptome from CF sputum was distinct from all other human infection contexts studied (Cornforth et al., 2018). This supports the hypothesis that the CF lung environment facilitates a unique *P. aeruginosa* infection compared with other human infection contexts. Overall, it was shown that a number of metabolic pathways and the QS regulon were downregulated in human infection, and pathways such as phenazine biosynthesis and antibiotic resistance-associated genes were upregulated, in comparison with *in vitro* growth. This led to the development of a support vector machine model to

classify whether *P. aeruginosa* transcriptomes from different environments classified as human infection, mainly based on the expression of nutrient acquisition and metabolism genes (Cornforth et al., 2018).

Building on this work, Cornforth et al. (2020) have developed a quantitative framework to evaluate and provide a score for models of *P. aeruginosa* infection in the CF context. It is based on CF sputum samples and *in vitro* grown *P. aeruginosa* transcriptomes from SCFM2, morpholinepropanesulfonic acid-succinate (MOPS-succinate), LB, and an *in vitro* CFTR mutant epithelial cell model, as well as a mouse model for lung infection. This framework calculated an accuracy score for each model to show the percentage of genes expressed within a defined number of standard deviations from CF sputum expression. It was found that none of the models tested were able to score 100%, however all models scored a minimum of 80% indicating they were valid models for use (Cornforth et al., 2020). The epithelial cell model and SCFM2 were shown to be optimal, although both still missed aspects of *P. aeruginosa* gene expression *in vivo*. SCFM2 was shown to cue overexpression of polyamine spermidine biosynthesis genes compared with CF, and the epithelial cell model growth caused inaccurate expression of protein synthesis genes (Cornforth et al., 2020). This work has provided a method to validate models, as well as showing that there are still aspects of chronic CF infection that are not replicated by the best models available. It has highlighted areas for improvement needed to replicate *in vivo* chronic *P. aeruginosa* infection.

1.3.3   The *ex vivo* pig lung model

As discussed, pigs are more similar to humans than mice, and have been shown to be comparable in their overall anatomy, physiology, immunology, and metabolic composition to humans (Meurens et al., 2012; Benahmed et al., 2014). Piglets have been previously used as models for *P. aeruginosa* lung infection contexts such as ventilator-associated pneumonia. They were used to investigate the host response to infection and for development of treatments (Luna et al., 2009; Meurens et al., 2012). Prior to starting the work in this thesis, preliminary data of an *ex vivo* pig lung (EVPL) model for *P. aeruginosa* lung infections in the CF context had been published (Harrison et al., 2014; Harrison and Diggle, 2016).

The EVPL model uses pig lungs sourced from a local butcher, considered a waste product from the meat industry. Therefore, there are no ethical considerations associated and the model works towards addressing the 3R's: Replacement, Refinement, and Reduction of the use of live animals in scientific research (Burden et al., 2015). The lung tissue is dissected into small squares, infected with *P. aeruginosa*, and surrounded by SCFM (Palmer et al., 2007). This original SCFM recipe has been shown to be suitable for the EVPL model, with no percieved benefit of using the further adapted SCFM2 (Harrington et al., 2020). Alveolar tissue was first used in the model to explore the growth of *P. aeruginosa lasR* mutants, and adaptation to the CF lung, which evidenced the validity of the model (Harrison et al., 2014). However alveolar tissue was subsequently replaced with bronchiolar tissue in the EVPL model, and has been used throughout this thesis, as it is known to be the main location of *P. aeruginosa* chronic infection in CF (Harrison et al., 2014; Harrison and Diggle, 2016). The initial work with bronchiolar tissue showed that a *P. aeruginosa* biofilm could be consistently replicated in the EVPL model and it had potential for capturing the clinical phenotype (Harrison and Diggle, 2016). Following this, the model has been used to investigate siderophore cheating by *P. aeruginosa* (Harrison et al., 2017), and to study the the antimicrobial activity of Manuka honey against *P. aeruginosa* isolates (Roberts et al., 2019).

The work in this thesis has led to further publications evidencing the validity of the EVPL as a clinically representative model for *P. aeruginosa* biofilms with a mature architecture (Harrington et al., 2020), and gene expression with key characteristics associated with human infection (Harrington et al., 2021a). Alongside this, use of the model for more accurate antibiotic susceptibility testing has been published (Harrington et al., 2021b), and studies of antibiotic activity have been performed (Hassan et al., 2020; Sweeney et al., 2020b). Optimisations have also begun for the study of other microorganisms in the model, including *S. aureus* (Sweeney et al., 2020a).

1.4   Multispecies interactions

1.4.1   Complexity of the CF lung

For a long time it was thought that the CF lung was predominantly infected with known pathogens such as *P. aeruginosa* and *S. aureus*, and there was little diversity. Rogers et al.

(2004) were one of the first studies to provide evidence for the complexity of the CF lung microbial community. Using 16S ribosomal ribonucleic acid (rRNA) sequencing and terminal restriction fragment length polymorphism profiling, they identified 19 different bacterial species in the lungs of people with CF, and 15 of these had not previously been associated with CF. Amongst these were *Prevotella* species, *Staphylococcus hominis*, and *Rothia mucilaginosa* (Rogers et al., 2004). The findings also highlighted the importance of species considered to be part of the lung flora, as well as pathogens. *R. mucilaginosa* is part of the flora in different locations of the human body, including the upper respiratory tract (Lim et al., 2013). It has now been shown to contribute to *P. aeruginosa* pathogenesis through production of metabolites used by *P. aeruginosa* (Gao et al., 2018). Hence both co-infecting pathogens and the interactions between pathogens and the lung microbiota are involved in pathogenesis. Therefore, further understanding of these interactions is important for developing new treatments.

It is considered unlikely that the microbial communities in the CF lung are consistent across all people with the condition. It has been proposed that there is a collective of communities that represent most CF airway infections (Jean-Pierre et al., 2021). Further profiling of the bacteria, fungi, and viruses involved may facilitate the development of better *in vitro* models to investigate the virulence, persistance, and antimicrobial resistance of infections influenced by interspecies interactions (Jean-Pierre et al., 2021). *P. aeruginosa* has been shown to be affected by its interactions with other microbial species in the CF lung. It modulates motility in response to *S. aureus* secreted products, driven by the type IV pili (Limoli et al., 2019), and the ability of *P. aeruginosa* to form a biofilm has been shown to be reduced when the two species co-infect (Hotterbeekx et al., 2017). Co-infection of *P. aeruginosa* with the species *Stenotrophomonas maltophilia* has also been shown to alter infection characteristics. It was demonstrated that co-infection causes increased resistance of *P. aeruginosa* to imipenem (Bottery et al., 2021). These examples demonstrate how *P. aeruginosa* interactions with other bacterial species affects its virulence, biofilm formation, and antibiotic resistance. *P. aeruginosa* also has an effect on the incidence of further infection, in the CF lung it has been shown to increase susceptibility to secondary infections including with the Bcc (Sajjan et al., 2001; O'Brien and Fothergill, 2017).

1.4.2 The *Burkholderia cepacia* complex

The Bcc are Gram negative bacteria, isolated from a range of locations including healthcare settings and environmental sources. They can be animal, plant, and human pathogens; in humans they affect immunocompromised individuals such as those with chronic granulomatous disease and CF (Sousa et al., 2010). The complex is made up of 22 *Burkholderia* species, and is associated with rapid lung function decline in people with CF (Scoffone et al., 2017).

There are three species most commonly isolated from the CF lung: *B. cenocepacia*, *B. multivorans*, and *B. dolosa*. They can cause a necrotizing pneumonia and sepsis, often referred to as cepacia syndrome, which has a high fatality rate (Sousa et al., 2010). *B. cenocepacia* used to be the predominant Bcc species that affected people with CF, however *B. multivorans* has now become the most prevalent Bcc species associated with CF (Kenna et al., 2017). There are low rates of *B. multivorans* adaptation within the CF lung and the diversity between people with CF is most likely driven by diverse environmental sources rather than cross-infection (Lood et al., 2021). This may also be associated with the low incidence of Bcc infection in people with CF, they are responsible for only approximately 5% of CF lung infections (Leitão et al., 2017; Shropshire et al., 2021). This may be such a small prevalance compared with *P. aeruginosa* because of infrequent cross infection. The high incidence of intrinsic antibiotic resistance, high transmissibility, and the severity of disease has led to extensive segregation measures in CF clinics to prevent cross patient infection (Kenna et al., 2017; Leitão et al., 2017). The Bcc share many similarities with *P. aeruginosa*; they also form biofilms during infection that exhibit high levels of antibiotic resistance and persistence (Scoffone et al., 2017). In fact, the *Burkholderia* genus was only confirmed to be independent of *Pseudomonas* in 1992 (Yabuuchi et al., 1992). Therefore, this was the next genera introduced into the EVPL model following establishment of the similar pathogen *P. aeruginosa*.

1.5 Aims and Objectives

The work in this thesis addressed the lack of a clinically relevant, laboratory model for *P. aeruginosa* chronic infections in the CF lung. The conditions in this context, as discussed throughout the introduction, cue *P. aeruginosa* adaptations that lead to the formation of

a chronic biofilm infection with specific characteristics. The determination of treatment plans that are effective *in vivo* is negatively affected by the lack of a clinically relevant model for the CF lung, which reduces quality of life. This also hinders development of new treatments and the identification of novel drug targets. Therefore, the primary aim was to investigate the cost effective, high-throughput EVPL model for *P. aeruginosa* infection and determine whether it could solve some of the issues with other CF lung infection models. Four key research questions were addressed, focusing on *P. aeruginosa* PA14, and are explored in depth in the subsequent chapters:

1. What are the *P. aeruginosa* virulence phenotypes exhibited in the EVPL model?

Using assays for *P. aeruginosa* virulence factor production and transposon insertion mutants for key genes, it was shown that the production of virulence factors in the EVPL was at low levels. Visualisation of the *P. aeruginosa* biofilm formed on the surface of the EVPL tissue revealed a clinically representative, mature structure dependent on the production of Pel and the Gac regulatory system. The biofilm also exhibited high levels of meropenem resistance.

2. How does *P. aeruginosa* gene expression in the EVPL model compare with SCFM, and in context with human infection?

RNA-seq analysis demonstrated that there was a distinction in gene expression between *P. aeruginosa* grown in the EVPL model, both as a biofilm associated with the lung tissue and in the surrounding SCFM, and SCFM *in vitro*. There was significant differential expression of antibiotic resistance-associated genes, and downregulation of QS genes in a similar pattern to CF sputum compared with SCFM.

3. How does *P. aeruginosa* gene expression change over time in the biofilm associated with the EVPL tissue?

RNA-seq was performed on *P. aeruginosa* samples from the EVPL biofilm at 24 h, 48 h, and 7 d. This revealed a number of changes including in nitrogen and sulfur metabolism.

4. Can *P. aeruginosa* and the Bcc co-exist in the EVPL model, and how are key phenotypes affected?

B. cenocepacia and *B. multivorans* were introduced to the EVPL model and were able to grow alongside *P. aeruginosa*. QS signalling and *P. aeruginosa* siderophore production

appeared to play a role in the interspecies interactions.

Overall this work has shown that the EVPL model can be used to study chronic-like *P. aeruginosa* biofilm infection in the CF lung, and appears to capture infection characteristics not observed in the current laboratory models. It can now be used to further understand *P. aeruginosa* infections to develop new treatments and prevention methods. It has also shown potential as a diagnostic platform to more accurately determine whether treatments will be effective. This will hopefully improve treatment outcomes and overall quality of life for people with CF.

Chapter 2

Materials and Methods

2.1 Bacterial strains and growth conditions

The bacterial strains used for this work are listed in Table 2.1, including where each isolate was obtained from. Each strain was grown on an agar plate at 37 °C prior to all experiments, and the agar and incubation length used for each strain are detailed in Table 2.1. The presence of the transposon in the correct locus for each *P. aeruginosa* PA14 transposon insertion mutant strain (Table 2.2) was confirmed by arbitrary Polymerase Chain Reaction (PCR) as per the PA14 Non-Redundant Transpson Mutant Set library instructions (Liberati et al., 2006a,b) and gel electrophoresis (0.7% agarose (Fisher BioReagents, US) with 1X SYBR® safe DNA gel stain (Invitrogen, Canada); 120 v for 30 min) (F Harrison, pers. Comm.).

Table 2.1: **All bacterial strains used for this work.** Each species and strain is listed and the media used for initial growth before each experiment. All strains were grown on Luria-Bertani (LB) agar (LB broth: Melford Laboratories, UK, agar: Formedium, UK) with selective antibiotics where appropriate. Clinical isolates used were all from cystic fibrosis (CF) and both *Escherichia coli* isolates were biosensors for acyl homoserine lactones (AHLs). The source details where each strain was acquired from and the original source where relevant are shown.

Species	Strain	Culture conditions	Source
Pseudomonas aeruginosa	PA14	LB agar overnight at 37 ℃	Prof. Leo Eberl, University of Zürich (originally University of Washington (Liberati et al., 2006a,b))
Pseudomonas aeruginosa	PA14 transposon mutants (Table 2.2)	LB agar + 15 µg ml^{-1} gentamicin (Sigma-Aldrich, USA) overnight at 37 ℃	PA14 Non-Redundant Tranposon Insertion Mutant Set (Liberati et al., 2006a,b)
Pseudomonas aeruginosa	LESB58 (CF isolate)	LB agar overnight at 37 ℃	Dr Steve Diggle, Georgia Insitute of Technology
Pseudomonas aeruginosa	SED20 (CF isolate)	LB agar for 48 h at 37 ℃	Dr Sophie Darch, Univeristy of South Florida (Darch et al., 2015)
Pseudomonas aeruginosa	SED43 (CF isolate)	LB agar for 48 h at 37 ℃	Dr Sophie Darch, Univeristy of South Florida (Darch et al., 2015)
Burkholderia cenocepacia	K56-2	LB agar + 50 µg ml^{-1} polymyxin B (Sigma-Aldrich, USA) for 48 h at 37 ℃	Dr Yin Chen, University of Warwick
Burkholderia multivorans	C5393 (CF isolate)	LB agar + 50 µg ml^{-1} polymyxin B for 48 h at 37 ℃	Prof. Leo Eberl, University of Zürich (originally *Burkholderia cepacia* complex experimental strain panel (Mahenthiralingam et al., 2000))
Escherichia coli	pSB1075 with a fusion of lasRI':: luxCDABE	LB agar + 10 µg ml^{-1} tetracycline (ABCR, Germany) overnight at 37 ℃	Dr Roman Popat and Prof. Paul Williams, University of Nottingham (Winson et al., 1998)

Table 2.1 – continued from previous page

Species	Strain	Culture conditions	Source
Escherichia coli	pSB536 with the *ahyR* of *Aeromonas hydrophyla* and the cognate *ahyI* gene promoter fused to luxCDABE	LB agar + 50 µg ml⁻¹ ampicillin (Merck KGaA, Germany) overnight at 37 °C	Dr Roman Popat and Prof. Paul Williams, University of Nottingham (Swift et al., 1997)

Table 2.2: *Pseudomonas aeruginosa* **PA14 transposon insertion mutants used for this work.** Each strain was obtained from the PA14 Non-Redundant Transposon Insertion Mutant set (Liberati et al., 2006a,b) and the insertion was confirmed using arbitrary polymerase chain reaction (PCR) following library instructions. The mutant and gene IDs are shown as well as the gene name and product.

Mutant ID	Gene ID	Gene name	Gene product
54630	GID3719	*gacA*	Response regulator gacA
52692	GID3659	*vfr*	Cyclic AMP recpetor-like protein
46879	GID1598	*sadR*	Probable two-component response regulator
47015	GID2130	*pqsR*	Transcriptional regulator MvfR
26187	GID86	*pelA*	Deacetylase required for Pel polysaccharide synthesis

2.2 Synthetic cystic fibrosis sputum medium

Synthetic cystic fibrosis sputum media (SCFM) was prepared based on the protocol published by Palmer et al. (2007) (see Table 2.3). Glucose was substituted with distilled water (dH$_2$O) as preliminary work found that, in the presence of lung tissue, glucose did not affect *P. aeruginosa* growth but did facilitate the growth of endogenous lung bacterial species (Harrison and Diggle, 2016). The same recipe was used for *in vitro* SCFM growth

for direct comparison. Each component was added in the order listed in Table 2.3 and each stock solution was prepared to the concentration shown in 40 ml sterile dH_2O, with the exception of those indicated in the table and footnotes. The media was prepared in 500 ml volumes then filter sterilised using a Nalgene™ Rapid-Flow™ sterile disposable filter unit (PES membrane: 75 mm x 0.1 µm x 500 ml) and stored at 4 °C for up to 1 month.

Table 2.3: **The protocol used to prepare 500 ml batches of synthetic cystic fibrosis sputum medium (SCFM) based on Palmer et al. (2007).** Each component is listed in the order they were added to the media. With the exception of components where the stock solution column shows '-', a 40 ml stock solution was prepared and an aliquot of each stock was added to the SCFM (volume added shown in amount added column). Each stock solution was prepared in dH_2O, except those described in the footnotes for which alternative stock preparation methods were used.

Component	Stock solution (40 ml)	Amount added	Manufacturer
NaCl	-	3.03 g	Fisher Scientific, UK
KCl	-	1.114 g	Fisher Scientific, UK
Sterile dH_2O	-	320 ml	-
Na_2HPO_4	0.125 M	5 ml	Acros Organics, Spain
NaH_2PO_4	0.13 M	5 ml	Acros Organics, India
NH_4Cl	0.228 M	5 ml	Fisher Scientific, UK
KNO_3	0.0348 M	5 ml	VWR Chemicals, Belgium
K_2SO_4	0.0271 M	5 ml	Acros Organics, Spain
MOPS	1 M	5 ml	Acros Organics, Taiwan
Aspartame[a]	82.7 mM	5 ml	Scientific Laboratory Supplies, UK
Threonine	107.2 mM	5 ml	Alfa Aesar, UK
Serine	144.6 mM	5 ml	Alfa Aesar, UK
Glutamic acid[b]	154.9 mM	5 ml	Sigma-Aldrich, China
Proline	166 mM	5 ml	Alfa Aesar, UK
Glycine	120.3 mM	5 ml	Sigma-Aldrich, USA
Alanine	178 mM	5 ml	Alfa Aesar, UK
Cysteine	16 mM	5 ml	Merck kGaA, Switzerland
Valine	111.7 mM	5 ml	Alfa Aesar, UK
Methionine	63.3 mM	5 ml	Sigma-Aldrich, Japan
Isoleucine[c]	112.1 mM	5 ml	Alfa Aesar, UK
Leucine[c]	160.9 mM	5 ml	Sigma-Aldrich, Germany
Tyrosine[d]	80.2 mM	5 ml	Alfa Aesar, USA
Phenylalanine	53 mM	5 ml	Alfa Aesar, UK
Ornithine-HCl	67.6 mM	5 ml	Park Scientific Limited, UK
Lysine	212.8 mM	5 ml	Sigma-Aldrich, China
Histidine	51.9 mM	5 ml	Alfa Aesar, UK
Tryptophan[e]	1.3 mM	5 ml	Alfa Aesar, UK
Arginine	30.6 mM	5 ml	Sigma-Aldrich, Japan
HCl	1 M	Adjust to pH 6.8	Fisher Scientific, UK
Sterile dH_2O	-	To final volume 480 ml	-

Table 2.3 – continued from previous page

Component	Stock solution (40 ml)	Amount added	Manufacturer
$CaCl_2$	0.175 M	5 ml	Alfa Aesar, UK
$MgCl_2$	0.0606 M	5 ml	Fisher BioReagents, India
L-Lactic acid[f]	0.93 M	5 ml	Alfa Aesar, UK
$Fe(III)SO_4.7H_2O$	0.00036 M	5 ml	Acros Organics, Spain

[a] Dissolved in 40 ml 0.5 M NaOH (Fisher Scientific, UK).

[b] Dissolved in 40 ml 1 M HCl.

[c] Dissolved in 40 ml dH_2O then heated to 50 °C for 30 min.

[d] Dissolved in 40 ml 1 M NaOH.

[e] Dissolved in 40 ml 0.2 M NaOH.

[f] Stock made with solution with density gradient of 1.209 g ml^{-1} : 2.77 ml solution was added to 30 ml dH_2O then adjusted to pH 7 with 5 M NaOH. The final stock volume of 40 ml was made using dH_2O.

2.3   Dissection of *ex vivo* pig lung tissue

The *ex vivo* pig lung (EVPL) bronchiolar tissue was dissected and subsequently infected following the published method (Harrington et al., 2021b), originally described by Harrison et al. (2014). Two to three independent lungs were used as repeats per experiment. Lungs used were provided by Steve Quigley and Sons Butchers Ltd. (Cubbington, UK) and Taylors Butchers (Coventry, UK), and were obtained on the day of arrival from the abattoir and transported to the University of Warwick in a sterile coolbox. All subsequent work was carried out under sterile conditions, around a bunsen burner. The pleura of the ventral surface was seared with a hot pallet knife for ~1 s to kill any potential lung surface contaminants that may have been introduced following slaughter. A sterile razor blade was used to cut the lung tissue to expose the bronchus cartilage, then make a transverse cut where the bronchus meets the trachea on each side as shown in Figure 2.1. The bronchi were cut where branching started (~6 cm in length) and removed from the surrounding tissue using flame sterilised forceps and the blade, any excess alveolar tissue that was attached was removed. The bronchiolar tissue was placed in a 50 ml falcon tube containing a 40 ml wash of 1:1 Roswell Park Memorial Institute (RPMI) 1640 medium and Dulbecco's modified Eagle medium (DMEM) (Sigma-Aldrich, UK), supplemented with 50 µg ml^{-1} ampicillin for ~10 min. Seperate wash sets were used

for independent lungs. The bronchi were removed from the wash using sterile forceps and any remaining excess alveolar and connective tissue removed with flame sterilised dissection scissors. The bronchioles were cut into~5 mm wide longitudinal strips using sterile dissection scissors (Figure 2.1), then briefly placed in a fresh 40 ml 1:1 RPMI 1640 and DMEM (+ ampicillin) wash. The tissue strips were removed from the wash then further cut into 5 mm x 5 mm squares and placed in a petri dish. A final 40 ml 1:1 RPMI 1640 and DMEM (+ ampicillin) wash was added to the petri dish then removed (Figure 2.1). Finally, ~20 ml SCFM was added to the petri dish with the bronchiolar tissue square sections then ultraviolet (UV) sterilised for 5 min.

1 Transverse cuts made where bronchi meet trachea and where branching starts (red lines) with sterile razor blade. Bronchi removed from lung using sterile forceps.

2 Excess tissue on the surface of extracted bronchi removed using sterile dissection scissors.

3 Bronchi placed in 40 ml 1:1 RPMI 1640 medium and DMEM + 50 µg ml^{-1} ampicillin for ~ 10 min then removed with sterile forceps.

4 Any external tissue remaining removed with sterile dissection scissors, and tissue sections cut into ~5 mm wide strips. Tissue placed in 40 ml 1:1 RPMI 1640 medium and DMEM + 50 µg ml^{-1} ampicillin wash using sterile forceps.

5 Tissue strips removed from the wash with sterile forceps and cut into ~5 mm x 5 mm squares using sterile dissection scissors.

6 Tissue squares placed in a petri dish with sterile forceps & 1:1 RPMI 1640 and DMEM + 50 µg ml^{-1} ampicillin added then removed (wash step). SCFM was added (~20 ml).

Figure 2.1: **Diagram showing the steps of the *ex vivo* pig lung model dissection protocol.** Drawings are representations of each step and are not to scale or biologically accurate. The forceps and dissection scissors were flame sterilised and the razor blades used were sterilised using an autoclave. The method was repeated for independent lungs used for this work, with fresh Roswell Park Memorial Institute (RPMI) 1640 medium and Dulbecco's modified Eagle medium (DMEM) washes with 50 µg ml^{-1} ampicillin used per step and per lung.

2.4   *Ex vivo* pig lung tissue infection

Following dissection, 0.8% agarose (w/v) was prepared in SCFM and 400 µl was added to each well of a tissue culture treated, flat bottom, individually wrapped 24 well plate (Corning Costar, USA) per tissue piece dissected. Each plate was sterilised with UV for 10 min. The UV sterilised bronchiolar tissue sections were then transferred using sterile

forceps to individual wells of the SCFM-agarose containing 24 well plates. The bacterial strains to be studied in the model were cultured on suitable Luria-Bertani (LB) (Melford Laboratories, UK) agar (Formedium, UK) plates as decribed in Table 2.1. A sterile 29G hypodermic needle (BD, France) was used to touch a colony from the LB plate and 'prick' the surface of the tissue piece then discarded; a sterile needle was used as a negative control. For lung pieces that were infected with multiple bacterial strains (mixed infection), a second needle was used in the same way to subsequently infect the tissue with the second strain. Three to five replicate tissue pieces per lung were infected per infection condition for each experiment. To recapitulate the lung environment, 500 µl liquid SCFM was added to each well. A Breathe-Easier® sealing membrane (Diversified Biotech, US) per plate was UV sterilised for 10 min, and was used to cover each plate. The 24 well plates were then incubated in plastic drawers at 37 °C, stationary, for the desired length of time.

2.5   Bacterial recovery from *ex vivo* pig lung tissue

Following incubation, infected tissue sections were washed in 500 µl phosphate-buffered saline (PBS) and transferred into individual, sterile tubes containing 1 g of 2.38 mm metal beads (Fisher Scientific, UK) and 1 ml PBS. To recover bacterial cells from the tissue-associated biofilm, the tissue-containing bead tubes were placed in a FastPrep-24 (MP Biomedicals, UK) and bead beaten for 40 s at 4 m s^{-1}. Homogenate that was not used to determine number of bacterial cells was filter sterilised using a 33 mm 0.2 µm syringe filter (Fisher Scientific, China) with a 2 ml syringe (Becton Dickinson, Spain) into individual, sterile 1.5 ml Eppendorf tubes (Germany) and stored at -20 °C. The homogenate samples were defrosted on ice for subsequent experiments.

2.6   *In vitro* SCFM growth

Each bacterial strain to be used was cultured on the relevant agar at 37 °C for the required time length (see Table 2.1). For RNA extractions to ensure for adequate amounts of RNA, colonies were taken from the plate using a plastic 10 µl loop and suspended in SCFM to an OD$_{600nm}$ of 0.05. Aliquots of 1 ml were then added to individual wells of a 24 well plate. For all other *in vitro* SCFM cultures, 1 ml sterile SCFM was added to individual wells of a 24 well plate. A sterile 29G hypodermic needle was used to touch a colony from the

agar plate then transferred to the 1 ml SCFM aliquot to mimic the lung tissue infection for comparison. For mixed infection cultures, a second needle was used to add the second bacterial strain to the SCFM. The plates, following both infection methods, were covered with a UV sterilised (10 min) Breathe-Easier® membrane and incubated at 37 °C in plastic drawers, stationary, for the desired length of time.

2.7 Determination of colony forming units

The samples for which colony forming units (CFU) were determined: either lung homogenate containing released bacteria or *in vitro* cultures, were serially diluted in PBS in sterile, polystyrene 96 well plates (Greiner Bio-One, Germany). This was performed on the same day as sampling. Initially, 200 µl of each undiluted sample was added to each well in the top row of the plate (10^0) then 180 µl PBS was added to the rest of the wells. A 20 µl aliquot was taken from the 10^0 well and added to the PBS in the well below and thoroughly mixed (10^{-1}). A 20 µl aliquot was then taken from the 10^{-1} well and added to the PBS in the well below and mixed (10^{-2}). This process was repeated sequentially to a 10^{-7} dilution in the final row, to produce a 10-fold series dilution and 10 µl of each dilution was plated on the relevant agar (see Table 2.1), in triplicate on two agar plates (Figure 2.2) per media. For mixed infections, samples were plated on duplicate agar plates for each relevant selection media per strain (Table 2.1). The plates were incubated at 37 °C for the required time (Table 2.1) then the number of colonies of each sample were counted for the two highest dilutions that were countable (~2 - 200 colonies) and the average determined from six repeats (3 repeats x 2 agar plates). The average dilution factor for the experiment was determined from the dilution factor calculated for each sample, excluding any values outside of 1-20: $\frac{AverageNumberOfColonies(dilution1)}{AverageNumberOfColonies(dilution2)}$. CFU ml^{-1} was determined using the following calculation for *in vitro* samples:

$$AverageNumberOfColonies(dilution1)\,x\,AverageDilutionFactor^{DilutionNumber}\,x\,\frac{1000}{10}$$

and CFU lung^{-1} was calculated with the following calculation, with 25 added to account for the extra volume introduced by the lung tissue:

$$AverageNumberOfColonies(dilution1)\,x\,AverageDilutionFactor^{DilutionNumber}\,x\,\frac{1025}{10}$$
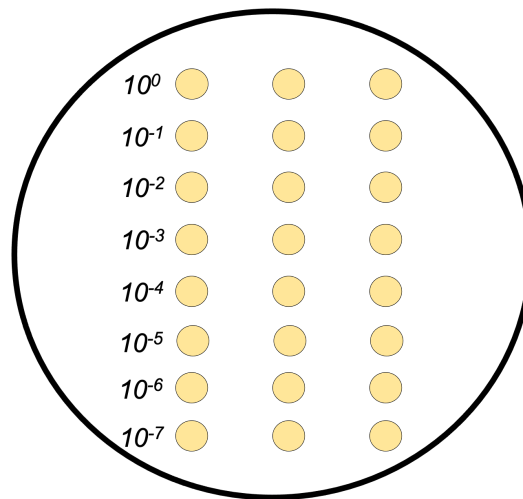
Figure 2.2: **Diagram of the layout of an agar plate used to determine the bacterial colony forming units (CFU) in a sample.** Each yellow circle represents 10 µl of sample and the three dots per row are aliquots from the same sample. Each row is a dilution as shown in the diagram, prepared in phosphate-buffered saline (PBS).

2.8   Enzyme-linked immunosorbent assay (ELISA)

An enzyme-linked immunosorbent assay (ELISA) for porcine interleukin-8 (IL-8) (Invitrogen, Austria) was performed on the filter sterilised homogenate from EVPL tissue infection and bacterial recovery at different time points post infection. The homogenate was diluted 1 in 5 using PBS in a 1.5 ml Eppendorf tube: ~600 µl homogenate and 2400 µl PBS. The assay was performed following the Invitrogen IL-8 porcine ELISA kit protocol and all reagents used were provided in the kit. Reagents were prepared as follows; the Wash Buffer Concentrate (25X) was allowed to reach room temperature then gently mixed and diluted to 1x using dH_2O to create the Working Wash Buffer, excess Working Wash buffer was stored at 4 °C. Swine IL-8 was used as a standard, and was initially reconstituted to 10,0000 pg ml^{-1} with Standard Diluent Buffer and left for 10 min. Following incubation, 120 µl of 10,0000 pg ml^{-1} swine IL-8 was added to 480 µl Standard Diluent Buffer in a 5 ml universal tube, and mixed to make standard one at a concentration of 2000 pg ml^{-1}. A two-fold dilution series in 5 ml universal tubes was then performed and 300 µl of the previous dilution was added to 300 µl Standard Diluent Buffer to create the following standards: 1000 pg ml^{-1}, 500 pg ml^{-1}, 250 pg ml^{-1}, 125 pg ml^{-1}, 62.5 pg ml^{-1}, 31.2 pg ml^{-1} and a blank (0 pg ml^{-1}). A 1X Streptavidin-HRP solution was also prepared, 10 µl of Streptavidin-HRP (100X) was added to 1 ml Streptavidin-HRP Diluent for every 8 well strip to be used (one well per sample) in a 10 ml universal tube.

The solution was mixed thoroughly.

The 8-well strips provided were placed in the frame, with one well per sample, standard and chromogen blank. The assay was repeated in triplicate for each sample, standard and chromagen blank. The sterile lung homogenate samples were further diluted 1 in 2: 50 µl PBS was added to each assay well then 50 µl sample, and the two were mixed. Following the dilution, 100 µl of each standard was added to individual non-sample wells, and three wells were left empty as chromogen blanks. Subsequently, 50 µl Incubation Buffer was added to each well except chromagen blanks and the side of the plate was tapped to mix the samples. The plate was covered with a provided plate cover and incubated at room temperature for 2 h. A wash step was then performed where the solution was thoroughly removed from each well, and the wells were washed with the provided 1X Wash Buffer four times. Each wash was performed by pipetting dH_2O into each well then removing it. The plate was tapped dry to ensure there was no remaining wash buffer then 100 µl Swine IL-8 Biotin Conjugate solution was added to each well (not chromgen blanks). The plate was covered and incubated at room temperature for 1 h and the wash steps were repeated. Once the wells were dry, 100 µl of prepared 1X Streptavidin-HRP solution was added to each well, excluding the chromagen blanks, and the plate was covered and incubated at room temperature for 30 min. The wash steps were repeated then 100 µl Stabilized Chromogen was added to each well, including the chromagen blanks. The plate was then placed in the dark at room temperature and incubated for 30 min. Following this, 100 µl Stop Solution was added to each well and mixed by tapping the plate; the solution went from blue to yellow.

The absorbance was then read at 450 nm using a Tecan Spark 10M multimode plate reader. A four parameter algorithm was used to fit a standard curve to the assay standards values (Figure 2.3), and determine the IL-8 concentration in the homogenate samples, using GraphPad Prism version 9.1.0 for Mac OS X (GraphPad, 2021). Each concentration was then multiplied by 2 to determine the concentration before the 1 in 2 assay dilution. This was further multiplied by 5 to account for the initial 1 in 5 dilution, to calculate the IL-8 concentration in the original sample.
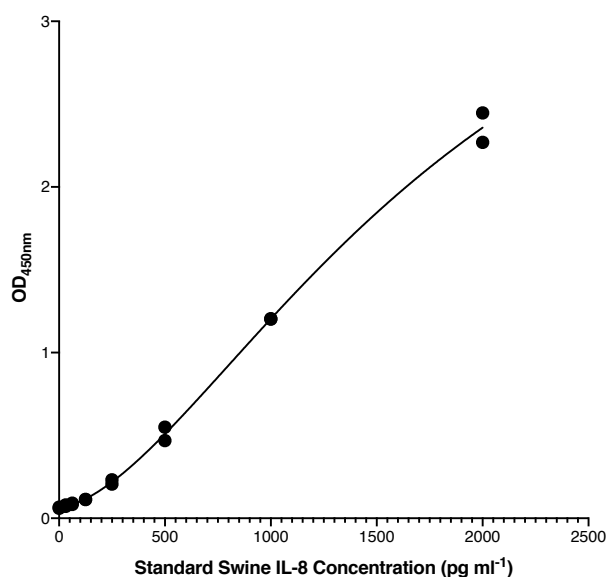
Figure 2.3: **Enzyme-linked immunosorbent assay (ELISA) porcine interleukin-8 (IL-8) standard curve.** The standard curve was produced using the OD_{450nm} value from three assay repeats of each swine IL-8 standard: 0 pg ml^{-1}, 31.2 pg ml^{-1}, 62.5 pg ml^{-1}, 125 pg ml^{-1}, 250 pg ml^{-1}, 500 pg ml^{-1}, 1000 pg ml^{-1} and 2000 pg ml^{-1}. A four parameter algorithm was used, produced in GraphPad Prism version 9.1.0 for Mac OS X (GraphPad, 2021).

2.9   Azocasein protease assay

The amount of protease produced in the EVPL tissue-associated *P. aeruginosa* biofilm was determined using azocasein as a substrate to measure proteolytic activity (Harrison et al., 2014). The assay was also performed on homogenate from uninfected tissue to determine whether there was any residual protease activity from the pig tissue. Following bacterial recovery and filter sterilisation, the lung homogenate was diluted 1 in 5 using PBS : ~600 µl homogenate and 2400 µl PBS, in a sterile 1.5 ml Eppendorf tube. The assay was performed on triplicate repeats of each sample; 100 µl sterile homogenate was added to each of three 1.5 ml Eppendorf tubes per sample. Proteinase K (Fisher BioReagents, Germany) was used as the known concentration of protease to produce a standard curve. A 5 ml master stock of proteinase K was made to a concentration of 1 mg ml^{-1} in dH$_2$O and from this stock 500 µl known standards of the following concentrations were prepared using dH$_2$O in 1.5 ml Eppendorf tubes: 500 µg ml^{-1}, 100 µg ml^{-1}, 75 µg ml^{-1}, 25 µg ml^{-1}, 10 µg ml^{-1}, 5 µg ml^{-1}, 1 µg ml^{-1} and a 0 µg ml^{-1} assay blank. Then, 100 µl of every standard concentration was added to each of three 1.5 ml Eppendorf tubes per standard. The azocasein buffer was prepared in a glass 500 ml Duran bottle, 1 ml was made for every tube (samples and standards): 100 mM Tris (Sigma-Aldrich, USA), 1 mM

CaCl$_2$ (Alfa Aesar, UK), pH 7.5, and 5 mg azocasein (Sigma-Aldrich, UK) was dissolved in the buffer for every tube to be assayed.

Following preparation, 900 μl of azocasein solubilised in the buffer was added to each assay tube. All tubes were incubated at 37 °C for 15 min with 170 rpm shaking. To stop the reaction, 100 μl stop solution was added (10% (v/v) trichloroacetic acid (TCA); PanReac AppliChem, ITW Reagents, Germany). The samples were centrifuged for 1 min at 13,000 rpm. A 200 μl aliquot was taken from the supernatant in each tube and transferred to individual wells of a 96 well plate (Corning, USA) and the abosrbance read at 400 nm using a Tecan Spark 10M multimode plate reader. A proteinase K standard curve was produced (Figure 2.4) and the total protease in each sample was calculated using the equation: $1.3935e^{(5.7822*OD_{400nm})}$ then the dilution was cancelled by multiplying by 5 and the total in each sample determined by finally multiplying by 1.025 (the extra 0.025 to account for the entire volume in the lung homogenate sample).
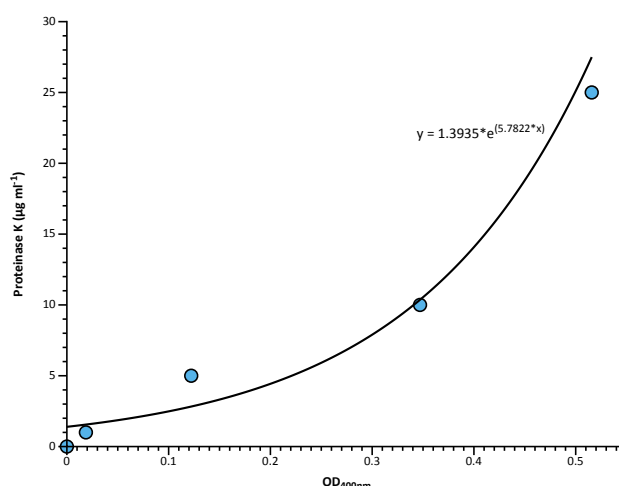
Figure 2.4: **Proteinase k (μg ml^{-1}) standard curve for azocasein protease assay.** The standard curve was produced using OD$_{400nm}$ values for triplicate repeats of known proteinase K concentrations: 500 μg ml^{-1}, 100 μg ml^{-1}, 75 μg ml^{-1}, 25 μg ml^{-1}, 10 μg ml^{-1}, 5 μg ml^{-1}, 1 μg ml^{-1} and 0 μg ml^{-1}. The data points represent the mean values for each concentration and the equation for the standard curve determined from all values is shown.

2.10   Pyoverdine and pyochelin assays

The production of the siderophores PVD and PCH by *P. aeruginosa* from EVPL tissue-associated biofilms was measured using fluorescence (Dumas et al., 2013; Harrison et al., 2014). The sterile lung homogenate from bead beating following lung dissection, infection and incubation at required time points, was diluted 1 in 5 in PBS as decribed in

Method 2.9. The assay was also performed on homogenate from uninfected tissue as a negative control. Duplicate aliquots of 200 µl each from every sample were transferred to individual wells of a 96 well flat, clear bottom, black tissue culture treated plate, with a lid (Corning, USA). PVD was measured by exciting the samples with light at 400 nm then measuring the fluorescence at 460 nm. PCH was measured by exciting the samples at 350 nm and measuring the fluorescence at 430 nm. Both were measured using a Tecan Spark 10M multimode plate reader.

2.11   Crystal violet biofilm assay

After EVPL dissection, infection and incubation at 37 °C for the desired length of time, tissue pieces were placed in individual wells of a 24 well plate, each containing 500 µl PBS. The lid was put on the plate and the plate was lightly shaken to remove non-biofilm associated *P. aeruginosa* cells. Crystal violet (Pro-Lab Diagnostics, UK) was prepared to 0.1% (v/v) in PBS in a 50 ml falcon tube, then 500 µl was added to individual wells of a new 24 well plate. The tissue sections were transferred to each crystal violet well and incubated at room temperature for 15 min, with 170 rpm shaking and the plate lid on. Each tissue piece was transferred to another 24 well plate, with 500 µl PBS in each well. The lid was put on the plate and it was lightly shaken to remove any unbound crystal violet. The tissue pieces were transferred to each well of a further, empty 24 well plate and left to dry in a laminar flow hood for 30 min, without the lid on. Following drying, 500 µl 95% ethanol (v/v) was added to each well and the plate was incubated with the lid on at room temperature, for 15 min with 170 rpm shaking. The tissue pieces were removed from each well using flame sterilised forceps and discarded. Finally, 200 µl of the ethanol solution from each well was transferred to individual wells of a 96 well plate. The absorbance was read at 590 nm using a Tecan Spark 10M multimode plate reader.

2.12   EVPL histology sample preparation

Following dissection, infection and the desired incubation time, *ex vivo* pig lung (EVPL) tissue sections were each placed in a tissue processing/embedding cassette (Simport Scientific, Canada) and placed in 10% neutral buffered formalin (VWR Chemicals, UK) overnight for fixation. Samples were then transferred to 70% ethanol (v/v) (VWR International, France), diluted to 70% using dH_2O, and stored at 4 °C for a maximum

of 7 d until all samples were ready. The sections were then prepared for histopathology; paraffin-embedded, sectioned and mounted on glass microscopy slides by an external service at the University of Manchester's histology core facility (UK). Following this, tissue sections were initially de-parraffinized in 2 changes of xylene (Avantor, Poland) for 10 min per change. The sections were then re-hydrated in 2 changes of 100% ethanol for 5 min per change, followed by 2 min in 95% ethanol then 2 min in 70% ethanol. All ethanol dilutions were prepared in dH_2O. Slides were then washed in dH_2O for 2-3 min prior to staining.

2.13 Gram staining

P. aeruginosa infected EVPL tissue pieces prepared for histological staining were also Gram stained, alongside *in vitro* SCFM *P. aeruginosa* cultures. The initial preparation steps prior to staining were different for each sample type. After the EVPL tissue samples were de-paraffinised in xylene (Method 2.12), the re-hydration process was altered from above. Re-hydration steps were performed using a combination of ethanol and isopropanol. The samples were re-hydrated in 100% ethanol for two changes, each 5 min. The slides were then placed in 95% isopropanol (Fisher Scientific, UK) (v/v; diluted in dH_2O) for 2 min, then 70% isopropanol (v/v; diluted in dH_2O) for 2 min. Residual alcohol was removed by washing the slides in dH_2O for 2-3 min. For *in vitro* SCFM cultures, ~20 µl of culture was added to a glass microscope slide (Fisher, UK) and heat fixed. Briefly, the slide was passed through a flame ~6 times then left to dry by the flame.

Gram staining was then performed on EVPL and *in vitro* SCFM samples following the same method. Crystal violet was briefly applied to the samples (~30 s) and rinsed with water. Iodine (Pro-Lab Diagnostics, UK) was applied for ~1 min then briefly rinsed using water, and acetone added for 10 - 15 s for decolourisation. Water was used to rinse off the acetone and 1% neutral red (v/v) (Pro-Lab Diagnostics, UK) applied for 1 min to counterstain. The slides were rinsed with water and blotted dry with filter paper.

The EVPL samples were finally dehydrated in 100% isopropanol (v/v) for ~5 s, then placed in two fresh changes of 100% xylene (v/v) for 5 min each. All samples were mounted using DPX mountant fluid and a 22 x 50 mm Hydrolytic Class 1 glass cover slip. Images were taken using a Zeiss Axio Scope. A1 light microscope with the Zeiss Axiocam Erc 5s

and Zeiss Zen 2.3 pro software.

2.14   Alcian blue staining of EVPL tissue

After re-hydration, the *P. aeruginosa* infected lung samples and uninfected tissue samples, as a negative control for biofilm, were stained with Alcian blue to identify the biofilm matrix. The slides were stained with 1% Alcian blue solution in 3% acetic acid (pH 2.5) (Sigma-Aldrich, USA) for 45 min, then rinsed well with dH$_2$O for 2 min. Slides were transferred to nuclear fast red solution (Alfa Aesar, UK) for 2 min to counterstain the samples then briefly washed in dH$_2$O. The samples were then dehydrated, first 'dipped' in 95% ethanol (v/v; diluted in dH$_2$O) 10 times then placed in fresh 95% ethanol (v/v) for 2 min. Slides were transferred to two changes of 100% ethanol for 2 min each and finally added to two changes of xylene for 5 min each. The samples were finally mounted using DPX mountant fluid (Sigma-Aldrich, UK) and a 22 x 50 mm Hydrolytic Class 1 glass cover slip (VWR Collection, UK). The samples were imaged using a Zeiss Axio Scope. A1 light microscope with the Zeiss Axiocam Erc 5s and Zeiss Zen 2.3 pro software.

2.15   Hematoxylin and eosin staining of EVPL tissue

The formation of *P. aeruginosa* biofilm on the surface of EVPL tissue sections was investigated using Hematoxylin and Eosin (H & E) staining, which stained both the lung tissue and bacterial biofilm (Figure 2.5). Uninfected tissue was also stained at each time point as a negative control for *P. aeruginosa* biofilm. Following histology preparation and re-hydration, the samples for staining were transferred to Mayer's hemalum solution (Merck Millipore, UK) for 10 min. Slides were washed in running 'tap water' (~1 L tap water with 2 teaspoons Na$_2$CO$_3$ (Prolabo, France)) for 5 min then transferred to the counterstain, eosin Y solution (Merck Millipore, Germany), for 1 min 30 s. The tissue samples were then dehydrated: first 'dipped' in 95% ethanol (v/v; diluted in dH$_2$O) 10 times, then transferred to 2 changes of 100% ethanol for 2 min per change. The slides were then transferred to 2 changes of xylene for 5 min each, and mounted using DPX mountant fluid and a 22 x 50 mm Hydrolytic Class 1 glass cover slip. Slides were imaged using a Zeiss Axio Scope. A1 light microscope with the Zeiss Axiocam Erc 5s and Zeiss Zen 2.3 pro software.
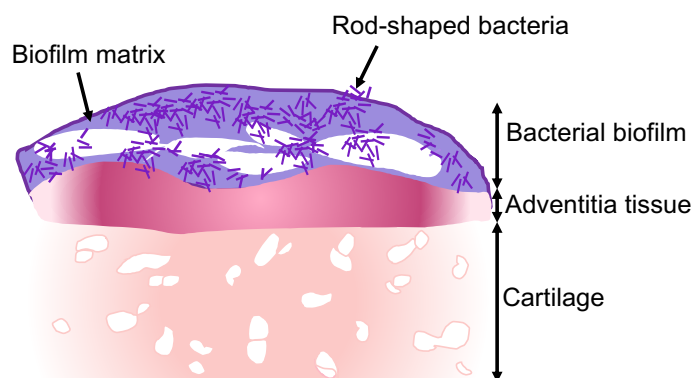
Figure 2.5: **Diagram of Hematoxylin & Eosin (H & E) stained *ex vivo* pig lung (EVPL) bronchiolar tissue sections infected with *Pseudomonas aeruginosa*.** The tissue structures that were visible from this staining are labelled, stained pink (with eosin Y solution). The bacterial biofilm is stained purple (with Mayer's hemalum solution) as shown and the rod-shaped bacteria within the biofilm, indicative of *P. aeruginosa*, were visible.

The depth of the stained biofilm on the surface of the tissue was measured using the Zeiss Zen 2.3 pro software. A line was drawn from the edge of the tissue (stained pink) where the biofilm started, to the outward edge of the biofilm (Figure 2.5) . The length (µm) was determined using the software, and measurements were taken at 7 points along each H & E stained biofilm image. The mean was calculated to determine the average *P. aeruginosa* biofilm depth on the surface of the EVPL tissue.

2.16   Minimum inhibitory concentration assay

All minimum inhibitory concentration (MIC) assays were performed following the broth microdilution method described by Wiegand et al. (2008). The MIC of different bacterial strains was tested for all antibiotics listed in Table 2.4. Assays were carried out using bacteria grown on EVPL tissue and using standard *in vitro* inoculum. For EVPL model MICs, the lung homogenate following bacterial recovery was diluted 1 in 100 in SCFM (~200 µl homogenate and 19.8 ml SCFM) in a 50 ml falcon tube, to prepare the bacterial inoculum. The *in vitro* inoculum were prepared as a MacFarland standard in a 25 ml, glass universal tube. *P. aeruginosa* PA14 was grown on an LB agar plate overnight and colonies were suspended in the required media for the assay: either SCFM or cation-adjusted Mueller Hinton broth (CAMHB) (Sigma-Aldrich, India), to an OD_{600nm} of 0.08 – 0.1, then diluted 1 in 100 in the media used to the required volume dependent on how many assays were performed per inoculum (~5 ml per antibiotic tested with the inoculum). Three replicate bacterial inoculums were prepared for each antibiotic MIC assay, both EVPL and *in vitro*.

Table 2.4: **The antibiotics for which the minimum inhibitory concentration (MIC) was determined for different bacterial strains.** Each antibiotic was prepared as a master stock as shown and stored at - 20 °C until required. Meropenem and polymyxin B master stocks were stored in 2 ml Eppendorf tubes and master stocks of colistin were stored in 2 ml clear, glass vials (Merck KGaA, Germany). The master stocks were then diluted to 256 µg ml^{-1} working concentrations to perform MIC assays as described.

Antibiotic	Master stock	Assay preparation	Manufacturer
Meropenem	5 mg ml^{-1}: 10 mg meropenem trihydrate + 1752 µl dH$_2$O	Diluted in SCFM to working concentrations	Sigma-Aldrich, USA
Colistin	10 mg ml^{-1}: 5 mg colistin sulfate salt + 500 µl dH$_2$O	Diluted in SCFM to working concentrations	Acros Organics, China
Polymyxin B	50 mg $^{-1}$: 50 mg polymyxin B sulfate salt + 1 ml dH$_2$O	Diluted in SCFM to working concentrations	Sigma-Aldrich, USA

The antibiotic to be tested was prepared to a concentration of 256 µg ml^{-1} in a 5 ml universal tube from the master stock in the same media used for the bacterial inoculum for that assay (Table 2.4). Subsequently, 200 µl of the antibiotic (256 µg ml^{-1}) was added to each well in the first column of a tissue culture treated, flat bottom, clear 96 well plate with a lid (Corning, USA). One row was prepared per assay performed for that antibiotic, then 100 µl media for the assay was added to the rest of the wells in each row (excluding the first antibiotic-containing well). The antibiotic was then serially diluted two-fold ten times (see Figure 2.6). Following dilutions, 100 µl of the bacterial inoculum were added to each antibiotic well, resulting in the final assay antibiotic concentrations, and the positive control wells (Figure 2.6). The negative control wells were then filled with 200 µl sterile media, as used for the rest of the assay. The plate was sealed with parafilm and incubated for 18 h at 37 °C, stationary without any plate stacking. Following incubation, the antibiotic concentration with no growth, visible as either turbidity or biofilm formation, was recorded as the MIC value.
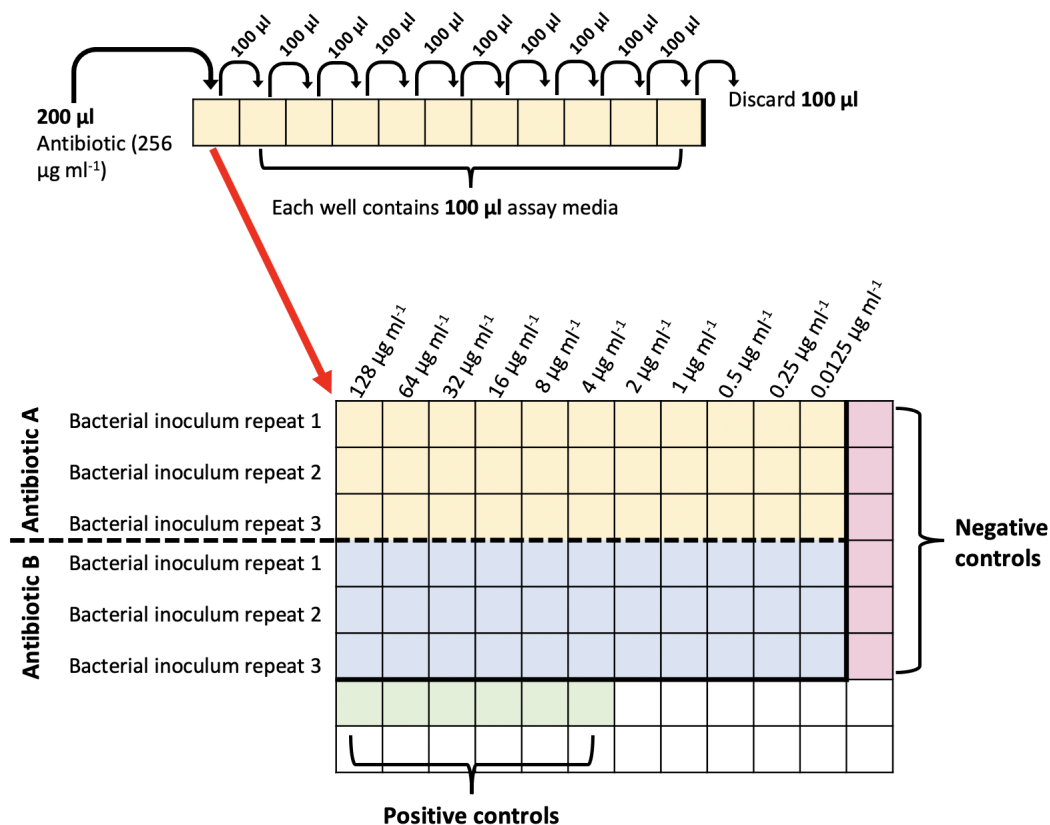
Figure 2.6: **Layout of a 96 well plate prepared for a minimum inhibitory concentration (MIC) assay for different bacteria of multiple anitbiotics.** MICs were performed in tissue culture treated, flat bottom, clear 96 well plates with a lid (Corning, USA), shown by the table above. Each square represents a well. The top diagram illustrates the two-fold dilution series performed in each antibiotic row to result in the final required antibiotic concentrations once the bacterial inoculum was added. The bottom diagram shows the whole plate layout for a 96 well plate where two sets of MICs were performed, three replicates per assay, and the final antibiotic concentrations.

2.17 Antibiotic susceptibility testing in the EVPL model

Lungs were dissected and infected as described, with three replicate lung pieces per lung and test condition. Antibiotics tested were prepared as a master stock and stored as described in Table 2.4 prior to use. The master stock was then used to make the required antibiotic concentrations for each experiment, diluted in SCFM in 15 ml falcon tubes.

Following the desired incubation time, tissue pieces were removed from the 24 well plate with flame sterilised forceps and washed in 500 µl PBS in individual wells of a tissue culture treated, flat bottom, individually wrapped 48 well plate (Corning Costar, USA) to remove non-biofilm associated bacterial cells. The tissue pieces were then transferred into 500 µl of the required antibiotic at the desired concentration in individual wells

of a 48 well plate. A replicate control, non-antibiotic treated set of tissue pieces were transferred into 500 µl PBS in individual wells of a 48 well plate. The plates were covered with a UV sterilised Breathe-Easier® sealing membrane and incubated in plastic drawers for 24 h at 37 °C. Tissue pieces were then removed and washed in PBS in a 48 well plate as above, and placed in individual tubes with 1 g 2.38 mm metal beads (Fisher Scientific, UK) and 1 ml PBS. The bacterial cells were recovered and CFU was determined as described above (Method 2.5, 2.7).

2.18   Microbial cell viability from EVPL tissue

To determine the cell viability of the *P. aeruginosa* biofilm grown on the EVPL tissue, a BacTiter-Glo™ microbial cell viability assay (Promega, USA) was performed to measure the amount of ATP (nM) present in samples to infer number of viable microbial cells. Uninfected tissue was used as a negative control condition for *P. aeruginosa* infection. After lung dissection, infection and incubation, the bacteria were recovered at 1 d, 2 d and 7 d; it was also done immediately after infection as a 0 d time point. The lung homogenate following bacterial recovery was equilibrated to room temperature and 100 µl of each homogenate was added to individual wells of a 96 well flat, clear bottom, black tissue culture treated plate, with a lid. Known concentrations of ATP were also prepared to produce a standard curve. In a polystyrene 96 well plate, three replicate dilution rows were prepared. In the first column 200 µl of 1 µM ATP solution (Jena Bioscience, Germany) was added to each well and in all subsequent wells in the row, 180 µl SCFM was added. A ten-fold series dilution was then performed, 20 µl was taken from the first well that contained 1 µM ATP and added to the adjacent well in each dilution row to produce a 0.1 µM concentration. This process was repeated sequentially four more times to produce the following concentrations: 0.01 µM, 0.001 µM, 0.0001 µM and 0.00001 µM. Following this, 100 µl of each ATP standard (3 replicates per concentration) was transferred to individual wells of the 96 well flat, clear bottom, black tissue culture treated plate, as was done for the homogenate samples, to perform the assay for known ATP concentrations.

The assay was then performed following the Promega BacTiter-Glo™ microbial cell viability assay kit instructions using the reagents provided. The BacTiter-Glo™ Buffer and lyophilised BacTiter-Glo™ Substrate were first equilibriated to room temperature then

the Buffer (10 ml) was transferred to the substrate and mixed using a vortex, to make the assay reagent. Once mixed, 100 µl of the reagent was added to each well of the 96 well plate containing a homogenate sample or ATP standard. The plate contents were mixed on an orbital shaker at 170 rpm, at room temperature for 1 min. The luminescence (RLU) was then read using a Tecan Spark 10M multimode plate reader. An ATP standard curve was produced (Figure 2.7) and the ATP concentration in each sample was calculated using the equation: $\frac{RLU - 21.33}{763.41}$.
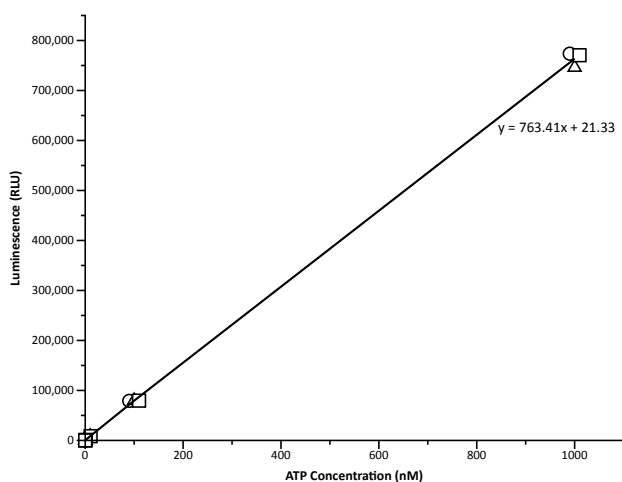
Figure 2.7: **ATP (nM) standard curve for BacTiter-Glo™ microbial cell viability assays (Promega, USA).** The standard curve was produced using the luminescence values (RLU) from three assay repeats of each ATP standard concentration: 0.01 nM, 0.1 nM, 1 nM, 10 nM, 100 nM and 1000 nM, after performing the assay following kit instructions. The different shape points represent each repeat. The standard curve is shown and the equation, which was used to determine the ATP concentration in *ex vivo* pig lung homogenate samples: uninfected negative controls and *Pseudomonas aeruginosa* infected, is shown.

2.19   *Pseudomonas aeruginosa* RNA extraction

All areas and equipment used for RNA experiments were cleaned using RNaseZap™ (Sigma-Aldrich, Lithuania) before the work started. *P. aeruginosa* PA14 ribonucleic acid (RNA) was extracted from the two environments of the EVPL model: the lung tissue-associated biofilm and surrounding SCFM media (see Figure 2.8) at 24 h, 48 h and 7 d post infection. The extractions were performed on double the amount of samples intended to be sequenced to account for any RNA loss during extraction, hence six replicate samples from each of two lungs were used at each time point. PA14 RNA was also extracted from *in vitro* SCFM cultures at 24 h and 48 h, similarly from double the number of samples to be sequenced - so six replicates per time point. At the required time, each culture was transferred to individual, sterile 2 ml DNA LoBind microcentrifuge

tubes (Eppendorf, Germany): 1 ml lung homogenate per tube, 500 µl surrounding SCFM per tube or 1 ml *in vitro* SCFM culture per tube. A 0.5 volume of sterile killing buffer (20 mM Tris-HCl pH 7.5, 5 mM $MgCl_2$, 20 mM NaN_3) was then added to each tube. The samples were centrifuged for 1 min at 13,000 rpm then snap frozen in dry ice and ethanol, and stored at -80 °C for a minimum of 1 h.
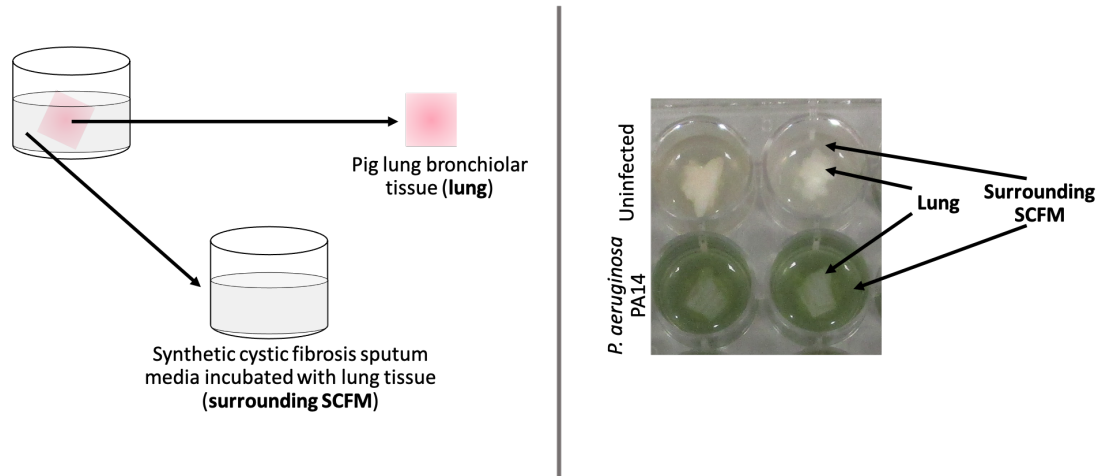
Figure 2.8: **The two environments of the *ex vivo* pig lung (EVPL) model from which *Pseudomonas aeruginosa* PA14 RNA was extracted.** The photos show the EVPL model following 7 d incubation at 37 °C as an example.

The samples were then defrosted on ice and the supernatant was carefully discarded so that the pellet was not disturbed. The pellet was re-suspended in 600 µl sterile LETs buffer (0.1 M LiCl, 0.01 M Na_2EDTA, 0.01 M Tris-HCl pH 7.5, 0.2% SDS) then transferred to 2 ml lysing matrix B tubes (MP Biomedicals, USA). Once transferred, the samples were bead beat in a FastPrep-24 5G for three cycles: 6 m s^{-1} for 40 s and 5 min incubation on ice, then further incubated to reach room temperature. The tubes were centrifuged at 13,000 rpm for 10 min, then 600 µl 125:24:1 Phenol Chloroform Isoamyl alcohol (PCI) pH 4.5 (Invitrogen, UK) was added. The samples were vortexed at ~14,000 rpm for 5 min then centrifuged for 5 min at 15,000 rpm, at 4 °C. The top layer of solution that had formed in each sample was transferred to sterile 2 ml RNase-free tubes (Sarstedt Ltd, Germany) and mixed with 1 volume 125:24:1 PCI (pH 4.5). The vortex, centrifugation and top layer transfer steps were repeated as decribed, then 1 volume 24:1 Chloroform Isoamyl alcohol (Sigma-Aldrich, UK) was added and samples were centrifuged for 5 min at 15,000 rpm, at room temperature. The top layer was transferred to another 2 ml RNase-free tube and 0.1 volume 3M $NaCH_3COO$ pH 5.2 and 1 volume 100% isoproponal (v/v) were added. The samples were mixed by inverting each tube ~six times then stored at -20 °C overnight.

2.20　RNA precipitation

The extracted RNA samples that had been stored at -20 °C overnight were defrosted on ice, then centrifuged for 15 min at 15,000 rpm. The supernatant was removed and the pellets were resuspended in 1 volume (~560 μl) 70% ethanol (v/v), then centrifuged at 4 °C for 15 min at 15,000 rpm. The supernatant was then removed and the pellets were dried by a flame for ~15 min. The dried pellets were resuspended in 50 μl RNase-free water (Invitrogen, UK) and incubated for 3 h on ice, then left to equilibriate to room temperature for 30 min. The concentration of precipitated RNA was determined as described in Method 2.21, then snap frozen and stored at -80 °C.

2.21　Determining RNA concentration

The concentration of RNA in each sample was determined using the Qubit™ RNA broad range (BR) Assay kit (Invitrogen, Netherlands) and Qubit® 2.0 Fluorometer. All reagents used were provided in the kit. The Qubit® RNA BR Reagent was diluted 1 in 200 in Qubit® RNA BR Buffer in a 15 ml falcon tube to produce the Qubit® working solution, to a total volume to ensure there was 200 μl per sample and standard (i.e. 200 μl x number of assay tubes). Subsequently, 190 μl Qubit® working solution was added to two individual Qubit® assay tubes (Invitrogen, USA) for standard 1 and standard 2, and then 10 μl of each Qubit® standard was added to the relevant tube and vortexed for ~2-3 s. Qubit® assay tubes were then prepared for each RNA sample, 199 μl Qubit® working solution was added then 1 μl of RNA sample. The samples were mixed by vortexing for ~2-3 s. All tubes (samples and standards) were incubated at room temperature for 2 min. The standards and samples were then read using a Qubit® 2.0 Fluorometer, to determine the RNA concentration of each RNA sample.

2.22　DNA removal from RNA samples

The precipitated, frozen RNA samples were defrosted on ice for deoxyribonucleic acid (DNA) removal. Samples that had a concentration above 200 μg ml^{-1} were diluted to less than 200 μg ml^{-1} using RNase-free water, to improve DNA removal success. Each sample was then transferred to sterile PCR tubes in volumes $\leq$ 50 μl, higher volumes were divided between multiple tubes. DNase I buffer (10X) (Invitrogen, Lithuania) was

added to each sample tube in a 9:1 ratio respectively (i.e. 46 µl sample and 9 µl buffer), then 2 µl DNase I (Invitrogen, Lithuania) was added. The tubes were incubated for 30 min at 37 °C then a further 2 µl DNase I was added and the incubation repeated. Another 2 µl DNase I was added and then the samples were incubated a third time for 30 min, at 37 °C. An equal volume of 100% ethanol (v/v) (~50 µl) was added and mixed to stop the reaction then samples were transferred to Zymo-Spin™ ICC columns (Direct-zol™ RNA MiniPrep Plus kit, Zymo Research, USA), with any separate high concentration samples combined in a single spin column. The samples were then centrifuged for 30 s at 13,000 rpm and the flow-through was discarded. The Direct-zol™ RNA MiniPrep Plus kit was used to clean up each RNA sample: 400 µl Direct-Zol RNA Prewash was added to each column and then the tubes were centrifuged for 30 s at 13,000 rpm and the flow-through discarded. This step was repeated then 700 µl RNA Wash Buffer was added and the samples centrifuged for 2 min at 13,000 rpm. The column was transferred to a sterile, RNase-free tube and 50 µl RNase-free water was added directly to the column matrix. Samples were incubated at 55 °C for 5 min then centrifuged for 30 s at 13,000 rpm to elute the RNA.

A 16s PCR (3 min at 95 °C; 25 x 1 min at 95 °C, 30 s at 50 °C, 1 min at 72 °C; 2 min at 72 °C) was performed to determine if any DNA was still present. Each reaction was made up of 1 µl sample, 1 µl forward primer, 1 µl reverse primer, 12.5 µl GoTaq® G2 green master mix (Promega, USA) and 9.5 µl nuclease-free water (Promega, USA), using the following primers (Merck, UK):

Forward: 5'-GGCTGGATCACCTCCTT

Reverse: 5'-TGCCAAGGCATCCACCG

Gel electrophoresis (0.7% agarose, 4 µl 1X SYBR® safe DNA gel stain) was run for 30 min at 120 v, using a 1 kb ladder (New England Biolabs, UK). For any samples that had detectable DNA, the entire DNA removal protocol was repeated. The final RNA concentration in each sample was confirmed using the Qubit™ RNA BR Assay kit (Method 2.21) and the samples were then snap frozen and stored at -80 °C until required.

2.23   RNA quality check and sequencing

The quality of the optimal RNA samples for sequencing was confirmed using the RNA 6000 Pico kit (Agilent Technologies, USA) and Agilent 2100 Bioanalyzer system.

Everything described was provided in the kit unless specified. The gel stock was prepared first; 550 μl RNA 6000 Pico gel matrix was added to a spin column and centrifuged at 4,000 rpm for 10 min. The spin column was discarded, and the gel filtered into the collection tube was divided into 65 μl aliquots (~8), each in 0.5 ml RNase-free microcentrifuge tubes. Any excess gel was stored at - 4 ℃ for 1 month. The RNA 6000 Pico dye concentrate was vortexed for 10 s then centrifuged for 30 s at 13,000 rpm, and 1 μl was added to a gel aliquot per RNA 6000 Pico chip used. The gel-dye mix was vortexed, left to reach room temperature whilst covered from light, then centrifuged at 14,000 rpm for 10 min.

Following preparation, the Bioanalyzer was cleaned using an electrode cleaner chip. The chip was slowly filled with 350 μl RNase-free water through one well, placed in the Agilent 2100 Bioanalyzer, and left for 5 min. The chip was removed and the lid was left open for ~30 s. The RNA 6000 Pico chip was placed in the chip priming station and 9 μl gel-dye mix was added into the bottom of the black well marked 'G'. The chip priming station was closed and the syringe pushed down from 1 ml and held for 30 s, then released. Once the syringe reached 0.3 ml, after ~5 s the syringe was pulled back to 1 ml and the chip removed from the chip priming station. Subsequently, 9 μl gel-dye mix was added to each of the two white wells marked 'G', then 9 μl RNA 6000 Pico conditioning solution was added to the well marked 'CS'. Finally, 5 μl RNA 6000 Pico marker was added to the well marked with a ladder and each of the sample wells, and 1 μl RNA ladder (Agilent RNA 6000 Pico Ladder; Agilent Technologies, Lithuania) was also added to the ladder well. RNA aliquots for testing (~5 μl) were denatured at 70 ℃ for 2 min then 1 μl was added to individual sample wells. For any sample wells where denatured RNA was not added, 1 μl RNase-free water was added. The chip was vortexed for 60 s at 2,400 rpm using an IKA vortex mixer then loaded into the Agilent 2100 Biolanalyzer. The 'Eukaryotic Total RNA Pico' assay using 2100 expert software was used to analyse the RNA samples. Once finished, the chip was removed and the electrode was cleaned again as described above, using the electrode cleaner chip.

Samples for RNA sequencing were then sent to Genewiz, where bacterial and mammalian rRNA depletion and Illumina library preparation for strand-specific RNA sequencing was performed. Genewiz then performed the sequencing on an Illumina NovaSeq. 150 bp paired-end run. Raw FASTQ files were then returned.

2.24   RNA sequencing data preparation

RNA sequencing reads in FASTQ format were quality checked using FastQC v0.11.8 (Andrews, 2018) before analysis and after each step of initial data preparation. All data preparation steps were performed using the cloud infrastructure for big data microbial bioinformatics (CLIMB) server. Trimmomatic v0.38 (Bolger et al., 2014) was used to trim reads, the minimum threshold for read length was set at 25 bp (Cornforth et al., 2018), then any residual bacterial rRNA and eukaryotic rRNA transcripts were filtered out using SortmeRNA v2.1b (Kopylova et al., 2012). Reads from EVPL model samples (lung-associated biofilm and surrounding SCFM) were aligned to the pig genome (*Sus scrofa*: NCBI, GCF_000003025.6) using HISAT2 v2.10 (Kim et al., 2019). Any reads that were mapped were removed using Seqtk v1.3-r106 (Li, 2015) and remaining reads and *in vitro* SCFM sample reads were then aligned to the *P. aeruginosa* UCBPP-PA14 genome (NCBI, GCF_000014625.1) using Burrows-Wheeler aligner (BWA) v0.7.17-r1188 with the maximal exact match (MEM) algorithm (Li, 2013).

Following read alignment all further analysis was performed in RStudio (Mac OS X 10.14.6 version 1.2.5042; R version 4.1.1) (Rstudio, www.rstudio.com). Reads that were mapped to coding sequences determined from the *P. aeruginosa* UCBPP-PA14 annotation sourced from Pseudomonas.com (Winsor et al., 2016) were counted using the function 'featureCounts' from the Rsubread v2.0.1 package (Liao et al., 2019). The count data was then normalised with the rlog Transformation function, part of the DESeq2 v1.26.0 package (Love et al., 2014). Principal component analysis (PCA) was performed on all genes in the analysis (5829) using the 'plotPCA' function from DESeq2 (Love et al., 2014) and 95% confidence ellipses were calculated and added to the plot using ggpubr v0.4.0 (Kassambara, 2020). A 3D PCA plot was produced using the plotly v4.9.4.1 package (Sievert, 2020) and ggplot2 v3.3.5 package (Wickham, 2016). Hierarchical clustering analysis was also performed and a heatmap produced, which visualised the pairwise correlation values from Pearson's correlation coefficient analysis for all sample comparisons using the 'HeatmapAnnotation' function from the ComplexHeatmap v2.2.0 package (Gu et al., 2016).

2.25 Differential expression analysis

All differential expression analysis was performed in RStudio (Mac OS X 10.14.6 version 1.2.5042; R version 4.1.1) (Rstudio, www.rstudio.com) and graphs were produced using the ggplot2 v3.3.5 package (Wickham, 2016) unless specified. Analysis of significant differentially expressed genes (DEGs) between different time points and growth environments in the RNA sequencing experiments was performed using DESeq2 v1.26.0 (Love et al., 2014). A gene was considered significant if the adjusted P value < 0.05 (Benjamini-Hochberg procedure to control false discovery rate) and the $\log_2$ fold change ($\log_2$FC) $\geq |1.5|$. MA plots were produced to show the mean of the normalized counts against the $\log_2$FC value for each contrast using 'plotMA' from the DESeq2 v1.26.0 package (Love et al., 2014). Venn diagrams were also produced to show the number of DEGs shared and unique between contrasts using the VennDiagram v1.7.0 package (Chen, 2021).

Kyoto encyclopedia of genes and genomes (KEGG) pathway enrichment analysis was then performed using 'enrichKEGG' from the clusterProfiler v3.14.3 (Yu et al., 2012) package and the *P. aeruginosa* UCBPP-PA14 KEGG code 'pau'. A KEGG pathway was considered to be significantly enriched using an adjusted P value < 0.05 (Benjamini-Hochberg). KEGG pathway maps were produced using 'pathview' from the clusterProfiler v3.14.3 package (Yu et al., 2012). Following this, gene ontology (GO) term enrichment analysis was carried out using the topGO v2.38.1 package (Alexa and Rahnenfuhrer, 2019) and a Fisher's exact test P value < 0.05. The significant differential expression of antimicrobial resistance genes was investigated based on the comprehensive antibiotic resistance database (CARD) predictions (Alcock et al., 2020) and sourced from Pseudomonas.com (Winsor et al., 2016). The gene names and functions described throughout this thesis were from Pseudomonas.com (Winsor et al., 2016). The genes associated with specific pathways, including quorum sensing (QS) and biofilm formation, were sourced from the KEGG database (Kanehisa and Goto, 2000; Kanehisa, 2019; Kanehisa et al., 2021).

2.26 Measurement of 3-oxo-C12-HSL and C4-HSL Production

All samples that the QS, acyl homoserine lactones (AHLs) signalling molecules were measured from (lung homogenate and *in vitro* cultures), were first filter sterilised using a 0.2 μm pore syringe filter into 2 ml Eppendorf tubes as described above (Method 2.5). Two *E. coli* bioreporter strains were used to measure 3-oxo-dodecanoyl homoserine lactone (3-oxo-C12-HSL) and N-butanoyl-L-homoserine lactone (C4-HSL): pSB1075 and pSB536 respectively (see Table 2.1). Each biosensor was grown in a sterile 50 ml falcon tube with 10 ml LB broth (Merck kGaA, Germany) overnight (pSB1075: + 10 μg ml^{-1} tetracycline, pSB536: + 50 μg ml^{-1} ampicillin), at 37 °C with 170 rpm shaking. Each overnight culture was diluted 1 in 100 in 15 ml LB broth (150 μl culture and 14.85 ml LB broth) with the relevant antibiotic concentration in a 50 ml falcon tube, then incubated for 3.5 h with 170 rpm shaking, at 37 °C.

Following incubation, the cultures were centrifuged for 2 min at 13,000 rpm then the supernatant was discarded and the pellet resuspended in 15 ml PBS. This step was repeated twice more and the final pellet was resuspended in 15 ml LB broth without antibiotics. The OD$_{600nm}$ was read and adjusted to 0.1 with LB broth; 100 μl culture was then added to each well of a 96 well flat, clear bottom, black tissue culture treated plate, with a lid. The sterile samples to be assayed were then diluted 1 in 10 in PBS and 100 μl was added to each well and mixed with the *E. coli* culture. Known concentration, standard wells were also set up, in triplicate repeat, using 3-oxo-C12-HSL (Sigma-Aldrich, India) and C4-HSL (Sigma-Aldrich, India) in place of the samples. A ten-fold series dilution in PBS was performed (see Method 2.18) in polystyrene 96 well plates for each standard to produce the following concentrations: 0.000001 nM, 0.00001 nM, 0.0001 nM, 0.001 nM, 0.01 nM, 0.1 nM and 1 nM. Three 0 nM (just PBS) controls were also set up; 100 μl of each standard and control were added to individual wells of the assay, black 96 well plate and mixed with the *E. coli* culture. The 96-well plate was incubated for 7.5 h at 37 °C in a Tecan Spark 10M multimode plate reader and the luminescence (RLU) and OD$_{600nm}$ were read every 15 min. The RLU/OD$_{600nm}$ was calculated at each time point, and the inflection time point was determined to create a standard curve (Figure 2.9). A standard curve was performed every time the assays were carried out. The final AHL concentrations were determined using the relevant standard curve equation from that experiment (see Figure

2.9).
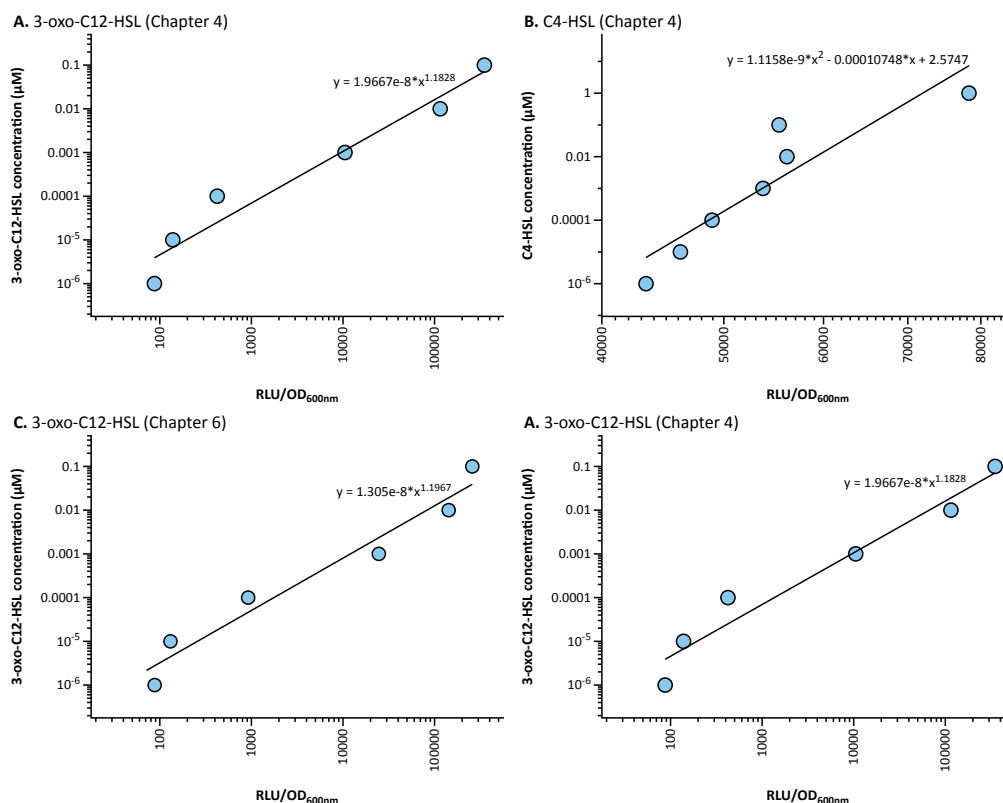
Figure 2.9: **Standard curves for 3-oxo-dodecanoyl homoserine lactone (3-oxo-C12-HSL) and N-butanoyl-L-homoserine lactone (C4-HSL) concentrations used to determine the concentrations in lung homogenate and *in vitro* samples.** The assay was performed using *Escherichia coli* bioreporter strains The standard curve was produced using luminescence (RLU) divided by OD_{600nm} at the inflection point for the known concentrations: 0 nM, 0.000001 nM, 0.00001 nM, 0.0001 nM, 0.001 nM, 0.01 nM, 0.1 nM and 1 nM. The data points represent the mean values for each concentration from three repeats, and the line shows the standard curve determined from all values. The equation of the line is shown, used to determine sample concentrations. All axes are $\log_{10}$ scale. **(A,B)** The standard curves used for the assays performed in chapter 4. **(C,D)** The standard curves used for the assays performed in chapter 6.

2.27   Cross streak inhibition assay

Cross streak inihibition assays were performed to determine whether a bacterial isolate (referred to as the inhibitor strain) inhibited the growth of a second isolate (referred to as the competitor strain). All LB agar plates used for these assays were made of 14 ml agar per plate. The inhibitor strains were grown in the EVPL model or SCFM as described above, for 48 h at 37 °C. The competitor strains were also grown in the EVPL model or SCFM 24 h later, and incubated for 48 h at 37 °C, so that they were ready 24 h after the inhibitor strains.

Following 48 h incubation of the inhibitor strains, 20 µl of either lung homogenate or *in vitro* SCFM culture for each strain was 'drip plated' vertically onto individual LB agar plates as shown in Figure 2.10, with the number of repeats required for each experiment. The plates were incubated at 37 °C overnight. Following this incubation the competitor strains had been incubated for 48 h, so 20 µl of competitor strain lung homogenate or *in vitro* SCFM culture was horizontally 'drip plated' 2 mm from the inhibitor strain on each plate (Figure 2.10). The plates were then incubated at 37 °C overnight and any inhbition of growth of the competitor strain was measured. The distance from the start of the competitor strain streak to the start of growth was measured using a ruler (mm).
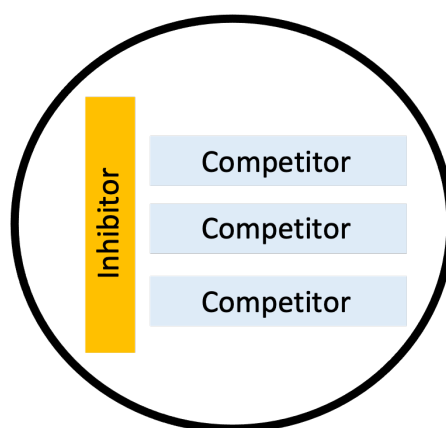
Figure 2.10: **The layout of the Luria-Bertani (LB) agar plates for cross streak inhibition assays**. The inhibitor strain was the bacterial isolate that was grown in the *ex vivo* pig lung (EVPL) model or synthetic cystic fibrosis sputum media (SCFM) *in vitro* for 48 h at 37 °C, then drip plated as shown (20 µl) and grown on the plate overnight at 37 °C. The competitor bacterial isolate was drip plated (20 µl) following the overnight incubation as shown, and the plate was further incubated overnight at 37 °C to determine any inhibition of competitor strain growth caused by the inhibitor strain. The competitor isolate was also grown in the EVPL model or SCFM for 48 h at 37 °C prior to plating. Also shown in chapter 6: Figure 6.2.

2.28   Graphs and statistical analysis

All graphs except those showing differential expression analysis, which is described in Method 2.25, were produced using DataGraph v4.7.1 on Mac OS Mojave v10.14.6 (Adalsteinsson and Schultz, 2020).

All statistical analyses were performed using RStudio (v1.2.1335 on Mac OS Mojave v10.14.6) (RStudio, https://www.rstudio.com), with $P < 0.05$ considered significant. Analysis of variance (ANOVA) tests were performed for comparisons of multiple groups where the data met the test assumptions and was normally distributed. If data was

not normally distributed, non-parametric Kruskal-Wallis tests were performed. Post-hoc comparisons, either a Tukey HSD test or Dunnett's test for ANOVAs where appropriate, or Dunn's test for Kruskal-Wallis tests, were performed using the multcomp v1.4.17 package (Hothorn et al., 2008). For comparisons with only two groups, Welch's two sample t-tests were performed. The statistical test performed for each analysis is specified where the data is presented.

2.29 Ethical statement

The pig lungs used as part of this work were sourced from local butchers and were obtained from animals slaughtered for human consumption, thus ethical approval was not required.

Chapter 3

Phenotypic characteristics of *Pseudomonas aeruginosa* biofilm infection in the *ex vivo* pig lung model

3.1 Introduction

P. aeruginosa adapts to form chronic biofilm infections that worsen disease outcomes in the lungs of people with CF, driven by the numerous environmental pressures that make these infections distinct from other infection contexts (Winstanley et al., 2016). These include, but are not limited to, nitrosative and oxidative stress, the inflammatory immune response, and the common occurence of infection with other microorganisms (Hogardt and Heesemann, 2011; Winstanley et al., 2016). Mutations in regulatory pathways have been shown to be positively selected for in the CF lung, including those involved in quorum sensing, motility, membrane modifications, biofilm, and antibiotic resistance (Dettman and Kassen, 2021). Hypermutable *P. aeruginosa* variants are frequently isolated from biofilm populations, which persist and display reduced virulence, proven to be key to survival (Cullen and McClean, 2015). However, during early acute infection *P. aeruginosa* produces a broad range of virulence factors and a biofilm is not yet established. This stage of infection is easier to treat but once the adaptation to chronic infection occurs, *P. aeruginosa* becomes almost impossible to eradicate (Cullen and McClean, 2015; Broder et al., 2016).

The virulence factors produced by *P. aeruginosa* in the CF lung include secreted proteases and the major siderophores PVD and PCH; each play a different role in

establishment and infection. Extracellular proteases are pivotal to invasion during initial infection, and *P. aeruginosa* produces a wide range including MucD, type IV protease, aminopeptidase, alkaline protease (AprA), *P. aeruginosa* small protease, large exoprotease A and the elastases LasA and LasB (Jurado-Martín et al., 2021). The quorum sensing transcriptional regulator LasR is involved in the regulation of acute infection associated virulence factor production. More specifically, LasR regulates production of AprA and LasB involved in immune evasion, host tissue damage, and *P. aeruginosa* cell proliferation; mutations in *lasR* are frequently seen during chronic infection. (Hennemann and Nguyen, 2021). This indicates that protease production is not positively selected for once a chronic biofilm infection is formed. The *lasR* mutants have also been shown to have a growth advantage using certain nitrogen and carbon sources, such as amino acids like phenylalanine (D'Argenio et al., 2007). Thus, loss of protease production may also be a result of selection for *lasR* mutants driven by nutrient availability. Alongside this, there is an overall loss of QS gene expression associated with the transition from acute to chronic infection lifestyle (Hogardt and Heesemann, 2011), which is linked to the reduction in virulence factor production, including proteases.

Similarly, there is increasing research to suggest that PVD and PCH are not essential during chronic infection. The formation of a chronic *P. aeruginosa* infection is associated with increased iron availability in the CF lung, as lung damage increases (Reid et al., 2007). A study using *ex vivo* airway mucus secretions found transposon mutants that could not produce PVD or PCH were able to survive. A novel iron uptake system was shown to be essential for *P. aeruginosa* growth in the airway mucus (Gi et al., 2015). It has also been proven that there is a significant decrease in production of PVD and PCH following the initial acute stages of CF infection. There is an accumulation of PVD mutants and it has been indicated that heme becomes the predominant iron source, thus heme uptake systems are utilised (Nguyen et al., 2014). Therefore PVD and PCH are likely only important for iron acquisition during acute infection, and *P. aeruginosa* uses other systems once a biofilm infection is established and there is increased iron availability.

Virulence is a key phenotype that characterises the different stages of *P. aeruginosa* infection in the CF lung, thus it was investigated in the EVPL model. Transposon insertion mutants for the following genes were grown in the model and the impact of loss of

gene function on virulence factor production was investigated: *gacA*, *vfr*, *sadR*, and *pqsR*. Each of these genes is implicated in virulence factor production or associated with the switch to chronic biofilm infection. Vfr is a cyclic adenosine monophosphate (cAMP)-dependent transcription factor that is involved in protease production and type 3 secretion. Disruption of *vfr* expression, such as common CF mutations in the anti-sigma factor *mucA* gene, blocks the production of invasive virulence factors such as proteases (Jones et al., 2010). The transcriptional regulator PqsR also plays a role in virulence factor gene expression, often known as MvfR: Multiple virulence factor regulator. The *Pseudomonas* quinolone signal (PQS) quorum sensing system activates *pqsR*, leading to the expression of multiple virulence factor genes including production of pyocyanin (Allegretta et al., 2017). PqsR has been shown to bind additional loci to play a pivotal role in quorum sensing regulation of infection and antibiotic tolerance (Maura et al., 2016).

P. aeruginosa also has more than 60 two component regulatory systems that control virulence and the switch in lifestyles from acute to chronic infection (Jimenez et al., 2012). SadR is the response regulator in one of these systems: SadARS, which is involved in biofilm maturation. The SadARS system is linked to repression of type 3 secretion, which is active during acute infection, and promotion of biofilm formation; mutants for *sadR* have been shown to cause a defect in the *P. aeruginosa* biofilm architecture (Gooderham and Hancock, 2009). However, the global activator of antibiotic and cyanide synthesis (GAC) system is arguably the most well studied of the *P. aeruginosa* two component systems. It is the predominant cause of the switch from acute to chronic infection in the CF lung, and is involved in interactions with the host tissue that often result in lung failure and increased mortality (Jimenez et al., 2012). GacA activity has also been linked to the regulation of biofilm maturation (Parkins et al., 2001), thus as well as investigating virulence factor production of *gacA*⁻ in the EVPL model, the biofilm formed was also studied. Figure 3.1 shows the signalling pathways involving the GAC system that switch the lifestyle of *P. aeruginosa* from acute to chronic biofilm infection in the CF lung (Jimenez et al., 2012; Bouillet et al., 2019).
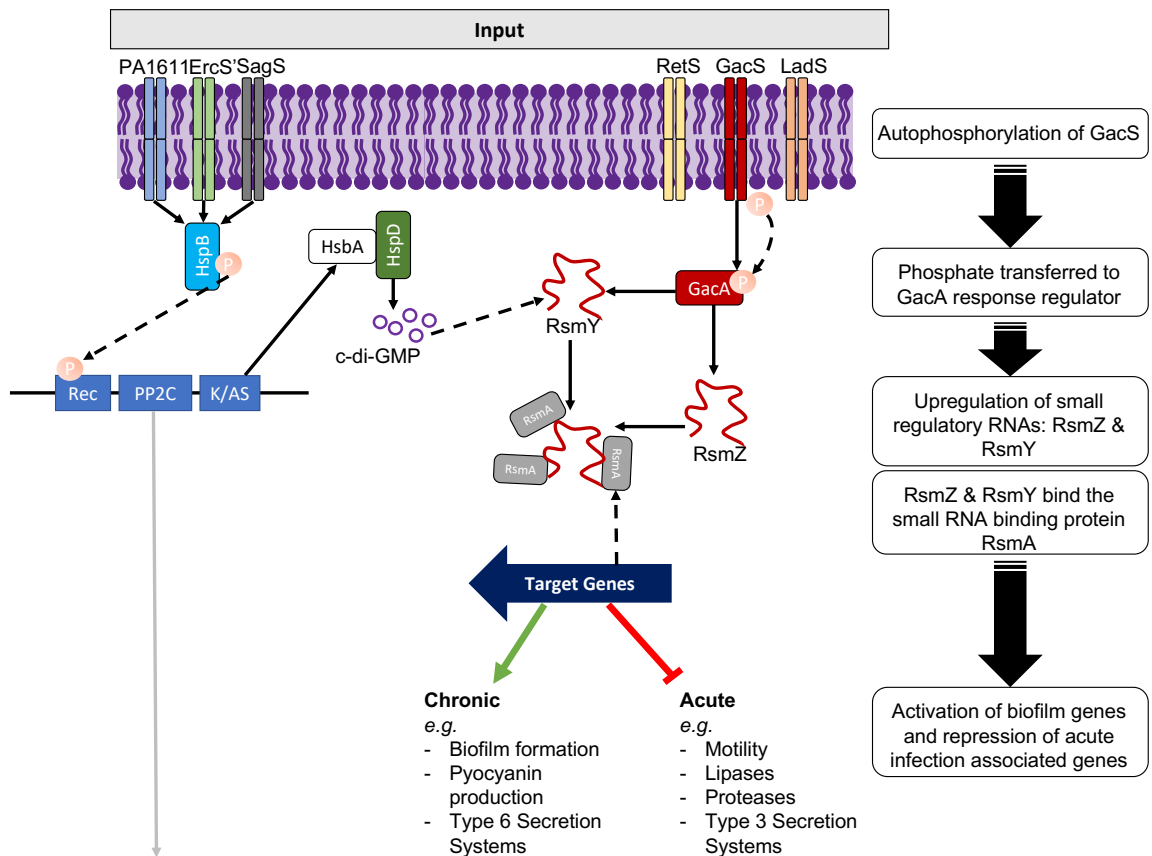
Figure 3.1: **Overview of the global activator of antibiotic and cyanide synthesis (GAC) system pathway known to drive the switch of *Pseudomonas aeruginosa* acute infection to chronic in the CF lung.** The steps of the GAC system pathway are outlined to the right of the diagram, however the secondary messenger cyclic diguanylate (c-di-GMP) is also able to upregulate RsmY. The figure was created based on information from Jimenez et al. (2012) and Bouillet et al. (2019).

The biofilm is made up of *P. aeruginosa* cells and a self-produced matrix of lipids, proteins, nucleic acids and polysaccharides (Flemming and Wingender, 2010). This stage of infection is so difficult to treat because this matrix provides protection from the immune response and causes increased antibiotic resistance (Høiby et al., 2010). Traditionally this stage of infection has been difficult to replicate *in vitro* so, research of *P. aeruginosa* persistence, virulence, and response to treatments during chronic infection is limited. The resistance phenotypes observed in *in vivo* biofilms differ from that seen *in vitro* (Müsken et al., 2017). Similarly, the structure of the biofilms grown in the lab is distinct from the biofilms seen in people with CF. Many aspects of chronic infection are dependent on the biofilm structure, particularly the pockets of dormant cells that affect quorum sensing and the nutrient gradients created (Høiby et al., 2010). As biofilm formation and structure is vital to the characteristics of *P. aeruginosa* chronic infection in the CF lung, it was investigated in the EVPL model and the impact on antibiotic resistance. As well as the impact of loss of *gacA* function, the biofilm

formed by a transposon mutant for *pelA* was also investigated. PelA is a periplasmic deacetylase and hydrolase enzyme involved in the production of the structural biofilm matrix polysaccharide Pel (Marmont et al., 2017). Pel is one of three exopolysaccharides produced by *P. aeruginosa* to form the biofilm matrix: Pel, Psl and alginate (Bjarnsholt et al., 2009). Pel has been shown to not only play a structural role in the biofilm but is also required for intercellular interaction and enhanced resistance to aminoglycosides (Colvin et al., 2011).

As detailed, the different stages of *P. aeruginosa* infection in the lungs of people with CF are characterised by changes in virulence factor production and the formation of a mature biofilm. Investigation of this in the EVPL model at two different time points (2 d and 7 d) was performed for *P. aeruginosa* PA14 and transposon insertion mutants for each of the genes discussed. Taking into account the role of each gene in the phenotypes observed in CF, the predictions in Table 3.1 were made for how each strain would behave in the EVPL model. It was shown that by 2 d, there were low levels of virulence factor production in the EVPL model that was maintained over 7 d, with little distinction between the mutants and wild type (WT). However, there were differences in the biofilm formed by the different mutants tested, and a mature biofilm established by the WT at 7 d. Thus indicating that the EVPL is a good model for the CF lung that drives *P. aeruginosa* into a chronic-like state of biofilm infection.

Table 3.1: **Predicted phenotypes for virulence factor production and biofilm formation of *Pseudomonas aeruginosa* PA14 transposon insertion mutants (Liberati et al., 2006a,b) compared with the wild type (WT) in the *ex vivo* pig lung model.** Based on the literature, as dicussed in the chapter introduction, in cystic fibrosis (CF) infection it is likely that loss of gene function will have the predicted phenotypes listed. The impact on biofilm was likely to affect antibiotic susceptibility so this was also tested for the mutants in th EVPL model. Those listed as not tested were not investigated for that phenotype as they were either not associated with changes compared to the WT (biofilm: *vfr*⁻, *pqsR*⁻; virulence: *pelA*⁻) or had similar effects to other genes so were not studied due to budget restrictions (biofilm: *sadR*⁻ likely similar to *gacA*⁻).

Transposon Mutant	Virulence compared with WT	Biofilm compared with WT
vfr⁻	Reduced production	*Not tested*
sadR⁻	No difference	*Not tested*
pqsR⁻	Reduced production	*Not tested*
gacA⁻	Increased production	Prevent biofilm maturation and increased antibiotic susceptibility
pelA⁻	*Not tested*	Unable to form biofilm and increased antibiotic susceptibility

3.2 Results

3.2.1 Growth of *P. aeruginosa* PA14 in the EVPL model and tissue immune response

To establish *P. aeruginosa* in the EVPL model and understand interaction with the pig lung bronchiolar tissue prior to addressing research hypotheses, *P. aeruginosa* PA14 growth over 7 d and any residual immune cells in the tissue were studied. These experiments were performed on three replicate tissue pieces per condition (i.e. time point, infection), from each of two independent pig lungs.

P. aeruginosa PA14 grew in the EVPL model and the bacterial load was maintained for 7 d.

Tissue pieces were infected with *P. aeruginosa* PA14 and incubated at 37 °C, then homogenised each day to recover the bacteria and determine CFU lung^{-1} (Figure 3.2). Uninfected tissue pieces were sampled as negative controls for PA14 growth, and confirmed that there was no *P. aeruginosa* contamination of the EVPL tissue or surrounding SCFM. Endogenous species growth was observed, but they were not detectable from *P. aeruginosa* PA14 infected tissue pieces.

The CFU ml^{-1} at infection was first calculated to determine the bacterial load at initial infection (0 d: Figure 3.2). Overall, a significant difference in CFU between time points was found (ANOVA: $F_{7,37}$ = 11.54, P < 0.01), the effect of lung was not included in the statistical analysis as this was not a factor for initial infection. Further post-hoc analysis showed that this difference was between infection (0 d) and every other time point (Tukey HSD: all P < 0.01). There was an increase in CFU from the time of infection (0 d) to 1 d of approximately 3 log$_{10}$ (Figure 3.2). A CFU lung^{-1} between 10^8 and 10^9 was then maintained from 1 d to 7 d (Figure 3.2) and no further significant differences were found. These results demonstrated that *P. aeruginosa* PA14 grows in the model, associated with the EVPL tissue, and the bacterial load of culturable *P. aeruginosa* is maintained for at least 7 d. The CFU numbers were also consistent with the *P. aeruginosa* CFU recovered from chronic CF lung infection, which is typically 10^8 - 10^{10} ml^{-1} in CF sputum (Palmer et al., 2005).
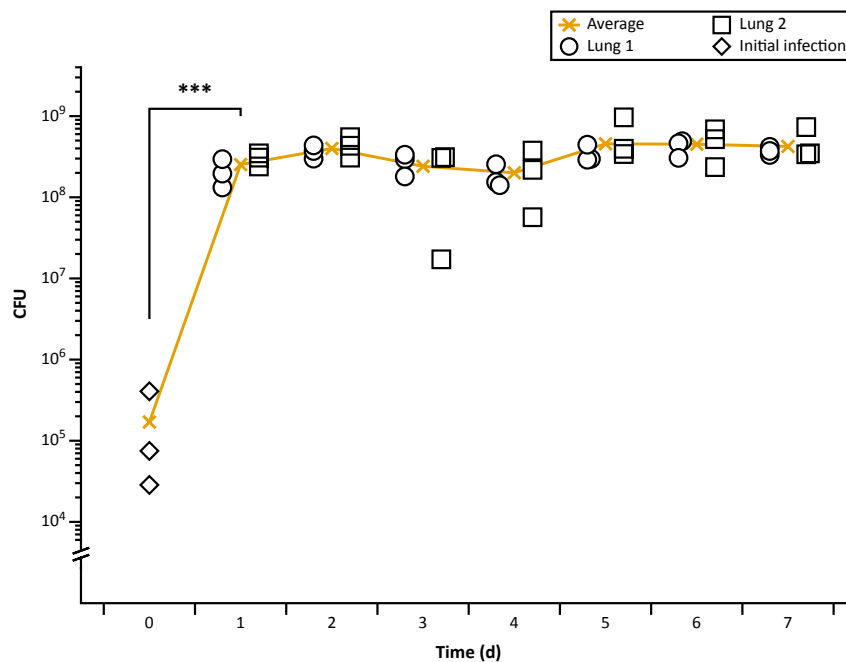
Figure 3.2: ***Pseudomonas aeruginosa* PA14 colony forming units (CFU) lung^{-1} in the *ex vivo* pig lung (EVPL) model every day for 7 d.** Destructive sampling was performed each day of three tissue pieces from each of two independent lungs infected with *P. aeruginosa* PA14 and the CFU lung^{-1} determined. Uninfected tissue pieces were sampled every day as a negative control and no PA14 growth was found. Each lung is represented by different shaped data points and the mean at each time point, across both lungs, is shown by the orange crosses and orange line (see key). Day 0 was the representative starting inoculum; a colony was taken using a 29G hypodermic needle and 'dipped' in 1 ml synthetic cystic fibrosis sputum media and the CFU ml^{-1} determined for three repeats. Asterisks represent a significant difference ('***' = $P < 0.001$) between time points. The y axis is $\log_{10}$ scale.

Interleukin-8 production was not consistently found in the EVPL tissue and did not increase with *P. aeruginosa* PA14 infection.

To provide preliminary insight into the potential residual immune repsonse in the EVPL bronchiolar tissue used in the model, the concentration of interleukin-8 (IL-8) in samples was measured using a porcine IL-8 ELISA. Uninfected EVPL tissue and *P. aeruginosa* PA14 infected tissue pieces 6 h, 18 h, 24 h and 48 h post incubation at 37 °C, after homogenisation and filter sterilisation, were tested. The aim was to identify if any residual immune response from the pig lung tissue was detectable, if the amount changed over time, and how this was affected by *P. aeruginosa* PA14 infection (Figure 3.3).
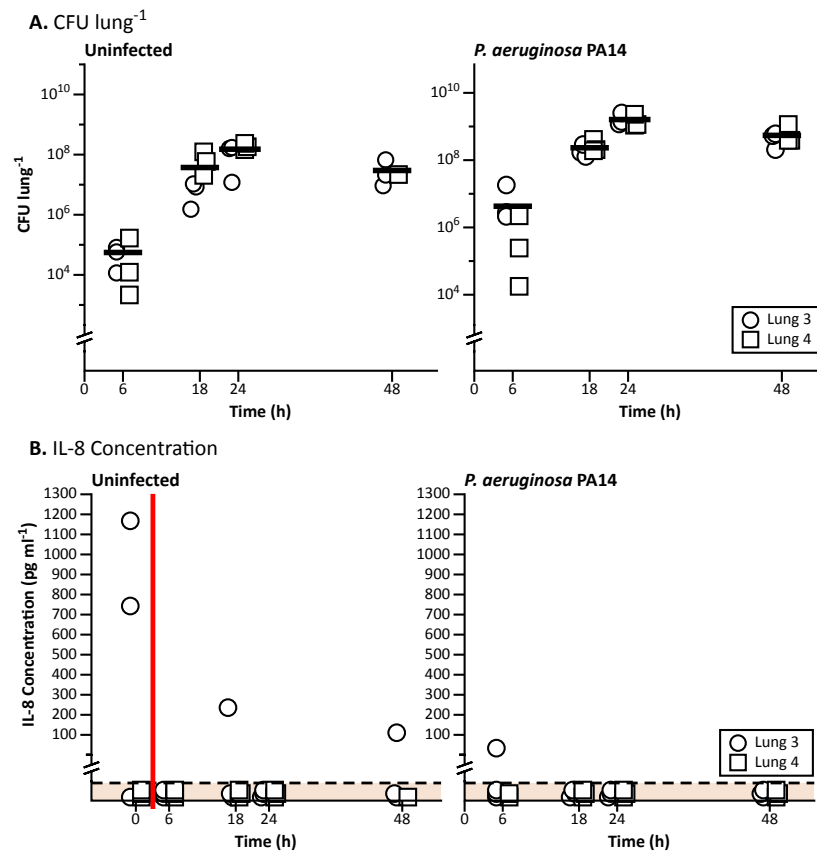
Figure 3.3: **Interleukin-8 (IL-8) production in *ex vivo* pig lung tissue infected with *Pseudomonas aeruginosa* PA14 or uninfected over 48 h.** Three pieces of tissue from each of two independent lungs per infection (uninfected or *P. aeruginosa* PA14) were sampled at 6 h, 18 h, 24 h and 48 h following incubation at 37 °C. Samples from each lung are represented by different data point shapes (see key). **(A)** Colony forming units (CFU) lung^{-1} for each sample. The uninfected CFU lung^{-1} was the endogenous species growth that was not observed for PA14 infected samples. No *P. aeruginosa* growth was seen in uninfected samples. The y-axes are a $\log_{10}$ scale and the horizontal lines represent the mean across both lungs at each time point. **(B)** IL-8 concentration (pg ml^{-1}) measured using a porcine ELISA kit. Data points below the horizontal dashed line did not have any detectable IL-8. The data points to the left of the red vertical line on the uninfected graph (0 h) are the samples that were assayed following dissection. The tissue pieces were not infected or incubated at 37 °C, and were tested to determine the IL-8 concentration from the pig bronchiolar tissue before experiments.

As shown in Figure 3.3A, the CFU lung^{-1} from each sample was also determined. The growth in uninfected tissue pieces was pig lung endogenous bacterial species that were not *P. aeruginosa* and did not appear to grow on PA14 infected tissue pieces. The IL-8 concentration from the pig tissue pieces prior to any experiments was first determined (Figure 3.3: Uninfected IL-8 concentration, 0 h). IL-8 was present in two EVPL samples from lung 3 at the time of dissection (1167.73 pg ml^{-1} and 742.81 pg ml^{-1}). One uninfected sample from lung 3, at each of 18 h and 48 h was also found to contain IL-8 (235.79 pg ml^{-1} and 110.61 pg ml^{-1} respectively), showing the amount decreased over time. No IL-8 was detected in any samples from lung 4. One sample from lung 3 infected with *P. aeruginosa*

PA14 was found to have 33.61 pg ml^{-1} IL-8 at 6 h but no other infected tissue pieces did (Figure 3.3). The presence of IL-8 was dependent on the lung and variable between tissue pieces. When IL-8 was present it was only in low concentrations and infection with *P. aeruginosa* PA14 reduced the amount. Following 6 h, no IL-8 was measured in PA14 infected samples.

3.2.2   *P. aeruginosa* PA14 virulence in the EVPL model

Following preliminary experiments confirming *P. aeruginosa* PA14 growth in the EVPL model, virulence and its regulation were investigated. Phenotypic assays for different virulence factors were performed on the PA14 WT and a biobank of transposon mutants for genes associated with virulence. Transposon mutants for the following genes were used: *gacA*, *vfr*, *sadR* and *pqsR*, to determine the role of each gene in *P. aeruginosa* virulence in the model. Experiments were performed at 2 d and 7 d post infection on five tissue pieces from each of three independent lungs, per condition.

Bacterial load of virulence associated transposon mutants in the EVPL model was comparable to the WT at 2 days and 7 days, but loss of *gacA* function caused visual differences in infection at 7 days.

Images were taken of EVPL tissue pieces infected with WT *P. aeruginosa* PA14, the virulence associated transposon mutants and uninfected tissue at 7 d (Figure 3.4). At 2 d there was no visible difference between PA14 strains in the model. The *gacA* transposon mutant appeared to produce an orange/yellow pigment at 7 d in all three lungs. This was distinct from the tissue infected with the WT and other strains, which appeared to produce a blue/green pigment (Figure 3.4). The *P. aeruginosa* blue pigment is known to be caused by production of the exotoxin pyocyanin, whereas orange/yellow pigment is associated with siderophore production (DeBritto et al., 2020). Initial visual observations thus indicated that loss of *gacA* function had an effect on virulence factor production compared with the WT.
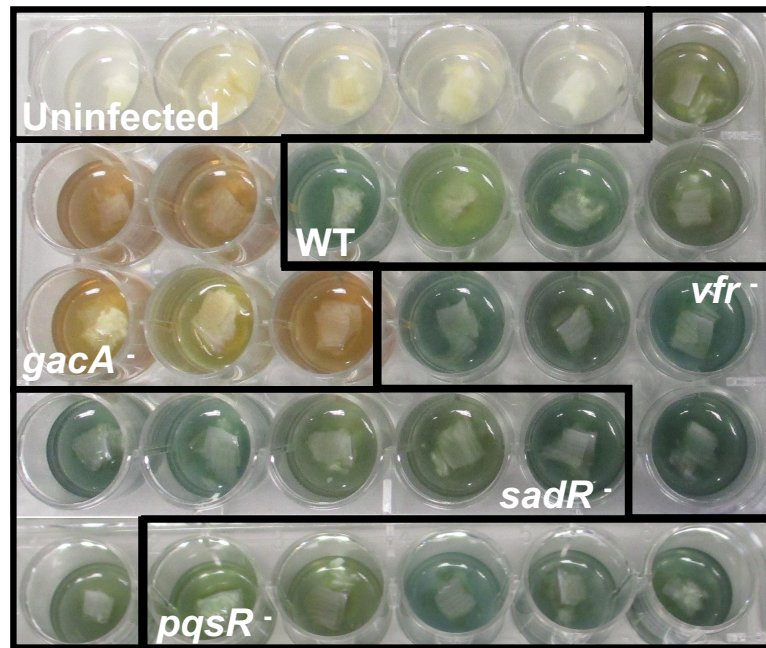
Figure 3.4: **Photographs of *ex vivo* pig lung tissue pieces infected with *Pseudomonas aeruginosa* PA14 wild type (WT) and virulence associated transposon mutants (Liberati et al., 2006a,b) following incubation at 37 °C for 7 d.** Tissue pieces are surrounded by 500 µl synthetic cystic fibrosis sputum media. The uninfected tissue was used as a negative control and showed no signs of *P. aeruginosa* growth. There are five replicates shown from one lung for each infection. The images were taken prior to homogenisation.

CFU lung^{-1} was then determined (Figure 3.5), to investigate any differences in bacterial load between the WT and transposon mutants. At 2 d (Figure 3.5A), a significant difference in CFU lung^{-1} was found between strains (ANOVA: strain $F_{4,60}$ = 7.22, *P* < 0.01, lung $F_{2,60}$ = 1.10, *P* = 0.34, interaction $F_{8,60}$ = 1.68, *P* = 0.12). There was no significant difference in lungs or the interaction between lung and strain, thus differences in CFU were not dependent on the lung tested. A post-hoc Dunnett's test showed the CFU lung^{-1} of *vfr*$^-$ (*P* < 0.01), *sadR*$^-$ (*P* = 0.01) and *pqsR*$^-$ (*P* = 0.03) was significantly less than the WT. At 7 d there was an increase in CFU lung^{-1} compared with 2 d for each strain (Figure 3.5B). There was also a significant difference in CFU lung^{-1} between strains (ANOVA: strain $F_{4,60}$ = 10.30, *P* < 0.01, lung $F_{2,60}$ = 3.43, *P* = 0.04, interaction $F_{8,60}$ = 2.30, *P* = 0.03). A post-hoc Dunnett's test showed that there was significantly more CFU lung^{-1} of *gacA*$^-$ than the WT (*P* < 0.01) however the interaction between strains and lung was significant suggesting that this may have been a result of lung variation rather than the mutation. Figure 3.5 shows that all CFU lung^{-1} values for the transposon mutants, at both time points, were within a 1 log$_{10}$ range of the WT. This indicates that although statistically significant, these differences were not likely of biological importance as all strains were within the expected range of *P. aeruginosa* bacterial load variability in CF (10^8 - 10^{10} ml^{-1}).
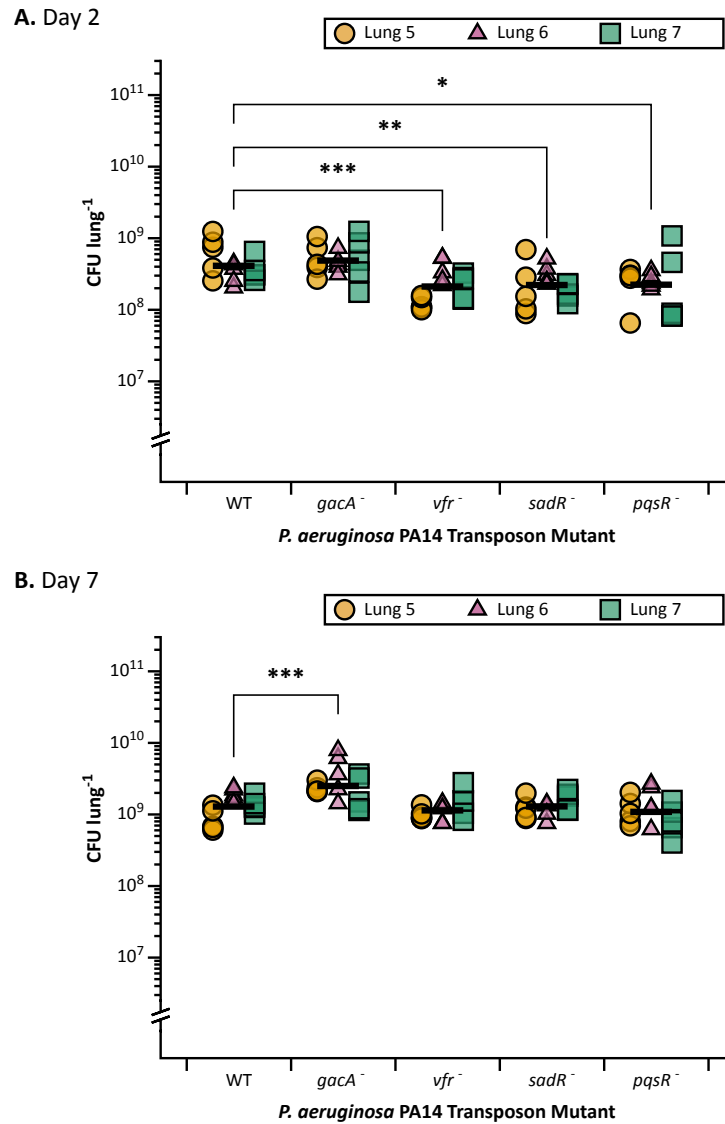
Figure 3.5: **Colony forming units (CFU) lung^{-1} of *Pseudomonas aeruginosa* PA14 wild type (WT) and virulence associated transposon mutants (Liberati et al., 2006a,b)**. The CFU lung^{-1} was calculated from five pieces of tissue from each of three independent pig lungs per infection strain, shown by individual data points. Each lung is represented by different data point shapes and colours (see key) and the asterisks represent a significant difference ('***' = $P < 0.001$, '**' = $P < 0.01$, '*' = $P < 0.05$). The horiztonal lines show the mean and the y axes are log$_{10}$ scale. **(A)** CFU lung^{-1} after 2 d incubation at 37 °C. **(B)** CFU lung^{-1} after 7 d incubation at 37 °C.

The *gacA* transposon mutant infected EVPL tissue pieces did not have significant amounts of protease, unlike the WT and other mutants, compared with uninfected tissue.

The lung homogenate samples from which CFU lung^{-1} was determined (Figure 3.5) were filter sterilised and the total protease was measured. The aim was to investigate the amount of extracellular proteases produced by *P. aeruginosa* PA14 and the transposon mutants in the EVPL model. Total protease in each sample was calculated equivalent to

known proteinase K concentrations, using an azocasein assay. Figure 3.6 shows that all lung samples had less than 20 µg protease, which was much lower than previous work using the EVPL model (50 - 300 µg) (Harrison et al., 2014). However the previous work used alveolar tissue in contrast with the bronchiolar tissue used in this work, which may account for the difference.
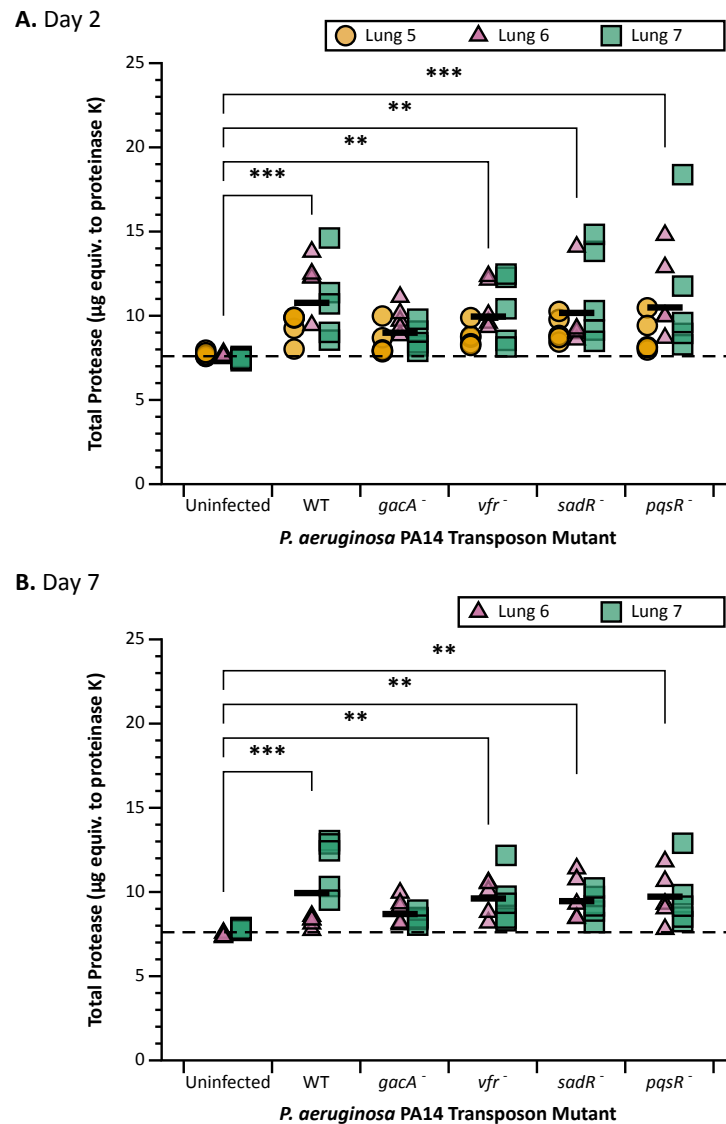
Figure 3.6: **Total protease (µg) euivalent to proteinase K activity in uninfected *ex vivo* pig lung (EVPL) tissue samples, and *ex vivo* pig lung tissue infected with *Pseudomonas* aeruginosa PA14 wild type (WT) and virulence associated transposon mutants (Liberati et al., 2006a,b).** The total protease was measured in five tissue pieces from each of three independent lungs per infection strain/uninfected tissue, shown by individual data points. The lungs are represented by different data point shapes and colours (see key) and the asterisks represent significant differences ('***' = $P < 0.001$, '**' = $P < 0.01$). The horiztonal, block lines how the mean and the dashed horizontal line is the mean total protease value for the uninfected tissue at that time point. **(A)** Total protease (µg) after 2 d incubation at 37 °C. **(B)** Total protease (µg) after 7 d incubation at 37 °C. Lung 5 was removed from this time point as it was an outlier.

As shown in Figure 3.6, at both 2 d and 7 d there were proteases in the uninfected

samples (mean: 2.76 µg and 2.59 µg respectively), which indicated that the EVPL bronchiolar tissue produced proteases. The mean amount of protease in uninfected tissue samples was calculated at each time point to determine an estimate for the amount of protease that may have been from the lung tissue rather than *P. aeruginosa* (Figure 3.6). ANOVA analysis showed a significant difference in total protease between strains at 2 d (strain $F_{5,72}$ = 6.68, $P < 0.01$, lung $F_{2,72}$ = 6.27, $P < 0.01$, interaction $F_{10,72}$ = 0.85, P = 0.58). Post-hoc Tukey HSD analysis showed there was no significant difference between *P. aeruginosa* PA14 WT and any of the transposon mutants at 2 d, however there were significant differences compared with the uninfected tissue (Figure 3.6A). There was significantly more protease than the uninfected tissue in the WT ($P < 0.01$), *vfr⁻* (P = 0.01), *sadR⁻* ($P < 0.01$) and *pqsR⁻* ($P < 0.01$) samples. There was no significant difference between uninfected tissue and *gacA⁻* (P = 0.27). Figure 3.6A shows that the mean total protease produced by *gacA⁻* was lower than the WT (8.99 µg and 10.77 µg respectively).

At 7 d lung 5 was considered an outlier as no protease was detected, so the data was removed from the analysis (Figure 3.6B). This was considered an experimental error as the EVPL tissue was found to have residual proteases without infection, so samples with no proteolytic activity were unlikely. As found at 2 d, there was a significant difference in total protease between infection conditions at 7 d (strain $F_{5,48}$ = 5.98, $P < 0.01$, lung $F_{1,48}$ = 2.77, P = 0.10, interaction $F_{5,48}$ = 4.20, $P < 0.01$). There were similarly no significant differences in total protease between the WT and any of the transposon mutants, and all mutants except *gacA⁻* appeared to produce significantly more protease than the tissue alone (WT $P < 0.01$, *vfr⁻* $P < 0.01$, *sadR⁻* P = 0.01, *pqsR⁻* $P < 0.01$ and *gacA⁻* P = 0.29). However the interaction between strains and lung was significant at this time, indicating that these differences may have been a result of lung to lung variation. The data shows that there was more total protease in the WT samples from lung 7 than the uninfected tissue and *gacA⁻*, but this was not seen in lung 6 (Figure 3.6B). Therefore, it could not be concluded whether there were any differences in total protease between any of the transposon mutants and the WT, or infected samples compared with uninfected at 7 d.

There was no difference in PVD or PCH production between *P. aeruginosa* PA14 WT and the virulence associated transposon mutants.

The production of two siderophores was also investigated, measured by fluorescence, at 2 d and 7 d. PVD is known to emit fluorescence at 460 nm when excited at 400 nm. Uninfected tissue samples were measured to determine whether fluorescence caused by *P. aeruginosa* PVD could be detected. A mean increase of 15,851.1 RFU at 2 d and 10,556.5 RFU at 7 d was observed in the WT samples compared with uninfected tissue samples (Figure 3.7). Both were found to be significant differences (T-test 2 d $t_{14.01}$ = 4.29, P < 0.01; 7 d $t_{16.92}$ = 3.52, P < 0.01). This confirmed that the assay measured PVD associated fluorescence, and not just fluorescence caused by any lung tissue or media that may have been present in the homogenate.

Comparisons were then made between the fluorescence in the PVD associated wavelength of WT samples and the virulence associated transposon mutants. Figure 3.7 shows that there was variability between repeats for each strain, at both time points, and some samples were above or below the detection threshold. At 2 d, there was no obvious difference between any of the strains (Figure 3.7A). Although a significant difference was found between the strains overall (ANOVA strain $F_{4,56}$ = 8.46, P < 0.01, lung $F_{2,56}$ = 24.79, P < 0.01, interaction $F_{8,56}$ = 2.02, P = 0.06), a post-hoc Dunnett's test showed there was no significant differences between the WT and any of the mutants (*gacA*[-] P = 0.15, *vfr*[-] P = 0.97, *sadR*[-] P = 1.00, *pqsR*[-] P = 0.49). There was also no obvious differences between the strains at 7 d and this was confirmed with ANOVA finding no significant difference in fluoresence (strain $F_{4,58}$ = 1.49, P = 0.22, lung $F_{2,58}$ = 7.37, P < 0.01, interaction $F_{8,58}$ = 0.76, P = 0.64). These results suggest that the loss of function of any of these genes did not have an effect on *P. aeruginosa* PA14 PVD production in the EVPL model at 2 d or 7 d.
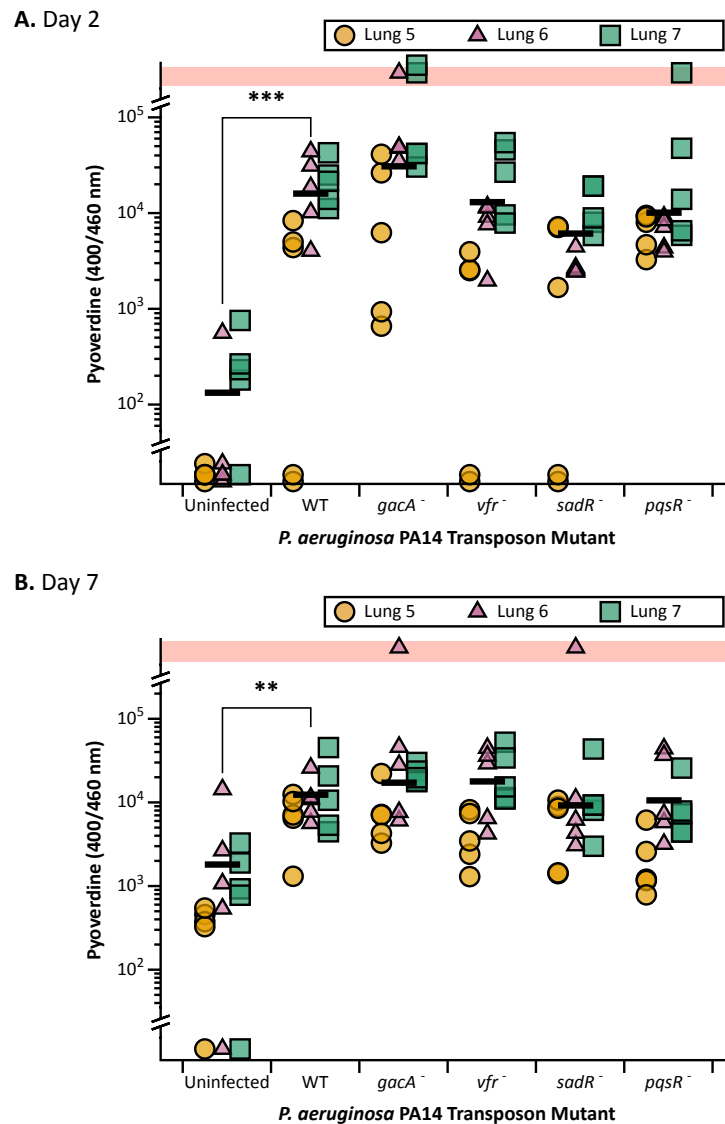
Figure 3.7: **Pyoverdine (PVD) measured as fluorescence (excitation 400 nm, emission 460 nm) from *ex vivo* pig lung (EVPL) sterile homogenate, from tissue pieces infected with *Pseudomonas aeruginosa* PA14 wild type (WT) and virulence associated transposon mutants (Liberati et al., 2006a,b).** The fluorescence in the PVD wavelength was measured from sterile lung homogenate samples, diluted 1 in 5 in PBS, from five tissue pieces from each of three independent lungs per infection strain. Uninfected tissue samples were also measured and there was significantly less fluorescence emitted compared with WT samples (T-test 2 d $t_{14.01} = 4.29$, $P < 0.01$; 7 d $t_{16.92} = 3.52$, $P < 0.01$) ('***' = $P < 0.001$, '**' = $P < 0.01$). The lungs are represented by different data point shapes and colours (see key). The horizontal lines show the mean and the red, horizontal block at the top of each graph shows samples that were above the detection threshold. Data points below the y axis break were below the detection threshold. The y axes are a $\log_{10}$ scale. **(A)** PVD fluorescence (RFU) after 2 d incubation at 37 °C. A post-hoc Dunnett's test found no significant differences between any of the mutants and WT. **(B)** PVD fluorescence (RFU) after 7 d incubation at 37 °C. ANOVA found no significant difference between strains.

PCH was then measured, known to emit fluorescence at 430 nm when excited at 350 nm. The same patterns were observed as for PVD (Figure 3.8). Initially the fluoresecence of uninfected tissue samples was compared with *P. aeruginosa* PA14 samples. There was

a mean increase of 17,946.43 RFU in the WT samples at 2 d compared with uninfected tissue, and 9,986.11 RFU increase at 7 d (Figure 3.8). Both of these differences were found to be significant (T-test 2 d $t_{17.29}$ = 4.40, P < 0.01; 7 d $t_{23.61}$ = 2.52, P = 0.02), hence the assay was valid to detect difference in $P.$ $aeruginosa$ PCH associated fluorescence between the WT and transposon mutants in the EVPL model samples.

There were no obvious differences in PCH fluorescence between WT samples and each of the virulence associated transposon mutants at both time points (Figure 3.8). ANOVA did find a significant difference in the fluorescence between the strains at 2 d (strain $F_{4,54}$ = 7.93, P < 0.01, lung $F_{2,54}$ = 36.71, P < 0.01, interaction $F_{8,54}$ = 1.68, P = 0.12) but post-hoc analysis showed no significant differences between the WT and any of the mutants (Dunnett's test $gacA^-$ P = 0.21, vfr^- P = 1.00, $sadR^-$ P = 0.99, $pqsR^-$ P =0.85). At 7 d, no significant difference in fluorescence between strains was found (ANOVA strain $F_{4,55}$ = 1.07, P = 0.38, lung $F_{2,55}$ = 39.47, P < 0.01, interaction $F_{8,55}$ = 0.49, P = 0.86). Therefore the loss of function of each gene also did not have an effect on $P.$ $aeruginosa$ PA14 PCH production at either time point.
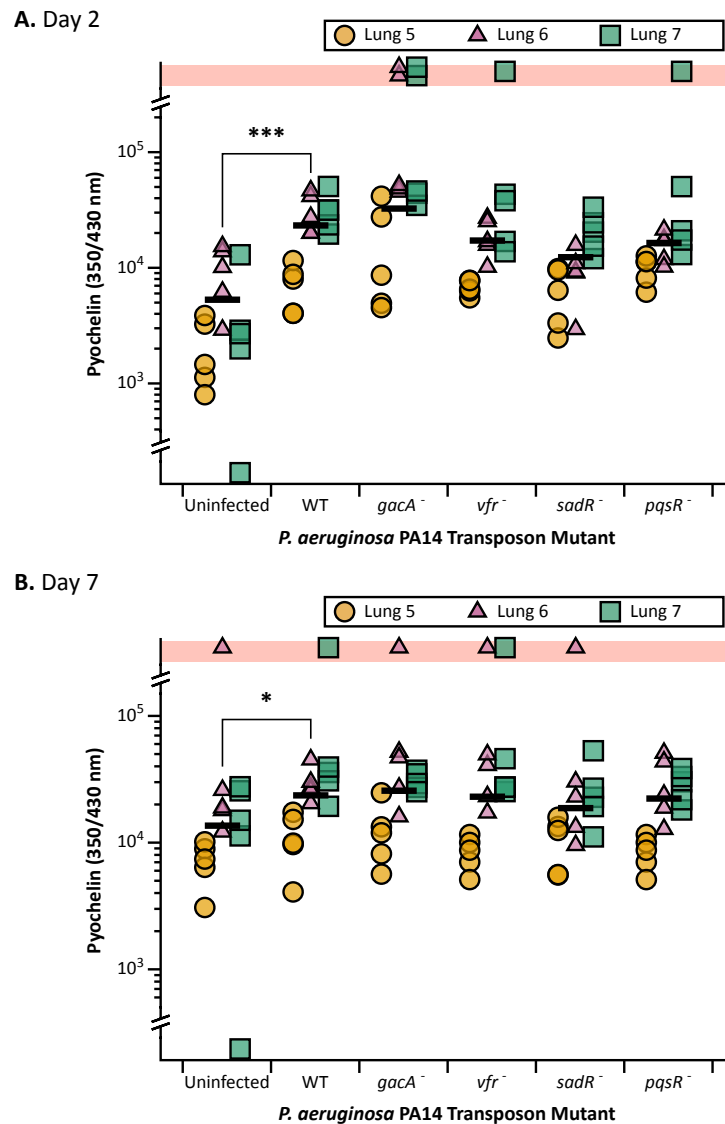
Figure 3.8: **Pyochelin (PCH) measured as fluorescence (excitation 350 nm, emission 430 nm) from *ex vivo* pig lung (EVPL) sterile homogenate, from tissue pieces infected with *Pseudomonas aeruginosa* PA14 wild type (WT) and virulence associated transposon mutants (Liberati et al., 2006a,b).** The fluorescence in the PCH wavelength was measured from sterile lung homogenate samples, diluted 1 in 5 in PBS, from five tissue pieces from each of three independent lungs per infection strain. Uninfected tissue samples were also measured and there was significantly less fluorescence emitted compared with WT samples (T-test 2 d $t_{17.29}$ = 4.40, P < 0.01; 7 d $t_{23.61}$ = 2.52, P = 0.02) ('*' = P < 0.05). The lungs are represented by different data point shapes and colours (see key). The horizontal lines show the mean and the red, horizontal block at the top of each graph shows samples that were above the detection threshold. Data points below the y axis break were below the detection threshold. The y axes are a $\log_{10}$ scale. **(A)** PCH fluorescence (RFU) after 2 d incubation at 37 °C. A post-hoc Dunnett's test found no significant differences between any of the mutants and WT. **(B)** PCH fluorescence (RFU) after 7 d incubation at 37 °C. ANOVA found no significant difference between strains.

3.2.3   *P. aeruginosa* PA14 biofilm formation in the EVPL model

P. aeruginosa PA14 biofilm formation on the EVPL tissue was then investigated. Similar to the study of virulence, the WT and two transposon insertion mutants for genes associated with biofilm infection - either directly (*pelA*) or via regulatory pathways (*gacA*) - were grown in the EVPL model for 2 d and 7 d.

Bacterial load of biofilm associated *P. aeruginosa* PA14 transposon mutants in the EVPL model was not distinctive from the WT but *gacA*⁻ was visibly different at 7 days.

Five pig lung bronchiolar tissue pieces from each of three independent lungs were infected with each strain for 2 d and 7 d. Five uninfected tissue pieces were also included from each lung per time point, as negative controls for *P. aeruginosa* growth. There were no visible differences observed between the strains at 2 d in the EVPL model. However at 7 d, *gacA*⁻ was lacking the blue pigment, associated with pyocyanin production, that was seen for the WT and *pelA*⁻ (Figure 3.9). This was consistent with observations of the *gacA* mutant in the model whilst investigating virulence (Figure 3.4).
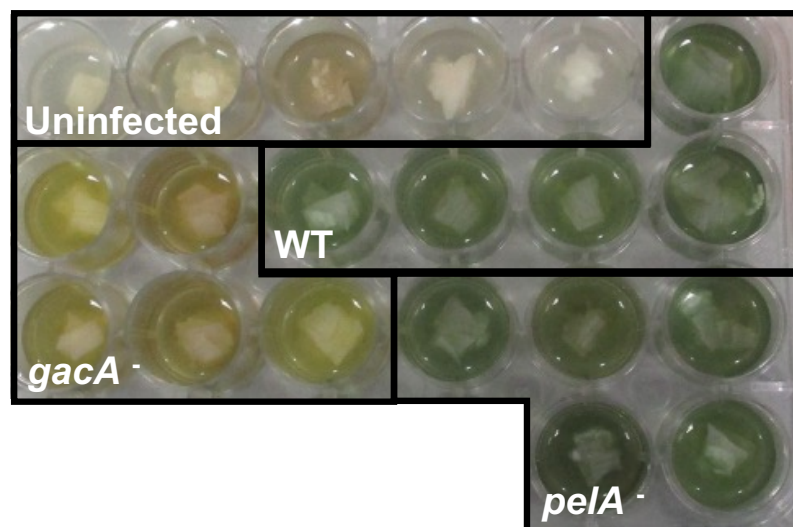
Figure 3.9: **Photographs of *ex vivo* pig lung (EVPL) tissue pieces infected with *Pseudomonas aeruginosa* PA14 wild type (WT) and biofilm associated transposon mutants (Liberati et al., 2006a,b), following incubation at 37 °C for 7 d.** Uninfected tissue was used as a negative control and showed no *P. aeruginosa* growth. There are five replicates shown from one lung per infection. Photos were taken prior to bacterial recovery.

The bacteria were recovered from the EVPL tissue associated biofilm at 2 d and 7 d, to calculate the CFU lung⁻¹ (Figure 3.10). ANOVA found a significant difference between the strains at 2 d (strain $F_{2,36}$ = 13.08, P < 0.01, lung $F_{2,36}$ = 11.89, P < 0.01, interaction $F_{4,36}$ = 1.82, P = 0.15) and the interaction between lung and strain was not significant. A post hoc

Dunnett's test comparing the mutants with the WT found a significant difference in the CFU lung^{-1} for *gacA$^-$* ($P < 0.01$) and *pelA$^-$* ($P = 0.01$) (Figure 3.10A). A significant difference between strains was also observed at 7 d (ANOVA strain $F_{2,36} = 9.28$, $P < 0.01$, lung $F_{2,36} = 59.40$, $P < 0.01$, interaction $F_{4,36} = 1.76$, $P = 0.16$). However, the only difference from the WT was *gacA$^-$* ($P = 0.04$) (Figure 3.10B). Consistent with the virulence associated transposon mutants' growth (Figure 3.10), these differences were within 1 log$_{10}$ at both time points. It was more likely that these difference were comparable to patient to patient variation seen clinically (Palmer et al., 2005), rather than growth differences caused by mutations.
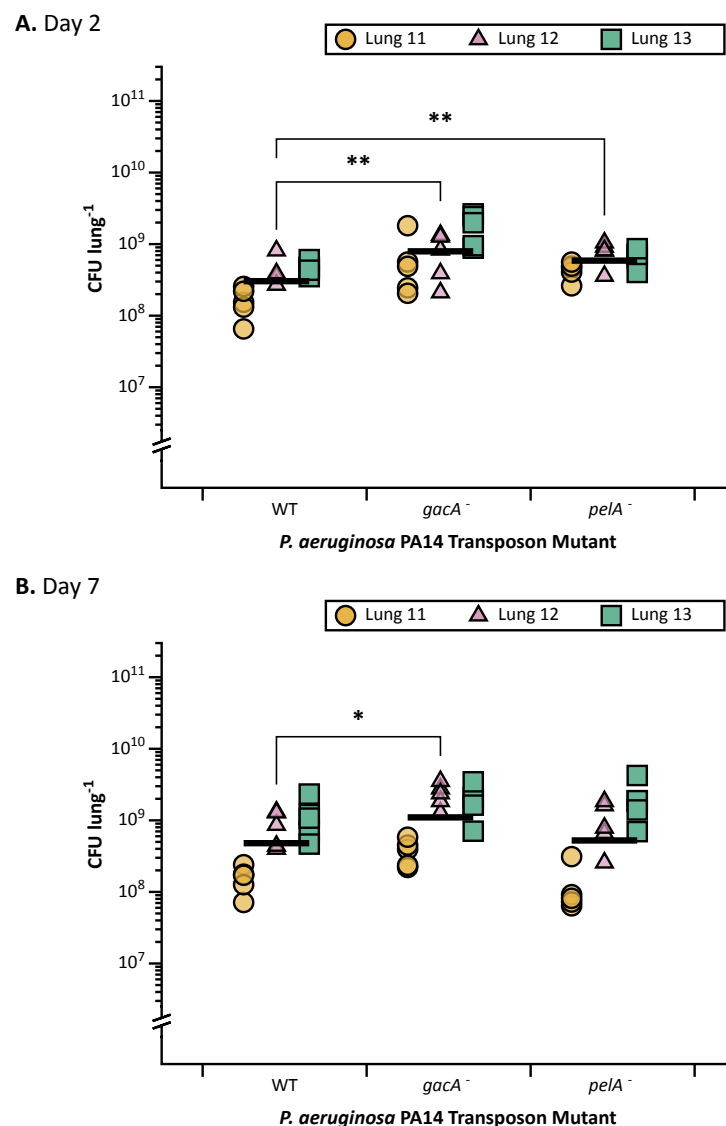
Figure 3.10: **Colony forming units (CFU) lung^{-1} of *Pseudomonas aeruginosa* PA14 wild type (WT) and biofilm associated transposon mutants (Liberati et al., 2006a,b)**. The CFU lung^{-1} was calculated from five pieces of tissue from each of three independent pig lungs per infection strain, shown by individual data points. Each lung is represented by different data point shapes and colours (see key) and the asterisks represent a significant difference ('**' = $P < 0.01$, '*' = $P < 0.05$). The horizontal lines show the mean and the y axes are log$_{10}$ scale. **(A)** CFU lung^{-1} after 2 d incubation at 37 °C. **(B)** CFU lung^{-1} after 7 d incubation at 37 °C.

P. aeruginosa PA14 biofilm formation on EVPL tissue recapitulated the morphology of *in vivo* CF biofilms, but was dependent on *gacA* and *pelA* function.

Two EVPL tissue pieces from each of two independent pig lungs were infected per strain (WT, *gacA*⁻, *pelA*⁻) for 2 d and 7 d. Uninfected tissue pieces were also prepared as negative controls for *P. aeruginosa* infection. The tissue pieces were then fixed, paraffin embedded and sectioned into two 100 μm step sections per piece, one section per slide.

One section of each *P. aeruginosa* PA14 infected tissue piece was Gram stained to identify bacterial growth. As shown in Figure 3.11, Gram negative rods were visible on the EVPL tissue surface infected with the WT or transposon mutants. This was indicative of *P. aeruginosa* infection. The growth on LB plates used to calculate CFU lung⁻¹ (Figure 3.10) was also morphologically characteristic of *P. aeruginosa*, thus it was confirmed that *P. aeruginosa* was the dominant species infecting the lung tissue in the EVPL model. Gram stain images in Figure 3.11 demonstrated the increase in bacterial cell density from 2 d to 7 d for all strains. The *gacA* transposon mutant appeared to form 'clumps' of cells distinct from the structure of WT cells seen.
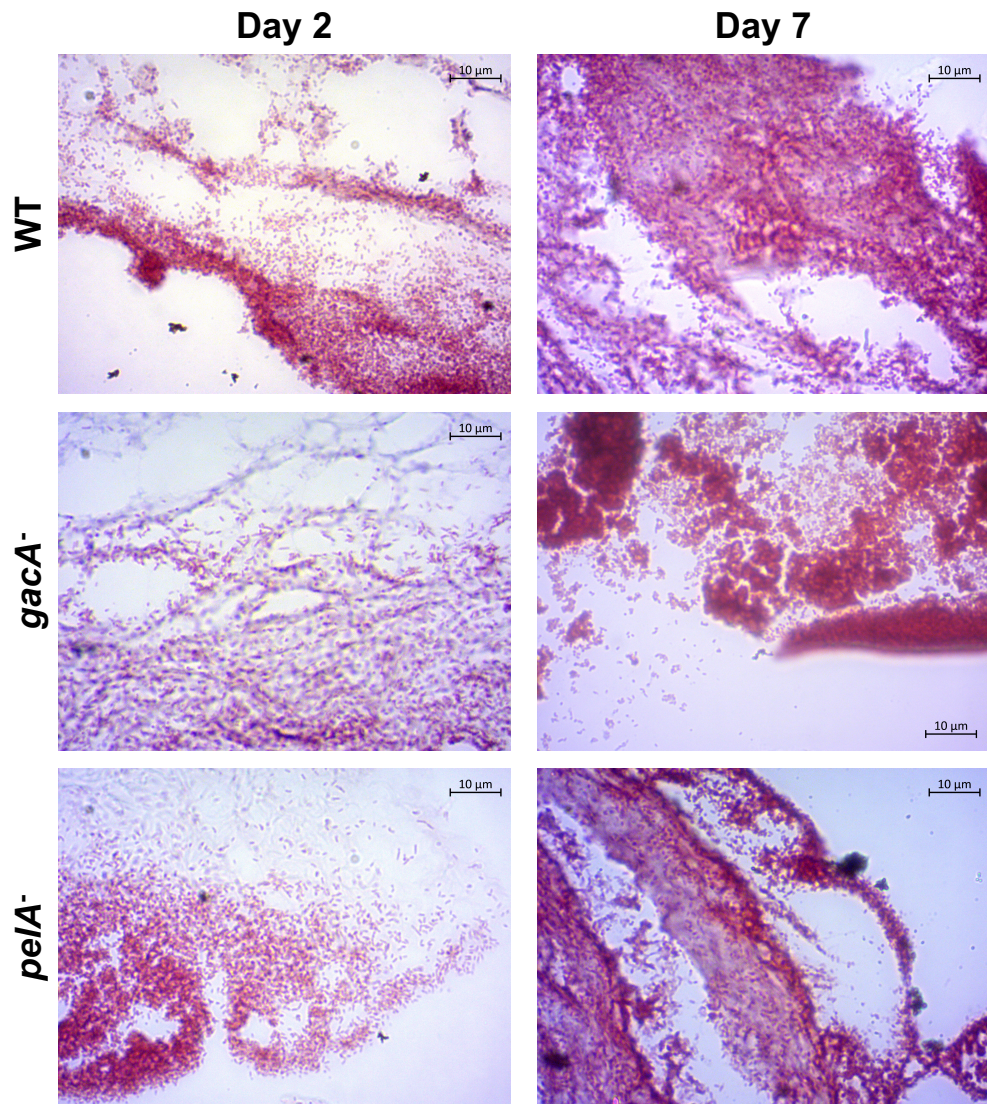
Figure 3.11: **Micrograph of Gram stained *ex vivo* pig lung bronchiolar tissue sections infected with *Pseduomonas aeruginosa* PA14 wild type (WT) or biofilm associated transposon mutants (Liberati et al., 2006a,b)**. All images are of tissue sections from the same pig lungs, fixed at either 2 d or 7 d after infection and incubation at 37 °C. The images were taken at x100 magnification.

A standard crystal violet biofilm assay was initially trialled on uninfected and PA14 WT infected EVPL tissue sections to determine its viability to identify biofilm biomass in the EVPL model. However as shown in Figure 3.12, the lung tissue preferentially bound crystal violet over the *P. aeruginosa* biofilm. Hence this was not suitable for identifying differences in the biofilms formed on the lung tissue by transposon mutants and the WT. This assay could not be performed on lung homogenate as the biofilm would not be intact. H & E staining was thus performed to visualise both the biofilm and tissue architecture, and Alcian blue staining to identify the biofilm matrix.
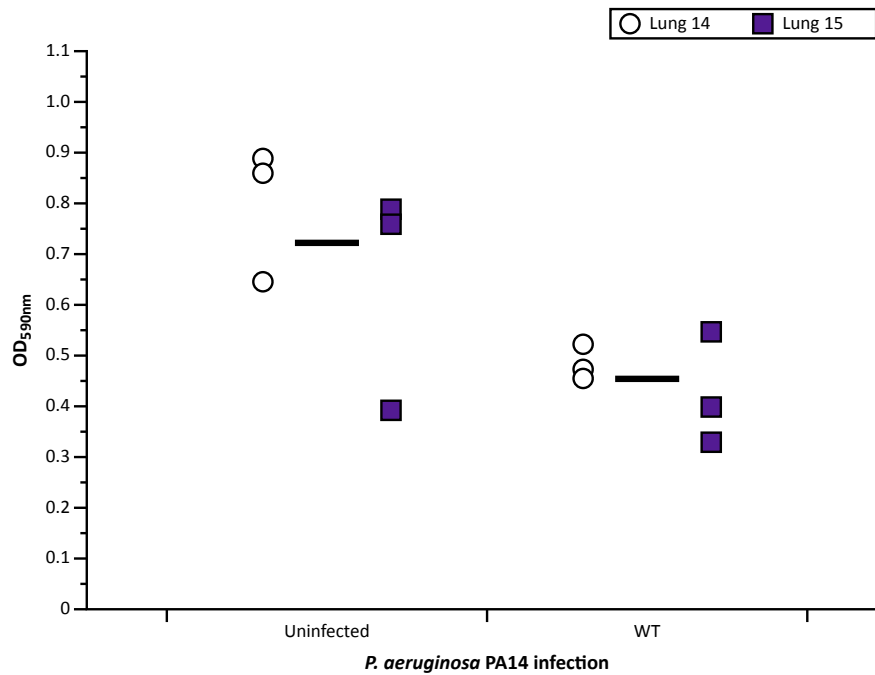
Figure 3.12: **The absorbance (590 nm) following a crystal violet biofilm assay on *ex vivo* pig lung tissue pieces infected with *Pseudomonas aeruginosa* PA14 wild type (WT) at 2 d after infection and incubation at 37 °C.** The assay was performed on three tissue pieces from each of two independent pig lungs shown by data points of different shapes and colours (see key). Uninfected tissue was stained with crystal violet as a negative control for *P. aeruginosa* infection. The horizontal lines represent the mean across both lungs.

H & E stained the biofilm matrix and basophilic bacteria purple (hematoxylin) and the connective tissue of the pig lung bronchiolar tissue sections pink (eosin). Alcian blue stained components of the biofilm matrix blue. Figure 3.13 shows stained tissue sections from 2 d post infection in the EVPL model. A hematoxylin stained *P. aeruginosa* biofilm was not clear on the x20 magnification images of *gacA*⁻ or *pelA*⁻. Although, the bacterial rods were evident in the x100 H & E images (Figure 3.13). There was Alcian blue staining on the lung tissue surface of the *pelA* transposon mutant infected tissue piece (Figure 3.13). The WT and *gacA* mutant infected pieces only had small regions of Alcian blue staining. However, the biggest contrast was the mass of hematoxylin staining on the surface of the WT infected lung tissue seen in the x20 H & E image, which showed the formation of a biofilm not seen for *gacA*⁻ or *pelA*⁻. Although, some lung tissue damage was evident for all strains (Figure 3.13).
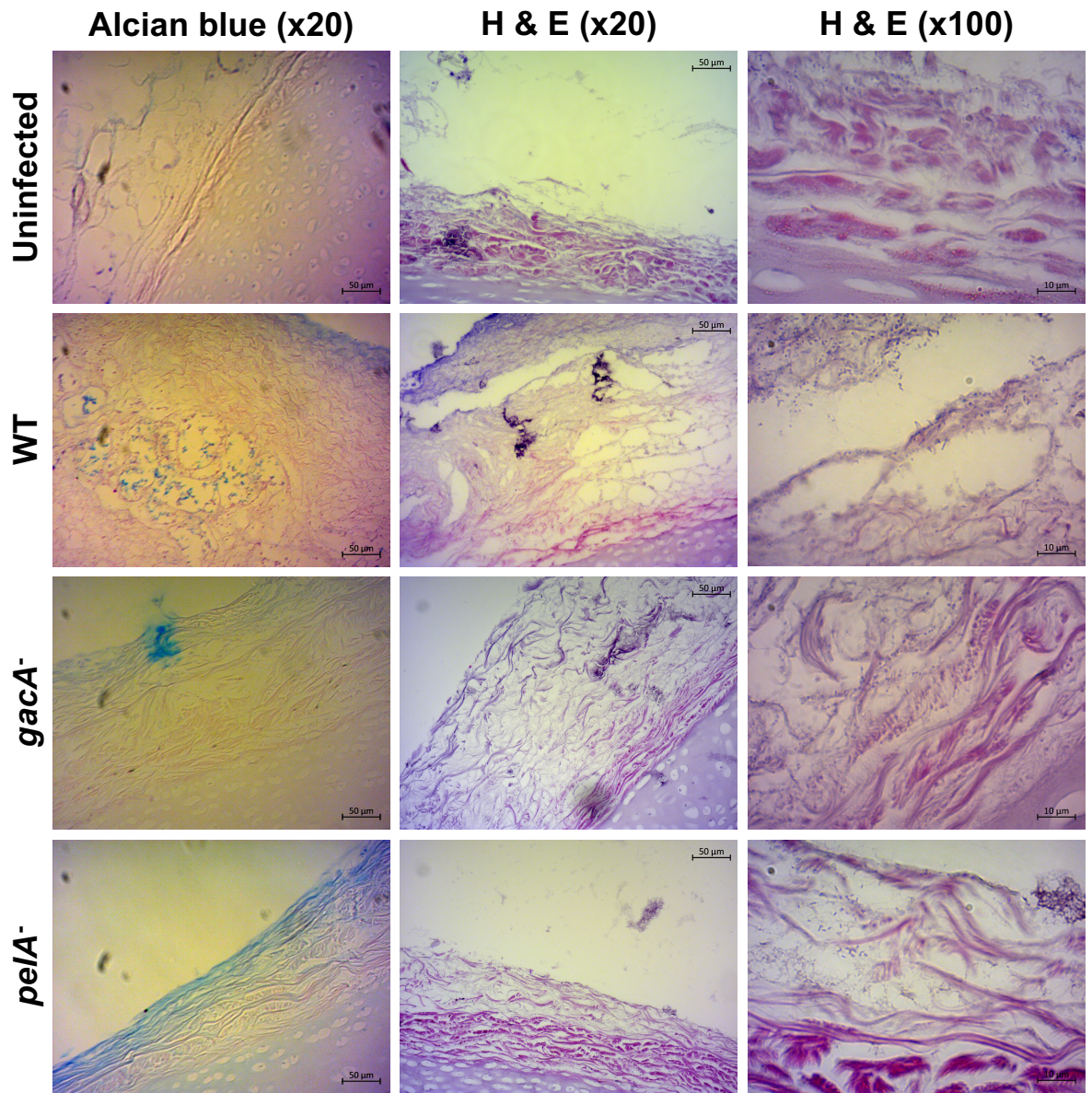
Figure 3.13: **Micrograph of stained *ex vivo* pig lung tissue sections infected with *P. aeruginosa* PA14 wild type (WT) or biofilm associated transposon mutants (Liberati et al., 2006a,b) for 2 d at 37 °C.** Uninfected tissue was also stained as a negative control for *P. aeruginosa* infection. Tissue sections from one lung were stained with Alcian blue and counterstained with nuclear fast red solution to stain the biofilm matrix and imaged at x20 magnification. Tissue sections from another lung (the same lung as Gram staining: Figure 3.11) were stained with Hematoxylin and Eosin (H & E) to identify both the pig lung tissue architecture and biofilm. H & E staining was imaged at x20 and x100 magnifcation, the x100 images were take from regions within the corresponding x20 image.

The staining was also performed on tissue sections from 7 d post infection (Figure 3.14). Clearer qualitative differences were observed between each transposon mutant and the WT compared with 2 d. There was no dense staining by Alcian blue on the uninfected tissue nor was there a biofilm or dense bacterial cells evident from H & E staining (Figure 3.14). These differences were less distinct at 2 d (Figure 3.13). This further confirmed that staining of infected tissue sections was *P. aeruginosa* infection and not an artefact of the

lung tissue.

The x20 magnification H & E images of the WT at 7 d showed a thick structure stained on the tissue surface. It was made up of layers of bacteria (Figure 3.14: x100 H & E) and matrix (Figure 3.14: x20 Alcian blue) that were punctuated with empty spaces. This structure was reminiscent of the *P. aeruginosa* biofilms found *in vivo* in CF chronic lung infections (Figure 3.15). The structured, dense biofilm was not observed on tissue pieces infected with *gacA*⁻ or *pelA*⁻ for 7 d. As shown in Figure 3.14, H & E staining at x20 magnification revealed a dense *gacA*⁻ biofilm associated with the pig lung tissue surface, which was homogenous without the spatial structure seen for the WT. There was only a thin layer of bacterial cells H & E stained on tissue infected with the *pelA* transposon mutant, which lacked both the structure and density of the WT biofilm (Figure 3.14). Alcian blue staining did stain a region within the surface of tissue infected with *pelA*⁻, similar to 2 d. However there was more Alcian blue staining of the WT and *gacA*⁻ infected tissue at 7 d than 2 d. This showed staining of a biofilm structure on the surface of the tissue infected with these strains rather than within the tissue, as observed for *pelA*⁻, with structures comparable to the H & E images (Figure 3.14).
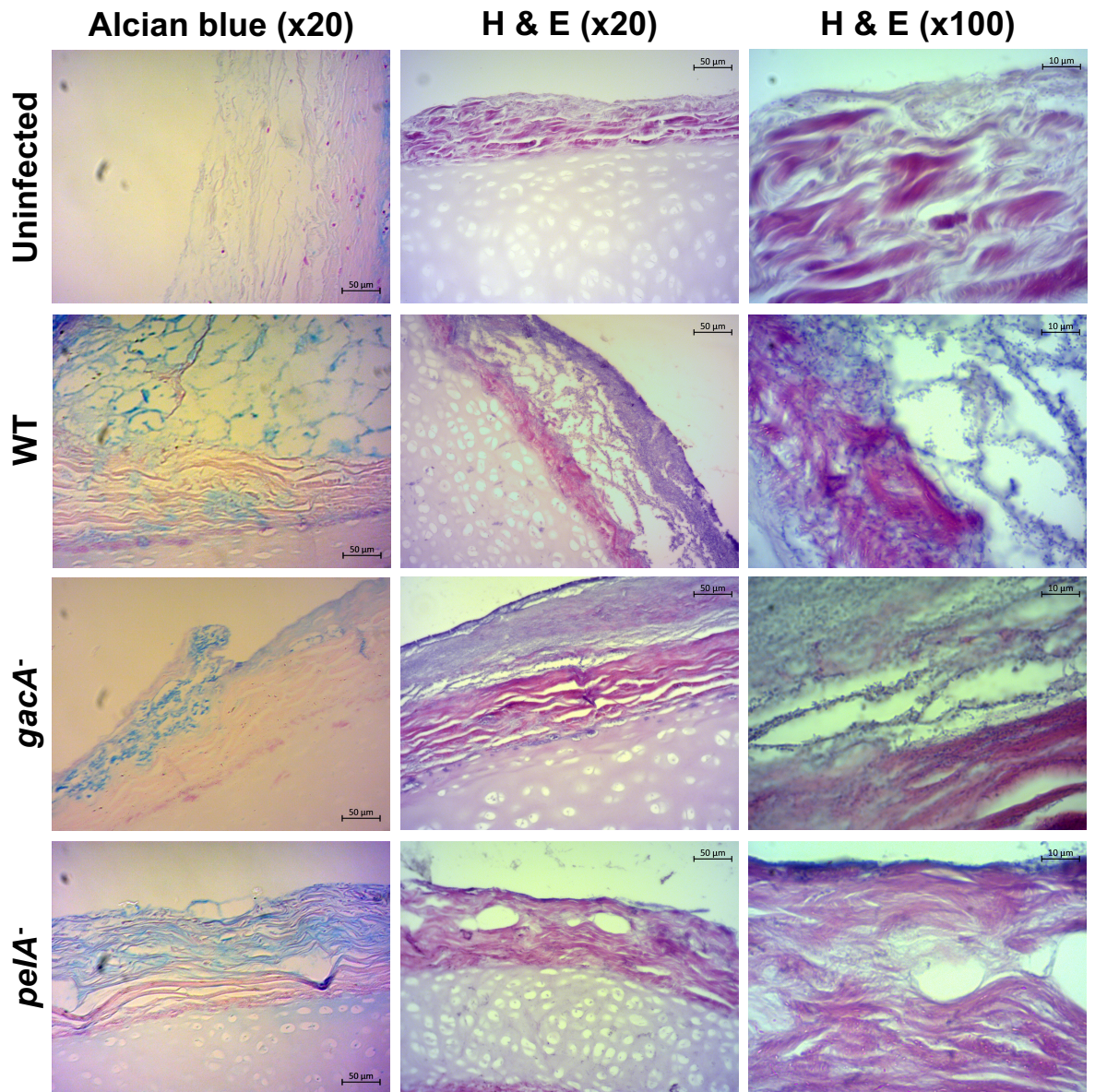
Figure 3.14: **Micrograph of stained *ex vivo* pig lung tissue sections infected with *P. aeruginosa* PA14 wild type (WT) or biofilm associated transposon mutants (Liberati et al., 2006a,b) for 7 d at 37 °C.** Uninfected tissue was also stained as a negative control for *P. aeruginosa* infection. Tissue sections from one lung were stained with Alcian blue and counterstained with nuclear fast red solution to stain the biofilm matrix and imaged at x20 magnification. Tissue sections from another lung (the same lung as Gram staining) were stained with Hematoxylin and Eosin (H & E) to identify both the pig lung tissue architecture and biofilm. H & E staining was imaged at x20 and x100 magnifcation, the x100 images were take from regions within the corresponding x20 image.
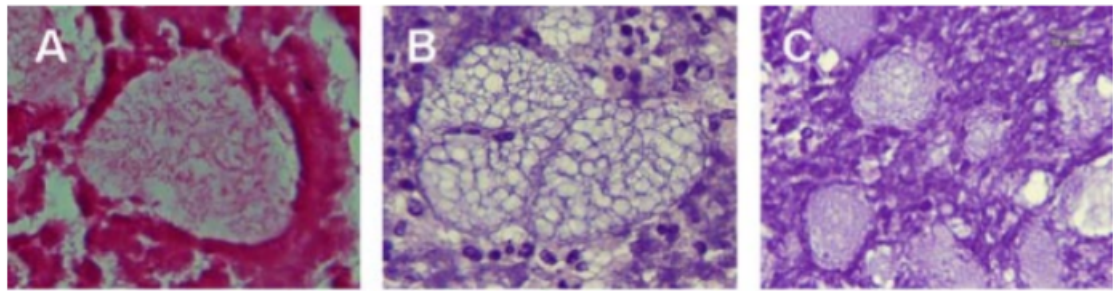
Figure 3.15: **Images taken from Bjarnsholt et al. (2009) (Figure 4) of biopsies taken from *in vivo* Pseudomonas aeruginosa chronic infection of a cystic fibrosis (CF) lung.** All three images show bronchiola samples. **(A)** A Gram stained biofilm from a person with CF and chronic *P. aeruginosa* infection for 28 y. **(B, C)** Hematoxylin and eosin (H & E) stains of bronchiole filled with bacteria, showing 'hollow zones and grid like structures'.

As a quanititative measure of biofilm differences, biofilm depth measurements were then taken from the tissue surface to the outward edge of the stained biofilm for each strain from x20 magnification H & E images. The mean depth was calculated from one tissue piece from each of two independent lungs. This was only performed for 7 d samples, as the biofilms were not clearly defined by staining at 2 d. As shown in Figure 3.16, there was a significant difference in the biofilm depth between the strains (ANOVA strain $F_{2,36}$ = 464.71, P < 0.01, lung $F_{1,36}$ = 73.31, P < 0.01, interaction $F_{2,36}$ = 25.11, P < 0.01). Although the interaction between strain and lung was significant, indicating that the differences observed may have been associated with lung variation. Post-hoc Tukey HSD analysis revealed that the *gacA*⁻ biofilm was significantly smaller than the WT in both lungs (P < 0.01) and the *pelA*⁻ biofilm was also significantly smaller than the WT (P < 0.01). The *pelA* transposon mutant formed a biofilm that was also significantly smaller than the *gacA* transposon mutant (P < 0.01). Hence both mutations reduced the depth of the biofilm formed compared with the WT, but *pelA*⁻ formed the smallest biofilm (mean depth WT: 102.19 μm, *gacA*⁻: 55.02 μm, *pelA*⁻: 3.10 μm). These results supported the qualitative differences observed.

The qualitative and quantitative data combined indicated that the *pelA* mutant was unable to form a dense biofilm in the EVPL model. Loss of *gacA* function did not prevent biofilm formation however the structured biofilm seen for WT infection in the EVPL model was not observed.
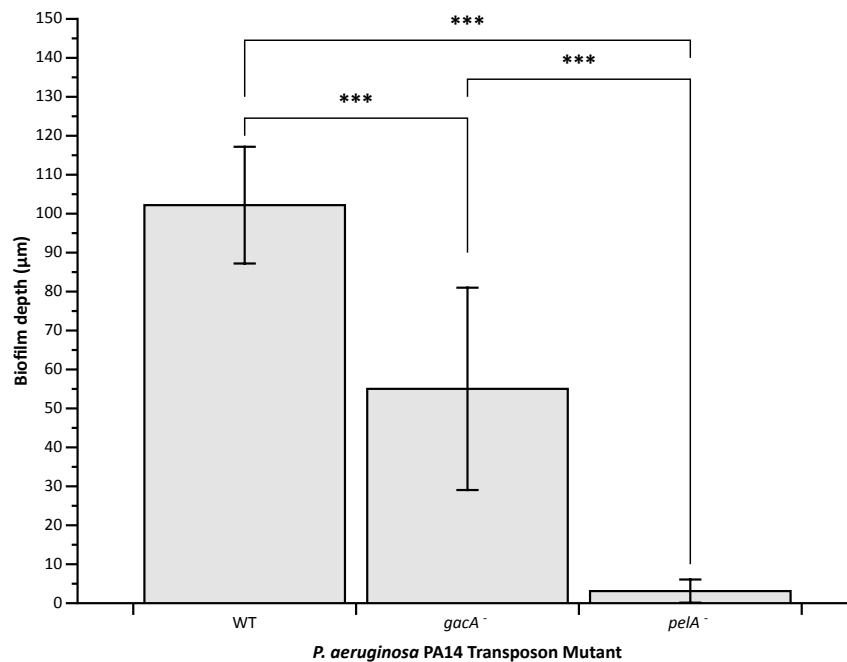
Figure 3.16: **The depth (μm) of the biofilm formed on the surface of *ev vivo* pig lung bronchiolar tissue by *Pseudomonas* aeruginosa PA14 wild type (WT) and biofilm associated transposon mutants (Liberati et al., 2006a,b), after incubation at 37 °C for 7 d.** The mean depth is shown for each strain from an infected tissue section from each of two independent lungs, the error bars show the standard deviation. The measurements were taken from x20 magnification, H & E stain images; seven measurements along the biofilm were taken, from the tissue surface to the outward edge of the biofilm, to determine the biofilm depth from each tissue section. The asterisks represent a significant difference ('***' = $P < 0.001$).

3.2.4   *P. aeruginosa* PA14 meropenem tolerance in the EVPL model

The *gacA* and *pelA* transposon mutants were found to produce distinct biofilms from the *P. aeruginosa* PA14 WT in the EVPL model; *pelA*⁻ appeared not to produce a biofilm at all (Figure 3.14). Therefore, the effect of differences in biofilm formation on antibiotic tolerance was investigated. The clinically relevant antibiotic meropenem was tested, which had an MIC value of 1 μg ml⁻¹ for *P. aeruginosa* PA14 in CAMHB. This was below the clinical breakpoint for non-meningitis *P. aeruginosa* (2), thus PA14 is susceptible to meropenem (The European Committee on Antimicrobial Susceptibility Testing, 2021). A starting concentration of 64 μg ml⁻¹ meropenem was used in the EVPL model (Harrington et al., 2021b). All antibiotic tolerance experiments were performed on three replicate tissue pieces per condition, from each of two independent pig lungs.

Meropenem treatment higher than the MIC value reduced *P. aeruginosa* PA14 bacterial load in the EVPL model during early infection but not by 24 hours, for both the WT and biofilm associated transposon mutants.

Tissue pieces were infected with *P. aeruginosa* PA14 WT, *gacA*⁻ and *pelA*⁻ strains then transferred to 64 µg ml⁻¹ meropenem at 2 h, 4 h, 6 h, 8 h and 24 h post infection. Replicate antibiotic untreated tissue pieces were transferred to PBS at the same time points. Following treatment for 24 h, the *P. aeruginosa* CFU lung⁻¹ was calculated. Uninfected tissue was used as a negative control for *P. aeruginosa* infection. Figure 3.17 shows that meropenem treatment significantly reduced *P. aeruginosa* CFU lung⁻¹ of all three strains at 2 h (Table 3.2). There was also a significant difference at the other time points for the WT, at 6 h and 8 h for *pelA*⁻, and 4 h and 8 h for *gacA*⁻ (Figure 3.17). However, this was not reflective of how effective the meropenem treatment was.
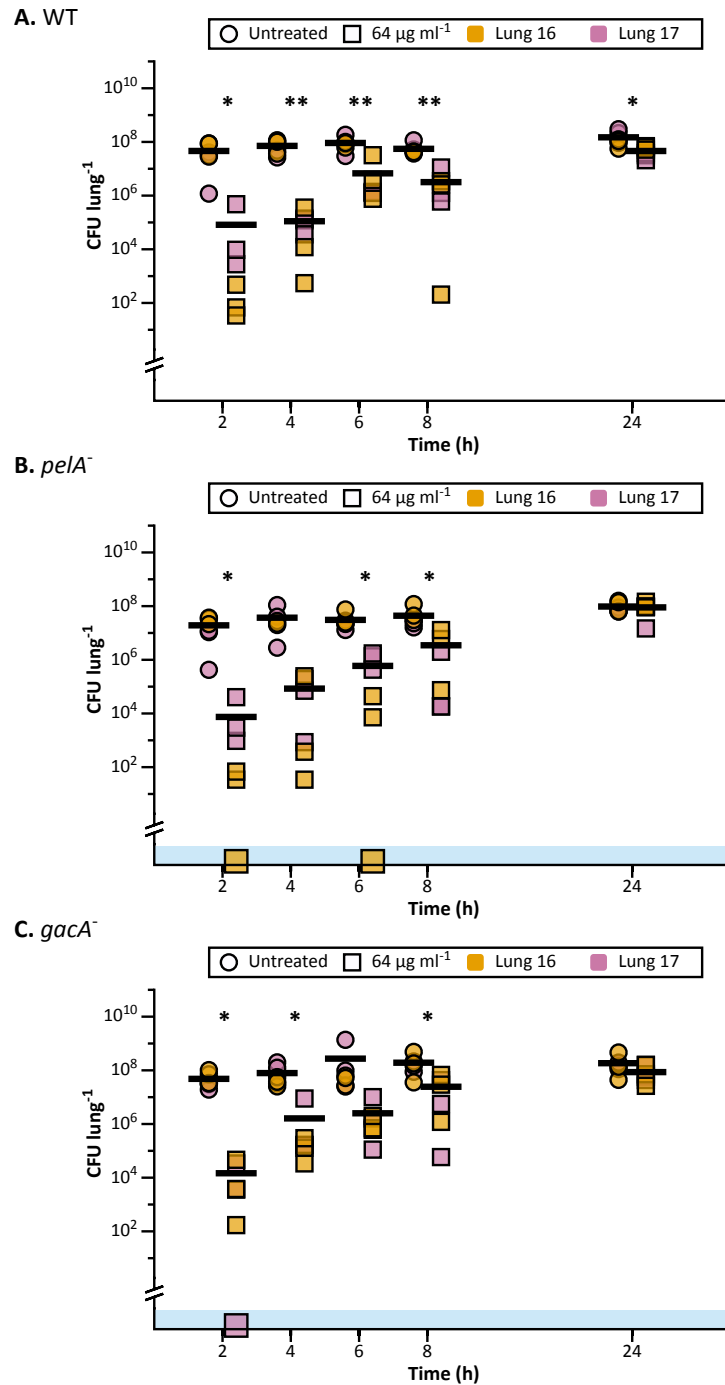
Figure 3.17: **Colony forming units (CFU) lung⁻¹ of *Pseudomonas aeruginosa* PA14 wild type (WT) and biofilm associated transposon mutants (Liberati et al., 2006a,b) in the *ex vivo* pig lung model treated with 64 µg ml⁻¹ meropenem over 24 h.** Six replicate tissue pieces from each of two independent pig lungs were infected with each strain per time point; three pieces were treated with 64 µg ml⁻¹ for 24 h at each time point and three pieces were transferred to phosphate-buffered saline (PBS) for 24 h (untreated). The treatment is represented by different shaped data points and each lung is a different colour (see key). The horizontal bars represent the mean across lungs and the asterisks represent statistical significance ('*' = P < 0.05, '**' = P < 0.01). The blue region at the bottom of the graph indicates samples below the detection threshold. The y axes are $\log_{10}$ scale. **(A)** CFU lung⁻¹ for the PA14 WT. **(B)** CFU lung⁻¹ for the *pelA* transposon mutant. **(C)** CFU lung⁻¹ for the *gacA* transposon mutant.

Table 3.2: **Results from Welch's two sample t-tests of the effect of meropenem treatment (64 µg ml^{-1}) on** *Pseudomonas aeruginosa* **PA14 wild type (WT) and biofilm associated mutants (Liberati et al., 2006a,b) over 24 h.** The table shows the degrees of freedom, *t*-value and *P* value at each time point for each strain, comparing untreated samples with meropenem treated. The underlined *P* values are significant reductions in CFU lung^{-1} caused by 64 µg ml^{-1} meropenem. The 0.05 *P* values were significant as they have been rounded up to two decimal places so the true value is < 0.05

Transposon mutant	Time (h)	Degrees of freedom	T-value	*P*-value
WT	2	5.00	3.26	0.02
WT	4	5.00	4.51	0.01
WT	6	5.57	3.89	0.01
WT	8	5.19	4.25	0.01
WT	24	5.44	2.74	0.04
pelA$^-$	2	5.00	3.31	0.02
pelA$^-$	4	5.00	2.42	0.06
pelA$^-$	6	5.01	3.32	0.02
pelA$^-$	8	5.18	2.58	0.05
pelA$^-$	24	10.00	0.28	0.78
gacA$^-$	2	5.00	3.72	0.01
gacA$^-$	4	5.03	2.76	0.04
gacA$^-$	6	5.00	1.23	0.27
gacA$^-$	8	5.30	2.57	0.05
gacA$^-$	24	6.54	1.54	0.17

The difference in CFU lung^{-1} between untreated and treated tissue pieces infected with both transposon mutants was greater than 3 log$_{10}$ CFU lung^{-1} at 2 h (Figure 3.18), and some samples were below detection (Figure 3.17). This threshold is often considered the minimum bactericidal concentration (Sweeney et al., 2020b). Hence at 2 h, 64 µg ml^{-1} was likely bactericidal to *pelA*$^-$ and *gacA*$^-$, but not the WT, in the EVPL model (Figure 3.18). After this time point, any reduction in CFU lung^{-1} of each strain was less than 3 log$_{10}$ so not considered bactericidal. As shown in Figure 3.17, there was a steep decrease in the CFU lung^{-1} log$_{10}$ reduction from 2 h to 6 h for each strain, which levelled out from 6 h to 24 h. There was a small increase in the mean log$_{10}$ reduction of *gacA*$^-$ from 4 h to 6 h, however there was no clear difference when all data points were visualised (Figure 3.17). At 24 h, meropenem did not appear to have a biological effect on the growth of any of the strains (Figure 3.18). Therefore, 64 µg ml^{-1} meropenem appeared to be most effective at 2 h when *pelA* or *gacA* were not functional.
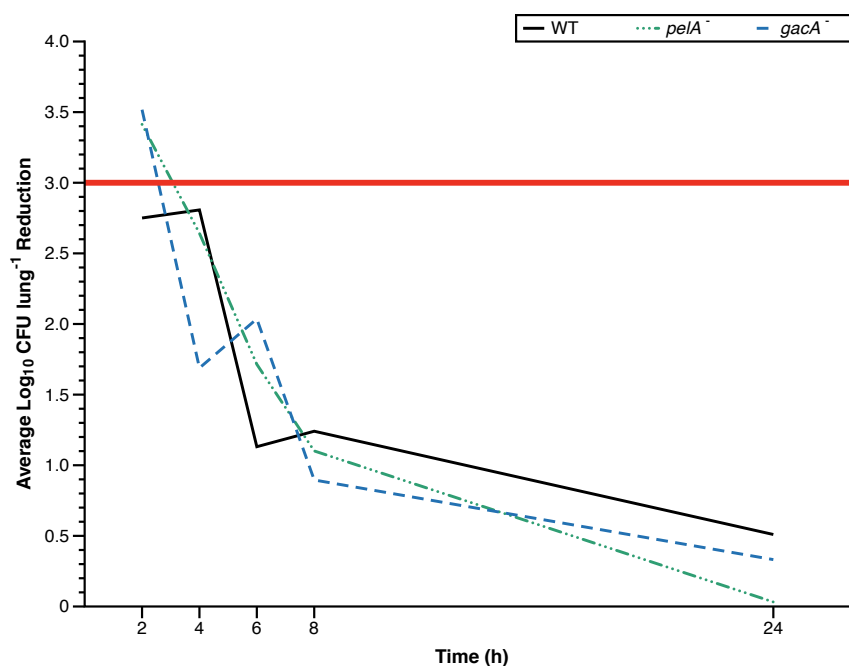
Figure 3.18: **Log$_{10}$ reduction in colony forming units (CFU) lung^{-1} of *Pseudomonas aeruginosa* PA14 wild type (WT) and biofilm associated transposon mutants (Liberati et al., 2006a,b) in the *ex vivo* pig lung model caused by 64 μg ml^{-1} meropenem, over 24 h.** The mean log$_{10}$ reduction in CFU lung^{-1} caused by 64 μg ml^{-1} meropenem was calculated from three replicate pieces from each of two independent pig lungs per strain, between untreated and antibiotic treated EVPL tissue pieces (Figure 3.17). Different line types represent each strain (WT = black, solid line; *pelA*$^-$ = green, dot & dashed line; *gacA*$^-$ = blue, dashed line). The horizontal, thick red line shows 3 log$_{10}$ reduction, often considered the minimum bactericidal concentration threshold (Sweeney et al., 2020b).

Increasing concentrations of meropenem did not affect the bacterial load of *P. aeruginosa* PA14 WT or the biofilm associated transpsoson mutants in the EVPL model at 48 hours.

As meropenem at a concentration of 64 μg ml^{-1} did not appear to have an effect on the bacterial load of *P. aeruginosa* PA14 WT or the transposon mutants after 2 h in the EVPL model, higher concentrations were tested. The strains were grown in the model for 48 h, then treated with double the concentration (128 μg ml^{-1}) and ten times (640 μg ml^{-1}) (Figure 3.19). There did not appear to be a difference in the CFU lung^{-1} between meropenem concentrations, including untreated (0 μg ml^{-1}), for any of the strains. ANOVA did find a significant difference for the WT (concentration $F_{3,16}$ = 10.52, P < 0.01, lung $F_{1,16}$ = 7.87, P = 0.01, interaction $F_{3,16}$ = 5.21, P = 0.01) and Tukey HSD post hoc analysis showed there was a significant difference between the 0 μg ml^{-1} treated samples and each meropenem treatment (all P <0.01). However the interaction term between concentration and lung was significant indicating these differences may be related to lung variation. This, alongside a lack of clear CFU lung^{-1} reduction (Figure 3.19A), suggested

that meropenem treatment of all concentrations did not have a biologically significant impact on WT bacterial load. ANOVA did not find a significant difference in CFU lung^{-1} between meropenem treatments for either *pelA*$^-$ (concentration $F_{3,16}$ = 1.18, *P* = 0.35, lung $F_{1,16}$ = 7.77, *P* = 0.01, interaction $F_{3,16}$ = 0.87, *P* = 0.48) or *gacA*$^-$ (concentration $F_{3,16}$ = 0.53, *P* = 0.67, lung $F_{1,16}$ = 0.06, *P* = 0.81, interaction $F_{3,16}$ = 0.65, *P* = 0.60). These results indicate, once established in the EVPL model, *P. aeruginosa* PA14 was able to survive high concentrations of meropenem even with the loss of *pelA* or *gacA* function. Therefore, growth in the model likely cued changes in *P. aeruginosa* physiology that increased antibiotic tolerance.
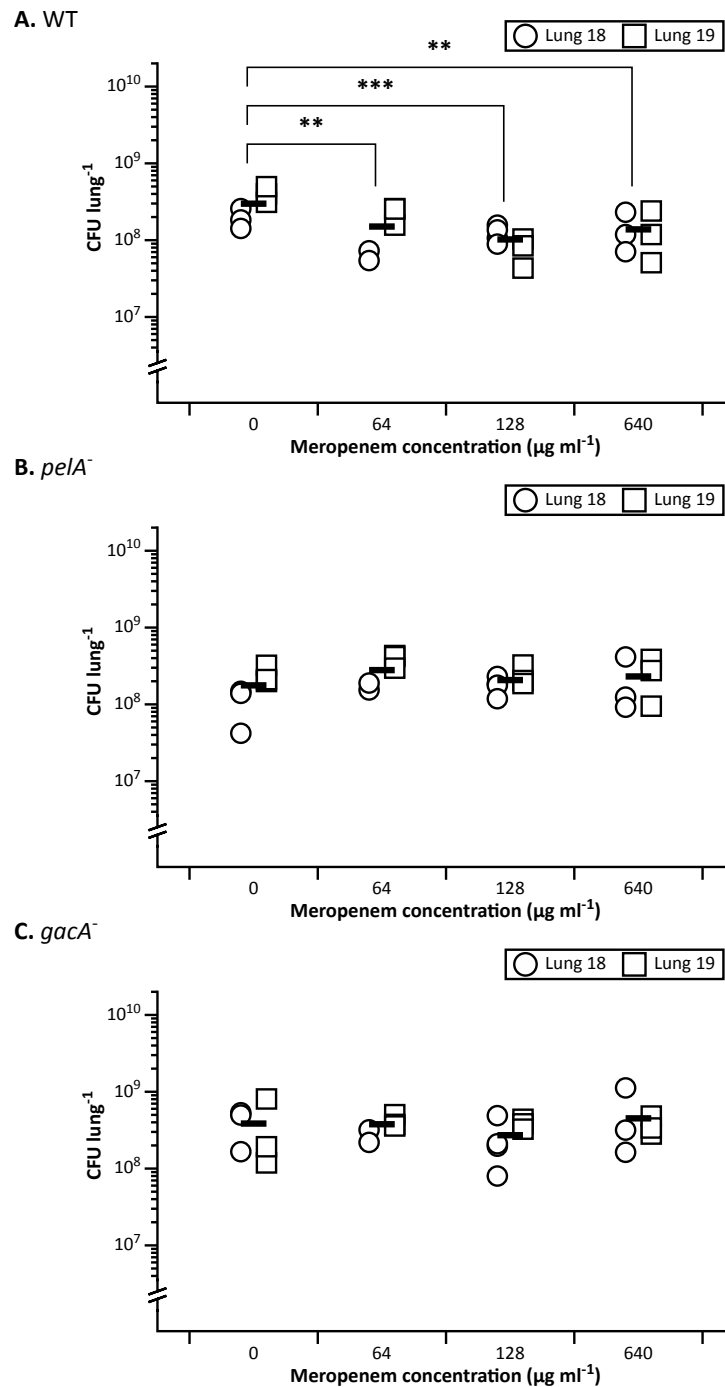
Figure 3.19: **Colony forming units (CFU) lung^{-1} of *Pseudomonas aeruginosa* PA14 wild type (WT) and biofilm associated transposon mutants (Liberati et al., 2006a,b) in the *ex vivo* pig lung model treated with different concentrations of meropenem (µg ml^{-1}) at 48 h.** Six replicate tissue pieces from two independent pig lungs were infected with each strain per concentration. The samples were transferred to meropenem and the untreated samples (0 µg ml^{-1}) were transferred to phosphate-buffered saline (PBS) for 24 h following 48 h incubation at 37 °C. Each lung is shown by different shaped data points (see key) and the horizontal bars show the mean. The y axes are log$_{10}$ scale. **(A)** CFU lung^{-1} for the PA14 WT. Significant differences are shown ('***' = $P < 0.001$, '**' = $P < 0.01$). **(B)** CFU lung^{-1} for the *pelA* transposon mutant. No significant differences were found. **(C)** CFU lung^{-1} for the *gacA* transposon mutant. No significant differences were found.

3.2.5 Summary of phenotypic analyses of *P. aeruginosa* PA14 tranposon mutants in the EVPL model

Table 3.3: **Summary of results from virulence factor, biofilm and antibiotic tolerance experiments on** ***Pseudomonas aeruginosa*** **PA14 wild type (WT) and selected transposon mutants (Liberati et al., 2006a,b) grown in the** ***ex vivo*** **pig lung model at 2 d and 7 d.** Virulence factor production was measured for the WT and virulence associated mutants (*gacA*⁻, *vfr*⁻, *sadR*⁻ and *pqsR*⁻). Biofilms were visualised and measured for the WT and biofilm associated mutants (*gacA*⁻ and *pelA*⁻), and meropenem tolerance. Overall differences are summaries of the results, considering biological and statistical differences.

Phenotype	Time (d)	Overall difference compared with the WT
Virulence associated mutants		
CFU lung⁻¹	2	None
	7	None
Total Protease	2	*gacA*⁻ may produce **less**
	7	None
Pyoverdine	2	None
	7	None
Pyochelin	2	None
	7	None
Biofilm associated mutants		
CFU lung⁻¹	2	None
	7	None
Biofilm Depth	7	*gacA*⁻ biofilm **lacked WT structure** & *pelA*⁻ appeared to be a **small layer** of cells
Meropenem tolerance	-	None

3.3   Discussion

P. aeruginosa PA14 phenotypic analyses indicated that the EVPL model may be a good laboratory model for *P. aeruginosa* chronic-like biofilm infection in the CF lung. The dominant pathogen was able to grow and survive associated with the pig lung bronchiolar tissue for 7 d.   Low levels of *P. aeruginosa* virulence factors and high meropenem tolerance were observed, regardless of any loss of gene function in different transposon mutant strains. These findings were consistent with the current

knowledge of how *P. aeruginosa* adapts to cause chronic infections of the CF lung; there is a reduction in virulence factor production and switch to a biofilm lifestyle typically associated with increased antibiotic resistance (Winstanley et al., 2016). The formation of a structured, dense *P. aeruginosa* WT biofilm comparable to *in vivo* infection was also observed on the surface of the tissue. These results suggest that *P. aeruginosa* PA14 was driven into a chronic-like infection state in the EVPL model. However, a lack of consistent recovery of IL-8 cells from EVPL tissue indicated that the model may not provide any immune response, which would better replicate host-pathogen interactions.

IL-8 concentration was measured to provide an insight into the immune response in the EVPL tissue. IL-8 is secreted by epithelial cells lining the bronchial lumen in both pigs and humans, and increased production is associated with the CF lung (Rimessi et al., 2018). The major role of IL-8 in causing progressive lung damage in CF, and its production at all stages of CF (Bonfield et al., 1995; Rimessi et al., 2018), meant it was of interest to establish the EVPL bronchiolar tissue as a model to mimic the CF lung environment. However, the tissue used in the EVPL model is from pigs post slaughter, transportation, and dissection. Hence, any IL-8 measured would have been present in the tissue section at the time of slaughter. An immune response to *P. aeruginosa* infection could not occur as it was unlikley the pig tissue was metabolically active, which may explain why IL-8 was not consistently found in the EVPL samples.

Other *ex vivo* porcine lung models are being developed with a particular focus on recapitulating the immune response, such as the perfusion model described by DeBritto et al. (2020). This work adapted the normothermic *ex vivo* lung perfusion method, increasingly used to maximise the time human lungs can be functionally assessed and still be viable for transplantation, for use with porcine lungs (Cypel et al., 2011; DeBritto et al., 2020). Following infection of the lung tissue with *Klebsiella pneumoniae*, inflammatory responses were detected and there was an increase of interleukin-10 cells (DeBritto et al., 2020). This method involves multiple steps at slaughter, lung extraction, and when whole lungs are processed in the lab to maintain this response. These steps may be incorporated in the EVPL model in the future to maintain immune response and provide better insight into the host-pathogen interactions. Conversely, It must be considered that the EVPL model is designed as a quick, cheap, high-throughput method to mimic the CF lung environment that could be used as a diagnostic platform in a clinical

setting. The addition of more complex preparation steps may reduce this functionality. Following establishment of the basic parameters for the EVPL model however, it may be adapted to address more specific research questions.

P. aeruginosa virulence in the EVPL model was then investigated. Virulence factor production is associated with the initial acute stage of infection, and mutations in virulence pathways are positively selected for in the CF lung (Smith et al., 2006). EVPL tissue was infected with *P. aeruginosa* PA14 WT or virulence associated transposon mutants for the following genes: *gacA*, *vfr*, *sadR* and *pqsR*. There was no difference in bacterial load between any of the strains at 2 d or 7 d, indicating that regardless of each mutation all strains were able to establish in the model. Interestingly, there were no significant differences in the total proteases produced by each transposon mutant compared with the WT either. Proteases were however measured from uninfected pig lung tissue. In both human and porcine lungs, neutrophils release neutrophil serine proteases. A study by Chevaleyre et al. (2016) infected pigs with *P. aeruginosa* and identified a neutropholic response that was comparable to human infection, important for studying CF as the lung inflammation observed is neutrophil-dependent. The presence of proteases in the EVPL tissue at 2 d and 7 d suggests that neutrophil serine proteases may be present in the model, thus it may be capturing this aspect of CF immune response. As *P. aeruginosa* elicits secretion of host neutrophils during *in vivo* infection, there is potential that the increase in total protease between the WT and all transposon mutants observed, except *gacA*⁻, may be response of the EVPL tissue not *P. aeruginosa* production. This would need to be further investigated to determine the source of these proteases. The amount of total protease was found to be much lower than previous work in the model (Harrison et al., 2014). However, it must be considered that previous work was done at 1 d post infection, whereas the current work sampled at 2 d and 7 d, and was set up using porcine alveolar tissue rather than bronchiolar. This may account for the differences.

P. aeruginosa is known to secrete a number of proteases during CF lung infection. The *P. aeruginosa* proteases cause damage to the host lung tissue, alter the immune response, and are linked with the pathogenesis of acute infection (Faure et al., 2018). As a large increase in protease was not observed in WT PA14 infected tissue compared to uninfected it is unlikely protease production was being upregulated in the EVPL model,

indicating this characteristic of acute infection was not present. It can not be determined whether *P. aeruginosa* was producing any proteases at all, or if it was a result of tissue response. More than a third of people with CF who have chronic *P. aeruginosa* infections have been shown to have *P. aeruginosa* variants that are deficient in LasR quorum sensing and proteases, driven by selection pressure by the host for persistance and survival (Faure et al., 2018). This may explain why low levels of protease were measured in all *P. aeruginosa* EVPL samples; *P. aeruginosa* was driven into a chronic state at 2 d, which was maintained for 7 d. If *P. aeruginosa* had entered a chronic-like state by 2 d then protease production would be switched off, and no difference between the transposon mutants would be expected, as observed.

Interestingly, Harrison et al. (2014) were unable to detect PVD or PCH in alveolar EVPL samples. The two siderophores were detected in EVPL bronchiolar samples infected with *P. aeruginosa* PA14 WT and the transposon mutants, however no difference was found between mutants and the WT. Pyoverdine production is significantly reduced in chronic infection caused by mutations resulting in inactivation of *lasR* (Hogardt and Heesemann, 2010). In fact, Nguyen et al. (2014) showed that primary siderophore production (PVD and PCH) is significantly reduced as CF lung infection progresses to a chronic state, and heme becomes the crucial iron source. Hence, this may explain why no differences were observed between mutants. If these siderophores were no longer dominant in the chronic-state of infection in the EVPL model, the function of each gene in production may not have been important. Hence, although virulence-associated transposon mutants did not reveal obvious differences with the WT it did suggest that the EVPL model was mimicking chronic style *P. aeruginosa* infection. As biofilm is a key characteristic of this stage of infection, this was subsequently investigated.

Visualisation of the biofilm was key to not only investigating the interaction between *P. aeruginosa* and the EVPL bronchiolar tissue and the structure of the biofilms, but also how the model compared with *in vivo* biofilms. H & E staining was the main approach used to study this as it has been reported as a cost-effective and practical method for detecting biofilms in clinical samples (Hochstim et al., 2010; Tóth et al., 2011; Hong et al., 2014). It stains both the bacteria and the lung tissue, which is not possible with bacteria specific microscopy techniques. Hence *P. aeruginosa* biofilm formation, its location on the tissue, and any potential lung tissue damage could be detected. Alcian blue was

used to confirm H & E was staining the biofilm, as it stains components of the biofilm matrix (Bjarnsholt et al., 2009; Høiby et al., 2017).

Using these techniques, it was shown that *P. aeruginosa* PA14 forms a biofilm associated with the EVPL tissue surface. The biofilm had a 'lace-like' structure at 7 d of bacterial aggregates punctuated with spaces of either fluid or air. This structure was reminiscent of the *P. aeruginosa* biofilms observed in explanted lung tissue from people with CF who had chronic *P. aeruginosa* infections (Figure 4 in Baltimore et al. (1989); Figure 4 in Bjarnsholt et al. (2009); Figure 8 in Henderson et al. (2014)). This structure is distinct and more heterogenous than the typical 'mushroom style' biofilms typically grown in flow cell biofilm models (Figure 8 in (Høiby et al., 2010)). This would indicate that the EVPL tissue provides the structure and physiological cues for *P. aeruginosa* biofilm formation that is representative of clinical infection.

The mechanisms underpinning *P. aeruginosa* biofilm in the pig lung model were explored by staining and imaging tissue infected with transposon mutants for *pelA* and *gacA*. The biofilms formed by both strains were distinctive from the WT. GacA is essential to *P. aeruginosa* PA14 biofilm maturation and loss of function has been shown to cause reduced antibiotic resistance and a reduction in the strains capacity to form a biofilm (Parkins et al., 2001). In the EVPL model, it was found that *gacA* function is required for the mature biofilm architecture observed for the WT. The *gacA* mutant did form a dense mass of bacterial aggregates on the surface of the pig lung tissue however it lacked the 'lace-like' appearance caused by the spaces. This confirmed the importance of established biofilm regulatory pathways, such as the GacAS system, in the formation of a mature, structured biofilm community associated with the EVPL tissue.

The gene *pelA* is involved in Pel synthesis, a biofilm exopolysaccharide that is required for the development of *P. aeruginosa* PA14 biofilms (Colvin et al., 2011; Marmont et al., 2017). *P. aeruginosa* produces three exopolysaccharides to form the biofilm matrix associated with antbiotic resistance and host immune response protection in infection: Pel, Psl and alginate (Bjarnsholt et al., 2009). *P. aeruginosa* PA14 is intrinsically Psl-deficient and alginate alone cannot form a structured biofilm, but is overproduced in the chronic stages of *P. aeruginosa* infection in CF (Xu et al., 2016). In fact, a *P. aeruginosa* PA14 mutant that could not produce Pel was found to arrest at the initial stages of biofilm

development, resulting in a flat monolayer of growth. (Colvin et al., 2011). Consistent with this, the *pelA* mutant was unable to form a biofilm in the EVPL model. Although, Alcian blue did stain the surface of the pig bronchiolar tissue infected with *pelA⁻*, which may have been lipopolysaccharides or alginate. Production of alginate would explain how the strain was able to attach to the tissue surface without forming a biofilm. Despite this, a similar CFU lung⁻¹ of *pelA⁻* was recovered from the EVPL model to the WT and *gacA* mutant, indicating the *P. aeruginosa* biofilms may have been made up of a large number of unculturable or dead bacterial cells.

Formation of a structured biofilm has been linked to increased *P. aeruginosa* antibiotic resistance, and plays a key role in the high levels of antibiotic resistance seen in the clinic compared to *in vitro* tests (Høiby et al., 2010). The clinically relevant, β-lactam antibiotic meropenem was tested against the PA14 WT and biofilm associated transposon mutants, as it has been shown to have a minimal effect on *P. aeruginosa* biofilm in the EVPL model (Hassan et al., 2020). Initially the MIC for WT PA14 in SCFM demonstrated that the strain was susceptible to meropenem, but it was able to grow in the EVPL model at concentrations ≥ 640 µg ml⁻¹. It has been found that the current antibiotic susceptibility testing methods, including MIC tests, do not accurately predict whether antibiotics will be effective *in vivo* in the CF lung, as *P. aeruginosa* clinical biofilm phenotypes are not captured by these tests (Smith et al., 2003; Hurley et al., 2012; Müsken et al., 2017). This indicates that the WT biofilm formed in the EVPL may be able to represent the antibiotic resistance phenotypes seen in the clinic. However this was not entirely caused by the biofilm structure as neither transposon mutant were more susceptible to meropenem treatment despite affecting biofilm formation. It was hypothesised that a *P. aeruginosa* biofilm that lacked structure (*gacA⁻*) or lack of biofilm formation (*pelA⁻*) may display increased meropenem susceptibility in the EVPL model. Previous studies have shown lack of *gacA* function in *P. aeruginosa* PA14 reduces antibiotic resistance *in vitro* (Parkins et al., 2001), but this was not the case in the EVPL model. The *pelA* mutant was not able to form a biofilm at all, however meropenem was still not bactericidal at 48 h at any concentrations tested. These results indicate that the biofilm is not the only important factor for antibiotic resistance in the CF lung. In fact, the microenvironment of the CF lung is now known to impact on the activity of antibiotics and can in part explain why differences are seen between patients. It has been found that the host environment factors including oxygen availability, iron availability, and mucus alter the resistance

profile of *P. aeruginosa* (Van den Bossche et al., 2021). The results suggest that the EVPL model is able to mimic some of these host interactions, supporting that the addition of EVPL bronchiolar tissue to SCFM drives *P. aeruginosa* into a chronic-state infection that displays reduced antibiotic susceptibility caused by a broad range of factors, as observed in the CF lung.

Future work in the model to investigate acute infection phenotypes should focus on earlier time points, even as early as 2 h where meropenem susceptibility was increased in biofilm associated transposon mutants. This may also provide insight into whether the EVPL model can mimic the *P. aeruginosa* switch from acute infection to chronic as seen in the CF lung, or if it enters a biofilm lifestyle upon infection. Additionally, the presence of other microbial species in the CF lung has an impact on *P. aeruginosa* and overall outcomes for quality of life and mortality. Incorporating these species alongside *P. aeruginosa* in the EVPL model would provide further understanding of these interactions during biofilm infection. More complex microscopy techniques such as scanning electron microscopy or fluorescence *in situ* hybridisation (FISH) would provide detail on the interspecies spatial interactions in the model.

3.4   Conclusion

Overall, I have shown that the EVPL model is able to drive *P. aeruginosa* into a chronic state of infection. *P. aeruginosa* PA14 formed a structured biofilm that displayed high meropenem resistance and reduced virulence by 2 d, maintained for a minimum of 7 d. Although the model does not reliably recapitulate the host immune response, the presence of pig bronchiolar tissue is able to mimic a *P. aeruginosa* biofilm infection reminiscent of chronic CF lung infection. Hence, the EVPL model is phenotypically relevant to study these infections. Therefore, I performed transcriptome analyses in the subsequent chapters to investigate the *P. aeruginosa* gene expression in the EVPL model to determine whether this was also indicative of chronic-like infection.

Chapter 4

Pseudomonas aeruginosa gene expression in the *ex vivo* pig lung model compared with *in vitro* synthetic cystic fibrosis sputum media growth

4.1 Introduction

P. aeruginosa infections in the CF lung are regarded as one of the most well studied biofilm infections within the field of medicine, however there are currently no treatments that are completely effective (Høiby et al., 2017). The biofilm structure, as explored in Chapter 3, is associated with complex cell-to-cell interactions that affect gene expression (Flemming et al., 2016). However, the lack of a laboratory model that recapitulates all the key aspects of *P. aeruginosa* chronic biofilm infection has caused limitations on research and treatment development (Cornforth et al., 2020; O'Toole et al., 2021).

There is a vast range of infection models to study CF lung infections, including live animal models, and *in vitro* systems and media. Artificial sputum media have been designed to mimic *in vivo* CF sputum, as well as epithelial cultures, and bead models. Each of these approaches to capture the CF lung environment have focused on different features but do not incorporate all infection characteristics. The difference between infection models and *in vivo* biofilm infection has led to RNA-seq research to determine which aspects of the chronic, biofilm-forming *P. aeruginosa* transcriptome is captured by different models (Cornforth et al., 2018; Rossi et al., 2018). This work has highlighted particular pathways that are not accurately replicated in the laboratory. The importance of the environment

P. aeruginosa is grown in for investigating key infection traits such as antimicrobial resistance (AMR), virulence, and persistence has been emphasised (Cornforth et al., 2018; Rossi et al., 2018; Kordes et al., 2019).

The increasing use of RNA-seq to study *P. aeruginosa* infection in the CF context, and to validate laboratory models, has led to a quantitative computational framework being developed to determine the accuracy of models, based on transcriptomic data (Cornforth et al., 2020). Briefly, it was shown that the *P. aeruginosa* transcriptome when grown in a revised version of the SCFM used with the EVPL model, referred to as SCFM2 (Turner et al., 2015), and an *in vitro* epithelial cell model were the most representative of CF sputum. Key *P. aeruginosa* metabolic pathways were found to be similarly expressed in both models to the CF lung, including fatty acid and phospholipid metabolism in epithelial cells, and nucleoside and nucleotide metabolism in SCFM2. Despite this, both models were still distinct from *in vivo P. aeruginosa* gene expression in a number of pathways. This was largely driven by distinct expression of genes associated with alginate production and QS. These pathways were found to be overexpressed *in vitro* compared with CF sputum (Cornforth et al., 2020).

Both pathways have been linked to virulence regulation and the persistence of *P. aeruginosa* infections in the CF lung (Winstanley and Fothergill, 2009; Kostylev et al., 2019). There are three *P. aeruginosa* QS systems that are involved in the regulation of a number of processes, including biofilm formation in human infection. These are the LasI/R and RhlI/R systems associated with AHL production, and the PQS associated with quinolone signalling molecules (Williams and Cámara, 2009; Mukherjee et al., 2017; Kostylev et al., 2019). *P. aeruginosa* expression of genes regulated by the *las* system specifically have been found to be a key point of distinction between CF sputum and *in vitro* growth conditions (Cornforth et al., 2018). The AHL encoded by the *las* system is 3-oxo-C12-HSL. It binds to the trancriptional regulator LasR to regulate the expression of multiple genes and pathways (Williams and Cámara, 2009).

These distinctions between the *P. aeruginosa* transcriptome in human infection and *in vitro* work is thought to have an impact on AMR. The lack of a representative lab model impacts the accuracy of diagnostics and drug development. This is associated with treatment plans guided by current antibiotic susceptibility testing methods often

having poor outcomes (Hurley et al., 2012). Cornforth et al. (2018) found that a number of AMR genes that were induced in human infection were not induced following *P. aeruginosa* antibiotic treatment *in vitro*, including the transcriptional regulator *mvaT*. This suggested that some key resistance mechanisms observed in human infection may be driven by the infection environment, which is not captured by standard lab media. This was hypothesised to be a potential explanation for why *P. aeruginosa* typically appears to be more sensitive to treatments *in vitro* than *in vivo* (Cornforth et al., 2018). It has been shown that *P. aeruginosa* grown in the EVPL model, associated with the tissue, is highly tolerant to antibiotic treatment in contrast with *in vitro* growth (Hassan et al., 2020; Sweeney et al., 2020b). Thus, the EVPL model has shown potential to more accurately mimic the AMR profile seen in human infection.

Overall, transcriptome analyses of *P. aeruginosa* in the CF lung and different research models has highlighted gaps in the current ability to reproduce CF-like infections in the laboratory. *P. aeruginosa* PA14 gene expression has been investigated in the EVPL model at different time points (24 h, 48 h, and 7 d) and compared with SCFM *in vitro* growth at 24 h and 48 h. The aim was to determine how *P. aeruginosa* gene expression differs when the pig lung tissue is added to SCFM, compared with SCFM alone. Hence, indicating the extent to which the EVPL model replicates *P. aeruginosa* gene expression in CF infection and potentially addresses some of the gaps observed in existing models. It was found that the EVPL model creates two *P. aeruginosa* growth environments with distinct transcriptomes: the lung tissue-associated biofilm and the surrounding SCFM population. These environments were also distinct from *P. aeruginosa* grown in SCFM *in vitro*. In particular, *P. aeruginosa* PA14 expression of QS-regulated genes and genes associated with antibiotic resistance in the lung-associated biofilm at 48 h, compared with *in vitro* SCFM, was similar to *P. aeruginosa* expression in CF sputum compared with *in vitro* conditions. This indicated that the EVPL model, particularly the pig lung tissue, cued *P. aeruginosa* gene expression that may be more representative of human infection than the current published models.

4.2   Results

All experiments in this chapter were performed on three replica tissue pieces from each of two independent pig lungs, per time point. For *in vitro* SCFM samples three repeats

were used per time point.

4.2.1 *P. aeruginosa* PA14 viability in the EVPL model for 7 days

The work in Chapter 3 showed *P. aeruginosa* PA14 grew in the EVPL model. The bacterial load was maintained for at least 7 d, and PA14 formed a mature biofilm phenotypically similar to CF lung infection. Therefore, 7 d was considered as a time point to include in RNA-seq analysis to investigate gene expression in a potentially more mature biofilm.

***P. aeruginosa* PA14 RNA was not consistently extracted from SCFM *in vitro* cultures after 7 days.**

RNA extractions were performed on 7 d EVPL *P. aeruginosa* PA14 biofilms and 7 d *in vitro* SCFM cultures, to identify whether RNA-seq was possible at this time point. No fresh media or lung tissue was added during the 7 d. The total RNA extracted from each of the *P. aeruginosa* PA14 lung samples was adequate for sequencing (Table 4.1). However as shown in Table 4.1, sufficient RNA could not be consistently extracted from the *in vitro* SCFM cultures. For four out of six samples no RNA was successfully extracted. This indicated that *P. aeruginosa* may not have been metabolically active at 7 d in SCFM *in vitro*, unlike the lung-associated biofilm.

Table 4.1: **The concentration of RNA (ng μl^{-1}) extracted from *Pseudomonas aeruginosa* PA14 *in vitro* synthetic cystic fibrosis sputum media (SCFM) cultures and PA14 infected *ex vivo* pig lung tissue pieces (Lung), following 7 d incubation at 37 °C**. RNA was extracted from six replica *in vitro* SCFM *P. aeruginosa* PA14 cultures and three *P. aeruginosa* PA14 infected lung tissue pieces from each of two independent lungs (lung 20 and lung 21). The total RNA was in an elution volume of 47 μl; final elution was in 50 μl but 3 μl was taken for concentration determination and RNA quality check. All RNA extractions for RNA sequencing were performed on samples from lung 20 and 21.

Environment	RNA concentration (ng μl^{-1})	Total RNA (ng)
SCFM	0	0
SCFM	0	0
SCFM	36.4	1710.8
SCFM	24.4	1146.8
SCFM	0	0
SCFM	0	0
Lung 20	27.4	1287.8
Lung 20	33.8	1588.6
Lung 20	25.8	1212.6
Lung 21	51.6	2425.2
Lung 21	14.2	667.4
Lung 21	60.2	2829.4

To visualise *P. aeruginosa* PA14 growing *in vitro* in SCFM to provide insight into whether the lack of RNA extracted at 7 d was caused by issues with the extraction method or lack of metabolic activity, Gram staining was performed. Gram staining of *in vitro* SCFM cultures at 48 h and 7 d was compared with Gram stain images of the PA14 biofilm associated with the EVPL tissue surface at both time points (Figure 4.1). *P. aeruginosa* PA14 did not visibly appear to be stressed in the lung-associated biofilm at 7 d and was comparable to cells at 48 h. There was an evident biofilm structure and clear rod shaped cells (Figure 4.1). However, the *in vitro* SCFM grown *P. aeruginosa* PA14, whilst rod-shaped at 48 h, appeared to become stressed by 7 d as the cells were a more rounded shape (Figure 4.1). This indicated that the RNA extraction protocol was not the problem. It was thus unlikely that an active PA14 population was maintained in SCFM alone for 7 d. RNA-seq of *P. aeruginosa* PA14 grown in SCFM *in vitro* for 7 d was therefore not performed, only 7 d lung samples.
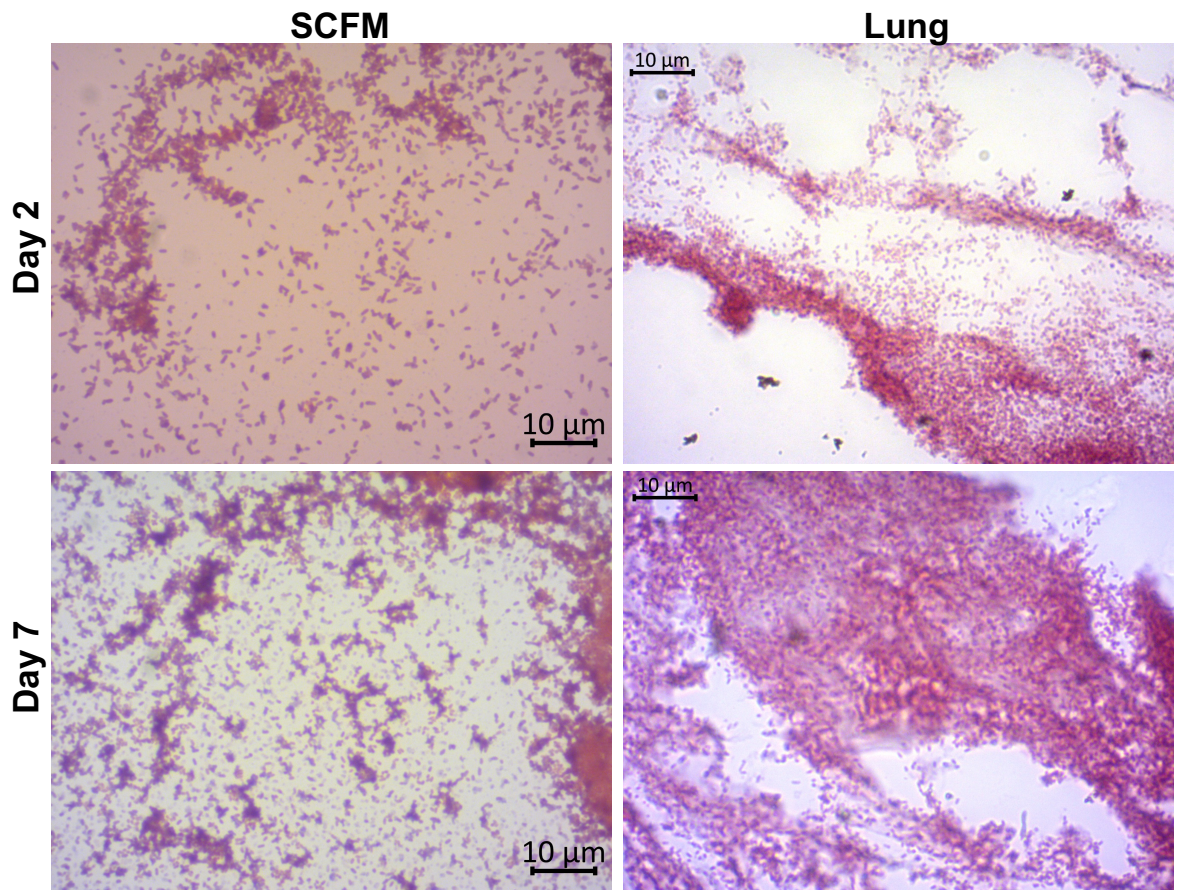
Figure 4.1: **Micrograph of Gram stained *Pseudomonas aeruginosa* PA14 grown in synthetic cystic fibrosis sputum media (SCFM) or *ex vivo* pig lung tissue sections (Lung) for 2 d and 7 d.** The lung images are also shown in Figure 3.11. All images were taken at x100 magnification.

P. aeruginosa PA14 cells remained viable in the EVPL-associated biofilm for 7 days.

Phenotypic analyses in Chapter 3 demonstrated that the *P. aeruginosa* PA14 biofilm associated with the EVPL tissue was maintained for 7 d; RNA was also successfully extracted at this time point. However, the viability of the bacterial cells in the biofilm was unknown. Prior to sequencing, a BacTiter-Glo™ microbial cell viability assay was performed to identify whether RNA-seq analysis of 7 d lung samples was of interest, or if cells were no longer viable. Viability was measured by the concentration of ATP produced. The assay was performed at initial infection (0 d) to measure the starting ATP concentration. Uninfected lung tissue was also included as a negative control for PA14 infection, to measure the ATP in the lung tissue. Measurements were subsequently taken at 24 h, 48 h, and 7 d (Figure 4.2). The CFU lung^{-1} was also calculated from each tissue piece to show bacterial growth alongside ATP production. Figure 4.2A shows that endogenous lung species grew in the uninfected tissue; these species were not seen for *P. aeruginosa* PA14 infected lung tissue. The CFU lung^{-1} of PA14 in infected tissue,

and endogenous species in the uninfected tissue was comparable at 7 d, however there was a higher concentration of ATP measured in *P. aeruginosa* infected samples (Figure 4.2B; means: 992.22 nM and 3.20 nM respectively). There was also an increase in ATP production from 48 h to 7 d in *P. aeruginosa* PA14 infected tissue (Figure 4.2). This indicated that there were *P. aeruginosa* PA14 cells still viable at 7 d in the lung-associated biofilm. The extracted RNA from the lung biofilm at 7 d was sequenced for analysis.

A. CFU lung^{-1}
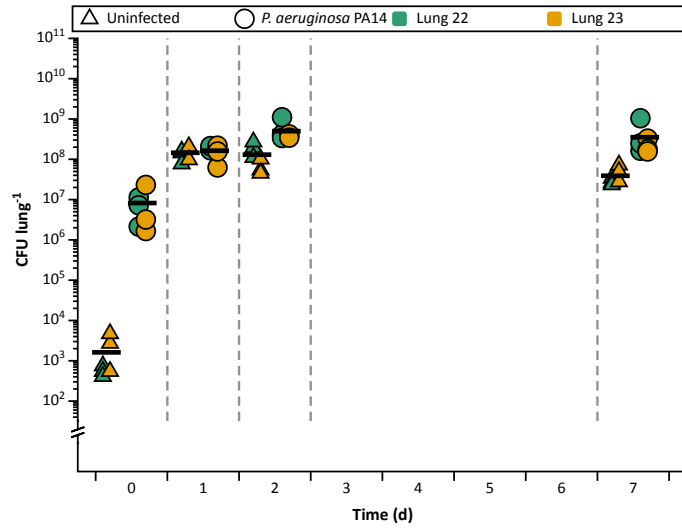
B. ATP concentration (nM)
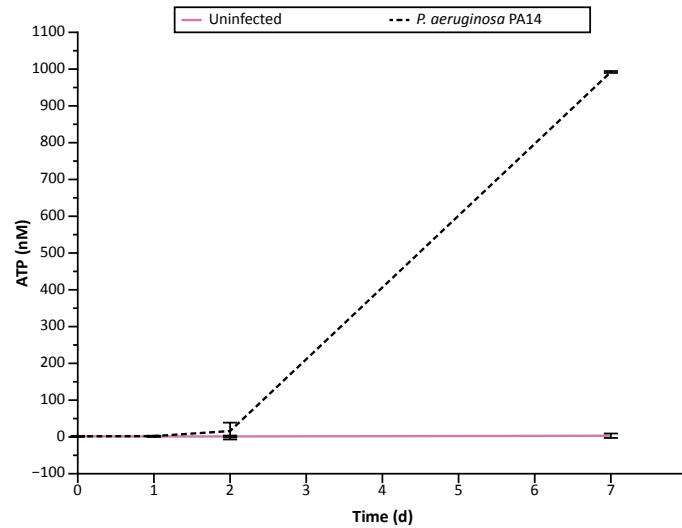
Figure 4.2: **Bacterial load and concentration of adenosine triphosphate (ATP) (nM) in *ex vivo* pig lung (EVPL) tissue samples at 0 d, 1 d, 2 d and 7 d.** Three replica tissue pieces from each of two independent pig lungs were infected with *Pseudomonas aeruginosa* PA14 for the time points tested. Uninfected tissue was also prepared as a negative control for PA14 infection. **(A)** Colony forming units (CFU) lung^{-1} for *P. aeruginosa* PA14 (circles) and endogenous bacterial species in uninfected tissue (triangles). These species were not detected on any of the PA14 infected tissue pieces. Each data point represents an EVPL tissue piece, and each lung is represented by different colours (see key). The horizontal lines show the mean and the y axes are log$_{10}$ scale. **(B)** The concentration of ATP (nM) present in each of the EVPL samples. The mean ATP concentration from six tissue pieces (three pieces each from two lungs) is shown for the *P. aeruginosa* PA14 (black, dashed line) and uninfected (purple, solid line) samples. Error bars represent the standard deviation.

4.2.2 *P. aeruginosa* PA14 transcriptome in the EVPL model and *in vitro* SCFM

P. aeruginosa PA14 gene expression was investigated in the two environments of the EVPL model to compare with *in vitro* SCFM growth at 24 h and 48 h. As well as the lung-associated biofilm, there was a *P. aeruginosa* PA14 population in the SCFM surrounding each tissue piece (surrounding SCFM). RNA was extracted from each EVPL environment individually to determine whether they were distinct *P. aeruginosa* PA14 populations or homogenous. The PA14 transcriptome in the lung and surrounding SCFM was compared with *P. aeruginosa* PA14 grown in SCFM *in vitro* at the two time points (24 h and 48 h). The RNA extracted from the infected lung samples at 7 d was also included in the analysis, as discussed.

P. aeruginosa PA14 bacterial load was consistent in all growth environments and PA14 RNA was successfully extracted and sequenced.

P. aeruginosa PA14 CFU lung^{-1} in the lung-associated biofilm and CFU ml^{-1} in the surrounding SCFM and *in vitro* SCFM was calculated. This was determined using representative repeats prepared alongside the RNA sequencing samples, from the same SCFM and lungs (Figure 4.3). The CFU was consistent between *in vitro* SCFM and lung-associated biofilm at 24 h and 48 h ($\sim 10^8$ - 10^9 CFU). The CFU lung^{-1} was maintained at 7 d in the lung-associated biofilm (Figure 4.3). In contrast, the CFU ml^{-1} in the surrounding SCFM was ~ 1 log$_{10}$ higher than both at 24 h and 48 h (Figure 4.3). However, the *P. aeruginosa* CFU in the three evironments, at all time points, was within the ranges of density and variability recovered from individuals with CF (Palmer et al., 2005), so were considered representative of *in vivo* bacterial load. Additionally, the LB agar plates used to determine CFU also confirmed *P. aeruginosa* PA14 infection by the distinct morphology and showed no endogenous species growth in any EVPL samples.
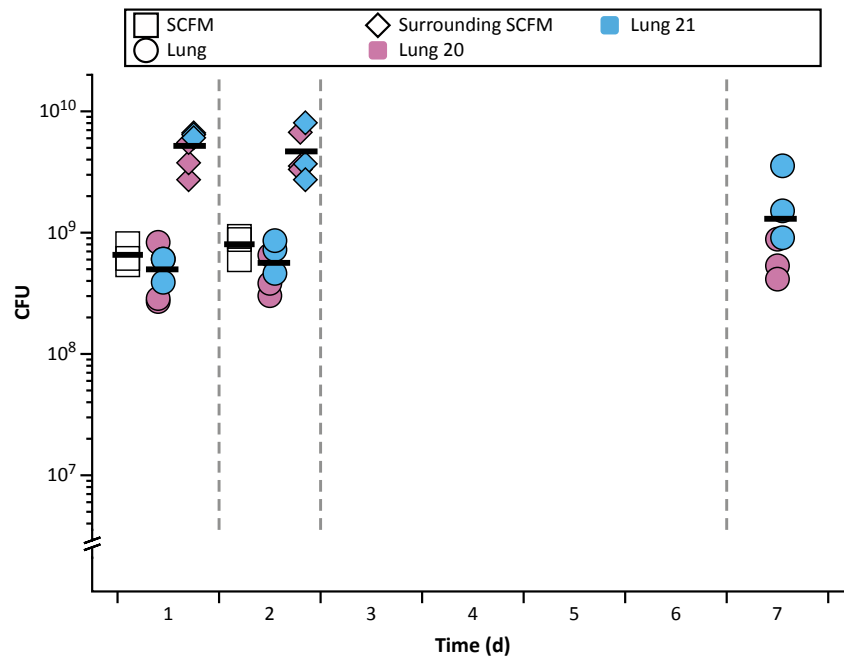
Figure 4.3: ***Pseudomonas aeruginosa* PA14 colony forming units (CFU) for samples prepared simultaneously to the samples RNA was extracted from.** Destructive sampling at 24 h, 48 h, and 7 d was performed for three *P. aeruginosa* PA14 infected *ex vivo* pig lung tissue pieces (Lung) and the surrounding synthetic cystic fibrosis sputum media (SCFM) (Surrounding SCFM), from each of two independent lungs. Three replica *in vitro* SCFM PA14 cultures (SCFM) were also prepared at each time point. The CFU lung^{-1} was calculated for the lung samples and CFU ml^{-1} calculated for the SCFM and surrounding SCFM samples. Each lung is represented by a different coloured data point and the different growth environments are shown by different shaped data points (see key). The y axis is log$_{10}$ scale and the horizontal lines represent the mean across all samples from each environment, at each time.

Following RNA extractions, sequencing and intial data preparation were performed. The sequencing statistics are shown in Appendix A (Table A.1). Reads from the EVPL samples (lung and surrounding SCFM) were aligned to the *Sus scrofa* genome to determine if any of the extracted RNA was from the pig lung tissue. As shown in Table 4.2, there were $\leq$ 1% of reads aligned to the pig genome in all EVPL samples (median 0.09%), which indicated that the RNA sequenced was predominantly microbial. Any reads that were mapped to the pig genome were removed, and all remaining reads and *in vitro* SCFM reads were aligned to the *P. aeruginosa* PA14 genome. The majority of reads in each sample were successfully aligned (median 98.9%). This showed that the RNA extracted was mainly *P. aeruginosa* PA14 (Table 4.2); it was considered unlikely that there was a large population of metabolically active endogenous microbes in the PA14 infected EVPL tissue.

Table 4.2: **The percentage of RNA sequencing reads aligned to the pig (*Sus scrofa*) genome or *Pseudomonas aeruginosa* PA14 genome.** RNA was sequenced from *ex vivo* pig lung tissue samples (Lung) and the synthetic cystic fibrosis sputum media surrounding each tissue piece (Surrounding SCFM), from three tissue pieces from each of two independent lungs at 24 h, 48 h, and 7 d. The reads from both environments were first aligned to the pig genome; reads that did not align were then aligned to the PA14 genome. The percentage of reads aligned to each genome are shown. RNA was also extracted from three *in vitro* SCFM cultures (SCFM) at each time point. The reads were aligned to just the *P. aeruginosa* PA14 genome and the percentage of reads aligned are shown. Each row represents an individual sample.

Environment	Time (d)	Aligned to pig (%)	Aligned to PA14 (%)
SCFM	1		95.30
SCFM	1		98.39
SCFM	1		99.30
SCFM	2		99.58
SCFM	2		98.88
SCFM	2		99.36
Lung 20	1	0.32	98.30
Lung 20	1	0.23	99.76
Lung 20	1	0.19	99.46
Lung 21	1	0.37	96.17
Lung 21	1	0.25	93.19
Lung 21	1	0.35	95.34
Lung 20	2	0.08	99.47
Lung 20	2	0.08	99.46
Lung 20	2	0.09	98.83
Lung 21	2	0.07	98.17
Lung 21	2	0.03	99.25
Lung 21	2	0.19	96.86
Lung 20	7	0.06	99.70
Lung 20	7	0.08	99.13
Lung 20	7	0.07	98.28
Lung 21	7	0.06	98.65
Lung 21	7	0.06	99.52
Lung 21	7	0.02	99.10
Surrounding SCFM (Lung 20)	1	0.12	99.39
Surrounding SCFM (Lung 20)	1	0.87	97.56
Surrounding SCFM (Lung 20)	1	0.39	98.57
Surrounding SCFM (Lung 21)	1	0.27	97.57
Surrounding SCFM (Lung 21)	1	0.16	97.84

Table 4.2 – continued from previous page

Environment	Time (d)	Aligned to pig (%)	Aligned to PA14 (%)
Surrounding SCFM (Lung 21)	1	1.04	94.61
Surrounding SCFM (Lung 20)	2	0.02	99.56
Surrounding SCFM (Lung 20)	2	0.08	99.27
Surrounding SCFM (Lung 20)	2	0.02	99.61
Surrounding SCFM (Lung 21)	2	0.08	98.71
Surrounding SCFM (Lung 21)	2	0.09	99.06
Surrounding SCFM (Lung 21)	2	0.10	98.92

The *P. aeruginosa* PA14 transcriptome revealed two distinct niches in the EVPL model, both distinct from *in vitro* SCFM growth.

Following quality control (Appendix A; Figure A.1), principal component analysis (PCA) of the expression of all considered genes (n = 5829) was used to investigate whether growth environment and infection time caused distinctions in the *P. aeruginosa* PA14 transcriptome. Figure 4.4 shows that PA14 in the lung-associated biofilm and surrounding SCFM had distinct expression profiles from each other, and also from *in vitro* SCFM. The changes in expression over time were also different in the EVPL environments compared with SCFM *in vitro*. There was a shift in the first two principal components from 24 h to 48 h in the lung and surrounding SCFM in opposing directions to the shift observed for *in vitro* SCFM grown *P. aeruginosa* PA14 (Figure 4.4). Expression at 7 d in the lung biofilm appeared to be similar to the lung-associated biofilm at 48 h.
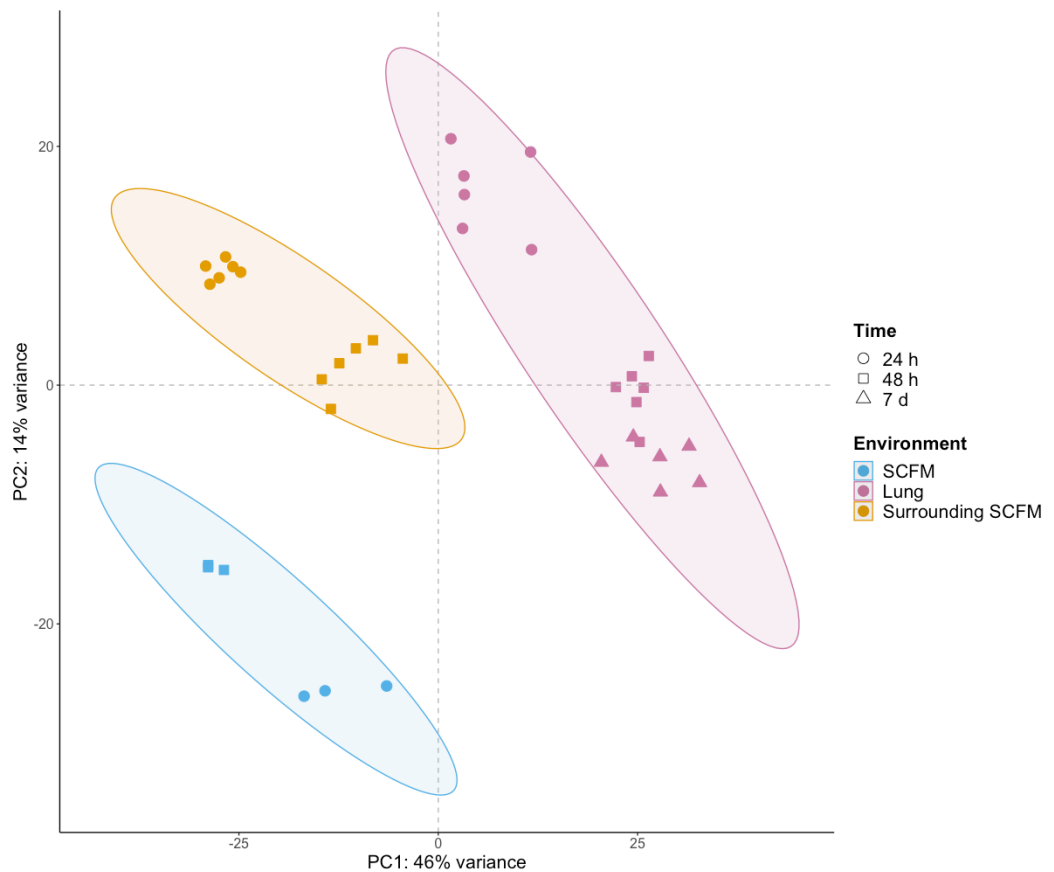
Figure 4.4: **Principal component analysis (PCA) plot of the *Pseudomonas aeruginosa* PA14 transcriptome, considering all genes (n = 5829), in the *ex vivo* pig lung (EVPL) model and synthetic cystic fibrosis sputum media (SCFM) *in vitro*.** RNA was sequenced from the 3 environments *P. aeruginosa* PA14 was grown in: *in vitro* SCFM (SCFM), and the two niches of the EVPL model (Lung and the Surrounding SCFM). Three replica *P. aeruginosa* PA14 cultures were sequenced at 24 h and 48 h from *in vitro* SCFM and three repeats from each of two independent lungs were sequenced at 24 h and 48 h from EVPL niches. *P. aeruginosa* PA14 infected lung tissue samples grown for 7 d were also sequenced. Each environment is shown by different colour data points and each time point is a different shaped data point (see key). The 95% confidence ellipses are shown.

Pearson's correlation coefficient analysis and hierarchical clustering, visualised in Figure 4.5, confirmed that the RNA-seq was a good quality as the Pearson's correlation coefficient (*r*) was > 0.9 for all comparisons. This was expected as all samples were the same strain: *P. aerugniosa* PA14, if the *r* value had been smaller it would indicate potential issues with the data. Hierarchical clustering analysis showed that the there was a distinction between the lung-associated biofilm at 48 h and 7 d, and all other samples (Figure 4.5). Pearson's correlation coefficient analysis provided further detail. It indicated that the greatest difference was between the lung biofilm at these two later time points, and all *in vitro* SCFM samples (24 h and 48 h) and the surrounding SCFM population at 24 h.
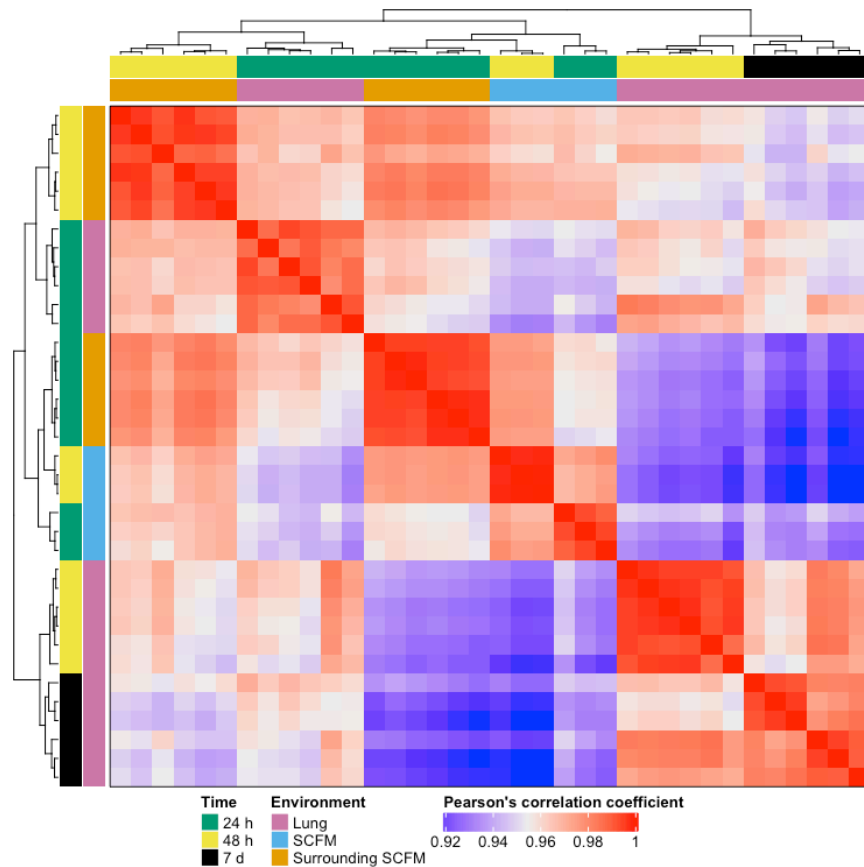
Figure 4.5: **Hierarchical clustering heatmap showing the Pearson's correlation coefficient values between** *Pseudomonas aeruginosa* **PA14 transcriptomes in the** *ex vivo* **pig lung (EVPL) model and synthetic cystic fibrosis sputum media (SCFM)** *in vitro*. *P. aeruginosa* PA14 RNA was extracted from *in vitro* SCFM cultures (SCFM: blue) at 24 h and 48 h, PA14 infected EVPL tissue pieces (Lung: pink) at 24 h, 48 h, and 7 d, and the EVPL surrounding SCFM (Surrounding SCFM: orange) at 24 h and 48 h. Three replica *in vitro* cultures were sampled at each time point and three EVPL tissue pieces from each of two independent lungs were used for the EVPL environments. Hierarchical clustering is shown on the left and top of the heatmap, and the samples are colour coded based on growth environment and infection time (see key). The heatmap shows the Pearson's correlation coefficient values on a blue to red scale (see key).

These analyses showed *P. aeruginosa* PA14 growth in the EVPL model resulted in clear differences in gene expression compared with *in vitro* SCFM growth. There was also a distinct difference between the lung-associated biofilm and surrounding SCFM populations. Further analyses of *P. aeruginosa* gene expression in the EVPL environments compared with *in vitro* SCFM growth were subsequently performed at 24 h and 48 h, to provide more information about these differences. The 7 d lung-associated biofilm transcriptome was explored in Chapter 5.

4.2.3 Differentially expressed *P. aeruginosa* PA14 genes in the EVPL model compared with *in vitro* SCFM and their functional importance

Gene expression in the lung-associated *P. aeruginosa* PA14 biofilm became more distinct from *in vitro* SCFM growth at 48 hours.

Differential expression analysis was performed to determine the significant differentially expressed genes (DEGs) for *P. aeruginosa* PA14 in the lung-associated biofilm compared with *in vitro* SCFM, and the surrounding SCFM compared with *in vitro* SCFM, at 24 h and 48 h ($P < 0.05$, log$_2$ fold change $\geq |1.5|$). There were a number of significant DEGs found for each contrast, some shared in the lung biofilm and surrounding SCFM population, and some unique (Figure 4.6).
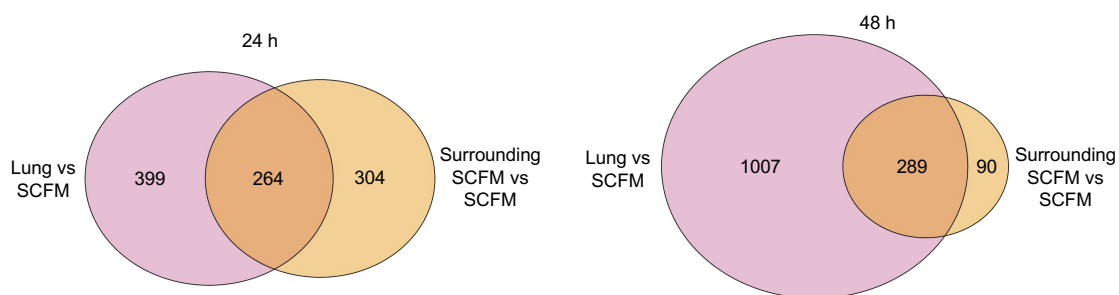
Figure 4.6: **Venn diagrams of the number of significant *Pseudomonas aeruginosa* PA14 differentially expressed genes (DEGs) for *ex vivo* pig lung (EVPL) model environments compared with *in vitro* synthetic cystic fibrosis sputum media (SCFM) at 24 h and 48 h.** Differential expression analysis was performed on three *in vitro* SCFM (SCFM) repeats and three repeats from each of two independent lungs for the EVPL environments: the lung-associated biofilm (Lung) and SCFM surrounding each tissue piece (Surrounding SCFM), per time point. The genes were considered significant if the log$_2$ fold change was $\leq$ -1.5 or $\geq$ 1.5, and $P < 0.05$. The shared genes at each time point were either overexpressed or underexpressed in both the lung and surrounding SCFM versus *in vitro* SCFM. Genes that were significant in both contrasts at each time point, but in opposing directions, were not considered shared.

At 24 h, a similar number of significant DEGs were found in the lung-associated biofilm and surrounding SCFM (663 and 568 genes respectively); 264 were shared in the same direction of expression (i.e. overexpressed in both contrasts or underexpressed in both). The number of shared DEGs in the same direction of expression at 48 h was comparable to 24 h (289), however there was a clear difference in the total number of significant DEGs in each contrast (Figure 4.6). There was an increase in the overall number of significant DEGs in the lung-associated biofilm compared with *in vitro* SCFM at 48 h (1296 genes). In contrast, the total number of significant DEGs in the surrounding SCFM compared

with *in vitro* SCFM decreased from 24 h to 48 h (568 and 379 genes respectively). This showed that as well as there being unique genes significantly differentially expressed at each time point in each environment, this distinction increased as *P. aeruginosa* PA14 established a biofilm associated with the lung tissue. It indicated that the dynamics of *P. aeruginosa* gene expression differences between *in vitro* growth and the two EVPL environments changed from 24 h to 48 h (Figure 4.6). As the biofilm established on the lung tissue, the PA14 population became more distinct from *in vitro* SCFM growth, whereas the surrounding SCFM population appeared to become more similar.

P. aeruginosa PA14 genes with the greatest difference in expression compared with *in vitro* SCFM growth were different in the lung-associated biofilm and surrounding SCFM.

The list of DEGs was then investigated and Table 4.3 shows the five significant DEGs in each contrast with the greatest $\log_2$ fold change in expression in each direction (i.e. overexpressed or underexpressed). These genes were not the same at 24 h and 48 h in the lung-associated biofilm or surrounding SCFM. There was also a difference in the genes found in the lung and surrounding SCFM, with the exception of genes most underexpressed at 24 h. As shown in Table 4.3, four out of the five most underexpressed genes in the lung biofilm compared with *in vitro* SCFM at 24 h were also in the list of most underexpressed genes in the surrounding SCFM at 24 h. This supported the results in Figure 4.6, which showed *P. aeruginosa* PA14 expression in the lung and surrounding SCFM may be more similar at 24 h than 48 h.

Table 4.3: **The five *Pseudomonas aeruginosa* PA14 significant differentially expressed genes (DEGs) with the greatest log$_2$ fold change (LFC) increase in the *ex vivo* pig lung (EVPL) environments compared with *in vitro* synthetic cystic fibrosis sputum media (SCFM) at 24 h and 48 h, and the five genes with the biggest LFC decrease.** RNA sequencing was performed on three replicate *in vitro* SCFM PA14 cultures (SCFM) grown for 24 h and 48 h, and three samples from each of two independent lungs from EVPL environments: the lung-associated biofilm (Lung) and SCFM surrounding each tissue piece (Surrounding SCFM) at 24 h and 48 h. DEGs were considered significant if the LFC compared with *in vitro* SCFM was ≤ -1.5 or ≥ 1.5, and *P* < 0.05. The locus tag, gene name and LFC value is shown for each gene in each contrast.

Contrast	Overexpressed			Underexpressed		
	Locus tag	Gene name	LFC	Locus tag	Gene name	LFC
24 h: Lung vs SCFM	PA14_49200	*oprH*	4.63	PA14_38850	*exaB*	-6.79
	PA14_52340		4.56	PA14_38860	*exaA*	-6.56
	PA14_49180	*phoP*	4.49	PA14_38880		-6.52
	PA14_49170	*phoQ*	4.37	PA14_64530		-6.44
	PA14_46900		4.25	PA14_38900		-6.37
48 h: Lung vs SCFM	PA14_37990		6.30	PA14_ 39945	*phzC2*	-5.68
	PA14_52340		6.18	PA14_21530		-5.60
	PA14_38190		5.08	PA14_09450	*phzD1*	-5.51
	PA14_18070		4.91	PA14_20960		-5.46
	PA14_07480		4.85	PA14_39910	*phzE2*	-5.40
24 h: Surrounding SCFM vs SCFM	PA14_06960		4.46	PA14_38850	*exaB*	-6.98
	PA14_05840	*gcdH*	4.19	PA14_38860	*exaA*	-6.69
	PA14_18070		4.16	PA14_38880		-6.53
	PA14_13170		3.95	PA14_38900		-6.11
	PA14_35240		3.94	PA14_38840		-5.19
48 h: Surrounding SCFM vs SCFM	PA14_18070		5.06	PA14_35240		-5.47
	PA14_38310		3.57	PA14_63920	*cntM*	-5.26
	PA14_13170		3.54	PA14_09950		-5.03
	PA14_32140	*antC*	3.36	PA14_73060		-4.94
	PA14_37590	*kynB*	3.23	PA14_63960	*cntO*	-4.72

The majority of the most overexpressed genes in the lung-associated biofilm at 24 h compared with *in vitro* SCFM were associated with the PhoP-PhoQ two component regulatory system (Table 4.3). Both *phoP* and *phoQ* were significantly overexpressed in the lung biofilm, as well as the porin gene *oprH*. The three genes are known to form an operon positively regulated by *phoP*, associated with increased polymyxin resistance (Chevalier et al., 2017; Yang et al., 2021). The other two genes, PA14_52340 and PA14_46900, are regulated by the PhoP-PhoQ system (Yang et al., 2021). PA14_52340

was the only gene found to be one of the five most overexpressed genes in the lung-associated biofilm at both 24 h and 48 h. However, unlike 24 h, there was no clear pattern or pathway differences in the genes most overexpressed at 48 h (Table 4.3). Only one gene was in the list of greatest overexpression in both environments: PA14_18070. There was a 4.16 $\log_2$ fold change in the surrounding SCFM at 24 h and 5.06 $\log_2$ fold change at 48 h compared with *in vitro* SCFM. There was also a 4.91 $\log_2$ fold change in the lung-associated biofilm contrast at 48 h (Table 4.3)). This gene is associated with increased antibiotic resistance (Dötsch et al., 2009). The majority of other most overexpressed genes in the surrounding SCFM at 24 h and 48 h were associated with metabolism, including *antC* and *kynB* (Table 4.3). Both genes are involved in the anthranilate metabolic pathway, which is linked to biofilm formation and PQS production (Costaglioli et al., 2012).

As described, there were more similarities in the most five underexpressed genes in the lung-associated biofilm and surrounding SCFM than the overexpressed genes, particularly at 24 h. The four shared most underexpressed genes found are involved in ethanol oxidation, including the *exaA* and *exaB* promoters (Görisch, 2003). PA14_38900 was also found to be highly underexpressed in both environments at 24 h (Table 4.3). It is a response regulator gene involved in ethanol oxidation that has been shown to play a role in antibiotic resistance linked with biofilm formation (Francis et al., 2017). This suggested the pathway was being downregulated in both EVPL environments compared with *in vitro* SCFM at 24 h. At 48 h, none of the most underexpressed genes in the lung biofilm were shared with the surrounding SCFM (Table 4.3). This supported the previous hypothesis that 48 h was the time point where *P. aeruginosa* PA14 expression in the two EVPL environments became more distinct.

The majority of the most underexpressed genes in the *P. aeruginosa* PA14 lung-associated biofilm compared with *in vitro* SCFM growth at 48 h were part of the phenazine biosynthesis pathway (Table 4.3). Expression of PA14_20960 was also found to be greatly reduced, by 5.46 $\log_2$ in the lung biofilm. This indicated that the gene may have been important for *P. aeruginosa* adaptation to the lung tissue. However, there is no known function for this gene and the gene product is uncharacterised. The most underexpressed genes in the surrounding SCFM compared with *in vitro* SCFM included a different set of genes than the lung biofilm contrast at 48 h. A number of these are part of the *cnt* operon

(Table 4.3). CntO is an outermembrane transporter and CntM is an enzyme, both involved in the biosynthesis and transportation of the metallophore pseudopaline (Gomez et al., 2021). Although not in the list of the five most underexpressed genes in the lung at 48 h, both *cntM* and *cntO* were also significantly underexpressed in lung-associated biofilm compared with *in vitro* SCFM (-4.92 and -4.69 log$_2$ fold change respectively).

The gene expression differences between *P. aeruginosa* PA14 in the two EVPL environments and *in vitro* SCFM have functional importance.

The functional importance of the significant DEGs in each contrast was then studied by investigating pathways that were significantly enriched. These were pathways where more significant DEGs in the contrast were attributed to a pathway than would occur by chance, thus indicating there was an effect on expression of the pathway overall. KEGG pathway enrichment analysis was initially performed to identify significantly enriched KEGG pathways ($P < 0.05$). Figure 4.7 shows all KEGG pathways that were significantly enriched in each contrast. There were a number of pathways enriched in both the lung-associated biofilm and surrounding SCFM compared with *in vitro* SCFM at 24 h, including quorum sensing. The majority of significant genes in each of these pathways were underexpressed, indicating these pathways were downregulated. However, glyoxylate and dicarboxylate metabolism appeared to be upregulated in the surrounding SCFM and downregulated in the lung biofilm (Figure 4.7), indicating a difference between the two EVPL environments.
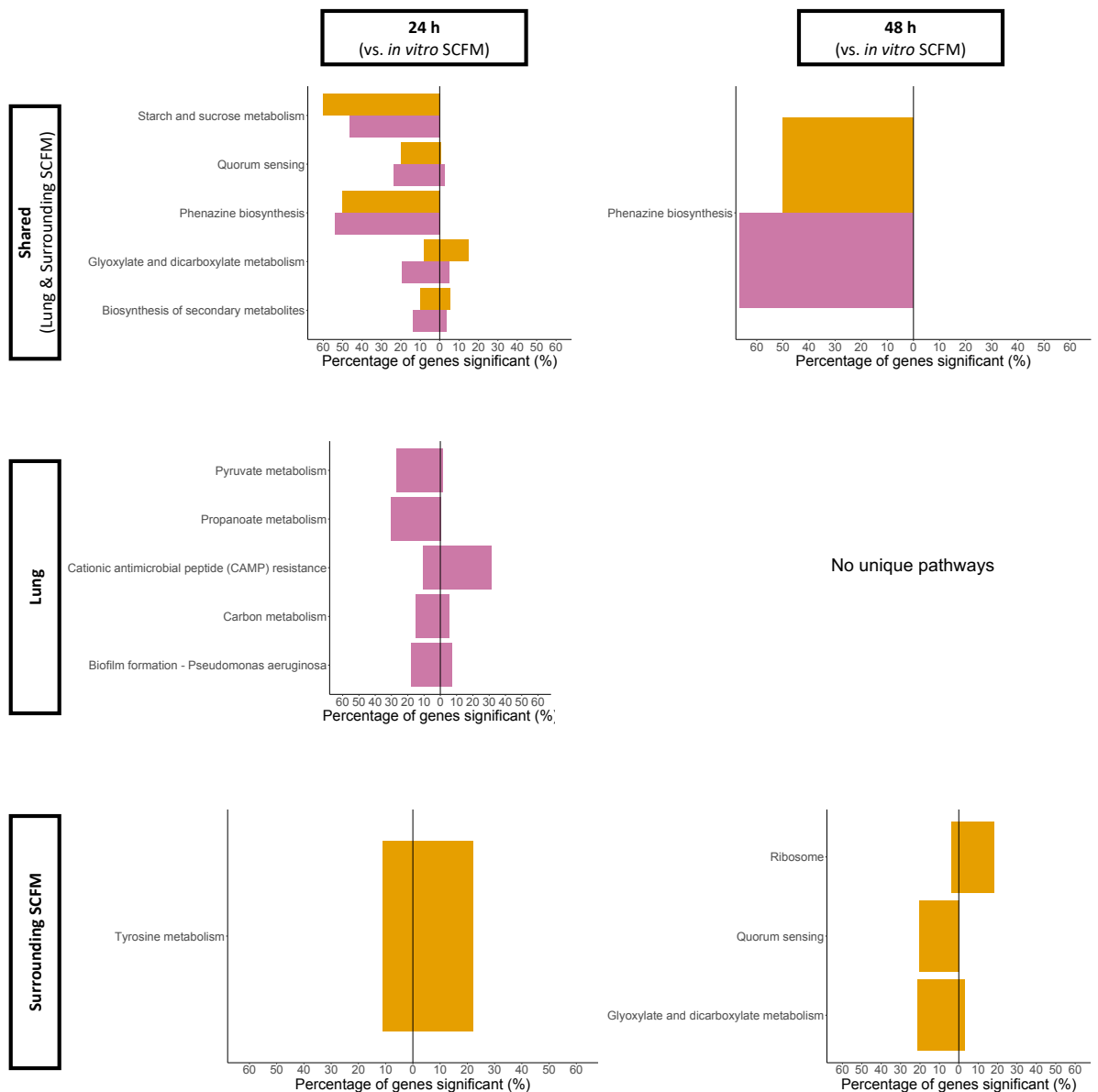
Figure 4.7: **Significantly enriched (*P* < 0.05) *Pseudomonas aeruginosa* PA14 Kyoto encyclopedia of genes and genomes (KEGG) pathways in the *ex vivo* pig lung tissue-associated biofilm (Lung) or surrounding synthetic cystic fibrosis sputum media (SCFM) (Surrounding SCFM) compared with *in vitro* SCFM growth (SCFM) at 24 h and 48 h.** The bar charts show the percentage of genes associated with each KEGG pathway that were significantly differentially expressed in the contrast (log$_2$ fold change $\geq$ |1.5|, *P* < 0.05). Three SCFM repeats and three repeats from each of two independent lungs for lung and surrounding SCFM were used to perform analysis. The percentage of genes to the left of the vertical lines (x = 0) were underexpressed in the lung or surrounding SCFM and percentage of genes to the right were overexpressed, compared with *in vitro* SCFM. The shared graphs are significantly enriched pathways in both contrasts at each time point and individual graphs show enriched pathways unique to that contrast. The lung contrasts are represented by purple bars (bottom in shared) and the surrounding SCFM by orange bars (top in shared).

There were five significantly enriched KEGG pathways unique to the lung-associated biofilm at 24 h; these included cationic antimicrobial resistance which appeared to be upregulated, and biofilm formation where there were genes upregulated (7.21% genes)

and downregulated (18.02% genes) (Figure 4.7). Tyrosine metabolism was the only pathway uniquely enriched in the surrounding SCFM at 24 h, and most associated genes were overexpressed (Figure 4.7). At 48 h, fewer enriched KEGG pathways were identified overall. The only pathway significantly enriched in both the lung biofilm and surrounding SCFM compared with *in vitro* SCFM was phenazine biosynthesis. This pathway was also significantly enriched at 24 h in both EVPL environments, downregulated in comparison with *in vitro* SCFM (Figure 4.7). These results indicated that downregulation of phenazine biosynthesis was a key distinction between EVPL model and *in vitro* growth. Genes associated with this pathway were also in the list of most underexpressed genes in the lung-associated biofilm at 48 h (Table 4.3). There were no unique, significantly enriched pathways in the lung-associated biofilm at 48 h, although three pathways were only significantly enriched in the surrounding SCFM. These included quorum sensing and glyoxylate and dicarboxylate metabolism, also enriched at 24 h (Figure 4.7). This analysis suggested that the significant DEGs found for each contrast had a functional context that may result in differing phenotypes compared with *in vitro* SCFM growth.

To further investigate these functional differences, the more detailed gene ontology (GO) term analysis was performed ($P < 0.05$), as KEGG pathway enrichment analysis found less significant pathways at 48 h despite there being more overall DEGs. The signficantly enriched *P. aeruginosa* PA14 biological process GO terms were studied to provide detailed information on pathways affected by EVPL growth compared with *in vitro* SCFM (Figure 4.8). The number of significantly enriched GO terms was higher at 48 h in the lung-associated biofilm compared with *in vitro* SCFM (Figure 4.8C) than at 24 h (Figure 4.8A). In contrast, the number of significantly enriched GO terms in the surrounding SCFM compared with *in vitro* SCFM at 48 h (Figure 4.8D) was smaller than at 24 h (Figure 4.8B). This supports the previous hypothesis that lung-associated growth caused increased *P. aeruginosa* PA14 transcriptome differences from *in vitro* SCFM between 24 h and 48 h. In contrast, differences between gene expression in the surrounding SCFM population and *in vitro* SCFM appeared to decrease over time.
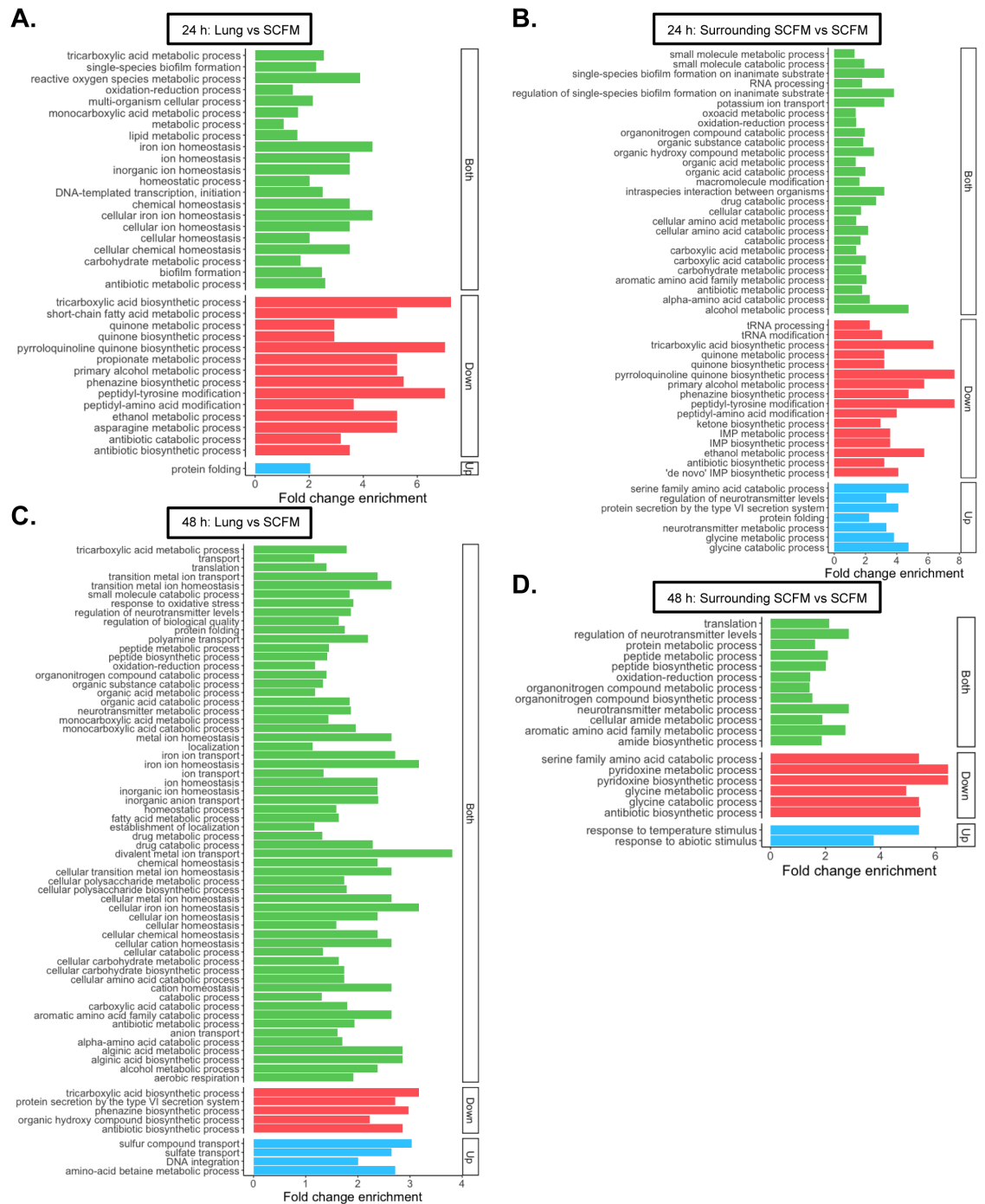
Figure 4.8: **Significantly enriched (*P* < 0.05) *Pseudomonas aeruginosa* PA14 biological processes gene ontology (GO) terms in the *ex vivo* pig lung tissue-associated biofilm (Lung) or surrounding synthetic cystic fibrosis sputum media (SCFM) (Surrounding SCFM), compared with *in vitro* SCFM growth (SCFM) at 24 h and 48 h.** Each bar graph shows the fold change enrichment (x axis) for each significantly enriched GO term, determined from the significant differentially expressed genes (DEGs) associated with each term ($\log_2 \geq |1.5|$, *P* < 0.05) in the contrasts. Fold change enrichment is the fold difference in the number of DEGs found for each term than expected by chance. Three SCFM repeats and three repeats from each of two independent lungs for lung and surrounding SCFM were used to perform analysis. The green bars represent GO terms where the associated significant DEGs were underexpressed and overexpressed (both) showing that the process was affected irrespective of the direction of expression. Red bars show GO terms where all significant DEGs were underexpressed compared with *in vitro* SCFM (down), and blue bars show GO terms where all the significant DEGs were overexpressed compared with *in vitro* SCFM (up).

The oxidation-reduction process was found to be significantly enriched in all contrasts, consistent with the underexpression of ethanol oxidation genes found in the list of most DEGs in both EVPL environments at 24 h (Table 4.3). This further supported the hypothesis that growth environment had an effect on ethanol oxidation. The GO term 'response to abiotic stimulus' was one of the terms significantly enriched in the surrounding SCFM versus *in vitro* SCFM at 48 h ($P = 0.04$, Figure 4.8). All genes were overexpressed indicating the process was upregulated. It was not significantly enriched in the lung comparisons at either time point. This response may have been caused by *P. aeruginosa* PA14 interaction with the SCFM-agarose pad, put in the base of each tissue culture plate well to support the lung tissue, at the interface with the surrounding SCFM. As the same tissue culture plates were used to grow PA14 in SCFM *in vitro*, the plate was unlikely to be the cause of expression differences. This indicated that the surrounding SCFM *P. aeruginosa* PA14 population may have been less *in vivo*-like than the lung-associated biofilm at 48 h, which was becoming more distinct from *in vitro* SCFM growth.

The phenazine biosynthetic process term was significantly enriched in the lung-associated biofilm at 24 h and 48 h, and surrounding SCFM at 24 h (Figure 4.8). This was consistent with the KEGG pathway 'phenazine biosynthesis' found to be enriched (Figure 4.7). These results further indicated that the distinction of the lung-associated biofilm and 24 h surrounding SCFM population compared with *in vitro* SCFM growth may have been largely associated with phenazine biosynthesis differences. Further investigation of this pathway revealed that all genes in the pathway for production of the phenazine exotoxin pyocyanin were significantly underexpressed in the lung biofilm at 48 h compared with *in vitro* SCFM (Figure 4.9). This pathway map for the other significant contrasts is shown in Appendix A (Figure A.2).
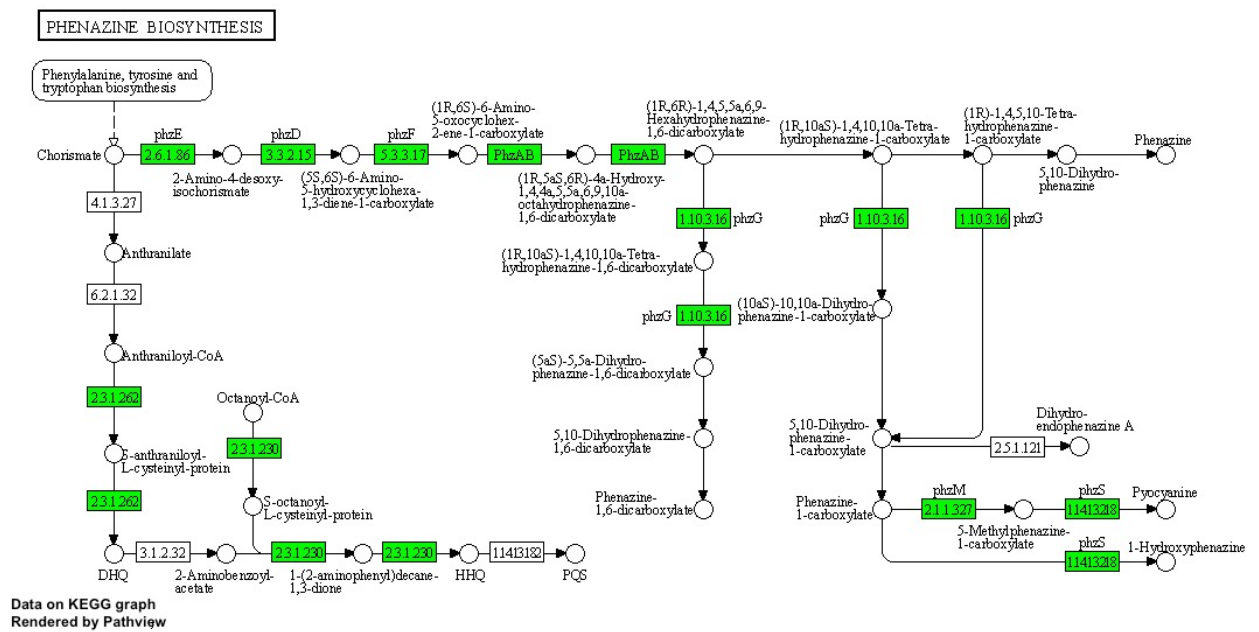
Figure 4.9: **The Kyoto encyclopedia of genes and genomes (KEGG)** *Pseudomonas aeruginosa* **PA14 phenazine biosynthesis pathway.** Genes that were significantly underexpressed ($\log_2$ fold change $\leq$ |-1.5|, $P < 0.05$) in the *P. aeruginosa* PA14 lung-associated biofilm compared with *in vitro* synthetic cystic fibrosis sputum media growth at 48 h are highlighted in green. No genes in the pathway were found to be significantly overexpressed in this contrast.

4.2.4 Differences in quorum sensing gene expression in the EVPL model compared with *in vitro* SCFM

The QS KEGG pathway was found to be significantly enriched in the surrounding SCFM and lung-associated biofilm at 24 h (Figure 4.7). The majority of the significant DEGs were underexpressed in the EVPL environments compared with SCFM *in vitro* growth, indicating the pathway was downregulated. QS is a key aspect of *P. aeruginosa* infection in CF, involved in biofilm establishment (Davies et al., 1998). It is also a pathway where *P. aeruginosa* expression has been shown to differ *in vitro* from CF sputum (Cornforth et al., 2018). Taking this into account, alongside QS being a potential novel therapeutic target (Scoffone et al., 2019; Defoirdt, 2018), QS associated gene expression was further investigated in the EVPL and *in vitro* SCFM contrasts. The aim was to determine whether the EVPL model environments could recapitulate the *P. aeruginosa* expression of QS genes seen in human infection.

Quorum sensing genes were downregulated in the *P. aeruginosa* PA14 lung-associated biofilm at 48 hours.

Table 4.4 shows all genes in the QS KEGG pathway that were significant DEGs in at least one contrast, and the $\log_2$ fold change in expression is shown where significant. The full table is shown in Appendix A (Table A.2). The majority of significant genes were underexpressed in the lung or surrounding SCFM compared with *in vitro* SCFM, most part of the phenazine biosynthesis operons. This supported the hypothesis that phenazine biosynthesis was a major distinction between *P. aeruginosa* PA14 grown in SCFM *in vitro* and the EVPL model. There was a greater reduction in expression of these genes in the lung-associated biofilm compared with SCFM *in vitro* than in the surrounding SCFM population, at both time points (Table 4.4). One of the few genes overexpressed in the EVPL model was a membrane-associated zinc metalloprotease in the lung-associated biofilm at 48 h (1.94 $\log_2$ fold change). This was consistent with the most DEGs list that indicated zinc availability was playing a role in the distinction between growth environments. Of the significantly overexpressed QS genes, two are involved in the production of PQS: *pqsC* and *pqsD*. This difference was found in the lung-associated biofilm at 48 h but significant differential expression of these genes was not observed in any of the other contrasts (Table 4.4). This indicated that this QS system (PQS) was downregulated from 24 h to 48 h in the lung biofilm compared with SCFM *in vitro*.

Table 4.4: ***Pseudomonas aeruginosa* PA14 genes in the quorum sensing Kyoto encyclopedia of genes and genomes (KEGG) pathway that were significantly differentially expressed in at least one contrast between the *ex vivo* pig lung (EVPL) environments and *in vitro* synthetic cystic fibrosis sputum media (SCFM) at 24 h or 48 h.** Differential expression analysis was performed on three replica *in vitro* SCFM cultures (SCFM) and three repeats from each of two independent lungs from the EVPL environments: the lung-associated biofilm (Lung) and the SCFM surrounding each tissue piece (Surrounding SCFM), at each time point. Genes were considered significant if the $\log_2$ fold change was $\leq$ -1.5 or $\geq$ 1.5 compared with *in vitro* SCFM and P < 0.05. The significant $\log_2$ fold change values are shown in the table. Contrasts where the gene was not significantly differentially expressed are denoted with '-'. The orange fill shows genes that were underexpressed in the EVPL environments, the darker the colour representing a higher $\log_2$ fold change. The green fill represents overexpressed genes, with bold and italicised font.

Locus tag	Gene name	Gene product	24 h Lung	48 h Lung	24 h Surrounding SCFM	48 h Surrounding SCFM
PA14_02720			-	-	-1.51	-
PA14_09050	*secY*	Preprotein translocase subunit SecY	-	*1.94*	-	-
PA14_09410	*hfq*	RNA-binding protein Hfq	-3.90	-4.38	-1.97	-2.55
PA14_09420	*phzF1*	Phenazine biosynthesis protein	-5.48	-4.90	-2.98	-3.07
PA14_09440	*phzE1*	Phenazine biosynthesis protein PhzE	-5.82	-5.04	-3.26	-3.33
PA14_09450	*phzD1*	Phenazine biosynthesis protein PhzD	-6.09	-5.51	-3.17	-3.09
PA14_09460	*phzC1*	Phenazine biosynthesis protein PhzC	-4.82	-5.15	-1.79	-2.92
PA14_09470	*phzB1*	Phenazine biosynthesis protein	-4.50	-4.19	-	-2.93
PA14_09480	*phzA1*	Phenazine biosynthesis protein	-3.68	-2.61	-2.68	-2.30
PA14_09520	*mexI*	RND efflux transporter	-1.97	-2.83	-1.73	-1.53
PA14_09530	*mexH*	RND efflux membrane fusion protein	-	-2.74	-	-
PA14_16250	*lasB*	Elastase LasB	-3.35	-3.01	-2.28	-1.62
PA14_17140		Membrane-associated zinc metalloprotease	-	*1.94*	-	-
PA14_19110	*rhlB*	Rhamnosyltransferase chain B	-1.79	-	-	-
PA14_20610	*lecB*	Fucose-binding lectin PA-IIL	-3.43	-2.90	-2.52	-1.95

Continued on next page

Table 4.4 – continued from previous page

Locus tag	Gene name	Gene product	24 h Lung	48 h Lung	24 h Surrounding SCFM	48 h Surrounding SCFM
PA14_21090			-2.20	-	-	-
PA14_27330			-	-3.18	-	-2.06
PA14_30850		TrbI-like protein	-	*1.81*	-1.77	-
PA14_30860		TrbG-like protein	-	*1.72*	-	-
PA14_31290	pa1L	PA-I galactophilic lectin	-3.94	*1.52*	-3.73	-
PA14_39880	phzG2	Pyridoxamine 5'-phosphate oxidase	-5.51	-5.15	-2.91	-3.14
PA14_39890	phzF2	Phenazine biosynthesis protein	-5.48	-4.86	-2.96	-3.09
PA14_39910	phzE2	Phenazine biosynthesis protein PhzE	-5.78	-5.40	-3.22	-3.42
PA14_39925	phzD2	Phenazine biosynthesis protein PhzD	-5.91	-5.36	-3.30	-3.16
PA14_39945	phzC2	Phenazine biosynthesis protein PhzC	-5.89	-5.68	-2.95	-3.75
PA14_39960	phzB2	Phenazine biosynthesis protein	-5.24	-5.09	-2.68	-3.97
PA14_39970	phzA2	Phenazine biosynthesis protein	-4.93	-4.40	-3.92	-4.52
PA14_40260			-2.17	-3.26	-	-
PA14_40290	lasA	LasA protease	-2.09	-2.22 -	-1.53	
PA14_49760	rhlC	Rhamnosyltransferase 2	-1.72	-1.61	-	-
PA14_50540	livM	Leucine/isoleucine/valine transporter permease subunit	-	-	-	-1.65
PA14_50550	livG	Leucine/isoleucine/valine transporter ATP-binding subunit	-	-	-	-1.65
PA14_50560	braG	Branched-chain amino acid transport protein BraG	-	-	-	-1.90
PA14_51390	pqsD	3-oxoacyl-ACP synthase	-	-1.83	-	-
PA14_51410	pqsC	PqsC	-	-1.87	-	-

Continued on next page

Table 4.4 – continued from previous page

Locus tag	Gene name	Gene product	24 h Lung	48 h Lung	24 h Surrounding SCFM	48 h Surrounding SCFM
PA14_58360	*dppA2*	Dipeptide ABC transporter substrate-binding protein DppA2	*2.25*	*2.33*	-	-
PA14_63150	*pmrA*	Two-component response regulator	*1.51*	-	-	-
PA14_64860		ABC transporter ATP-binding protein	-2.97	-1.62	-2.12	-
PA14_64870		ABC transporter ATP-binding protein	-2.29	-	-1.71	-
PA14_64880		Branched chain amino acid ABC transporter permease	-2.04	-	-1.82	-
PA14_65310		RNA-binding protein Hfq	*1.59*	-	*1.87*	-
PA14_72560	*np20*	Transcriptional regulator np20	-	-2.17	-	-

P. aeruginosa PA14 expression of conserved quorum sensing regulated genes in the lung-associated biofilm at 48 hours was comparable to CF sputum.

One of the key aspects of QS where the *P. aeruginosa* transcriptome *in vitro* has been shown to differ from *in vivo* CF infections is the expression of a set of *las*-regulated genes. The majority of genes were significantly underexpressed in CF sputum compared with lab conditions (Cornforth et al., 2018). This set of 42 genes was of particular interest as they have been shown to be conserved amongst *P. aeruginosa* isolates from the CF lung (Chugani et al., 2012). Expression of the equivalent *P. aeruginosa* PA14 genes was studied in each EVPL contrast with *in vitro* SCFM, and compared with the expression of this gene set in the CF sputum versus *in vitro* conditions investigated by Cornforth et al. (2018). The aim was to identify whether either EVPL environment more accurately represented this aspect of human infection than other laboratory models.

In the lung-associated biofilm at 24 h, the *P. aeruginosa* PA14 gene expression differences compared with *in vitro* SCFM was similar to the CF sputum versus *in vitro* contrast (Figure 4.10A). Two key genes were similarly underexpressed: *lasA* (-2.09 $\log_2$ fold change in

the lung and -3.38 $\log_2$ fold change in CF sputum) and *lasB* (-3.35 $\log_2$ fold change in the lung and -3.30 $\log_2$ fold change in CF sputum). At 48 h, the expression profile increased in similarity with the CF sputum contrast (Figure 4.10B), which suggested that the lung-associated biofilm at 48 h may have been representative of QS *in vivo*. However, there were some genes where the expression changes observed by Cornforth et al. (2018) in CF sputum were not consistently seen in the lung-associated biofilm (Figure 4.10).

A. 24 h

B. 48 h
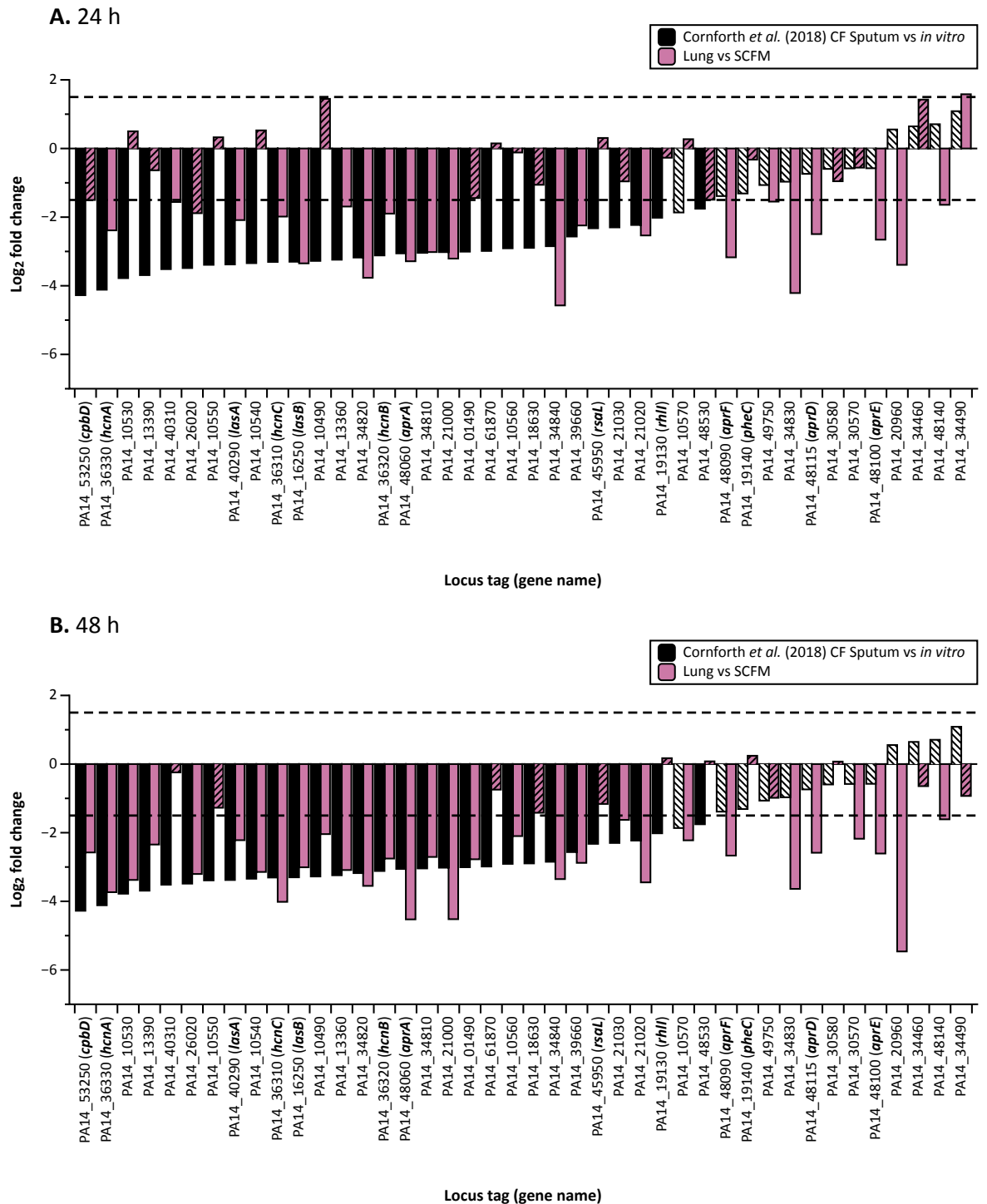
Figure 4.10: **The log$_2$ fold change in expression of 42 *Pseudomonas aeruginosa* PA14 quorum sensing regulated genes, controlled by the *las* regulon, in the *ex vivo* pig lung-associated biofilm (Lung) compared with *in vitro* synthetic cystic fibrosis sputum media (SCFM), and in Cystic Fibrosis (CF) sputum compared with *in vitro* conditions taken from Cornforth et al. (2018).** The locus tags shown are for *P. aeruginosa* PA14 and where possible, gene names are also shown. The black bars represent the log$_2$ fold change in CF sputum compared with *in vitro* determined by Cornforth et al. (2018). The purple bars show the lung biofilm compared with *in vitro* SCFM. Solid fill bars are genes that were significantly differentially expressed (log$_2$ fold change $\geq |1.5|$, $P < 0.05$) and stripe filled bars were genes that were not significantly differentially expressed. The horizontal dashed lines represend the log$_2$ fold change threshold for significance (y = 1.5, y = -1.5). Analysis was performed on lung and *in vitro* SCFM samples at **(A)** 24 h and **(B)** 48 h.

Three genes involved in type 1 secretion systems (T1SS) were found to be significantly underexpressed in the lung-associated biofilm compared with *in vitro* SCFM at 24 h and 48 h (PA14_48090, PA14_48100, PA14_48115), but there was no significant difference in expression in CF sputum (Cornforth et al. (2018)). These genes are associated with alkaline protease secretion, a function of *P. aeruginosa* T1SS in the CF lung (Depluverez et al., 2016). As well as this, expression of genes associated with the oxidation-reduction pathway were distinct from the CF sputum comparison. The sulfite/nitrite reductase involved in sulphur metablism (PA14_10550) was significantly underexpressed in CF sputum but not in the lung-associated biofilm at either time point (Figure 4.10; -3.39 $\log_2$ fold change in CF sputum, 0.33 $\log_2$ fold change in the lung at 24 h and -1.27 $\log_2$ fold change in the lung at 48 h). The oxidation-reduction regulatory gene PA14_34830 was however underexpressed in both contrasts, but only significant in the the lung biofilm (Figure 4.10: 24 h and 48 h). This was also found for PA14_34460, however this was only significantly underexpressed at in the lung biofilm at 48 h (Figure 4.10B). These findings indicated that aspects of the ethanol oxidation pathway were also underexpressed in CF sputum compared with *in vitro*. Another gene only significantly underexpressed in the lung-associated biofilm was the periplasmic sperimidine/putrescine-binding protein involved in polyamine transport: PA14_30570. There were other genes where differences were seen (Figure 4.10), however these were not indicative of specific functional or pathway differences.

This comparison was also performed for the surrounding SCFM and *in vitro* SCFM contrasts (Figure 4.11). The similarities between this environment and the CF sputum versus *in vitro* contrast were less obvious than the lung-associated biofilm. At 24 h, only five genes were significantly underexpressed in the surrounding SCFM and CF sputum (Figure 4.11A). Two of these genes encode non-ribosomal peptide synthetases (PA14_34810 and PA14_34840), one is involved in fatty acid biosynthesis (PA14_40310) and the others have unknown functions (PA14_10490 and PA14_39660). At 48 h there were more similarities (Figure 4.11), however expression was still more distinct than the lung biofilm comparison. Although, there was similar differential expression of the T1SS genes as observed in the lung-associated biofilm at 48 h.

A. 24 h

B. 48 h
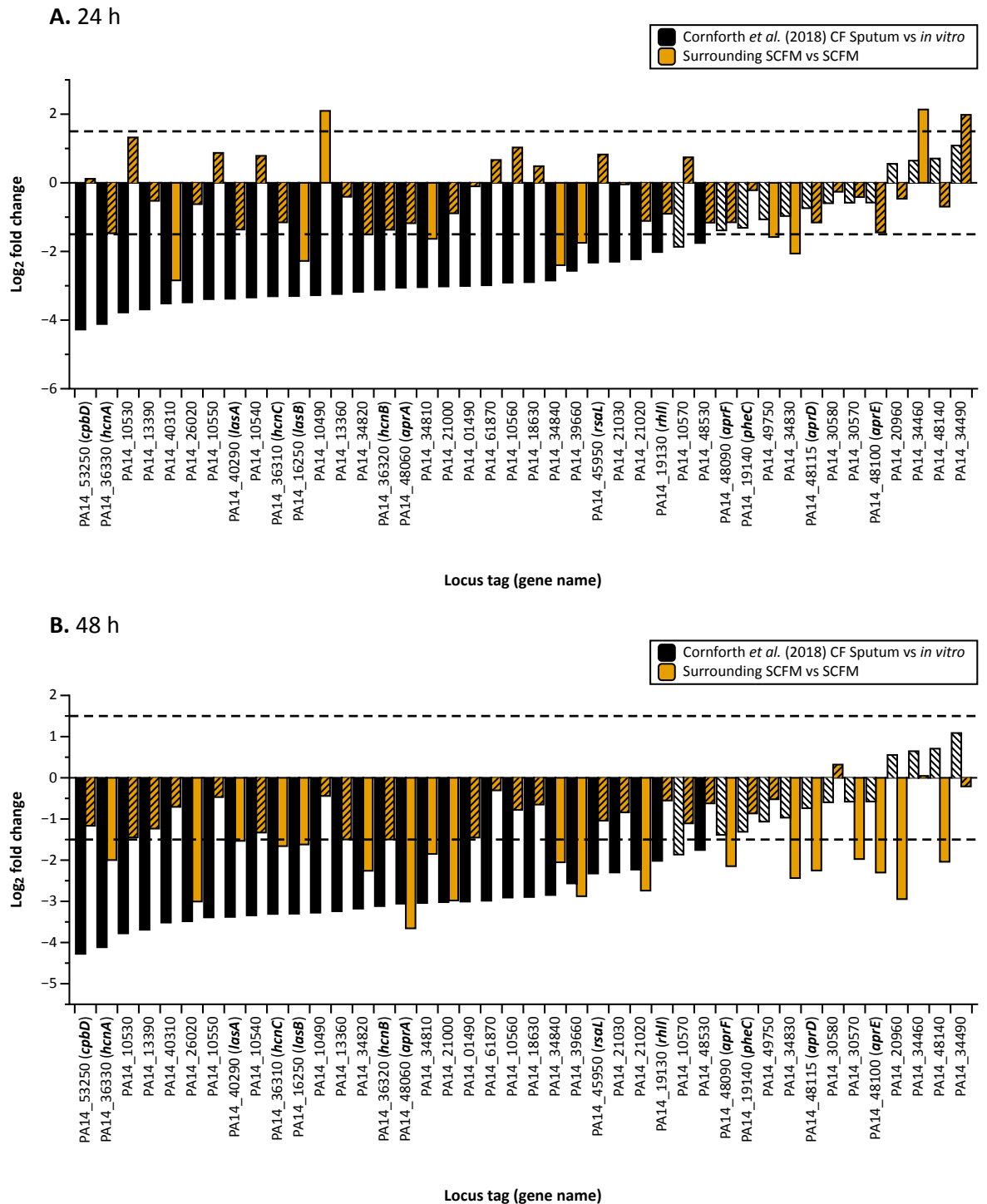
Figure 4.11: **The log$_2$ fold change in expression of 42 *Pseudomonas aeruginosa* PA14 quorum sensing regulated genes, controlled by the *las* regulon, in the synthetic cystic fibrosis sputum media (SCFM) surrounding each *ex vivo* pig lung tissue piece (Surrounding SCFM) compared with *in vitro* synthetic cystic fibrosis sputum media (SCFM), and in Cystic Fibrosis (CF) sputum compared with *in vitro* conditions taken from Cornforth et al. (2018).** The locus tags shown are for *P. aeruginosa* PA14 and where possible, gene names are also shown. The black bars represent the log$_2$ fold change in CF sputum compared with *in vitro* determined by Cornforth et al. (2018) and the orange bars show the surrounding SCFM population compared with *in vitro* SCFM. Solid fill bars are genes that were significantly differentially expressed (log$_2$ fold change $\geq |1.5|$, $P < 0.05$) and stripe filled bars were genes that were not significantly differentially expressed. The horizontal dashed lines represend the log$_2$ fold change threshold for significance (y = 1.5, y = -1.5). Analysis was performed on surrounding SCFM and *in vitro* SCFM samples at **(A)** 24 h and **(B)** 48 h.

146

3-oxo-C12-HSL production was reduced in the EVPL model compared with *in vitro* SCFM at 48 hours.

Production of the QS molecules 3-oxo-dodecanoyl homoserine lactone (3-oxo-C12-HSL) and N-butanoyl-L-homoserine lactone (C4-HSL) was investigated to determine whether QS related gene expression differences likely had a phenotypic effect. The *P. aeruginosa* PA14 CFU lung^{-1} for each sample that QS molecules were measured from is shown in Appendix A (Figure A.3). C4-HSL production could not be detected as the assay was unable to differentiate between uninfected EVPL samples and sterile SCFM, and the *P. aeruginosa* PA14 samples (Figure 4.12). This may have been due to interference of SCFM components and the lung tissue, or an issue with the bioreporter strain. However, this meant that the effect of growth environment on C4-HSL production could not be determined.
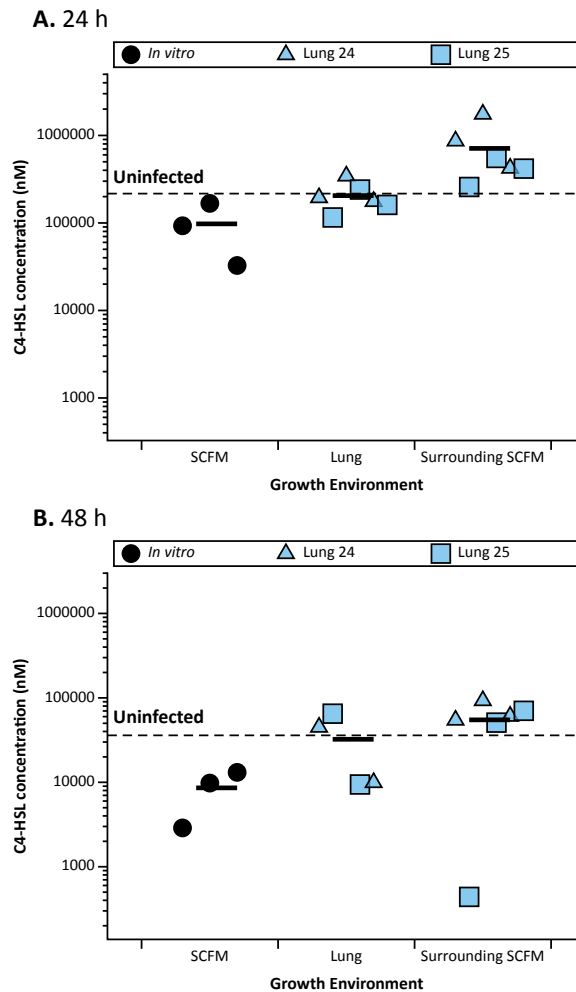
Figure 4.12: **Concentration of N-butanoyl-L-homoserine lactone (C4-HSL) produced by *Pseudomonas aeruginosa* PA14 in synthetic cystic fibrosis sputum media (SCFM) *in vitro* (SCFM) and the two environments of the *ex vivo* pig lung (EVPL) model: the lung-associated biofilm (Lung) and SCFM surrounding each tissue piece (Surrounding SCFM).** The *in vitro* SCFM samples used for this experiment were prepared by Jenny Littler. Each data point represents an individual sample; *in vitro* SCFM cultures were prepared in triplicate per time point and three tissue pieces from each of two independent lungs were prepared for the EVPL model environments. The environments and individual lungs are represented by different shaped and coloured data points (see key). The dashed line shows the mean C4-HSL concentration measured in uninfected samples across the three environments at the time point. The horizontal, bold lines represent the mean concentration. The y axes are $\log_{10}$ scale. Measurements were performed on *P. aeruginosa* PA14 samples at **(A)** 24 h and **(B)** 48 h.

The production of 3-oxo-C12-HSL was successfully detected in *P. aeruginosa* PA14 samples at 24 h and 48 h (Figure 4.13). As shown in Figure 4.13A, there was no significant difference in 3-oxo-C12-HSL concentration between *in vitro* SCFM samples, the lung-associated biofilm, and the surrounding SCFM at 24 h (ANOVA $F_{2,12}$ = 2.53, P = 0.12). There was however some variation observed in the lung biofilm that was not seen for either *in vitro* SCFM or surrounding SCFM. At 48 h, there was a lower concentration of 3-oxo-C12-HSL in the lung and surrounding SCFM than SCFM *in vitro* (Figure 4.13B). These differences

were significant (ANOVA $F_{2,12}$ = 32.83, P < 0.01) and a post hoc Dunnett's test confirmed that there was a significantly lower concentration of 3-oxo-C12-HSL in the lung biofilm (P < 0.01) and surrounding SCFM (P = 0.02) than SCFM *in vitro*.
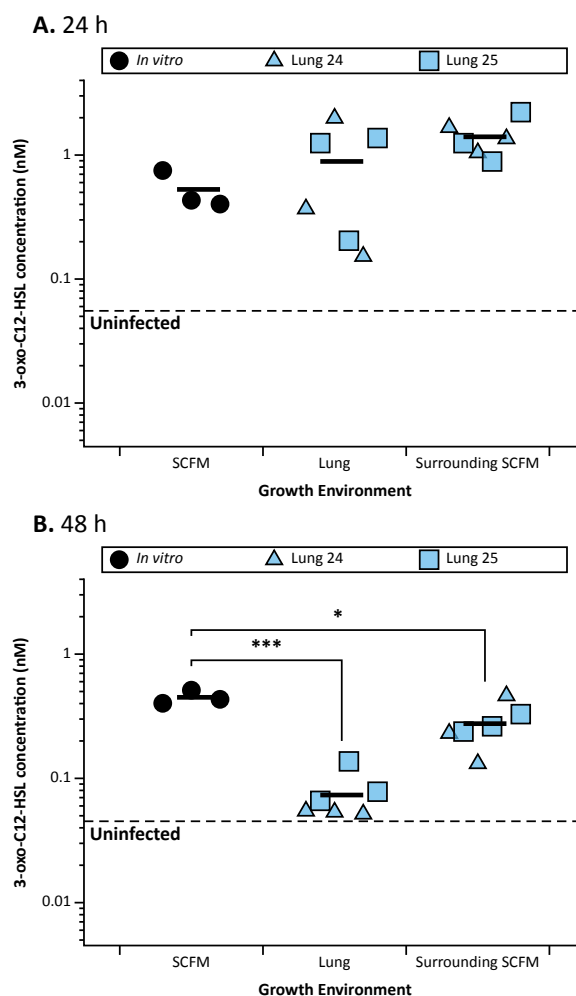
Figure 4.13: **Concentration of 3-oxo-dodecanoyl homoserine lactone (3-oxo-C12-HSL) produced by** *Pseudomonas aeruginosa* **PA14 in synthetic cystic fibrosis sputum media (SCFM)** *in vitro* **(SCFM) and the two environments of the** *ex vivo* **pig lung (EVPL) model: the lung-associated biofilm (Lung) and SCFM surrounding each tissue piece (Surrounding SCFM).** The *in vitro* SCFM samples used for this experiment were prepared by Jenny Littler. Each data point represents an individual sample; *in vitro* SCFM cultures were prepared in triplicate per time point and three tissue pieces from each of two independent lungs were prepared for the EVPL model environments. The environments and individual lungs are represented by different shaped and coloured data points (see key). The dashed line shows the mean 3-oxo-C12-HSL concentration measured in uninfected samples across the three environments at the time point. The horizontal, bold lines represent the mean concentration. The y axes are $\log_{10}$ scale. Measurements were performed on *P. aeruginosa* PA14 samples at **(A)** 24 h and **(B)** 48 h.

Figure 4.13 shows that the concentration of 3-oxo-C12-HSL produced by *P. aeruginosa* PA14 grown in SCFM *in vitro* only slightly decreased from 24 h to 48 h (means 0.53 nM and 0.45 nM respectively) however there was a large reduction in the lung-associated biofilm (means 24 h: 0.89 nM; 48 h: 0.07 nM) and surrounding SCFM (means 24 h:

1.40 nM; 48 h: 0.28 nM). This suggested that production was downregulated in the EVPL model at 48 h. This was consistent with the RNA-seq findings, which showed the conserved set of *las*-regulated genes were underexpressed in the lung, and to a lesser extent the surrounding SCFM, at 48 h. Despite this, neither *lasI* or *lasR* were significantly differentially expressed (Appendix A; Table A.2). *P. aeruginosa* PA14 expression of genes that have been associated with self-degradation of AHL signals, such as 3-oxo-C12-HSL, were thus investigated to determine if this was the cause. As shown in Table 4.5, none of these genes were found to be significantly upregulated. In fact, *pvdQ* was found to be significantly underexpressed in the lung biofilm at 48 h compared with *in vitro* SCFM grown PA14. Thus, self-degradation of was not the cause of the reduction in 3-oxo-C12-HSL measured in the EVPL model environments at 48 h.

Table 4.5: **The log$_2$ fold change in expression of three genes associated with *Pseudomonas aeruginosa* self-degradation of acyl homoserine lactone signals (Grandclément et al., 2016) in the *ex vivo* pig lung (EVPL) model environments compared with *in vitro* synthetic cystic fibrosis sputum media (SCFM) growth at 24 and 48 h.** The *P. aeruginosa* PA14 locus tags are also shown, and the gene name and product. The log$_2$ fold change for EVPL lung-associated biofilm (Lung) and surrounding SCFM compared with *in vitro* SCFM are shown. Significant changes are in bold and underlined (log$_2$ fold change $\geq$ |1.5|, *P* <0.05).

Locus tag	Gene name	Gene product	24 h Lung	48 h Lung	24 h Surrounding SCFM	48 h Surrounding SCFM
PA14_03980		Hypothetical protein	0.41	-0.48	0.52	-0.35
PA14_33820	*pvdQ*	Penicillin acylase-related protein	-1.15	**-1.88**	0.11	-0.39
PA14_50980	*pac*	Penicillin amidase	-0.09	0.04	-0.15	-0.29

4.2.5 Differences in antibiotic resistance associated gene expression in the EVPL model compared with *in vitro* SCFM

Expression of antibiotic resistance associated genes in the EVPL model environments compared with *in vitro* SCFM was then investigated. The set of 52 *P. aeruginosa* genes predicted to be involved in resistance by the comprehensive antibiotic resistance database (CARD) were studied (Alcock et al., 2020). As *P. aeruginosa* PA14 was not exposed to antimicrobials prior to, or during infection, the aim was to determine whether the growth environment alone influenced expression of resistance associated genes. Table 4.6 shows resistance genes found to be significantly differentially expressed in at

least one of the contrasts. There were genes found to be significantly underexpressed and overexpressed. The full gene list is shown in Appendix A (Table A.3).

Table 4.6: *Pseudomonas aeruginosa* **PA14 genes predicted to be involved in antibiotic resistance by the Comprehensive Antibiotic Resistance Database (CARD) (Alcock et al., 2020) that were significantly differentially expressed in at least one contrast between the** *ex vivo* **pig lung (EVPL) environments and** *in vitro* **synthetic cystic fibrosis sputum media (SCFM) at 24 h or 48 h.** Differential expression analysis was performed on three replica *in vitro* SCFM cultures (SCFM) and three repeats from each of two independent lungs from the EVPL environments: the lung-associated biofilm (Lung) and the SCFM surrounding each tissue piece (Surrounding SCFM), at each time point. Genes were considered significant if the $\log_2$ fold change was $\leq$ -1.5 or $\geq$ 1.5 compared with *in vitro* SCFM and $P < 0.05$. The significant $\log_2$ fold change values are shown in the table. Contrasts where the gene was not significantly differentially expressed are denoted with '-'. The orange fill shows genes that were significantly underexpressed in the EVPL environments, the darker the colour representing a higher $\log_2$ fold change. The green fill represents significantly overexpressed genes, with bold and italicised font.

Locus tag	Model name	Gene product	24 h Lung	48 h Lung	24 h Surrounding SCFM	48 h Surrounding SCFM
PA14_01960	TriB	RND efflux membrane fusion protein	-	-1.72	-	-
PA14_09500	OpmD	Outer membrane protein	-2.77	-3.41	-1.87	-1.79
PA14_09520	MexI	RND efflux transporter	-1.97	-2.83	-1.73	-1.53
PA14_09530	MexH	RND efflux membrane fusion protein	-	-2.74	-	-
PA14_09540	MexG	Hypothetical protein	-	-2.32	-	-
PA14_10470	bcr-1	MFS transporter	*2.06*	-	-	-
PA14_16300	ArmR	Hypothetical protein	-1.52	-	-	-
PA14_16790	MexL	TetR family transcriptional regulator	-	-1.62	-	-
PA14_18080	nalD	TetR family transcriptional regulator	-	-	*2.22*	*2.04*
PA14_18350	arnA	Bifunctional UDP-glucuronic acid decarboxylase/UDP-4-amino-4-deoxy-L-arabinose formyltransferase	*2.34*	-	-	-
PA14_18760	mexP	RND efflux membrane fusion protein	-	*1.84*	-	*1.76*

Continued on next page

Table 4.6 – continued from previous page

Locus tag	Model name	Gene product	24 h Lung	48 h Lung	24 h Surrounding SCFM	48 h Surrounding SCFM
PA14_18790	opmE	Outer membrane efflux protein	-	-	-	*1.61*
PA14_31870	MuxA	RND efflux membrane fusion protein	-	*1.67*	-	-
PA14_31900	MuxC	Efflux transporter	*1.55*	-	-	-
PA14_31920	OpmB	Outer membrane protein	*1.68*	-	-	-
PA14_45910	mexM	RND efflux membrane fusion protein	-	*1.72*	-	-
PA14_49780	FosA	Fosfomycin resistance protein	-1.61	-	-	-
PA14_59160	CrpP	CrpP	-	*1.68*	-	-
PA14_60820	OprJ	Outer membrane protein OprJ	-	-	*1.55*	-
PA14_60830	MexD	Multidrug efflux RND transporter MexD	-	*1.61*	-	*1.58*
PA14_60850	MexC	Multidrug efflux RND membrane fusion protein	-	*2.09*	-	*2.25*
PA14_65750	OpmH	Outer membrane efflux protein	-	-1.57	-	-

There was significant differential expression of genes associated with three efflux pumps in the EVPL model compared with *in vitro* SCFM.

There were three efflux pumps where significant DEGs were associated (Figure 4.14). All genes that encode MexG/HI-OpmD were significantly underexpressed in the lung-associated biofilm compared with *in vitro* SCFM at 48 h (Figure 4.14A). The two efflux pumps encoded by these genes are known to play roles in antibiotic resistance: MexHI-OpmD is associated with fluoroquinolone resistance and MexGHI-OpmD affects antibiotic sensitivity via post-transcriptional regulation of 3-oxo-C12-HSL (Wolloscheck et al., 2018). Mutations in MexGHI-OpmD have been shown to stop *P. aeruginosa* from producing 3-oxo-C12-HSL (Aendekerk et al., 2005). Hence, underexpression of these genes may also have been associated with the reduced 3-oxo-C12-HSL production observed in the lung biofilm.

A. *mexGHI-opmD*

B. *mexJK-oprM* (repressor *mexL*)

C. *mexAB-oprM* (repressor *nalD*)
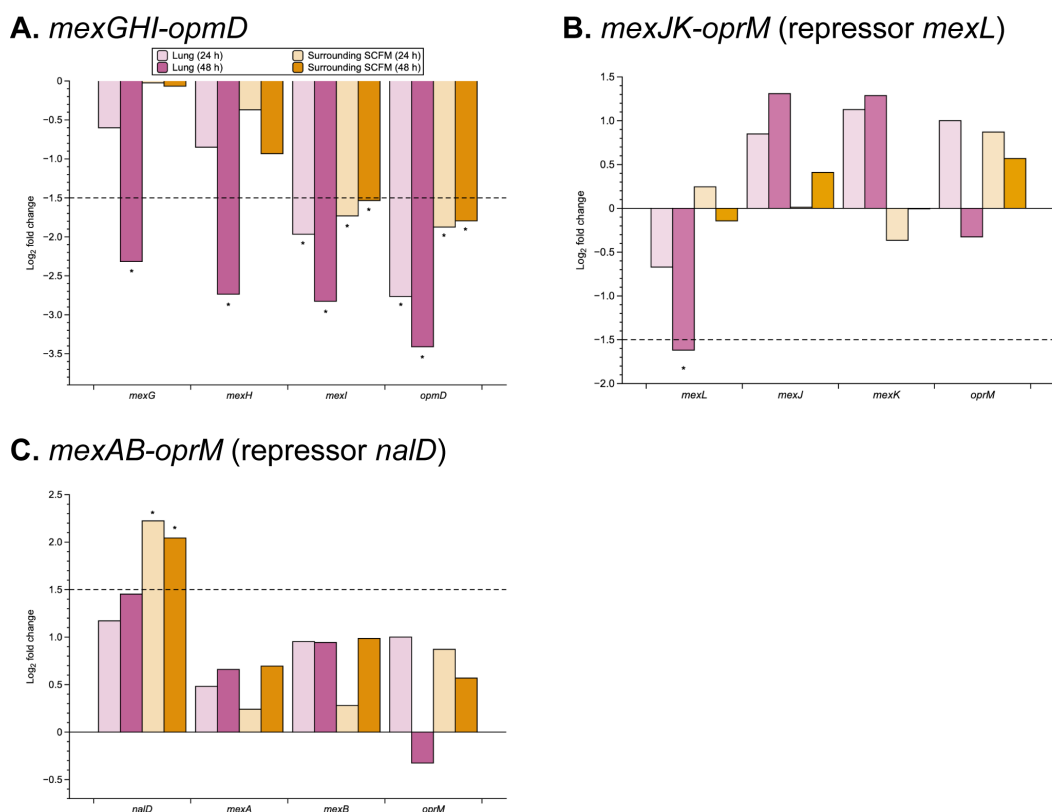
Figure 4.14: **Log$_2$ fold change of *Pseudomonas aeruginosa* PA14 expression of efflux pumps where associated genes were found to be significantly differentially expressed in at least one contast between the *ex vivo* pig lung (EVPL) environments and *in vitro* synthetic cystic fibrosis sputum media (SCFM), at 24 h or 48 h.** Differential expression analysis was performed on three replica *in vitro* SCFM cultures (SCFM) and three repeats from each of two independent lungs from the EVPL environments: the lung-associated biofilm (Lung) and the SCFM surrounding each tissue piece (Surrounding SCFM), at each time point. Genes were considered significant if the log$_2$ fold change was $\leq$ -1.5 or $\geq$ 1.5 compared with *in vitro* SCFM and $P <$ 0.05. The dashed horizontal lines represent the log$_2$ threshold for significance. Each bar colour represents a different contrast and time (see key). Significant contrasts are denoted with an asterisk. Each graph (**A-C**) shows the genes involved in individual efflux pumps, and repressors where appropriate.

The MexJK-OprM efflux pump also appeared to be affected by *P. aeruginosa* PA14 growth as a biofilm associated with the lung tissue, compared with *in vitro* SCFM, at 48 h (Figure 4.14B). This efflux pump has been linked to resistance to triclosan (Chuanchuen et al., 2002). The transcriptional repressor-encoding gene for this pump, *mexL*, was significantly underexpressed in the lung biofilm at 48 h. This indicated that expression of this efflux pump may have been switched on. Although, the MexJK-OprM genes were not significantly differentially expressed (Figure 4.14), so this expression difference may not have had a phenotypic effect at 48 h. In contrast, a gene encoding a transcriptional repressor (*nalD*) of the MexAB-OprM efflux pump, which is associated with carbapenem resistance (Pan et al., 2016), was significantly overexpressed in the surrounding SCFM compared with *in vitro* SCFM at 24 h and 48 h (Figure 4.14C). This indicated that expression

of the pump was being downregulated. As differences in gene expression of the efflux pump genes were not observed, it is unlikely that this has had a phenotypic effect by 48 h. The pump has previously been shown to no longer be required following mature biofilm formation and is also associated with 3-oxo-C12-HSL transportation (Pan et al., 2016). Although, as differential expression was not observed for components of the efflux pump, it is unlikely this was responsible for the differences in 3-oxo-C12-HSL concentration observed.

There was significant differential expression of individual resistance genes in the *arn* locus in the lung-associated biofilm compared with *in vitro* SCFM at 24 hours and 48 hours.

There were two individual genes of interest found to be significantly differentially expressed, predicted to be involved in antibiotic resistance (Figure 4.15); both are part of the *arn* locus. The genes were significantly overexpressed in the lung-associated biofilm compared with *in vitro* SCFM at 24 h (*arnA*: Figure 4.15A) or 48 h (*crpP*: Figure 4.15). The locus is associated with cationic antimicrobial peptide (CAMP) resistance (Gutu et al., 2015). Thus indicating that there may have been increased *P. aeruginosa* PA14 CAMP resistance in the lung-associated biofilm compared with SCFM *in vitro* growth at both time points.
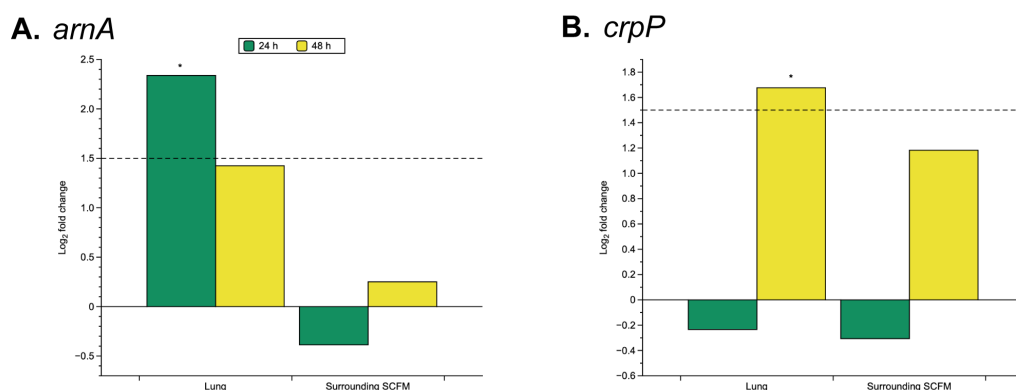
Figure 4.15: **Log$_2$ fold change of *Pseudomonas aeruginosa* PA14 expression of antibiotic resistance genes found to be significant in at least one contast between the *ex vivo* pig lung (EVPL) environments and *in vitro* synthetic cystic fibrosis sputum media (SCFM), at 24 h or 48 h.** Differential expression analysis was performed on three replica *in vitro* SCFM cultures (SCFM) and three repeats from each of two independent lungs from the EVPL environments: the lung-associated biofilm (Lung) and the SCFM surrounding each tissue piece (Surrounding SCFM), at each time point. Genes were considered significant if the log$_2$ fold change was $\leq$ -1.5 or $\geq$ 1.5 compared with *in vitro* SCFM and P < 0.05. The dashed horizontal lines represent the log$_2$ threshold for significance. Each bar colour represents a time point (see key). Significant contrasts are denoted with an asterisk. Each graph (**A-B**) shows an expression changes for an individual gene in the EVPL model environments compared with *in vitro* SCFM growth.

The MIC of colistin and polymyxin B for *P. aeruginosa* PA14 was higher when grown as a biofilm associated with the EVPL tissue than *in vitro* SCFM.

The significant differential expression of resistance genes led to the determination of the MIC of two CAMPs; colisitin and polymyxin B, for *P. aeruginosa* PA14 cells from the lung-associated biofilm at 24 h and 48 h. The *P. aeruginosa* PA14 MIC in SCFM and the MIC standard media CAMHB was also tested for comparison. As shown in Table 4.7, the MIC of both antibiotics was higher for the lung biofilm cells at both time points than either *in vitro* medias. This demonstrated that the resistance associated gene expression differences in the lung biofilm compared with *in vitro* SCFM likely had a phenotypic effect. This was also linked to the most overexpressed genes; *oprH* was one of the five genes most overexpressed in the lung-associated biofilm compared with *in vitro* SCFM at 24 h (Table 4.3). It was also significantly overexpressed in the lung biofilm at 48 h (3.52 $\log_2$ fold change). The upregulation of this gene has previously been shown to increase resistance to polymyxin B (Chevalier et al., 2017), as found for the lung biofilm cells compared with *in vitro* (Table 4.7).

Table 4.7: **The minimum inhibitory concentration (MIC) of colistin and polymyxin B (µg ml^{-1}) for *Pseudomonas aeruginosa* PA14 in different growth conditions.** These experiments were performed by Freya Allen as part of an undergraduate Master's project. The MIC value in cation-adjusted Mueller Hinton broth (CAMHB), the clinical standard, and synthetic cystic fibrosis sputum media (SCFM) was determined based on three replicates. The MIC values for the lung samples were from MIC tests performed using *P. aeruginosa* PA14 cells retrieved from the *ex vivo* pig lung tissue-associated biofilm at 24 h and 48 h. The MIC was determined for three replicate lung pieces from each of two independent lungs (lung 26 and lung 27).

Antibiotic	CAMHB	SCFM	24 h Lung	48 h Lung
Colistin	2	2	8	16
Polymyxin B	1	2	8	4

4.3   Discussion

Transcriptome analysis of *P. aeruginosa* PA14 growing in the EVPL model revealed that the formation of a biofilm associated with the lung tissue surface may have cued gene expression comparable to *in vivo* infection. Comparison of *P. aeruginosa* gene expression in the model with *in vitro* growth in SCFM focused on the two environments of the model individually: the lung tissue and the surrounding SCFM. Analysis was performed

on samples from 24 h and 48 h post infection. It was found that the *P. aeruginosa* PA14 lung-associated biofilm and surrounding SCFM population were distinct from each other, as well as *in vitro* SCFM growth. This indicated that the environmental cues encountered by *P. aeruginosa* were different when associated with the lung tissue than the surrounding SCFM, included in the model to mimic the CF airway mucus. Accumulation of mutations typically occurs over years of infection in the CF lung, to facilitate *P. aeruginosa* adaptation to the environment and form a chronic biofilm infection (Folkesson et al., 2012). These results demonstrated that the EVPL model may have rapidly driven *P. aeruginosa* PA14 into an infection state reminiscent of these chronic infections.

The difference in the gene expression over time was also distinct between *P. aeruginosa* PA14 grown in the EVPL model environments and *in vitro* SCFM. Therefore, as the lung environment was driving a chronic-like state of infection, the *in vitro* SCFM culture may have been becoming less comparable to *in vivo* infection. To investigate the validity of this hypothesis and hence the viability of the EVPL tissue as a model for chronic-like infection, quorum sensing and antibiotic resistance gene expression were focused on. They are two key aspects of *in vivo* infection that have been shown to be poorly replicated *in vitro* (Cornforth et al., 2018). A clear difference in expression of genes associated with these pathways was observed in the EVPL model and *in vitro* SCFM. In particular, *P. aeruginosa* PA14 expression in the lung-associated biofilm at 48 h appeared to be similar to CF sputum expression of QS regulated genes, and significant differential expression of key antibiotic resistance genes was also observed at this time point. This indicated that the lung-associated biofilm at 48 h was the most clinically relevant population. It was also found that the EVPL model was likely to maintain a viable *P. aeruginosa* PA14 population for longer than *in vitro* SCFM, as RNA could be successfully extracted at 7 d. Measurement of ATP production suggested this population was viable; the PA14 cells also appeared not to be stressed, unlike those grown in SCFM *in vitro*.

The *P. aeruginosa* PA14 genes with the highest $\log_2$ fold change in expression between the EVPL environments and *in vitro* SCFM also highlighted pathways where the lung-associated biofilm appeared be more representative of the human infection environment. In particular, ethanol oxidation genes were on the list of most significantly underexpressed genes in the EVPL model at 24 h. The majority of these were still

significantly underexpressed in the lung-associated biofilm at 48 h, compared with *in vitro* SCFM. These genes are known to be required when *P. aeruginosa* grows in the presence of ethanol (Görisch, 2003). Ethanol oxidation is regulated by a number of *P. aeruginosa* pathways that form a complex network required during aerobic growth (Mern et al., 2010). Thus, this suggested that the *in vitro* SCFM may have created an aerobic environment in contrast to the lung biofilm. The CF lung is a diverse environment that is typically oxygen-limited, which is responsible for many of the *P. aeruginosa* physiological changes observed (Schobert and Jahn, 2010). Therefore, these results further indicated that the lung environment may have been more representative of the CF lung than *in vitro* SCFM.

Expression of a number of pathways was found to be affected by *P. aeruginosa* PA14 growth in the different environments studied, however the phenazine biosynthetic pathway appeared to be one of the predominant functional differences. The KEGG phenazine biosynthesis pathway was significantly enriched in the lung-associated biofilm and surrounding SCFM population at both time points compared with *in vitro* SCFM. The GO term for the phenazine biosynthetic process was also found to be significantly enriched in the lung-associated biofilm at both time points and the surrounding SCFM at 24 h, downregulated in all contrasts. Phenazines have been shown to affect antibiotic susceptibility and the expression of a number of genes through antimicrobial acitivity and their function as redox-active pigments (Schiessl et al., 2019). The greatest number of genes in the pathway significantly differentially expressed compared with *in vitro* SCFM was in the lung-associated biofilm at 48 h. All genes in the pathway for biosynthesis of the virulence factor phenazine, pyocyanin, were underexpressed in the lung biofilm compared with *in vitro* SCFM at 48 h. Overall, as discussed in Chapter 3, virulence factor production is known to be downregulated in the chronic stages of *P. aeruginosa* infection in the CF lung. Overproduction of the exotoxin pyocyanin is actually reported as an unusual phenotype in an established biofilm infection (Fothergill et al., 2007). Hence, the downregulation of its synthesis at 48 h further supported the conclusion that the lung tissue environment captured key aspects of *in vivo* chronic infection.

Virulence factor production is predominantly regulated by the three QS systems in *P. aeruginosa*: *las*, *rhl*, and PQS; this includes the production of phenazines (Higgins et al., 2018). Alongside the phenazine biosynthesis pathways being found to be significantly

downregulated in the lung-associated biofilm, differences in other QS associated gene expression were found. QS systems are known to be pivotal in regulating biofilm maturation, virulence factor production, interactions with the host, and antibiotic resistance associated efflux pumps (Williams and Cámara, 2009). It is also an aspect of infection where previous transcriptome analyses indicated that current laboratory models were cueing significant overexpression of genes in comparison with *in vivo* infection (Cornforth et al., 2018). More specifically, expression of a set of conserved, *las* controlled genes was found to be underexpressed in CF sputum. Similarly, the majority of these genes were underexpressed in the lung-associated biofilm compared with *in vitro* SCFM at 48 h. This is consistent with the knowledge that mutations in QS pathways accumulate over time in the CF lung, and that these systems are most important during the initial, acute infection stage (Winstanley and Fothergill, 2009). Therefore, investigation of QS related expression in the EVPL model suggested that the pig lung tissue is driving *P. aeruginosa* PA14 to form a biofilm with characteristics of chronic infection, not seen in *in vitro* models (Cornforth et al., 2018; Rossi et al., 2018). It must also be considered that the study by Cornforth et al. (2018) mapped all reads from clinical *P. aeruginosa* isolates to the *P. aeruginosa* PAO1 genome, which may have missed more subtle differences. For example, if there was differential expression of genes in the clinical *P. aeruginosa* isolates from CF sputum for which there is not a corresponding PAO1 locus, then this would not have been found. Therefore, there may have been more differences between CF sputum and the *in vitro* conditions than reported by Cornforth et al. (2018).

The differences in *P. aeruginosa* PA14 QS gene expression in the lung-associated biofilm and *in vitro* SCFM were only seen in downstream genes regulated by the *las-* and *rhl-* systems. The AHL molecule produced by the *las* system, 3-oxo-C12-HSL, was also a much lower concentration in the lung-associated biofilm and surrounding SCFM at 48 h than in SCFM *in vitro*. However, the two component response regulators *lasI/R* and *rhlI/R* were not significantly differentially expressed in either of the EVPL environments at 24 h or 48 h. Genes known to encode amidases that degrade AHL signals (PA14 homologues of *pvdQ, quiP, hacB*) (Grandclément et al., 2016) were similarly found to not be differentially expressed in any of the EVPL contasts. This alongside comparable expression of the regulatory genes indicated that the difference between environments was likely caused by other factors under QS regulation.

Interestingly, *P. aeruginosa* mutants for *mexI* and *opmD*, both efflux pump genes, have previously demonstrated an inability to produce 3-oxo-C12-HSL, driven by the accumulation of a toxic PQS precursor that occurs when the pump acitivity is lost (Aendekerk et al., 2005). Aendekerk et al. (2005) used reverse transcription-polymerase chain reaction (RT-PCR) to show that the reduction in extracellular 3-oxo-C12-HSL they observed may have been driven by overall downregulation of the efflux pump MexGHI-OpmD. These findings did not correlate with any inhibition of *lasI* or *rhlI* transcription, suggesting the effect of MexGHI-OpmD on 3-oxo-C12-HSL is post-transcriptional. All of these efflux pump genes were underexpressed in the *P. aeruginosa* PA14 lung-associated biofilm at 48 h. The genes *mexI* and *opmD* were also significantly underexpressed in the lung biofilm at 24 h and in the surrounding SCFM population at both time points, compared with *in vitro* SCFM. Overall, this suggested that the differences in QS expression in the EVPL model versus *in vitro* SCFM growth were likely involved in a wider regulatory network. These differences may have also had implications on antibiotic resistance so this was further explored. However, proteomic analysis would be required to confirm this hypothesis.

Significant underexpression of the MexGHI-OpmD efflux pump genes at 48 h in the lung-associated biofilm may have also caused an AMR phenotype. Mutations in the *mexI* and *opmD* genes have been shown to increase *P. aeruginosa* resistance to β-lactams, aminoglycosides, and quinolones (Aendekerk et al., 2005). Other efflux pumps potentially affected by *P. aeruginosa* PA14 growth in the EVPL model included MexAB-OprM. The transcriptional regulator *nalD* for the MexAB-OprM pump was significantly overexpressed in the surrounding SCFM population compared with *in vitro* SCFM at 24 h and 48 h. Although the genes encoding the efflux pump were not significantly differentially expressed, which indicated that expression of this pump may have been downregulated with a phenotypic effect after 48 h. This will be further explored at 7 d in the lung-associated biofilm in Chapter 5. This pump is known to be involved in the pseudopaline system (Gomez et al., 2021), a PQS precursor that was significantly underexpressed in the EVPL model environments. MexAB-OprM has also been linked with heterogeneity within the *P. aeruginosa* chronic biofilm population in the CF lung. A higher proportion of the MexAB-OprM pump has been found in dense biofilm cells than the rest of the infection population (De Kievit et al., 2001). No

significant differences in expression for *nalD* or the efflux pump genes were found in the lung-associated biofilm at either time point, which indicated that as the infection progressed, the pump was being switched off in the surrounding SCFM but not the lung biofilm. This further supported the lung-associated biofilm at 48 h as a chronic-like biofilm infection. As well as demonstrating *P. aeruginosa* gene regulation comparable to what is known of *in vivo* infection dynamics, this also showed that the distinction between the surrounding SCFM and lung tissue may have represented the heterogenous infection population seen in CF. This difference in potential sub-populations is an important consideration to determine the efficacy of antibiotic treatment approaches.

As discussed, the pseudopaline system, regulated by zinc, was downregulated in the EVPL environments compared with *in vitro* SCFM growth. It is known to be important for zinc uptake in low metal environments such as the CF lung, but also nickel uptake in poor media conditions (Lhospice et al., 2017). Upregulation of this system is thought to be a *P. aeruginosa* adaptation driven by the CF lung environment to increase metal ion intake and facilitate metabolism in the low metal CF lung environment (Hermansen et al., 2018). Thus, this may be an incidence where *in vitro* SCFM better replicates the metabolism of *in vivo* infection. However, these genes were still expressed in the EVPL model, just to a lesser extent, and QS gene expression analysis found some genes associated with the pseudopaline system to be underexpressed in CF sputum compared with *in vitro*. Further research using *in vivo* samples is required to determine whether this is *in vitro* SCFM cueing expression reminiscent of metabolic pathways *in vivo* or if it is overcompensating, as is the case for many QS-regulated genes, and in fact the EVPL model may be more reflective of true infection.

The clinical relevance of the EVPL model was supported by the significant differential expression of AMR genes in the lung-associated biofilm, which may be associated with the increased resistance observed in *P. aeruginosa in vivo* infections. Two individual genes of clinical interest were significantly differentially expressed in the lung-associated biofilm: *arnA* overexpressed at 24 h and *crpP* overexpressed at 48 h. These genes have been associated with CAMP resistance, *arnA* is associated with a locus that increases resistance through modifications to lipid A (Gutu et al., 2015). As this gene was overexpressed compared to *in vitro* SCFM at 24 h but not 48 h, this suggested the pathway was downregulated as the biofilm established. The resistance mechanism may

have been important during initial infection when the biofilm matrix was not formed to protect against antimicrobials. However, CrpP confers resistance to the antibiotic ciprofloxacin through phosphorylation (Chávez-Jacobo et al., 2018) and was significantly overexpressed in the lung-associated biofilm at 48 h, thus resistance mechanisms were also upregulated after 24 h. Overall, the upregulation of these resistance pathways and genes, despite no antibiotic treatment in the EVPL model, suggested that AMR phenotypes may be driven by the lung environment rather than treatments *in vivo*. A similar conclusion from transcriptome analysis was made by Cornforth et al. (2018).

These findings provided insight into resistance mechanisms that play an important role in the CF lung, but also highlighted the importance of using a clinically realistic model such as the EVPL to understand *in vivo* antibiotic resistance. Despite this, it must be taken into account that individuals with CF with chronic *P. aeruginosa* infections undergo rigorous antibiotic treatments, which will impact *P. aeruginosa*. Future work in the model using clinical isolates that have been exposed to these treatments may provide further insight into antibiotic resistance and thus how to combat it, as they are likely to have altered behaviour compared with *P. aeruginosa* PA14 (Rossi et al., 2018). This transcriptome analysis has however demonstrated that the EVPL model, in particular the lung tissue-associated biofilm at 48 h, drives *P. aeruginosa* into a chronic-like state of infection with pathways regulated in a comparable way to human infection. This was consistent with the phenotypic findings in Chapter 3, which demonstrated acute infection characteristics were not detectable in the model but a biofilm reminiscent of *in vivo* infection was seen.

To build upon this in the future and to address more specific research questions, the RNA-seq data must be explored to ensure appropriate pathways are regulated as expected and hence the EVPL model is suitable for indivudual hypotheses. This would also indicate whether the lung-associated biofilm or surrounding SCFM population is most relevant to the question. This work has focused on gene expression of the *P. aeruginosa* population in each environment as a whole. As *P. aeruginosa* chronic biofilms are likely a heterogenous population, single-cell analysis may provide more detailed information on the infection dynamics to aid more effective treatment development and infection management. Future work on *P. aeruginosa* gene expression in the EVPL model could also incorporate other species, both commensals and other pathogens to explore

interactions and the implications of these on infection.

4.4   Conclusion

Through transcriptome analysis I have shown that the EVPL model creates two distinct *P. aeruginosa* growth environments that differ from *in vitro* SCFM. Gene expression in the lung-associated biofilm at 48 h appeared to be most representative of an established chronic infection in the CF lung. Although there are still many aspects of infection that I have not explored, I have demonstrated that key pathways where *in vitro* SCFM does not recapitulate human infection appear to be more clinically realistic in the lung-associated biofilm. This chapter has built upon the phenotypic analyses in Chapter 3 to show that the gene expression causing these phenotypes is also comparable to *in vivo* infection thus validating EVPL as a *P. aeruginosa* biofilm model. Hence, I have used the EVPL model to further understanding of *in vivo* infections in the following chapters. RNA was not sequenced from *P. aeruginosa* PA14 grown in SCFM at 7 d, as discussed. Therefore, analysis of 7 d EVPL biofilm samples was not performed in this chapter as there was no *in vitro* comparison. This will be explored in chapter 5 to investigate *P. aeruginosa* gene expression over time in the EVPL-associated biofilm.

Chapter 5

Transcriptome changes in the *Pseudomonas aeruginosa* biofilm in the *ex vivo* pig lung model over time

5.1 Introduction

Chronic *P. aeruginosa* biofilm infection in the CF lung involves adaptation to the environment over years. This adaptation is characterised by a reduction in phenotypic diversity and loss of virulence (Rossi et al., 2020). It is driven by a range of environmental selection pressures, including osmotic, nitrosative, and oxidative stress. Any interactions with the lung microbiome and co-infecting pathogens also have an influence, as well as antibiotic exposure (Winsor et al., 2016). Chronic *P. aeruginosa* biofilm infections exhibit increased antibiotic resistance, which makes them almost impossible to eradicate. Formation of the biofilm matrix protects the bacterial cells from the host immune response and antibiotics (Høiby et al., 2010), as discussed in chapter 3, contributing to resistance. However, there are other biofilm factors that also influence resistance. A study by Wilton et al. (2016) found that the extracellular DNA in the biofilm created an acidic environment, which caused increased aminoglycoside resistance. This resistance arose from lipid A modifications and spermidine production, and was reversed upon neutralisation of the pH. Hence indicating that changes in conditions, such as pH, cause gene expression changes in the biofilm population that influence resistance. These findings also highlight the importance of accurately replicating *in vivo* biofilms in laboratories, as the structure and components of the biofilm influence a number of processes important for persistence and antimicrobial resistance.

Alongside this, there are numerous other lifestyle changes associated with *P. aeruginosa* adaptation to the CF lung. *P. aeruginosa* isolates from a person with CF at initial infection have been compared with isolates taken 20 years later. A loss of swimming motility, impaired PVD production, increased adherence, and an increase in resistance to a range of antibiotics were identified in the chronic, lung-adapted isolates (Wardell et al., 2021). These adaptations improved the ability of *P. aeruginosa* to persist in the CF lung environment, and demonstrated how *P. aeruginosa* traits change over time during chronic biofilm infection. Taking this into account, if expression of genes involved in the regulatory pathways that control these traits is not replicated in the laboratory, then the change in lifestyle can not be fully understood. Therefore, studying the progression of *P. aeruginosa* biofilm infection over time in a more clinically relevant model, such as the EVPL model, may provide better understanding of these adaptations.

One of the key environmental factors that affects *P. aeruginosa* adaptation is oxygen availability. There is a build up of thick mucus in the CF lung that is not effectively cleared, which results in mucus plugs that block the airways. This creates an oxygen gradient with regions of low oxygen availability (hypoxic) and no oxygen (anoxic) (Filkins and O'Toole, 2015). *P. aeruginosa* has been shown to occupy a hypoxic niche in the CF lung, and the oxygen gradient is steepened by cell proliferation (Worlitzsch et al., 2002). Despite low oxygen availability, there has been research to suggest that *P. aeruginosa* can grow by microaerobic respiration in regions of the CF lung. *P. aeruginosa* utilises an oxygen supply in the lumen, from the host, to respire at the surface of the mucus layer (Alvarez-Ortega and Harwood, 2007). However, anaerobic respiration is believed to be predominant as growth is mainly in hypoxic regions, and is associated with increased antibiotic tolerance (Schobert and Jahn, 2010). Thus, it has been proposed that microaerobic and anaerobic respiration occur in parallel in *P. aeruginosa* chronic biofilm infections of the CF lung (Alvarez-Ortega and Harwood, 2007). These mechanisms for respiration, driven by the CF lung environment, have an impact on the changes in *P. aeruginosa* growth and physiology over time.

Microorganisms able to survive in low oxygen environments have an increased ability to form chronic infections (Filkins and O'Toole, 2015). Hence, adaptation of the facultative anaerobe *P. aeruginosa* to anaerobic respiration in hypoxic regions of the CF lung may

contribute to the establishment of long term infections. *P. aeruginosa* uses a number of processes including arginine and pyruvate fermentation, and nitrogen metabolism to survive in the low oxygen (Schobert and Jahn, 2010), predominantly respiring using nitrite and nitrate (Filkins and O'Toole, 2015). Denitrification is the *P. aeruginosa* pathway for nitrogen metabolism, regulated by the QS system PQS and associated with iron availability. When there is low iron availability, PQS represses nitrogen metabolism (Toyofuku et al., 2008). The CF lung creates a growth environment that drives changes in respiration, which has an effect on *P. aeruginosa* physiology and is associated with increased antibiotic tolerance (Schobert and Jahn, 2010). Thus indicating that changes in processes such as nitrogen metabolism over time in the biofilm may contribute to difficulty treating these infections, and hence causing reduced quality of life.

Sulfur metabolism is also linked to growth in anoxic conditions, and may play a role in chronic *P. aeruginosa* infection of the CF lung. A study of *P. aeruginosa* PA14 growth in SCFM found that sulfur metabolism was upregulated in anaerobic biofilms, induced by a lack of oxygen and not sulfur starvation (Tata et al., 2016). This may explain the role of sulfur metabolism in the CF lung, where sulfur is not limited. There is actually an increase in sulfation of the airway mucins in CF compared with a non-CF lung (Cheng et al., 1989; Xia et al., 2005). This has been proposed to be, in part, caused by inflammation (Lamblin et al., 2001). Although *P. aeruginosa* chronically adapted to the CF lung is able to use host mucin as a sulfur source, unlike isolates from non-clinical settings, it has been shown that there is enough inorganic sulfate in CF sputum to facilitate *P. aeruginosa* growth without mucin as a sulfur source (Robinson et al., 2012). Sulfur is essential for *P. aeruginosa* to synthesise cofactors for two regulators of anaerobic respiration: Anr and Dnr, and for a number of the enzymes involved in denitrification (Zhang et al., 1995; Xia et al., 2005; Robinson et al., 2012). Thus, sulfur metabolism may play an important role in adaptation over time to the growth conditions in the CF lung. As *P. aeruginosa* adapts to the CF lung and forms a biofilm in the hypoxic conditions, it is likely that sulfur metabolism is upregulated.

Metabolism and respiration changes are accompanied by other adaptations in the chronic *P. aeruginosa* biofilm population during the course of infection. Phenotypic changes including reduced virulence factor production are controlled by different regulatory pathways, predominantly under QS control. The expression of *P. aeruginosa*

social traits such as QS have been shown to decline over time (Jiricny et al., 2014). This includes a reduction in production of two QS signals: 3-oxo-C12-HSL and PQS. Interestingly, there is no change in production of two other QS signals reported: C4-HSL and HHQ (Jiricny et al., 2014). This is indicative of complex changes over time rather than overall downregulation of all processes. QS plays a key role in the development of a biofilm with mature architecture. It is estimated to influence the expression of approximately 10% of all *P. aeruginosa* genes, which also includes genes involved in motility, chemotaxis, and metabolism (Hogardt and Heesemann, 2011). Despite a reduction in elastase, PVD, and total protease production, there is no significant change in capacity for biofilm formation (Jiricny et al., 2014). This further supports downregulation of numerous pathways is accompanied by changes that favour long term infection, such as anaerobic respiration and biofilm formation.

As outlined, there are changes in *P. aeruginosa* gene expression during infection in the CF lung that affect key characteristics. The work in this chapter investigated *P. aeruginosa* gene expression changes in the EVPL-associated biofilm from 24 h to 48 h, and 7 d, and from 48 h to 7 d, using the RNA-seq data generated in chapter 4. The overall aim was to identify whether the EVPL model captured *P. aeruginosa* gene expression changes associated with chronic adaptations to the CF lung, to further understand these processes as well as the dynamics of biofilm infection in the EVPL model. There were distinct *P. aeruginosa* PA14 transcriptomes found at 24 h, 48 h, and 7 d in the EVPL biofilm, suggesting there were changes over the 7 d studied.

QS-associated gene expression in *in vitro* models has been shown to be distinct from CF sputum (Cornforth et al., 2018), and the RNA-seq analysis in chapter 4 demonstrated that the EVPL model may more accurately capture this gene expression. Therefore, changes over time in QS gene expression in the EVPL model lung-associated biofilm was a specific focus to further understand the role of QS in any adaptations. The expression of genes in metabolic pathways were also investigated to determine whether processes significantly upregulated or downregulated were reminiscent of the changes in expression known for the CF lung. Nitrogen metabolism and sulfur metabolism were both found to be significantly enriched over time in the *P. aeruginosa* PA14 EVPL biofilm. The association of *P. aeruginosa* gene expression changes over time in the EVPL model with increased antibiotic resistance was also studied, to provide insight into

the mechanisms underpinning the antibiotic resistance observed in the EVPL model (Sweeney et al., 2020b; Hassan et al., 2020; Harrington et al., 2021b), and thus in the CF lung.

In addition to the original aim, this work has also shown the optimal time point to study *P. aeruginosa* in the EVPL model to replicate a chronic-like infection: 48 h, and highlighted potential aspects of the model that could be optimised to address specific research questions in the future.

5.2   Results

In chapter 4, *P. aeruginosa* PA14 gene expression in the EVPL model was compared with *in vitro* SCFM growth at two time points (24 h and 48 h). However, RNA from the lung-associated biofilm from three time points was sequenced: 24 h, 48 h, and 7 d, as shown in the initial analysis in chapter 4. Gene expression at each of these time points was compared in this chapter to provide insight into the biofilm formed on the surface of the EVPL tissue and the phenotypes observed in chapter 3. RNA was extracted at each time point from three *P. aeruginosa* PA14 infected tissue pieces from each of two independent lungs.

5.2.1   *P. aeruginosa* PA14 transcriptome in the EVPL tissue-associated biofilm over 7 days

The RNA was sequenced, data preparation, and quality control (Appendix B; Figure B.1) was performed on all RNA samples as described in chapter 4. To further investigate the *P. aeruginosa* PA14 transcriptome in the lung-associated biofilm, PCA was performed using only the lung-associated biofilm samples at each time point: 24 h, 48 h, and 7 d, considering all genes (n = 5829). As shown in Figure 5.1, there was a clear distinction in PA14 gene expression between samples from each time point. Most variation between samples was explained by principal components 1 and 2; 43 % of variance was caused by the genes in principal component 1 (Figure 5.1A). The 24 h biofilm appeared to be most distinct from 48 h and 7 d in principal component 1. This indicated that *P. aeruginosa* PA14 gene expression in the lung-associated biofilm may have been more similar at 48 h and 7 d than the initial 24 h time point (Figure 5.1A).
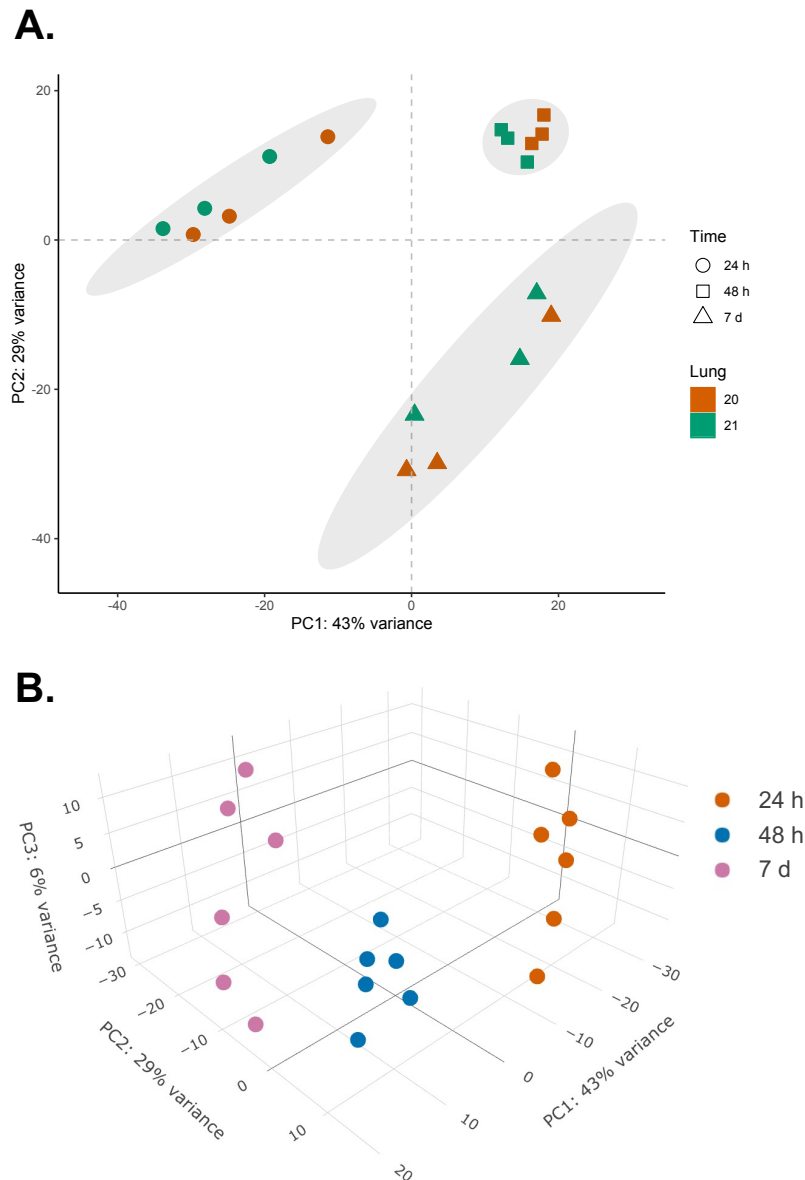
Figure 5.1: **Principal component analysis (PCA) plots of the *Pseudomonas aeruginosa* PA14 transcriptome, conisdering all genes (n = 5829), in the *ex vivo* pig lung (EVPL) model tissue-associated biofilm at 24 h, 48 h, and 7 d.** RNA was sequenced from the lung-associated biofilm at each time point from three repeats from each of two independent pig lungs. **(A)** PCA plot showing principal component (PC) 1 and PC2. Each time point is shown by a different shaped data point and the individual pig lungs shown by different colours (see key). The 95% confidence ellipses are shown. **(B)** PCA plot showing PC1, PC2, and PC3. The different time points are shown by different coloured data points (see key).

The samples from each set of lungs were also identified in the PCA plot, to visualise whether the distinctions observed between samples at different time points was affected by the lung *P. aeruginosa* PA14 was grown on (Figure 5.1A). However, there was no clear difference in gene expression observed between the two lungs. The two clusters made up of three 7 d samples were not grouped by the individual lungs (Figure 5.1A). A third prinicipal component was also considered in the analysis to determine if there were

other differences between samples not captured by the first two principal components. However, as shown in Figure 5.1B, prinicpal component 3 accounted for only 6% of the variance between samples and did not provide any further insight into how the samples compared.

5.2.2 *P. aeruginosa* PA14 differential expression in the EVPL tissue-associated biofilm over 7 days

Differential expression analysis was then performed using the same threshold for significance as in chapter 4 ($P < 0.05$, $\log_2$ fold change $\geq |1.5|$). The number of significant DEGs in each contrast is shown in Figure 5.2. Each gene contrast was between two time points and the earliest time point was used as the baseline for comparison. For example, the contrast between gene expression at 24 h and 48 h determined the $\log_2$ fold change at 48 h compared with 24 h. This showed the change in gene expression from 24 h to 48 h. Each contrast is referred to in this format for the rest of the chapter: 24 h to 48 h, 24 h to 7 d, and 48 h to 7 d.

The greatest number of gene expression changes was found from 24 hours to 7 days in the *P. aeruginosa* PA14 lung-associated biofilm.

As shown in Figure 5.2, differential expression analysis found more significant DEGs overexpressed in each contrast than underexpressed. This indicated that gene expression was upregulated over time in the lung-associated biofilm. Consistent with PCA, the greatest number of significant DEGs was found in the 24 h contrasts: 435 significant genes 24 h to 7 d, and 432 significant genes 24 h to 48 h. There were approximately half the number of significant DEGs found 48 h to 7 d (Figure 5.2B: 205 genes). These results demonstrated that the greatest difference in gene expression occured from 24 h to 7 d in the lung-associated biofilm (Figure 5.2C).
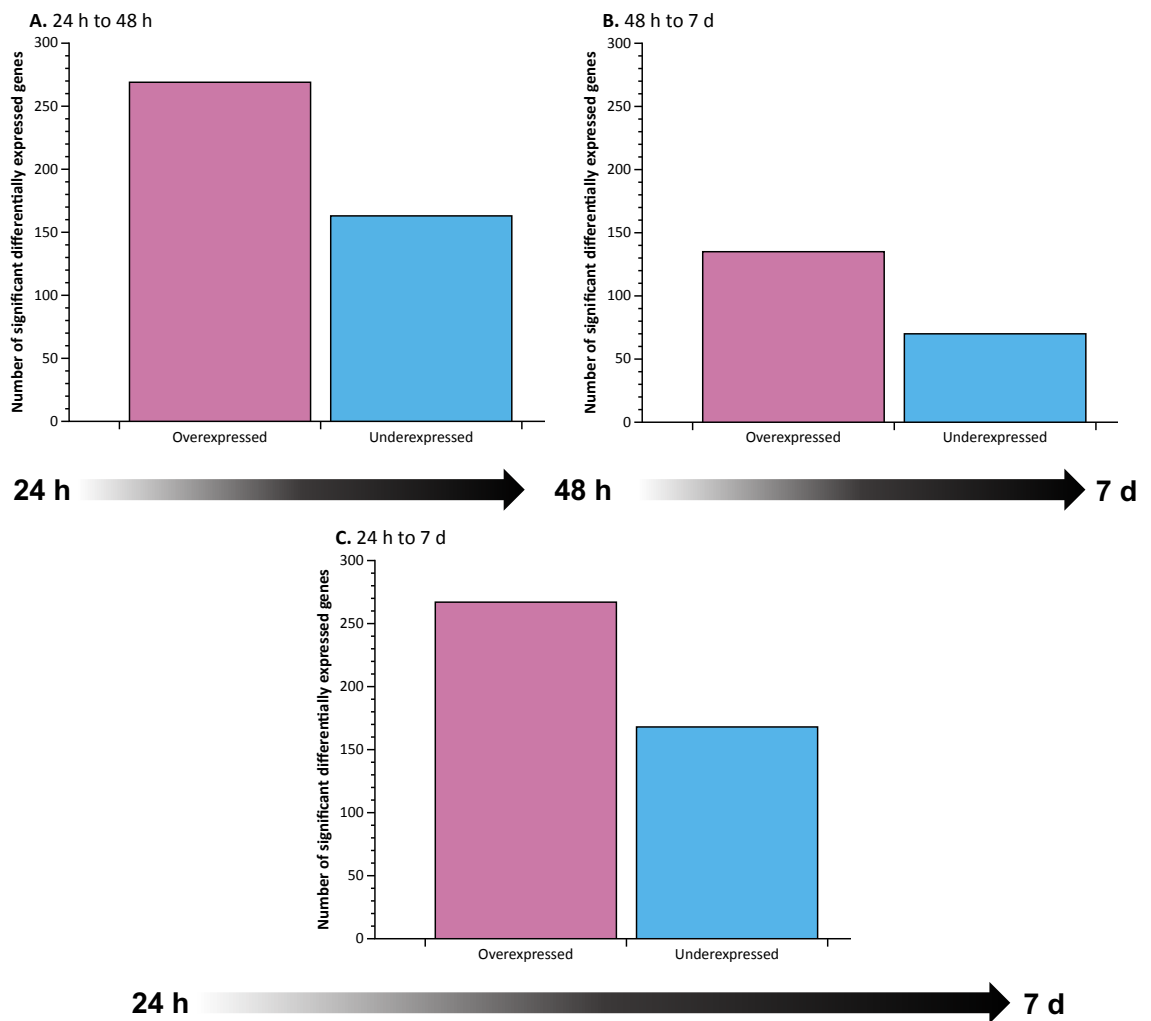
Figure 5.2: **The number of *Pseudomonas aeruginosa* PA14 significant differentially expressed genes (DEGs) (*P* < 0.05, log$_2$ fold change ≥ |1.5|) at each time point in the *ex vivo* pig lung model tissue-associated biofilm.** RNA was sequenced from three lung-associated biofilms from each of two independent pig lungs and differential expression analysis performed. The number of significantly overexpressed genes are shown in pink and the number of significant underepxressed genes shown in blue. The time points investigated were 24 h, 48 h, and 7 d as shown by the arrow timelines under each graph. **(A)** The significant DEGs at 48 h compared with 24 h, indicating the number of genes that were overexpressed/underexpressed from 24 h to 48 h. **(B)** The number of significant DEGs at 7 d compared with 48 h, indicating the number of genes overexpressed/underexpressed from 48 h to 7 d. **(C)** Significant DEGs at 7 d compared with 24 h, indicating the number of genes overexpressed/underexpressed from 24 h to 7 d.

There were a number of metabolic pathways significantly enriched in the lung-associated biofilm 24 hours to 7 days, including upregulation of sulfur metabolism.

The number of significant DEGs did not determine whether the gene expression changes found were likely to have an effect on functional pathways. Therefore, KEGG pathway enrichment analysis of DEGs was performed to identify the significantly enriched *P. aeruginosa* PA14 pathways in each time contrast (*P* < 0.05). GO term analysis was not

performed as in chapter 4, as the present analysis focused on *P. aeruginosa* PA14 samples grown in the same environment to provide a more detailled study of gene expression in the EVPL model biofilm. Hence, the KEGG pathway analysis was considered sufficient detail to provide functional information for the more specifc RNA-seq analysis.

There were no KEGG pathways found to be significantly enriched 24 h to 48 h despite the highest number of significant DEGs found in this contrast (Figure 5.2). However, four KEGG pathways were found to be significantly enriched 24 h to 7 d, including two metabolic pathways (Figure 5.3). The largest percentage of significant DEGs were associated with the sulfur metabolism pathway; the majority of these genes were significantly overexpressed at 7 d. This indicated that sulfur metabolism was upregulated in the *P. aeruginosa* PA14 lung-associated biofilm 24 h to 7 d (Figure 5.3). There was only one gene significantly underexpressed from 24 h to 7 d associated with sulfur metabolism: a sulfite/nitrite reductase PA14_10550 (-1.56 $\log_2$ fold change). The significantly overexpressed sulfur metabolism genes included sulfate transport genes *cysA*, *cysW*, and *cysT* ($\log_2$ fold changes: 3.04, 2.87, and 3.14 respectively), and a number of ATP-binding cassette (ABC) transporters.
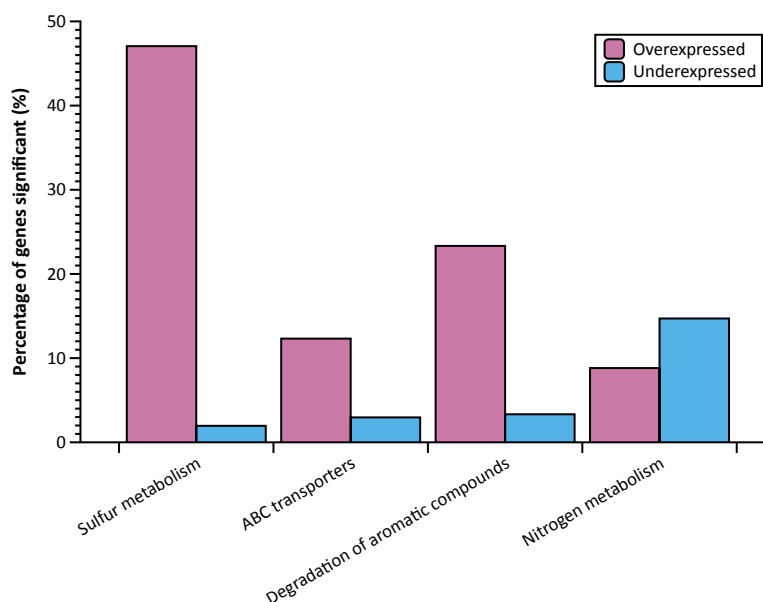
Figure 5.3: **Significantly enriched (P < 0.05) *Pseudomonas aeruginosa* PA14 Kyoto encyclopedia of genes and genomes (KEGG) pathways in the *ex vivo* pig lung-associated biofilm at 7 d compared with 24 h.** The bars show the percentage of significant differentially expressed genes (DEGs) associated with each pathway ($\log_2$ fold change $\geq$ |1.5|, P <0.05). The percentage of significant underexpressed (right bar) and overexpressed (left bar) genes associated with each pathway are shown by different colour fills (see key). Three repeats from each of two independent pig lungs were studied at each time point.

The KEGG pathway for ABC transporters was also found to be significantly enriched 24 h to 7 d (Figure 5.3), and the majority of significant DEGs associated with this pathway were involved in sulfur metabolism. However there were other ABC transporter genes found to be significantly differentially expressed, including overexpression of genes in the phosphate-specific transporter PstSCAB: *pstB* (1.52 log$_2$ fold change), *pstA* (1.83 log$_2$ fold change), and *pstC* (1.88 log$_2$ fold change). This transporter has been shown to be overepressed by *P. aeruginosa* under phosphate stress (Bains et al., 2012; Jones et al., 2021). Alongside these pathways, degradation of aromatic compounds and nitrogen metabolism were also found to be significantly enriched (Figure 5.3). In contrast with the other significant KEGG pathways 24 h to 7 d, there were more nitrogen metabolism associated genes significantly underexpressed than overexpressed.

Nitrogen metabolism was significantly enriched in the lung-associated biofilm from 24 hours to 7 days.

It has previously been shown that *P. aeruginosa* in CF sputum samples move towards mixed anaerobic and micro-aerophilic respiration, associated with upregulation of the nitrogen metabolism operons *nor*, *nir*, *nap*, *nar*, and *nos*, compared with *in vitro* growth (Rossi et al., 2018). As nitrogen metabolism was found to be significantly enriched in the *P. aeruginosa* PA14 lung-associated biofilm from 24 h to 7 d, expression of these operons was investigated. Significant DEGs were only found in the *nor* and *nir* operons in each time contrast (Table 5.1). All genes in the *nor* operon were significantly underexpressed in the lung-associated biofilm from 24 h to 48h, and 24 h to 7 d. This indicated that there was downregulation of this operon by 48 h that was maintained for 7 d (Table 5.1). The expression changes in the *nir* operon did not follow the same pattern as the *nor* operon. All significant DEGs 24 h to 48 h were underexpressed, and all significant DEGs 48 h to 7 d were overexpressed (Table 5.1). The significant *nir* DEGs were also different in each time contrast, with the exception of *nirH*. This gene was significantly underexpressed 24 h to 48 h, then significantly overexpressed 48 h to 7 d resulting in no significant change 24 h to 7 d (Table 5.1). There was no clear pattern for the changes in nitrogen metabolism gene expression, and there was only differential expression in two of the five associated operons. Therefore, no obvious change in nitrogen metabolism gene expression over time in the EVPL biofilm could be determined.

Table 5.1: ***Pseudomonas aeruginosa* PA14 expression of genes in two nitrogen metabolism operons: *nor* and *nir*, in the *ex vivo* pig lung-associated biofilm across three time points.** Differential expression analysis was performed on three replica tissue pieces from each of two independent pig lungs at 24 h, 48 h, and 7 d. Genes were considered significant if the $\log_2$ fold change was $\leq$ -1.5 or $\geq$ 1.5, and $P < 0.05$. The significant $\log_2$ fold change values are shown in the table and were determined at the later time point compared with the earlier time point (i.e. 24 h to 48 h shows expression at 48 h compared with 24 h). Contrasts where the gene was not significantly differentially expressed are denoted with '-'. The orange fill shows genes that were underexpressed at the later time point, the darker the colour representing a higher $\log_2$ fold change. The green fill represents overexpressed genes, with bold and italicised font.

Locus tag	Gene name	Gene product	24 h to 48 h	48 h to 7 d	24 h to 7 d
nor operon					
PA14_06810	*norC*	Nitric-oxide reductase subunit C	-2.12	-	-4.22
PA14_06830	*norB*	Nitric-oxide reductase subunit B	-2.38	-1.69	-4.40
PA14_06840		Dinitrification protein NorD	-3.37	-	-4.26
nir operon					
PA14_06650	*nirN*	C-type cytochrome	-	*2.41*	*2.13*
PA14_06660	*nirE*	Uroporphyrin-III c-methyltransferase	-	*2.51*	*1.56*
PA14_06670	*nirJ*	Heme d1 biosynthesis protein NirJ	-	*2.21*	*1.78*
PA14_06680	*nirH*	Hypothetical protein	-1.57	*2.01*	-
PA14_06690	*nirG*	Transcriptional regulator	-	*1.85*	-
PA14_06700	*nirL*	Heme d1 biosynthesis protein NirL	-1.77	-	-
PA14_06710		Transcriptional regulator	-	-	-
PA14_06720	*nirF*	Heme d1 biosynthesis protein NirF	-2.46	-	-
PA14_06730	*nirC*	C-type cytochrome	-	-	-
PA14_06740	*nirM*	Cytochrome c-551	-3.47	-	-3.11
PA14_06750	*nirS*	Nitrite reductase	-2.12	-	-2.68

Phenazine biosynthesis was upregulated in the lung-associated biofilm from 48 hours to 7 days, associated with QS.

Significantly enriched KEGG pathways were also found in the *P. aeruginosa* PA14 lung-associated biofilm from 48 h to 7 d (Figure 5.4). These pathways were distinct from the significant KEGG pathways enriched 24 h to 7 d (Figure 5.4). Phenazine biosynthesis was significantly upregulated from 48 h to 7 d; all of the associated significant DEGs were overexpressed (Figure 5.4). QS was similarly found to be significantly enriched, and nine out of the eleven associated significant DEGs were also part of the phenazine biosynthesis pathway. The two significantly differentially expressed QS genes not associated with phenazine biosynthesis were the two component response regulator *pmrA* (1.65 log$_2$ fold change) and the only underexpressed gene, *hfq* (-1.56 log$_2$ fold change). Hfq is a global regulator that has been shown to regulate expression of ~5% of the *P. aeruginosa* genome including type III secretion (Janssen et al., 2020). Therefore underexpression of this gene at 7 d may have implications for the *P. aeruginosa* PA14 lung biofilm at later time points. The third KEGG pathway significantly enriched 48 h to 7 d was biosynthesis of secondary metabolites (Figure 5.4). However as found for QS, the majority of the associated genes were involved in phenazine biosynthesis. These results indicated that changes in phenazine biosynthesis may have been the predominant change in the lung-associated biofilm from 48 h to 7 d.
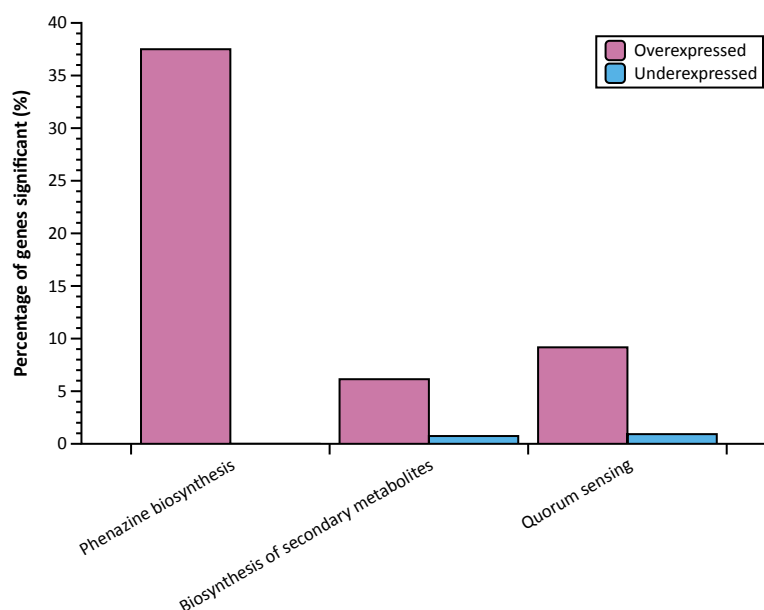
Figure 5.4: **Significantly enriched (*P* < 0.05) *Pseudomonas aeruginosa* PA14 Kyoto encyclopedia of genes and genomes (KEGG) pathways in the *ex vivo* pig lung-associated biofilm at 7 d compared with 48 h.** The bars show the percentage of significantly differentially expressed genes (DEGs) associated with each pathway (log$_2$ fold change $\geq$ |1.5|, *P* <0.05); the percentage of significant underexpressed (right bar) and overexpressed (left bar) genes associated with each pathway are shown by different colour fills (see key). Three repeats from each of two independent pig lungs were studied at each time point.

5.2.3 *P. aeruginosa* PA14 expression profiles in the EVPL tissue-associated biofilm

Analyses of gene expression comparing each pair of time points in the *P. aeruginosa* PA14 lung-associated biofilm identified a number of significant DEGs 24 h to 48 h, 48 h to 7 d, and 24 h to 7 d, that also appeared to affect expression pathways. However, this did not show the pattern of expression changes for individual genes over the 7 d. Therefore, the different gene expression profiles over the timeline: 24 h to 48 h to 7 d, were investigated.

There were seven different *P. aeruginosa* PA14 expression profiles in the lung-associated biofilm.

The number of shared and unique DEGs between each contrast were determined, as shown in Figure 5.5. Genes were considered shared if they were differentially expressed in the same direction (i.e. always overexpressed or always underexpressed). There were more than 100 significant DEGs found to be unique to each contrast, and only four shared by all contrasts (Figure 5.5). The greatest number of unique DEGs was from 24 h to 48 h (280 genes). There were also significant DEGs found to be shared by each pair of contrasts. As shown in Figure 5.5, the highest number of shared genes was from 24 h

175

to 48 h and from 24 h to 7 d (148 genes).
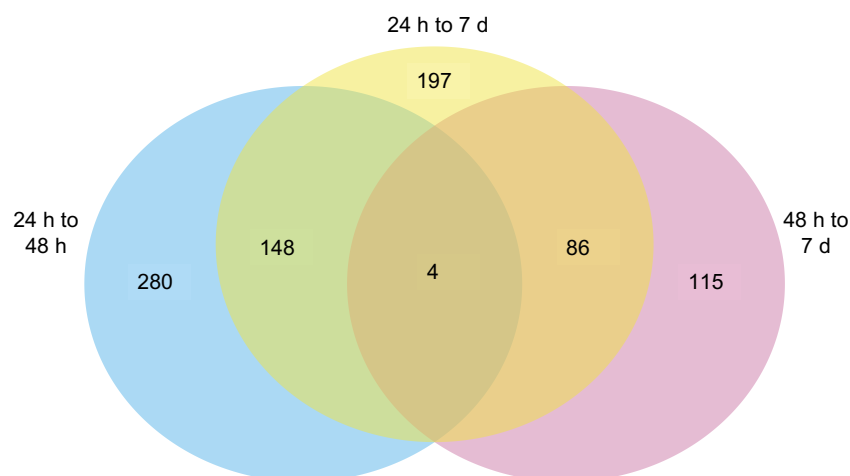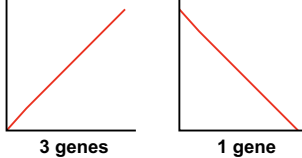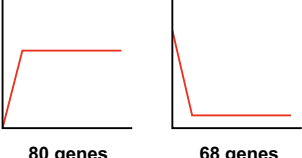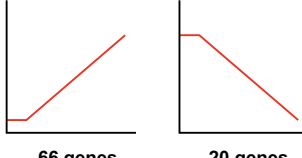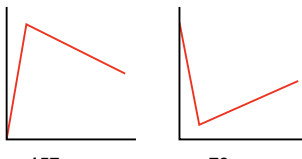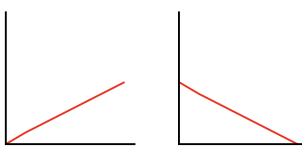
Figure 5.5: **Venn diagram of the number of significant *Pseudomonas aeruginosa* PA14 differentially expressed genes (DEGs) in the *ex vivo* pig lung-associated biofilm in each time point contrast.** Differential expression analysis was performed on three repeats from each of two independent pig lungs at 24 h, 48 h, and 7 d. The genes were considered significant if the $\log_2$ fold change was $\leq$ -1.5 or $\geq$ 1.5, and *P* < 0.05. The shared genes were either significantly overexpressed or underexpressed in all contrasts compared. Genes that were significant in multiple contrasts but in opposing directions were not considered shared.

The expression profiles from 24 h to 48 h to 7 d were determined for each significant DEG based on when changes in expression were shared, unique, or non-significant. Table 5.2 shows the seven different expression profiles found for *P. aeruginosa* PA14 in the lung-associated biofilm over 7 d, divided into individual gene sets. The four genes shared by all three contrasts (Figure 5.5) formed gene set 1. These genes were significantly differentially expressed 24 h to 48 h, then significantly differentially expressed in the same direction 48 h to 7 d, resulting in a cumulative significant difference in expression 24 h to 7 d (Table 5.2). Gene set five had a similar expression profile, where genes were expressed in the same direction from 24 h to 7 d. However, this change was only significant 24 h to 7 d and not between 24 h and 48 h, or 48 h and 7 d (Figure 5.2). Therefore, the change in expression of genes in this set was more gradual than gene set one. The remaining gene sets had expression profiles that were different from 24 h to 48 h than 48 h to 7 d (Table 5.2). The greatest number of genes were found to be part of gene set four. These genes were only significantly differentially expressed 24 h to 48 h, and the non-significant change in expression in the opposite direction 48 h to 7 d
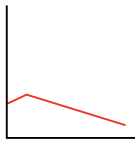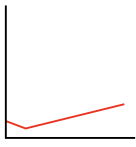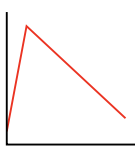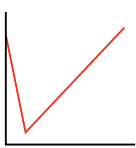
resulted in no significant difference 24 h to 7 d (Table 5.2). Most of the genes in set four were significantly overexpressed at 48 h, suggesting that expression of these genes was upregulated initially then no longer required.

Table 5.2: **The *Pseudomonas aeruginosa* PA14 gene expression profiles found in the *ex vivo* pig lung-associated biofilm at 24 h, 48 h, and 7 d.** Differential expression analysis was performed on three repeats from each of two independent pig lungs at 48 h compared with 24 h, 7 d compared with 48 h, and 7 d compared with 24 h. The changes in expression of each differentially expressed gene (DEG) in each time contrast were investigated to determine the expression changes over the time points investigated. The seven expression profiles found were grouped into gene sets, described below. The graphical representations demonstrate the changes in expression of DEGs over the three time points. Below each graph is the number of significant DEGs found to follow that expression profile in the lung-associated biofilm.

Gene set	Expression profile	Graphical representation
1	A significant change 24 h to 48 h then a significant change in the same direction 48 h to 7 d, resulting in a significant change 24 h to 7 d.	3 genes 1 gene
2	A significant change 24 h to 48 h, maintained 48 h to 7 d (no significant change), resulting in a significant change 24 h to 7 d.	80 genes 68 genes
3	No significant change 24 h to 48 h then a significant change 48 h to 7 d, resulting in a significant change 24 h to 7 d.	66 genes 20 genes
4	A significant change 24 h to 48 h then a small but not significant change in the opposite direction 48 h to 7 d, resulting in no significant change 24 h to 7 d.	157 genes 79 genes
5	A small, not significant change 24 h to 48 h then a small, not significant change in the same direction 48 h to 7 d, resulting in a significant change 24 h to 7 d.	118 genes 79 genes

Continued on next page

Table 5.2 – continued from previous page

Gene set	Expression profile	Graphical representation
6	A small, not significant change 24 h to 48 h then a significant change in the opposite direction 48 h to 7 d, resulting in no significant change 24 h to 7 d.	**20 genes** **51 genes**
7	A significant change 24 h to 48 h then a significant change in the opposite direction 48 h to 7 d, resulting in no significant change 24 h to 7 d.	**29 genes** **15 genes**

As gene set one was made up of genes that had the greatest change over time in the lung-associated biofilm, they were further investigated. There was no association found between these four genes suggesting that there were no operons being upregulated or downregulated following this expression profile (Table 5.3). The only gene that was significantly underexpressed over the 7 d was *norB,* part of the *nor* operon discussed above.

Table 5.3: ***Pseudomonas aeruginosa* PA14 genes that were significantly differentially expressed in all time contrasts in the *ex vivo* pig lung-associated biofilm.** Differential expression analysis was performed on three repeats from each of two independent pig lungs at 48 h compared with 24 h, 7 d compared with 48 h, and 7 d compared with 24 h. Genes significantly differentially expressed in the same direction (i.e. overexpressed/underexpressed) in every contrast formed gene set 1 ($\log_2$ fold change $\geq$ |1.5|, $P < 0.05$). The $\log_2$ fold change value is shown for each gene in each contrast.

Locus tag	Gene name	Gene product	24 h to 48 h	48 h to 7 d	24 h to 7 d
PA14_06830	*norB*	Nitric-oxide reductase subunit B	-2.38	-1.69	-4.40
PA14_22160		Hypothetical protein	1.73	1.61	3.45
PA14_34740		Hypothetical protein	1.59	2.46	4.24
PA14_48460		Polyamine ABC transporter substrate-binding protein	1.63	2.17	3.95

The upregulation of sulfur metabolism in the lung-associated biofilm followed two different gene expression profiles.

The KEGG pathways significantly enriched in each *P. aeruginosa* PA14 gene set were determined to provide insight into the expression profiles of different pathways in the lung-associated biofilm. Although gene set four was made up the largest number of genes, there were no significantly enriched KEGG pathways. However, there were significantly enriched pathways found for three of the gene sets (Figure 5.6). Sulfur metabolism was significantly enriched amongst the genes in gene set two (Figure 5.6A) and gene set five (Figure 5.6B), upregulated in both. This supported the results above, which showed that sulfur metabolism was upregulated in the lung-associated biofilm over 7 d. It also demonstrated that significant sulfur metabolism DEGs were following one of these two expression profiles in the lung-associated biofilm (see Table 5.2: gene sets 2 & 5). Sulfur metabolism was the only KEGG pathway significantly enriched following the expression profile of gene set two, however there were other significantly enriched pathways in gene set five. Degradation of aromatic compounds and benzoate degradation were also significantly enriched in gene set five (Figure 5.6B). Both pathways were upregulated from 24 h to 7 d, and all significant DEGs in the degradation of aromatic compounds pathway were part of the benzoate degradation pathway.

A. Gene set 2

B. Gene set 5
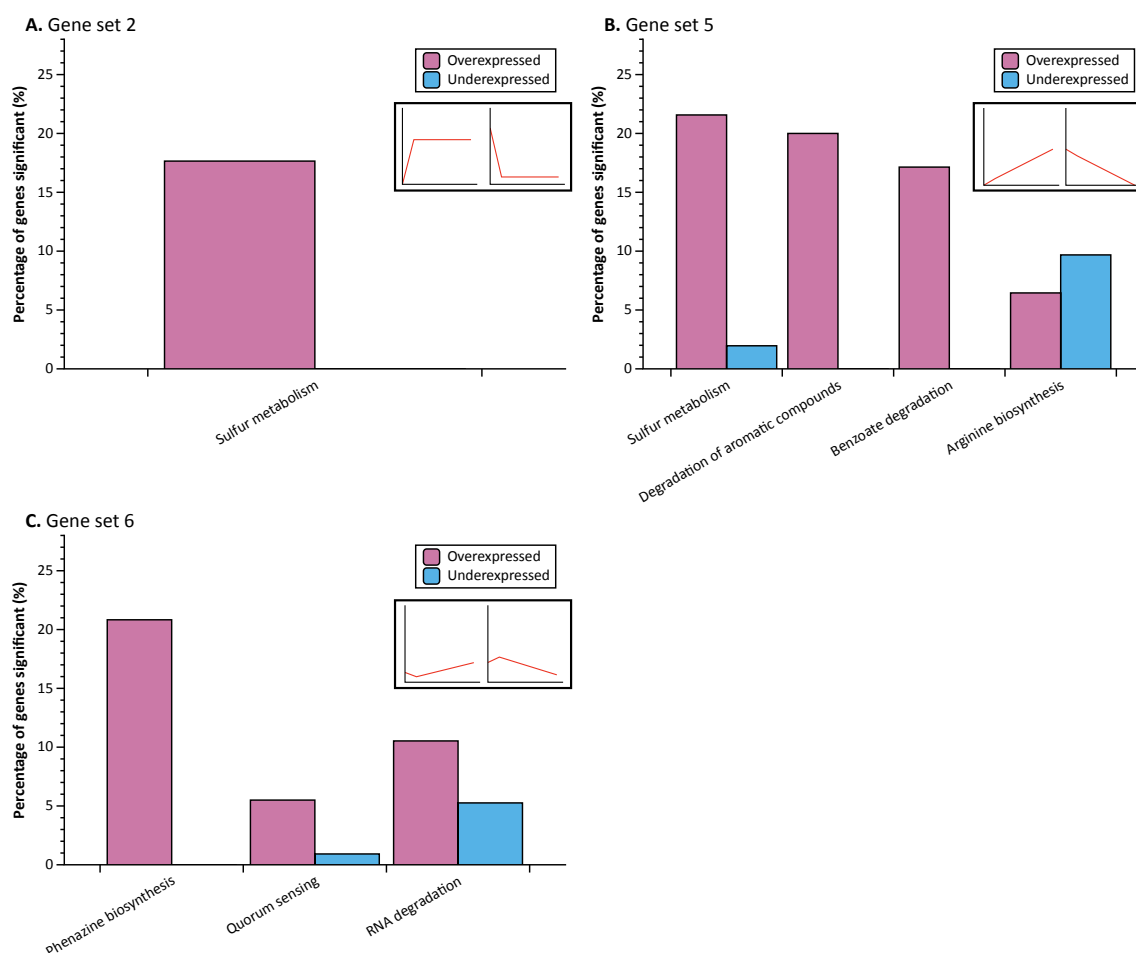
C. Gene set 6

Figure 5.6: **Significantly enriched (*P* < 0.05) *Pseudomonas aeruginosa* PA14 Kyoto encyclopedia of genes and genomes (KEGG) pathways in the *ex vivo* pig lung-associated biofilm in the expression profile gene sets (see Table 5.2).** The bars show the percentage of significant differentially expressed genes (DEGs) associated with each pathway ($\log_2$ fold change $\geq |1.5|$, *P* <0.05); the percentage of significant underexpressed (right bar) and overexpressed (left bar) genes associated with each pathway are shown by different colour fills (see key). The graphical representation of the change in gene expression for each gene set are shown below the keys; the left graph image shows the overexpressed genes and the right shows the underexpressed genes. Three repeats from each of two independent pig lungs were studied at each time point. **(A)** Significantly enriched KEGG pathways in gene set 2, where there was a significant change in the direction specified 24 h to 48 h, which was maintained 48 h to 7 d resulting in a significant change 24 h to 7 d also. **(B)** Significantly enriched KEGG pathway in gene set 5, where there was a significant change in the direction specified 24 h to 7 d caused by non-significant changes in the same direction 24 h to 48 h and 48 h to 7 d. **(C)** Significantly enriched KEGG pathways in gene set 6, where there was a significant change in the direction specified only at 7 d compared with 48 h.

Arginine biosynthesis was also found to be significantly enriched in gene set five (Figure 5.6B). Two of the associated significant DEGs were overexpressed 24 h to 7 d, and three were underexpressed. Two of the significantly underexpressed arginine biosynthesis genes 24 h to 7 d were arginine fermentation enzymes (Schreiber et al., 2006): *arcB* (-2.25 $\log_2$ fold change) and *arcC* (-2.16 $\log_2$ fold change).

The significantly enriched KEGG pathways in gene set six (Figure 5.6C) were different from those in gene sets two and five. This gene set was composed of genes only significantly differentially expressed from 48 h to 7 d (see Table 5.2: gene set 6). The pathways following this expression profile were phenazine biosynthesis, QS, and RNA degradation (Figure 5.6). All associated phenazine biosynthesis DEGs were also associated with the QS pathway, and were significantly overexpressed 48 h to 7 d. These genes were initially underexpressed from 24 h to 48 h, however this change in expression was not found to be significant.

5.2.4 Expression of antibiotic resistance associated genes and biofilm genes in the EVPL tissue-associated biofilm over 7 days

There was underexpression of two individual antibiotic resistance associated genes in the lung-associated biofilm from 24 hours to 48 hours.

Analysis of the *P. aeruginosa* PA14 transcriptome in the EVPL model in chapter 4, compared with *in vitro* SCFM growth, found significant differential expression of genes associated with antibiotic resistance. These results indicated that *P. aeruginosa* PA14 growth as a biofilm associated with the lung-tissue had an effect on resistance. Therefore, the expression of genes predicted to be involved in antibiotic resistance were also investigated in the lung-associated biofilm over 7 d. The expression profile gene set that each significant gene was part of was also determined. Table 5.4 shows the antibiotic resistance genes where expression significantly changed over time. Two of the genes were part of gene set four: *mexG* and *arnA* (Table 4.6). These genes were significantly underexpressed 24 h to 48 h, then expression increased 48 h to 7 d although this was not significant. This resulted in no significant difference in expression 24 h to 7 d.

Table 5.4: ***Pseudomonas aeruginosa* PA14 antibiotic resistance associated genes found to be significantly differentially expressed in at least one time contrast in the *ex vivo* pig lung-associated biofilm.** Differential expression analysis was performed on three repeats from each of two independent pig lungs at 48 h compared with 24 h, 7 d compared with 48 h, and 7 d compared with 24 h. The locus tag, gene name, and gene product is shown as well as the expression profile gene set each gene was found to be a part of in the lung-associated biofilm (see Table 5.2). The $\log_2$ fold change (FC) in the contrast that was significant is also shown. A $\log_2$ fold change was found to be significant if it was $\geq$ 1.5 or $\leq$ -1.5 and *P* < 0.05. These genes were not significantly differentially expressed in the contrasts not shown.

Locus tag	Gene name	Gene product	Gene Set	Time: $\log_2$FC
PA14_09540	*mexG*	Hypothetical protein	4	24 h to 48 h: -1.52
PA14_18350	*arnA*	Bifunctional UDP-glucuronic acid decarboxylase/UDP-4-amino-4-deoxy-L-arabinose formyltransferase	4	24 h to 48 h: -1.59
PA14_10470	*bcr-1*	MFS transporter	5	24 h to 7 d: -2.49

No other components of the efflux pumps *mexG* is part of were found to be significantly differentially expressed over time, thus it was unlikely that changes in this gene had phenotypic effect in the lung-associated biofilm. However, as explored in Chapter 4, *arnA* is part of the *arn* locus associated with CAMP resistance (Gutu et al., 2015). As this gene was significantly underexpressed at 48 h, it may have caused increased resistance at 24 h in comparison with 48 h. This is consistent with the MIC for the CAMP polymyxin B determined in chapter 4; the MIC for lung-associated biofilm *P. aeruginosa* PA14 cells at 24 h was 8 µg ml^{-1} and 4 µg ml^{-1} at 48 h (Table 4.7).

The third *P. aeruginosa* PA14 antibiotic resistance assoicated gene signficiantly differentially expressed over time in the lung-associated biofilm was *bcr-1* (Table 5.4). This gene was part of gene set five; expression was non-significantly reduced from 24 h to 48 h, and 48 h to 7d, which resulted in significant underexpression 24 h to 7 d (Table 4.6). The gene *bcr-1* encodes a transmembrane protein that has been associated with bicyclomycin resistance (Fonseca et al., 2015). Overall, these results indicate that some *P. aeruginosa* PA14 antibiotic resistance mechanisms may have been downregulated over time in the lung-associated biofilm.

There was downregulation of biosynthesis of the biofilm exopolysaccharide Pel over time in the *P. aeruginosa* PA14 lung-associated biofilm.

In chapter 3, visualisation of the *P. aeruginosa* PA14 biofilm formed on the surface of the EVPL tissue identified a structure that was similar to the biofilm architecture observed in the CF lung for chronic *P. aeruginosa* infection. In chapter 4, the transcriptome comparison between the EVPL model and *in vitro* SCFM demonstrated that expression of a number of genes under QS control was comparable to CF sputum. This suggested that QS-regulated genes were expressed similarly to human infection in the EVPL *P. aeruginosa* PA14 biofilm. Therefore, the expression pathways involved in biofilm formation and QS pathways were investigated over 7 d in the lung-associated biofilm. The aim was to determine whether there were changes in expression of these genes that underpin the previous findings. The *P. aeruginosa* PA14 locus tags corresponding to each gene studied are shown in Appendix B (Table B.1).

The expression of genes in these pathways was initially investigated from 24 h to 7 d. As shown in Figure 5.7, there were no QS genes significantly differentially expressed. There was also only one gene associated with virulence factor production in these pathways significantly differentially expressed; *lec*A was overexpressed from 24 h to 7 d (Figure 5.7). LecA is an internal lectin, often referred to as PA-IL, that binds D-galactose and has been associated with adhesion to host cells, *P. aeruginosa* aggregation, and shown to be involved in the formation of mature biofilm architecture (Diggle et al., 2006). In contrast, all genes for Pel biosynthesis were found to be significantly underexpressed from 24 h to 7 d in the lung-associated biofilm (Figure 5.7). Pel has been shown to be an essential exopolysaccharide for biofilm development by *P. aeruginosa* PA14 (Colvin et al., 2011). Hence, this indicated that the formation of biofilm was downregulated from 24 h on the EVPL tissue over 7 d. However, genes involved in biosynthesis of another biofilm exopolysaccharide, alginate, did not appear to be differentially expressed (Figure 5.7). There were other genes in the regulatory pathways for biofilm formation and QS found to be significantly differentially expressed 24 h to 7 d, however they did not appear to be associated with clear differences in expression of the pathway overall (Figure 5.7).

Figure 5.7: **Diagram showing expression changes in the *Pseudomonas aeruginosa* PA14 Kyoto encyclopedia of genes and genomes (KEGG) biofilm formation and quorum sensing (QS) pathways in the *ex vivo* pig lung-associated biofilm from 24 h to 7 d.** Three repeats from each of two independent pig lungs were studied at each time point, and genes were considered significantly differentially expressed if the $\log_2$ fold change was $\geq$ 1.5 or $\leq$ -1.5 and P < 0.05. The diagram shows all genes involved in each pathway, including signalling pathways and the Pel exopolysaccharide biosynthesis pathway. The $\log_2$ fold change value from 24 h to 7 d is shown below each gene name; genes shown in red were significantly underexpressed and genes shown in green were significantly overexpressed. The blocked arrows represent gene activation and the dashed arrows show indirect gene activation. The solid blocked solid lines (ending with |, not an arrow) show inhibition and the dashed blocked lines show indirect inhibition. The blue 'P' represents phosphorylation.

Figure 5.8 shows these pathways with the $\log_2$ fold change in expression of each gene from 24 h to 48 h in the lung-associated biofilm. Consistent with the findings from 24 h to 7 d (Figure 5.7), the majority of Pel biosynthesis genes were also significantly underexpressed from 24 h to 48 h (Figure 5.8). This indicated that the downregulation of Pel biosynthesis found 24 h to 7 d began prior to 48 h. Conversely, the *lecA* gene was not found to be significantly differentially expressed 24 h to 48 h, however *lecB* was overexpressed (Figure 5.8: 1.54 $\log_2$ fold change). LecB is the second *P. aeruginosa* internal lectin, often referred to as PA-IIL, that binds fucose and mannose. It has been shown to play a role as a biofilm matrix protein, associated with increased cell and exopolysaccharide retention within the biofilm (Passos da Silva et al., 2019). Despite there being other significant DEGs found in these pathways from 24 h to 48 h, as at 24 h to 7 d, there were no clear pathway effects (Figure 5.8).
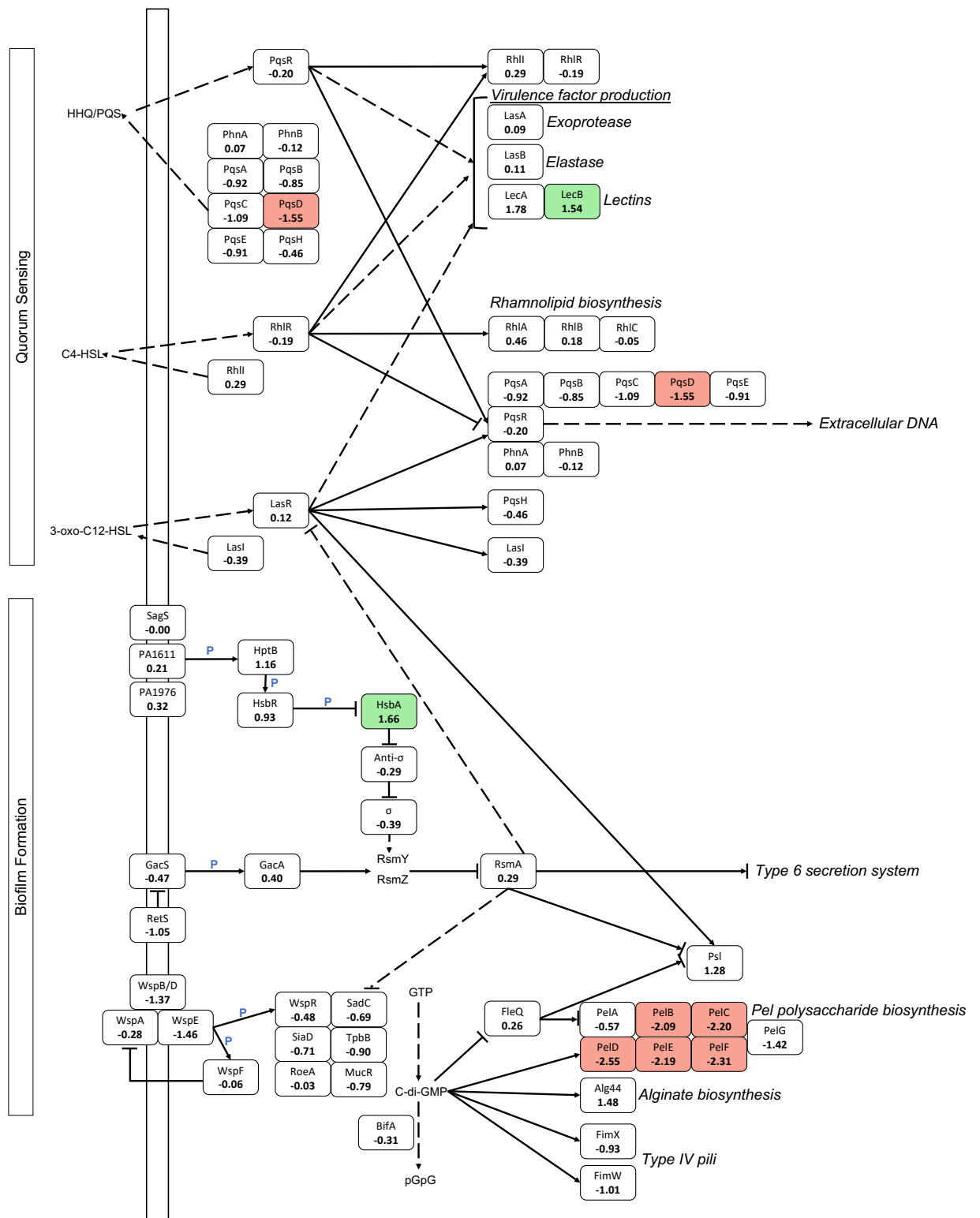
Figure 5.8: **Diagram showing expression changes in the *Pseudomonas aeruginosa* PA14 Kyoto encyclopedia of genes and genomes (KEGG) biofilm formation and quorum sensing (QS) pathways in the *ex vivo* pig lung-associated biofilm from 24 h to 48 h.** Three repeats from each of two independent pig lungs were studied at each time point, and genes were considered significantly differentially expressed if the $\log_2$ fold change was ≥ 1.5 or $\leq$ -1.5 and $P < 0.05$. The diagram shows all genes involved in each pathway, including signalling pathways and the Pel exopolysaccharide biosynthesis pathway. The $\log_2$ fold change value from 24 h to 48 h is shown below each gene name; genes shown in red were significantly underexpressed and genes shown in green were significantly overexpressed. The blocked arrows represent gene activation and the dashed arrows show indirect gene activation. The solid blocked solid lines (ending with |, not an arrow) show inhibition and the dashed blocked lines show indirect inhibition. The blue 'P' represents phosphorylation.

Figure 5.9 shows the same pathways with the $\log_2$ fold change in expression of each gene from 48 h to 7 d; there were only two genes found to be significantly differentially expressed in this contrast. The Pel biosynthesis genes were not differentially expressed unlike 24 h to 7 d, and 24 h to 48 h. This indicated that biosynthesis of biofilm exopolysaccharide Pel followed the gene set two expression profile (see Table 5.2). Biosynthesis was downregulated 24 h to 48 h then expression of these genes was maintained at the same level from 48 h to 7 d (Figure 5.9). There was however one gene of interest significantly differentially expressed 48 h to 7 d; *rsmA* was significantly underexpressed in the lung-associated biofilm from 48 h to 7 d (Figure 5.9; -1.57 $\log_2$ fold change). The regulatory protein RsmA is involved in global regulation of *P. aeruginosa* virulence, the KEGG pathway shows that it is involved in repression of type VI secretion (Figure 5.9), and is also known positively regulate type III secretion and directly repress Pel genes (Mikkelsen et al., 2011).

Quorum Sensing

HHQ/PQS

PqsR
0.56

RhlI
-0.14

RhlR
-0.07

Virulence factor production

PhnA -0.00	PhnB -0.36
PqsA 0.18	PqsB 0.26
PqsC 0.71	PqsD 0.94
PqsE 0.58	PqsH -0.48

LasA
-0.18 *Exoprotease*

LasB
-0.46 *Elastase*

LecA 0.90 | LecB -0.07 *Lectins*

C4-HSL

RhlR
-0.07

Rhamnolipid biosynthesis

| RhlA -0.21 | RhlB 0.25 | RhlC -0.23 |

RhlI
-0.14

| PqsA 0.18 | PqsB 0.26 | PqsC 0.71 | PqsD 0.94 | PqsE 0.58 |

PqsR
0.56 → *Extracellular DNA*

PhnA -0.00 | PhnB -0.36

3-oxo-C12-HSL

LasR
-0.73

PqsH
-0.48

LasI
-0.65

LasI
-0.65

Biofilm Formation

SagS
-0.55

PA1611
-0.42 **P**

HptB
-0.34 **P**

PA1976
0.59

HsbR
-0.69 **P**

HsbA
-0.83

Anti-σ
0.36

σ
0.61

GacS
-0.31 **P**

GacA
-0.18

RsmY
RsmZ

RsmA
-1.57

Type 6 secretion system

RetS
0.29

Psl
-1.25

WspB/D
0.21

WspA -0.50 | WspE -0.05 **P**

WspR 0.49 | SadC -0.09

SiaD -0.50 | TpbB 0.29

RoeA 1.54 | MucR 1.08

WspF
0.17

GTP

FleQ
-1.19

| PelA -0.89 | PelB -0.29 | PelC 0.07 | *Pel polysaccharide biosynthesis* |
| PelD 0.14 | PelE 0.16 | PelF 0.08 | PelG -0.09 |

C-di-GMP

Alg44
-1.11 *Alginate biosynthesis*

FimX
0.30

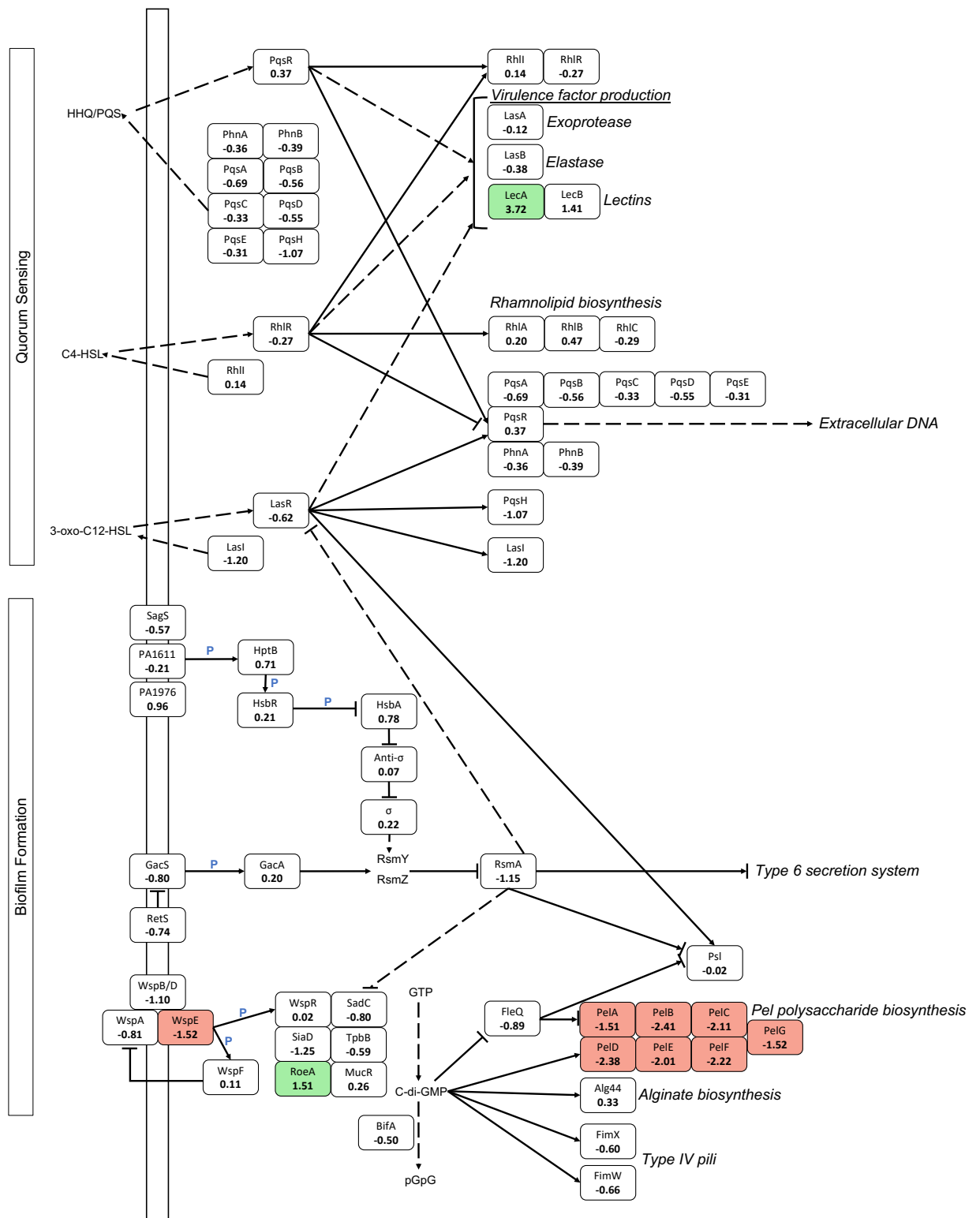FimW
0.32 *Type IV pili*

BifA
-0.18

pGpG

Figure 5.9: **Diagram showing expression changes in the *Pseudomonas aeruginosa* PA14 Kyoto encyclopedia of genes and genomes (KEGG) biofilm formation and quorum sensing (QS) pathways in the *ex vivo* pig lung-associated biofilm from 48 h to 7 d.** Three repeats from each of two independent pig lungs were studied at each time point, and genes were considered significantly differentially expressed if the $\log_2$ fold change was $\geq$ 1.5 or $\leq$ -1.5 and P < 0.05. The diagram shows all genes involved in each pathway, including signalling pathways and the Pel exopolysaccharide biosynthesis pathway. The $\log_2$ fold change value from 48 h to 7 d is shown below each gene name; genes shown in red were significantly underexpressed and genes shown in green were significantly overexpressed. The blocked arrows represent gene activation and the dashed arrows show indirect gene activation. The solid blocked solid lines (ending with |, not an arrow) show inhibition and the dashed blocked lines show indirect inhibition. The blue 'P' represents phosphorylation.

More genes associated with *P. aeruginosa* PA14 virulence factor production were also investigated, including motility, type III secretion, type VI secretion, and alginate biosynthesis. There was no significant differential expression found in the lung-associated biofilm for any of these factors. However, *cpdA* was found to be significantly underexpressed from 24 h to 7 d (-2.44 $\log_2$ fold change) and 24 h to 48 h (-1.70 $\log_2$ fold change). This gene followed the gene set two expression profile; there was a significant reduction in expression from 24 h to 48 h, which was then maintained to 7 d (Table 5.2). CpdA is involved in cyclic adenosine monophosphate (cAMP) homeostasis and regulates the production of virulence factors (Fuchs et al., 2010).

5.3   Discussion

Transcriptome analysis of the *P. aeruginosa* PA14 biofilm associated with the EVPL tissue at 24 h, 48 h, and 7 d identified changes in metabolic pathways and genes associated with antibiotic resistance. The comparison of gene expression at different time points found non-significant changes in expression of key regulatory genes, suggesting that the biofilm population was maintained throughout 7 d infection. These findings demonstrated that the EVPL model may provide an environment for formation of *P. aeruginosa* biofilms that not only phenotypically exhibit characteristics of a mature biofilm, but also maintains the *P. aeruginosa* PA14 population for 7 d.

A distinct *P. aeruginosa* PA14 transcriptome was identified at each time point studied, indicating that there were changes in expression in the lung-associated biofilm. As there was no distinction between samples grown on tissue from independent pig lungs this indicated that these changes were true differences in the biofilm population not caused by variation between lungs. This further supported the EVPL model as a reliable model for growing *P. aeruginosa* biofilms that mimic CF lung infection. The greatest difference in PA14 gene expression was observed between the first time point, 24 h following infection, and the two later time points (48 h and 7 d). The majority of genes were overexpressed, which indicated that many pathways were being upregulated in the EVPL biofilm. There were also a number of different expression profiles identified that demonstrated the progression of *P. aeruginosa* infection in the EVPL model following biofilm formation.

The signifcant changes in gene expression were associated with a number of different KEGG pathways. Sulfur metabolism was found to have the highest percentage of significant DEGs associated. It was upregulated from 24 h to 7 d, and associated genes followed two different expression profiles; a gradual overexpression from 24 h to 7 d, or a significant increase 24 h to 48 h that was maintained to 7 d. More specifically, all genes in the sulfur transporter operon associated with cysteine biosynthesis: *cysTWA*, were found to be significantly overexpressed 24 h to 7 d. In *E. coli*, upregulation of this operon has been linked to sulfate starvation (Gyaneshwar et al., 2005). However, the role of these genes in *P. aeruginosa* biofilms is less clear. Investigation of the sulfate starvation response in *P. aeruginosa* PAO1 and a cystic fibrosis clinical isolate found genes involved in cysteine biosynthesis, including *cysTWA*, were only weakly upregulated when sulfate was limited (Tralau et al., 2007). Therefore, despite the upregulation of this pathway indicating that there may be sulfate starvation by 7 d in the lung-associated biofilm, which is possible as there was no mucin added to the SCFM or media supplementation, there are other explanations that must be considered.

There have been links made with iron starvation and sulfur metabolism, in fact during iron starvation proteins involved in cysteine biosynthesis and sulfur assimilation are reduced (Nelson et al., 2019). Therefore, upregulation of sulfur metabolism may have been caused by changes in iron availability in the lung-associated biofilm; if upregulation occurs when iron is in abundance. Sulfur metabolism has also been associated with anaerobic respiration. In particular, *P. aeruginosa* PA14 grown in SCFM using the same protocol for SCFM as in the EVPL model demonstrated upregulation of sulfur metabolism genes despite no sulfur starvation (Tata et al., 2016). Hence, sulfur availability in the EVPL model should be determined in the future to identify whether sulfur starvation arises at 7 d and media supplementation is required, or if this expression change is representative of other environment conditions.

Nitrogen metabolism was also significantly enriched from 24 h to 7d , however there was no clear overall change in expression of nitrogen metabolism genes. There were associated genes significantly overexpressed and genes significantly underexpressed. Further investigation of denitrification operons, the process of nitrogen metabolism in *P. aeruginosa*, did not reveal any obvious differences. In contrast, these operons have been shown to be upregulated in CF sputum showing a shift towards anaerobic

respiration alongside microaerophilic respiration (Rossi et al., 2018). There were some genes significantly differentially expressed including significant overexpression of five genes in the *nir* denitrification operon from 48 h to 7 d: *nirN*, *nirE*, *nirJ*, *nirH*, and *nirG*. These genes are part of the *nirSMCFDLGHJEN* cluster that is induced by the regulator of anaerobic respiration, Anr, under denitrifying conditions (Kawasaki et al., 1997). Conversely, *nirM* and *nirS* were both significantly underexpressed from 24 h to 48 h, then the level of expression was maintained to 7 d. These genes are part of the *nirSMC* operon, which is induced under anaerobic conditions. In fact, during aerobic growth expression of these genes is not detected at all (Trunk et al., 2010), and *nirS* is upregulated in anoxia (Line et al., 2014). These findings showed that there were indications of denitrification being upregulated and downregulated in the lung-associated *P. aeruginosa* PA14 biofilm over 7 d. There is an oxygen gradient in the CF lung, where oxygen availability is reduced with depth (Worlitzsch et al., 2002). Hence, these conflicting gene expression changes may have been caused by different mechanisms for respiration in different regions. Measurements of oxygen at different points in the lung-associated biofilm would provide more information on this.

Another pathway associated with *P. aeruginosa* growth in low oxygen environments was also significantly enriched over time in the lung-associated *P. aeruginosa* PA14 biofilm. Significant DEGs associated with arginine biosynthesis were found from 24 h to 7 d, caused by a gradual change in expression from 24 h to 48 h, then a continued gradual change from 48 h to 7 d. Two of these genes are involved in arginine fermentation, *arcB* and *arcC*. They encode enzymes which, alongside the arginine deminiase ArcA, produce ATP from converting arginine to ornithine, supporting anaerobic growth (Schobert and Jahn, 2010). These genes have been shown to be induced during *P. aeruginosa* growth in anaerobic conditions over 7 d (Schreiber et al., 2006). These results suggest that anaerobic respiration was not upregulated in the lung-associated biofilm. However, it is proposed that microaerobic and anaerobic respiration occur simultaneously in the CF lung. Therefore, sequencing of all messenger RNA (mRNA) may not reveal changes within different regions of the biofilm (Alvarez-Ortega and Harwood, 2007), as hypothesised based on nitrogen metabolism gene expression.

Among the pathways upregulated was phenazine biosynthesis, the associated genes were slightly underexpressed from 24 h to 48 h, then significantly overexpressed from

48 h to 7 d. The virulence factor pyocyanin is one of the most frequently researched phenazines, and genes associated with its biosynthesis were upregulated over time in the lung-associated biofilm. It has been shown to act as a signalling molecule for *P. aeruginosa* PA14 by upregulating genes involved in efflux pumps, iron acquisition, and redox, and appears to link the PQS QS system with expression of the key efflux pump discussed in chapter 4, MexGHI-opmD (Dietrich et al., 2006). It has been shown that all three QS systems are involved in the regulation of phenazine biosynthesis operons, including production of phenazine-1-carboxylic acid (PCA) and pyocyanin (Higgins et al., 2018). The differential expression of phenazine biosynthesis genes thus shows that there were changes in QS regulated pathways over time in the lung-associated biofilm. In flow-cell *P. aeruginosa* PA14 biofilms, phenazines, specifically pyocyanin, have been proven to play a role in the formation of a biofilm with defined architecture, and phenazine-deficient mutants were unable to form a structured biofilm (Ramos et al., 2010). Thus, the upregulation of this pathway may be associated with the development of a mature, structured *P. aeruginosa* PA14 biofilm on the surface of the EVPL tissue at 7 d, as observed in chapter 3.

P. aeruginosa PA14 changes in expression of genes in the three QS pathways was also investigated: LasI/R, RhlI/R, and PQS. There were no significant differences found in any of the time contrasts, indicating that expression of these pathways did not change from 24h to 7 d in the *P. aeruginosa* PA14 lung-associated biofilm. Other regulatory pathways involved in lifestyle changes, including the switch from acute to chronic infection, were also investigated however no clear differences in expression were found either. There were also no significant changes in virulence factor gene expression found. It is known that as part of adaptation to the CF lung and formation of a chronic infection, *P. aeruginosa* positively selects for mutations in virulence pathways and virulence factor production is significantly reduced (Smith et al., 2006). As the phenotypic analyses in chapter 3 demonstrated that virulence factor production was limited at 48 h in the lung-associated biofilm, maintained for 7 d, these results may indicate that *P. aeruginosa* PA14 had already switched off virulence factor production by 24 h hence no change was observed. This would also explain why the expression of regulatory pathways was maintained. This further supported the EVPL as a model for chronic-like *P. aeruginosa* biofilm infection of the CF lung.

There were some individual genes of interest found to be significantly differentially expressed over time in the EVPL biofilm. The gene *cpdA* was significantly underexpressed from 24 h to 48 h, and expression was maintained to 7 d. This resulted in significant underexpression from 24 h to 7 d. CpdA is a cAMP phosphodiesterase; it has been shown that loss of gene function causes an accumulation of cAMP within cells, which in turn affects the regulation of virulence factor expression (Fuchs et al., 2010). The activity of *cpdA* also affects biofilm formation, however there is conflicting evidence of what this impact is. It has been demonstrated that loss of *cpdA* results in the build up of intracellular cAMP and inhibition of biofilm formation in a study using *P. aeruginosa* PAO1 (Almblad et al., 2019). However, a study that investigated the role of *cpdA* in *P. aeruginosa* PA14 showed that a mutant for *cpdA* experienced a build up of c-di-GMP, which resulted in increased biofilm formation (Luo et al., 2015). As work in the EVPL model used *P. aeruginosa* PA14, the underexpression of *cpdA* over time may have caused an increase in biofilm formation.

There were significant changes in biofilm associated genes in the lung-associated biofilm. Pel biosynthesis genes were significantly underexpressed from 24 h to 48 h, then maintained at the same expression level from 48 h to 7 d, resulting in significant downregulation from 24 h to 7 d. This suggested that production of Pel was reduced after 24 h then kept at the same level from 48 h onwards. As mentioned, Pel is a biofilm exopolysaccharide that is essential to biofilm development by *P. aeruginosa* PA14, and is only expressed during biofilm growth (Colvin et al., 2011; Marmont et al., 2017). It must be considered that Pel was significantly underexpressed in the lung-associated biofilm at 48 h and 7 d, compared with 24 h. This did not indicate that there was no Pel being produced at the later time points, just less than the initial stage of infection in the EVPL model. This may have been caused by upregulation of Pel biosynthesis as the biofilm was established at 24 h, which was reduced once the biofilm was formed at 48 h, and gene expression was maintained over 7 d for the level of Pel production required. This was also an indication that the *P. aeruginosa* PA14 biofilm was maintained over 7 d in the EVPL model, as there was consistent expression of exopolysaccharide biosynthesis genes. The focus of gene expression may have been on the formation of a mature structure, rather than further biofilm formation. This was also supported by the upregulation of two lectin genes observed in the lung-associated biofilm from 24 h to 7 d, and from 24 h to 48 h. Both have been associated with a mature biofilm; *lecA* is

indicated to play a role in formation of a mature architecture (Diggle et al., 2006), and *lecB* involved in increased cell and exopolysaccharide retention in the biofilm (Passos da Silva et al., 2019). This retention may also have been responsible for the reduction in Pel production, as less new Pel was required.

A significant reduction in expression of two individual antibiotic resistance genes was seen from 24 h to 48 h: *arnA* and *bcr-1*, associated with resistance to CAMPs (Gutu et al., 2015) and bicyclomycin (Fonseca et al., 2015) respectively. This was consistent with the reduced polymyxin B MIC determined for *P. aeruginosa* PA14 cells from the lung-associated biofilm at 48 h compared with 24 h. This suggested that the changes in expression had a phenotypic effect, and certain mechanisms of antibiotic resistance may have been reduced as the *P. aeruginosa* PA14 biofilm established in the EVPL model. This coincided with the reduction in expression of Pel biosynthesis genes at 48 h, and the formation of a biofilm visualised in chapter 3. Potentially the formation of a biofilm, of which the matrix facilitates antibiotic resistance (Høiby et al., 2010), led to other mechanisms of antibiotic resistance being downregulated as they were not required. This supports the use of biofilm disrupters to improve treatment regimens as the *P. aeruginosa* cells within the biofilm may not be expressing some genes associated with antibiotic resistance.

However, there were other mechanisms of antibiotic resistance found to be significantly overexpressed, associated with environmental pressures. Phosphate transporters were significantly overexpressed from 24 h to 7 d, indicative of phosphate stress. Under phosphate stress *P. aeruginosa* has been shown to undergo lipid modifications that confer resistance to polymyxin B. There is a transition from phospholipids to glycolipids, which confer protection against polymyxin B (Jones et al., 2021). Therefore, this expression change may have conferred increased antibiotic resistance. Future investigation of *P. aeruginosa* lipid modifications in the EVPL model environment would provide more information. This analysis has indicated that these pathways may be induced, thus further understanding of the mechanisms of resistance triggered by the EVPL model may highlight novel targets for treatments.

The work in this chapter has shown that there are changes in the *P. aeruginosa* lung-associated biofilm population in the EVPL model over 7 d. Introduction of other

factors that influence *P. aeruginosa* gene expression in the CF lung, such as other microbes and antibiotic treatment, to the EVPL model may reveal further changes in the biofilm population that facilitate survival in these conditions. Further insight into these mechanisms may provide better understanding as to how to eradicate chronic *P. aeruginosa* infections. The transcriptome analysis has also indicated that there may be heterogeneity within the biofilm population, particularly in respiration and metabolism. However, future studies of individual niches within the lung-associated biofilm are required to confirm this. The nutrient and oxygen availability in the EVPL model across 7 d should also be investigated, to understand the cause of changes in gene expression. This will also be important in developing the model as a platform for long term evolution experiments, determing any supplementation that is required to maintain the *P. aeruginosa* biofilm population for longer than 7 d.

5.3.1 Conclusion

I have demonstrated that there were distinct *P. aeruginosa* transcriptomes at different time points in the lung-associated biofilm in the EVPL model. The greatest differences in gene expression were between 24 h and the two later time points, 48 h and 7 d. At 48 h, the *P. aeruginosa* biofilm appeared to become reminiscent of chronic infection. Although I have shown a number of key changes related to metabolism, biofilm formation, and antibiotic resistance, further investigation of the conditions created in the EVPL model over longer infection periods is required to better understand these mechanisms. This work built upon the findings in chapters 3 and 4, which showed that *P. aeruginosa* formed a biofilm reminiscent of *in vivo* infection and gene expression was more comparable to human infection than *in vitro* media, to show that there are changes in the *P. aeruginosa* population in the EVPL biofilm over time that likely affect infection dynamics. Other factors can now be introduced in the model to determine the effect they have on *P. aeruginosa* infection over time.

Chapter 6

Pseudomonas aeruginosa and *Burkholderia cepacia* complex mixed infection

6.1   Introduction

The CF lung is a polymicrobial environment; although *P. aeruginosa* is the most common pathogen, infections are caused by a range of miroorganisms. There is a shift in the dominant pathogens over time in the CF lung; *S. aureus* and *H. influenzae* are primarily found in the airways of children with CF, then *P. aeruginosa* and the *Burkholderia cepacia* complex (Bcc) are associated with infections later in life (Filkins and O'Toole, 2015). CF lung infections have traditionally been investigated using culture-based techniques, however it is now known that this does not detect all microbes. Therefore, there are microbial species that may have previously been overlooked. Rogers et al. (2004) were the first to show that the CF lung is a complex, polymicrobial environment composed of a diverse microbial community, including pathogens and the microbiota. It has since been shown that the CF lung microbiota may be an indicator of lung disease state, with reduced diversity associated with worsened lung function and obligate anaerobes dominant when lung function is better (Cuthbertson et al., 2020). As more is discovered about the range of microorganisms in the CF lung, their interactions, and the effect on AMR, this may provide more information on infection dynamics and reveal novel treatment approaches. This requires development of a laboratory model that is able to accurately replicate mixed infections, which has become a key research focus for those who study CF lung infections (O'Toole et al., 2021).

Following establishment, and investigation, of *P. aeruginosa* biofilm infection in the EVPL model in chapters 3, 4, and 5, another Gram negative, biofilm-forming pathogen was introduced: the Bcc. The Bcc is highly similar to *P. aeruginosa* and was only re-classified in 1992, previously considered *Pseudomonas* (Yabuuchi et al., 1992). Due to the recent re-classification and relatively low incidence of Bcc infection (~5% of CF lung infections; Leitão et al. (2017)), co-infection of *P. aeruginosa* with the Bcc in the CF lung has not been fully explored. The literature is conflicting over whether they form a mixed biofilm and how they may interact. There have been three possible outcomes outlined for their co-infection in the CF lung: the incidence of cepacia syndrome, gradual lung function decline over time, or asymptomatic carriage (Isles et al., 1984; Riedel et al., 2001). *P. aeruginosa* infection typically occurs first, followed by secondary infections such as those caused by the Bcc (Filkins and O'Toole, 2015).

An early study showed that iron availability may be involved in interactions, and that Bcc production of the siderophore ornibactin may induce the expression of numerous *P. aeruginosa* genes (Weaver and Kolter, 2004). Since then, their co-infection has been investigated in a number of different laboratory models; a flow cell model has been used to demonstrate that the presence of *B. cenocepacia* caused an increase in *P. aeruginosa* biofilm biomass and altered biofilm architecture (Bragonzi et al., 2012). The same study also used a mouse model for CF, and demonstrated that in this environment *P. aeruginosa* was able to establish a chronic biofilm infection when co-infected with *B. cenocepacia* (Bragonzi et al., 2012). As well as highlighting potential impacts of co-infection, this work also showed the variability in findings depending on the model used, which may in part be responsible for conflicting findings. In explanted CF lungs, it has been shown that *P. aeruginosa* and the Bcc may actually inhabit different niches; the Bcc can exist as single cells in mucus and small clusters within phagocytes, as opposed to the biofilm formed by *P. aeruginosa* (Schwab et al., 2014). Thus, investigation of co-infection of the two genera in a more clinically relevant laboratory model is needed to gain further insight into potential interactions, and to determine whether a mixed biofilm forms in the CF lung. The most frequently used animal model, mice, are not able to replicate the airway secretions of people with CF, even mice with CFTR mutations (Benahmed et al., 2014) so are unlikely to be able to facilitate growth in different niches. The EVPL model may be better able to capture this, as the work in previous chapters has

shown *P. aeruginosa* forms a chronic-like biofilm infection in the model, and pigs are more comparable to humans than mice (Meurens et al., 2012).

Type VI secretion has also been shown to be important for the co-existence of both genera in CF. This secretion system is associated with interbacterial competition; *P. aeruginosa* and the Bcc both possess type VI secretion systems (Perault et al., 2020). Type VI is the most recent *P. aeruginosa* secretion system to be described (Diggle and Whiteley, 2020), and is important for bacterial competition (Jurado-Martín et al., 2021). However, mutations in genes associated with these mechanisms are commonly found in *P. aeruginosa* isolates from chronic infection. It has been shown that *B. cenocepacia*, *B. multivorans*, and *B. dolosa* that have functional type VI secretion systems can outcompete *P. aeruginosa* when their type VI secretion is impaired (Perault et al., 2020). In contrast, *P. aeruginosa* inhibits the growth of *B. multivorans* and *B. cenocepacia in vitro*, dependent on pyoverdine biosynthesis and QS (Costello et al., 2014). This may further explain why *P. aeruginosa* and the Bcc can co-exist in the CF lung alongside the incidence of mutations for type VI secretion, as *P. aeruginosa* virulence factor production and QS is downregulated during chronic infection (Winstanley et al., 2016). It also highlights distinctions between *in vitro* co-infection and in the CF lung, further supporting the need for a clinically relevant model to study *P. aeruginosa* and Bcc mixed infection.

To determine whether the EVPL model may be the answer, two species of the Bcc: *B. cenocepacia* and *B. multivorans*, were each co-infected with *P. aeruginosa* in the model. Initially, the inhibition caused by each strain to the others was investigated on LB agar following growth in either the EVPL model or SCFM *in vitro*. It was found that *P. aeruginosa* PA14 and LESB58 inhibited both *B. cenocepacia* K56-2 and *B. multivorans* C5393 regardless of the initial growth environment, however the Bcc strains did not inhibit the *P. aeruginosa* strains. This was not observed when *P. aeruginosa* PA14 was co-infected with each Bcc strain in the EVPL model, with both genera recovered from tissue pieces for at least 3 d following co-infection. The CFU lung^{-1} for each was determined using two different agars. The *P. aeruginosa* PA14 bacterial load was determined on LB agar as it outcompeted the Bcc strains on this media, as shown in the initial inhibition assay. The Bcc bacterial load was determined on LB agar supplemented with 50 µg ml^{-1} polymyxin B. The Bcc are intrinsically resistant to polymyxins due to

a lipopolysaccharide modification (Rhodes and Schweizer, 2016) but *P. aeruginosa* is not, so only Bcc colonies grew on the polymyxin agar. Uninfected tissue samples were also plated on both agars, and in a small number of samples the endogenous lung species were able to grow on the polymyxin B agar. When indistinguishable from Bcc colonies, these samples were discounted. Following identification of this issue, any lungs with endogenous microbial species resistant to polymyxin B were not used for experiments. Super-infection experiments were also performed to reflect the typical timeline of infection in the CF lung: *P. aeruginosa* establishes followed by Bcc infection. *B. cenocepacia* K56-2 and *B. multivorans* C5393 were super-infected in the EVPL model following *P. aeruginosa* infection, as shown in Figure 6.1. *B. multivorans* C5393 appeared to better survive when introduced to a *P. aeruginosa* PA14 biofilm compared with simultaneous infection.
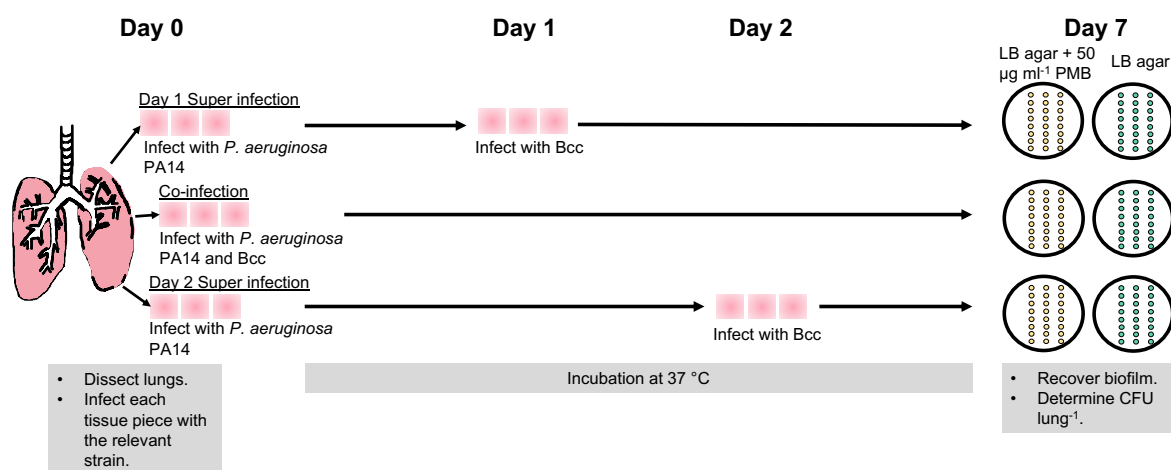
Figure 6.1: **The method for super-infection in the *ex vivo* pig lung (EVPL) model.** Two independent pig lungs were dissected on day 0 and infected with *Pseudomonas aeruginosa* PA14. Three replicate tissue pieces per co-infection were also infected with the relevant *Burkholderia cepacia* complex (Bcc) strain: *B. cenocepacia* K56-2 or *B. multivorans* C5393. These tissue pieces were incubated at 37 °C for 7 d. Three tissue pieces per super-infection were incubated at the same time at 37 °C, following infection with just *P. aeruginosa* PA14. After 1 d incubation, half of the super-infection pieces were removed and infected with the relevant Bcc strain, then incubated at 37 °C for a further 6 d. After 2 d incubation, the other half of the super-infection tissue pieces were removed and infected with the relevant Bcc strain. These tissue pieces were then incubated at 37 °C for a further 5 d. All tissue pieces were then retrieved 7 d after initial infection (6 d after 1 d super-infection and 5 d after 2 d super-infection). The biofilm was recovered and the CFU lung^{-1} of each species determined using Luria-Bertani (LB) agar plates (green spot plates), supplemented with 50 µg ml^{-1} polymyxin B (PMB) for the Bcc (yellow spot plates).

Both genera have QS systems that use AHL signal molecules to regulate virulence and biofilm formation. A study using a flow chamber model and mouse lung tissue showed that *B. cepacia* could recognise and respond to *P. aeruginosa* AHL signals, however

P. aeruginosa did not respond to the *B. cepacia* AHL signal molecules (Riedel et al., 2001). This suggests that the Bcc may be able to alter their behaviour in response to *P. aeruginosa* QS signals in the CF lung. As discussed in chapters 4 and 5, the *P. aeruginosa* transcriptome analysis from different laboratory models and CF sputum by Cornforth et al. (2018) showed that QS-regulated gene expression during chronic biofilm infection was not accurately replicated by current models. The RNA-seq analysis of *P. aeruginosa* PA14 in the EVPL model performed indicated that QS-related gene expression may be more comparable to human infection in this model. Therefore, the production of QS signal molecules during co-infection and super-infection of each Bcc and *P. aeruginosa* combination in the EVPL model was also measured. It was found that there may be an effect on QS signalling depending on when *B. cenocepacia* K56-2 is introduced to the *P. aeruginosa* PA14 biofilm in the EVPL model.

These intial experiments showed that *P. aeruginosa* and the Bcc strains were able to co-exist in the EVPL model and there may be interactions, which must be explored further in the future. Clinical *P. aeruginosa* CF isolates were then studied to be more representative of *in vivo* infection. The effect of co-infection with *B. cenocepacia* K56-2 and *B. multivorans* C5393 in the EVPL model was compared with *in vitro* SCFM co-infection. The aim was to determine whether the presence of lung tissue was facilitating co-infection or if SCFM alone was a viable model. The presence of lung tissue did appear to have an effect on Bcc recovery, and the Bcc bacterial load appeared to be higher during co-infection with the *P. aeruginosa* clinical isolates compared with PA14.

There was upregulation of phenazine biosynthesis genes observed in the EVPL *P. aeruginosa* biofilm over 7 d in chapter 5. As the phenazine PVD has been implicated in *P. aeruginosa* interactions with the Bcc during co-infection (Costello et al., 2014), the production of the siderophores PVD and PCH was also measured for the different *P. aeruginosa* strain co-infections with *B. cenocepacia* K56-2 and *B. multivorans* C5393. This highlighted another potential interaction to be further investigated. Overall the work in this chapter has shown that the EVPL model maintains a Bcc infection population, and *P. aeruginosa* and the Bcc are able to co-exist. The results in this chapter also indicate that QS and siderophore production play a role in their interactions to be explored in the future. This preliminary work has also highlighted key questions for future research, and evidenced that the use of clinical CF isolates is important.

6.2 Results

All SCFM experiments in this chapter were performed using three repeats per condition, and EVPL experiments included three repeats from each of two independent pig lungs.

6.2.1 Establishment of *P. aeruginosa* and Bcc mixed infection

***P. aeruginosa* inhibited *B. cenocepacia* and *B. multivorans* independent of growth in SCFM or the EVPL model. However, there was a difference in the inhibition within the *P. aeruginosa* strains and the Bcc between the growth environments.**

The growth inhibition of two Bcc strains caused by *P. aeruginosa* PA14 and *P. aeruginosa* LESB58, and vice versa, was first determined. The Bcc studied were the laboratory strain *B. cenocepacia* K56-2 and CF clinical isolate *B. multivorans* C5393. The aim was to identify whether each Bcc strain and *P. aeruginosa* were able to grow alongside each other. This would indicate whether they were likely to form a co-infection. The strains were grown individually in SCFM and the EVPL model for 48 h to determine whether there was a change when pig lung tissue was present. The *in vitro* SCFM cultures and biofilm recovered from the EVPL were each then streaked on an LB agar plate overnight, referred to as the inhibitor strain. A second strain, also grown in each environment for 48 h, was then streaked perpendicular to the first the following night, referred to as the competitor strain. Any inhibition of growth of the competitor strain was measured (see Figure 6.2). Each *P. aeruginosa* and Bcc strain were also tested against each other to identify any intraspecies inhibition. Statistical analysis was not performed as these experiments were carried out to give an overall idea of growth inhibition rather than definitive inhbition measurements.
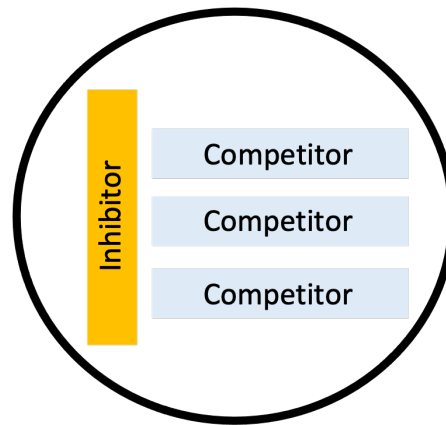
Figure 6.2: **The layout of the Luria-Bertani (LB) agar plates for cross streak inhibition assays**. The inhibitor strain was the bacterial isolate that was grown in the *ex vivo* pig lung (EVPL) model or synthetic cystic fibrosis sputum media (SCFM) *in vitro* for 48 h at 37 °C, then drip plated as shown (20 µl) and grown on the plate overnight at 37 °C. The competitor bacterial isolate was drip plated (20 µl) following the overnight incubation as shown, and the plate was further incubated overnight at 37 °C to determine any inhibition of competitor strain growth caused by the inhibitor strain. The competitor isolate was also grown in the EVPL model or SCFM for 48 h at 37 °C prior to plating. Also shown in the chapter 2: Figure 2.10.

P. aeruginosa PA14 grown in SCFM *in vitro* was found to inhibit all competitor strains regardless of the environment they were intially grown in (Figure 6.3A). However, there was increased inhibition of *P. aeruginosa* LESB58 grown as a biofilm associated with the EVPL tissue, compared with when it was grown in SCFM (mean inhibition: 13.42 mm and 1.17 mm respectively). There was also a small increase in inhibition of *B. multivorans* C5393 grown in the EVPL model compared with SCFM (13.67 mm and 8.17 mm respectively). This was not seen for *B. cenocepacia* K56-2, and the inhibition was similar regardless of the environment it was grown in (Figure 6.3A).

Figure 6.3: **Growth inhibition caused by *Pseudomonas aeruginosa* PA14.** *P. aeruginosa* PA14 was grown in **(A)** synthetic cystic fibrosis sputum media (SCFM) or **(B, C)** the *ex vivo* pig lung (EVPL) model, at 37 °C for 2 d. The SCFM cultures or biofilm recovered from each of two independent pig lungs were each plated on Luria-Bertani (LB) agar in one horizontal strip, and incubated at 37 °C overnight. Each competitor strain was also grown in either SCFM or the EVPL model, using two independent pig lungs, for 2 d: *P. aeruginosa* LESB58, *Burkholderia cenocepacia* K56-2, and *Burkholderia multivorans* C5393. Following overnight incubation of PA14 on LB agar, the competitor strains were plated perpendicular to PA14 and the agar plate was incubated again overnight. Any inhibition of growth of the competitor strain was measured in mm. For each culture, two repeats were performed on LB agar plates and the data points represent the mean. There were three individual cultures tested for each condition, shown by individual data points on the graphs. The two pig lungs used for the EVPL model are represented by different colour data points (see key) and for the growth of the inhibitor strain, *P. aeruginosa* PA14, they are shown on different graphs. The horizontal lines show the mean for the SCFM and EVPL samples, and above the dashed horizontal line (shown by the blue region) shows samples where no growth of the competitor strain was seen on the LB agar plate.

The inhibition caused by *P. aeruginosa* PA14 when it was grown in the EVPL model did not show the same patterns as seen for SCFM *in vitro* growth (Figure 6.3). There was a small region of *P. aerugnosa* LESB58 inhibition measured regardless of the environment it was grown in, and for some samples there was no inhibition observed (Figure 6.3B). There was similarly no clear distinction in the inhibition of *B. multivorans* C5393 caused by *P. aeruginosa* PA14 grown in the EVPL model, whether it was grown in SCFM or the EVPL model (Figure 6.3B,C). The inhibition of *B. multivorans* C5393 was also comparable to that caused by PA14 grown in SCFM (Figure 6.3). However, there was a clear difference

in *B. cenocepacia* K56-2 inhibition depending on the environment it was grown in. There was complete inhibition of some *B. cenocepacia* K56-2 samples grown in SCFM by *P. aeruginosa* PA14 grown in the EVPL model (Figure 6.3B,C). Conversely, *B. cenocepacia* K56-2 that had been grown associated with the lung tissue from both lungs in the EVPL model was inhibited less than SCFM growth (mean across both lungs 16.29 mm and 49.25 mm respectively).

The inhibition of competitor strains caused by *P. aeruginosa* LESB58 did not appear to be as different whether it was grown in SCFM or the EVPL model as seen for PA14 (Figure 6.4). However, *P. aeruginosa* PA14 was only inhibited when LESB58 was grown in SCFM. As shown in Figure 6.4A, only one of three PA14 samples also grown in SCFM were inhibited, whereas all PA14 samples from the EVPL model were inhibited by *P. aeruginosa* LESB58 grown in SCFM (mean 4.83 mm). There was also greater inhibition of *B. multivorans* C5393 grown in the EVPL model than SCFM caused by *P. aeruginosa* LESB58 in SCFM (mean 18.17 mm and 5.17 mm respectively). However, there was comparable inhibition of C5393 from each environment by *P. aeruginosa* LESB58 grown in the EVPL model (Figure 6.4B,C). The greatest inhibition was observed for *B. cenocepacia* K56-2, and was caused by *P. aeruginosa* LESB58 grown in both SCFM and the EVPL model (Figure 6.4). *B. cenocepacia* K56-2 grown in SCFM was inhibited more than when it was grown in the EVPL model, regardless of where LESB58 was grown; there was no growth of some K56-2 SCFM samples observed for each (Figure 6.4).
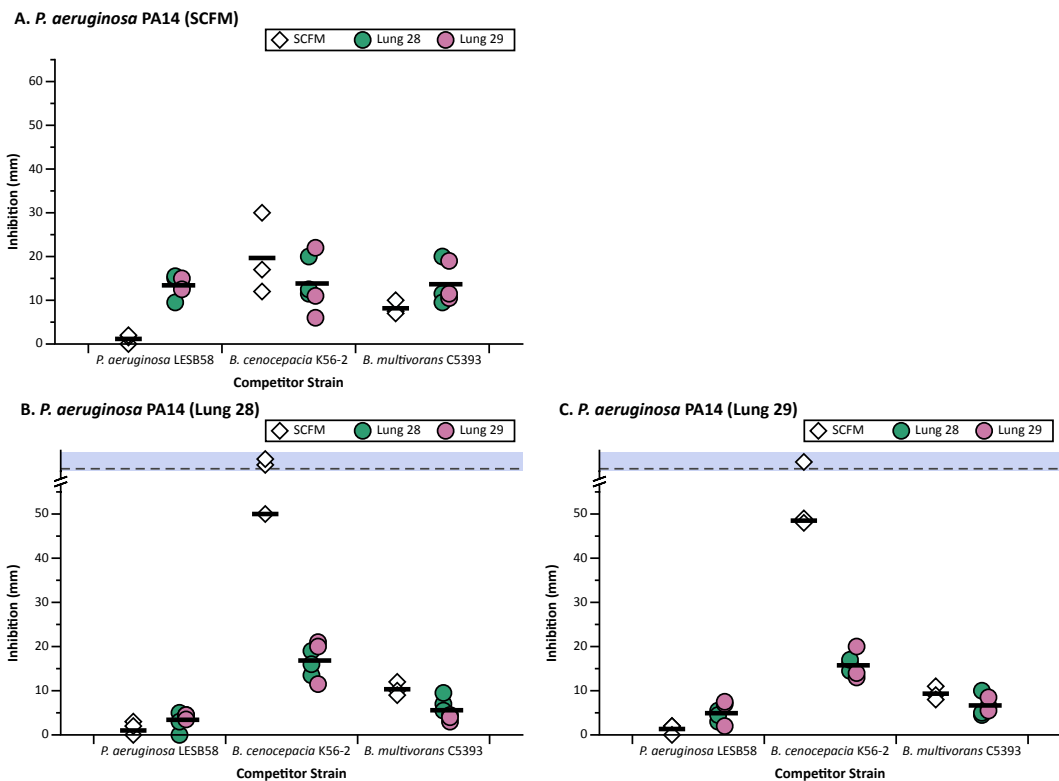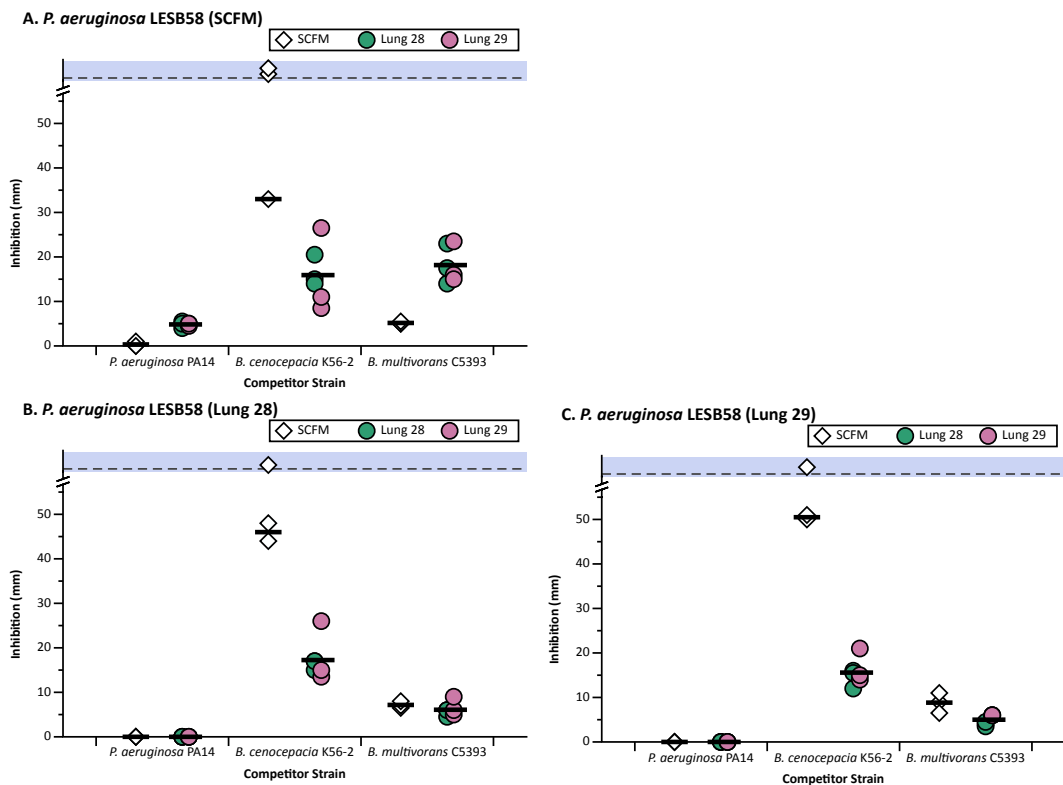
Figure 6.4: **Growth inhibition caused by *Pseudomonas aeruginosa* LESB58.** *P. aeruginosa* LESB58 was grown in **(A)** synthetic cystic fibrosis sputum media (SCFM) or **(B, C)** the *ex vivo* pig lung (EVPL) model, at 37 °C for 2 d. The SCFM cultures or biofilm recovered from each of two independent pig lungs were each plated on Luria-Bertani (LB) agar in one horizontal strip, and incubated at 37 °C overnight. Each competitor strain was also grown in either SCFM or the EVPL model, using two independent pig lungs, for 2 d: *P. aeruginosa* PA14, *Burkholderia cenocepacia* K56-2, and *Burkholderia multivorans* C5393. Following overnight incubation of LESB58 on LB agar, the competitor strains were plated perpendicular to LESB58 and the agar plate was incubated again overnight. Any inhibition of growth of the competitor strain was measured in mm. For each culture, two repeats were performed on LB agar plates and the data points represent the mean. There were three individual cultures tested for each condition, shown by individual data points on the graphs. The two pig lungs used for the EVPL model are represented by different colour data points (see key) and for the growth of the inhibitor strain, *P. aeruginosa* LESB58, they are shown on different graphs. The horizontal lines show the mean for the SCFM and EVPL samples, and above the dashed horizontal line (shown by the blue region) shows samples where no growth of the competitor strain was seen on the LB agar plate.

Following this, inhibition caused by the Bcc species was investigated. *B. cenocepacia* K56-2 did not inhibit the growth of any competitor strains tested: *P. aeruginosa* PA14, *P. aeruginosa* LESB58, and *B. multivorans* C5393 (Figure 6.5). This was consistent for both *in vitro* SCFM and EVPL model growth.
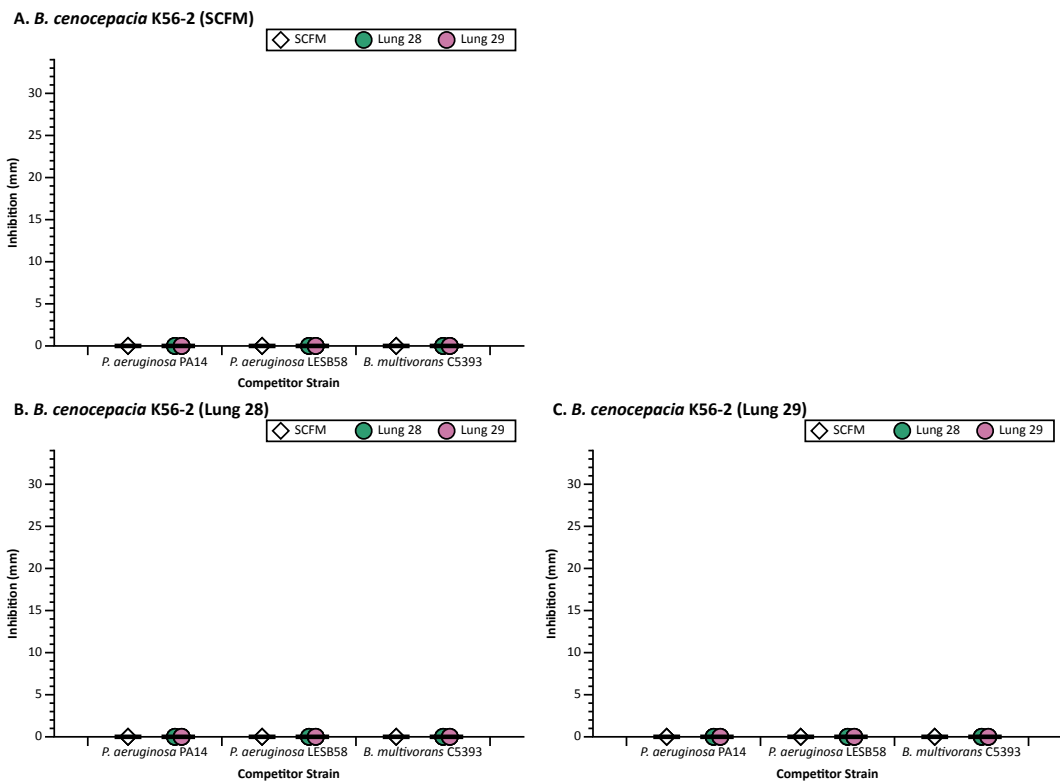
Figure 6.5: **Growth inhibition caused by *Burkholderia cenocepacia* K56-2.** *B. cenocepacia* K56-2 was grown in **(A)** synthetic cystic fibrosis sputum media (SCFM) or **(B, C)** the *ex vivo* pig lung (EVPL) model, at 37 °C for 2 d. The SCFM cultures or biofilm recovered from each of two independent pig lungs were each plated on Luria-Bertani (LB) agar in one horizontal strip, and incubated at 37 °C overnight. Each competitor strain was also grown in either SCFM or the EVPL model, using two independent pig lungs, for 2 d: *Pseudomonas aeruginosa* PA14, *P. aeruginosa* LESB58, and *Burkholderia multivorans* C5393. Following overnight incubation of K56-2 on LB agar, the competitor strains were plated perpendicular to K56-2 and the agar plate was incubated again overnight. Any inhibition of growth of the competitor strain was measured in mm. For each culture, two repeats were performed on LB agar plates and the data points represent the mean. There were three individual cultures tested for each condition, shown by individual data points on the graphs. The two pig lungs used for the EVPL model are represented by different colour data points (see key) and for the growth of the inhibitor strain, *B. cenocepacia* K56-2, they are shown on different graphs. The horizontal lines show the mean for the SCFM and EVPL samples.

B. multivorans C5393 was also shown to not inhibit the growth of *P. aeruginosa* PA14 or *P. aeruginosa* LESB58, regardless of the environment the strains were initially grown in (Figure 6.6). However, there was inhibition of *B. cenocepacia* K56-2 observed. As shown in Figure 6.6A, *B. multivorans* C5393 grown in SCFM inhibited the growth of *B. cenocepacia* K56-2 grown in SCFM (mean 35.33 mm) but not K56-2 grown in the EVPL model. A similar pattern was observed for inhbition caused by *B. multivorans* C5393 grown in the EVPL model. *B. cenocepacia* K56-2 grown in SCFM *in vitro* was inhibited by C5393 grown in this environment (mean across both lungs 28.25 mm). However, there was also one *B. cenocepacia* K56-2 EVPL sample that exhibited some growth inhibition

206

caused by *B. multivorans* C5393 grown in the EVPL model (Figure 6.6C).
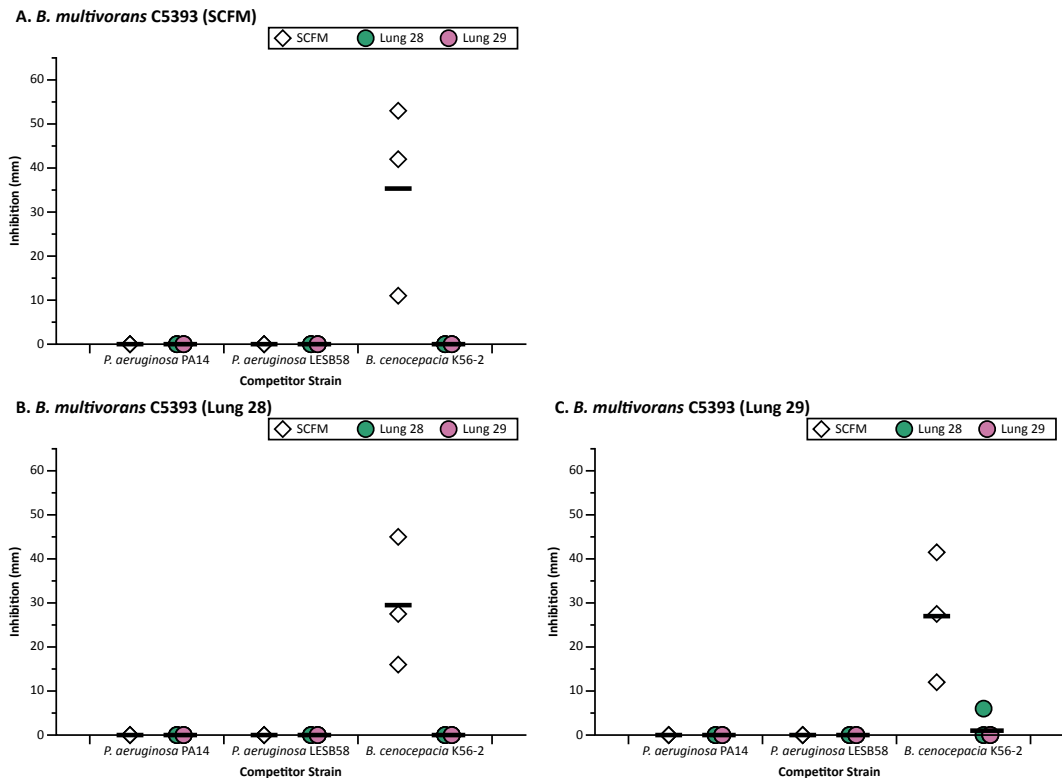
Figure 6.6: **Growth inhibition caused by *Burkholderia multivorans* C5393.** *B. multivorans* C5393 was grown in **(A)** synthetic cystic fibrosis sputum media (SCFM) or **(B, C)** the *ex vivo* pig lung (EVPL) model, at 37 °C for 2 d. The SCFM cultures or biofilm recovered from each of two independent pig lungs were each plated on Luria-Bertani (LB) agar in one horizontal strip, and incubated at 37 °C overnight. Each competitor strain was also grown in either SCFM or the EVPL model, using two independent pig lungs, for 2 d: *Pseudomonas aeruginosa* PA14, *P. aeruginosa* LESB58, and *Burkholderia cenocepacia* K56-2. Following overnight incubation of C5393 on LB agar, the competitor strains were plated perpendicular to C5393 and the agar plate was incubated again overnight. Any inhibition of growth of the competitor strain was measured in mm. For each culture, two repeats were performed on LB agar plates and the data points represent the mean. There were three individual cultures tested for each condition, shown by individual data points on the graphs. The two pig lungs used for the EVPL model are represented by different colour data points (see key) and for the growth of the inhibitor strain, *B. multivorans* C5393, they are shown on different graphs. The horizontal lines show the mean for the SCFM and EVPL samples.

To provide an overview of the inhbition observed, the results were divided into different categories (Figure 6.7). There was considered to be no inhibition when there was growth of the competitor strain adjacent to the inhibitor strain, as shown in Figure 6.7A. There was measured inhibition when a measurable zone of no growth was seen (Figure 6.7B). Figure 6.7C shows complete inhibition, which was when there was no growth of the competitor strain observed on the plate. This was typically inhibition greater than 55 mm, which could not be measured on the width of an LB agar plate.

A. <u>No inhibition</u>

B. multivorans C5393 **(Lung)**

B. cenocepacia K56-2 (**SCFM**)

B. <u>Measured inhibition</u>

B. cenocepacia K56-2 **(Lung)**

P. aeruginosa PA14 **(Lung)**

C. <u>Complete inhibition</u>

B. cenocepacia K56-2 **(SCFM)**

P. aeruginosa PA14 **(Lung)**
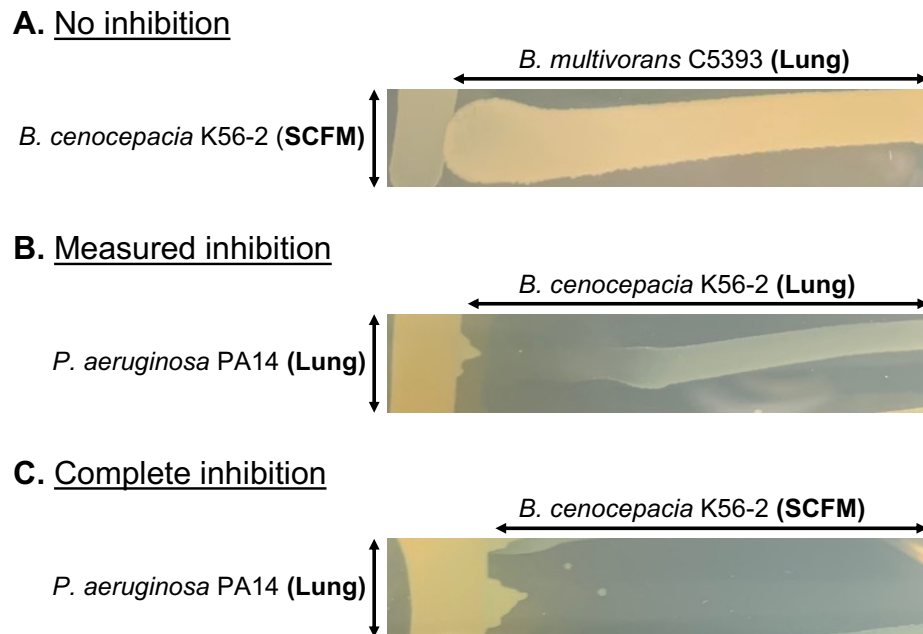
Figure 6.7: **Images to represent each category of inhibition.** The vertical growth is the inhibitor strain and the horizontal growth is the competitor strain, which was grown overnight following the initial overnight growth of the inhibitor strain. Each strain was initially grown in either synthetic cystic fibrosis sputum media (SCFM) or as a biofilm associated with the lung tissue of the *ex vivo* pig lung (EVPL) model (Lung) for 2 d. The assay was then performed on Luria-Bertani (LB) agar plates, which the images show. **(A)** An example of no inhibition. The competitor strain was able to grow adjacent to the inhibitor strain, with no zone of clearance. This example shows *Burkholderia cenocepacia* K56-2 grown in SCFM as the inhibitor strain and *Burkholderia multivorans* C5393 grown in the EVPL model as the competitor strain. **(B)** An example of measured inhibition. There was a measureable zone of no growth of the competitor strain adjacent to the inhibitor strain. This example shows *Pseudomonas aeruginosa* PA14 grown in the EVPL model as the inhibitor strain and *B. cenocepacia* K56-2 grown in the EVPL model as the competitor strain. **(C)** An example of complete inhibition. There was no growth of the competitor strain observed on the LB agar plate, therefore the inhibition was greater than ~55 mm. This example shows *P. aeruginosa* PA14 grown in the EVPL model as the inhibitor strain, which grew into the streak of the competitor *B. cenocepacia* K56-2 grown in SCFM, which did not grow on the LB agar plate.

A heatmap was produced of each inhibition assay performed, showing the category of inhibition for comparison (Figure 6.8). There were intermediate categories used to represent where there were repeats exhibiting different levels of inhibition (i.e. some repeats were completely inhibited and some showed measurable inhibition). There was no inhibition of the *P. aeruginosa* strains caused by the two Bcc species. However, the *P. aeruginosa* strains inhibited the Bcc species when they were grown in SCFM and the EVPL model (Figure 6.8). *P. aeruginosa* PA14 also inhibited *P. aeruginosa* LESB58, however LESB58 only inhibited PA14 when it was grown in SCFM (Figure 6.8). *B. cenocepacia* K56-2 did not inhibit *B. multivorans* C5393 at all. Conversely, *B. multivorans* C5393 did inhibit *B. cenocepacia K56-2* when it was grown in SCFM. Overall, inhibition between *P. aeruginosa*

and the Bcc did not appear to be affected by growth environment, however inhibition within the *P. aeruginosa* or Bcc strains was found to be affected by growth environment (Figure 6.8).
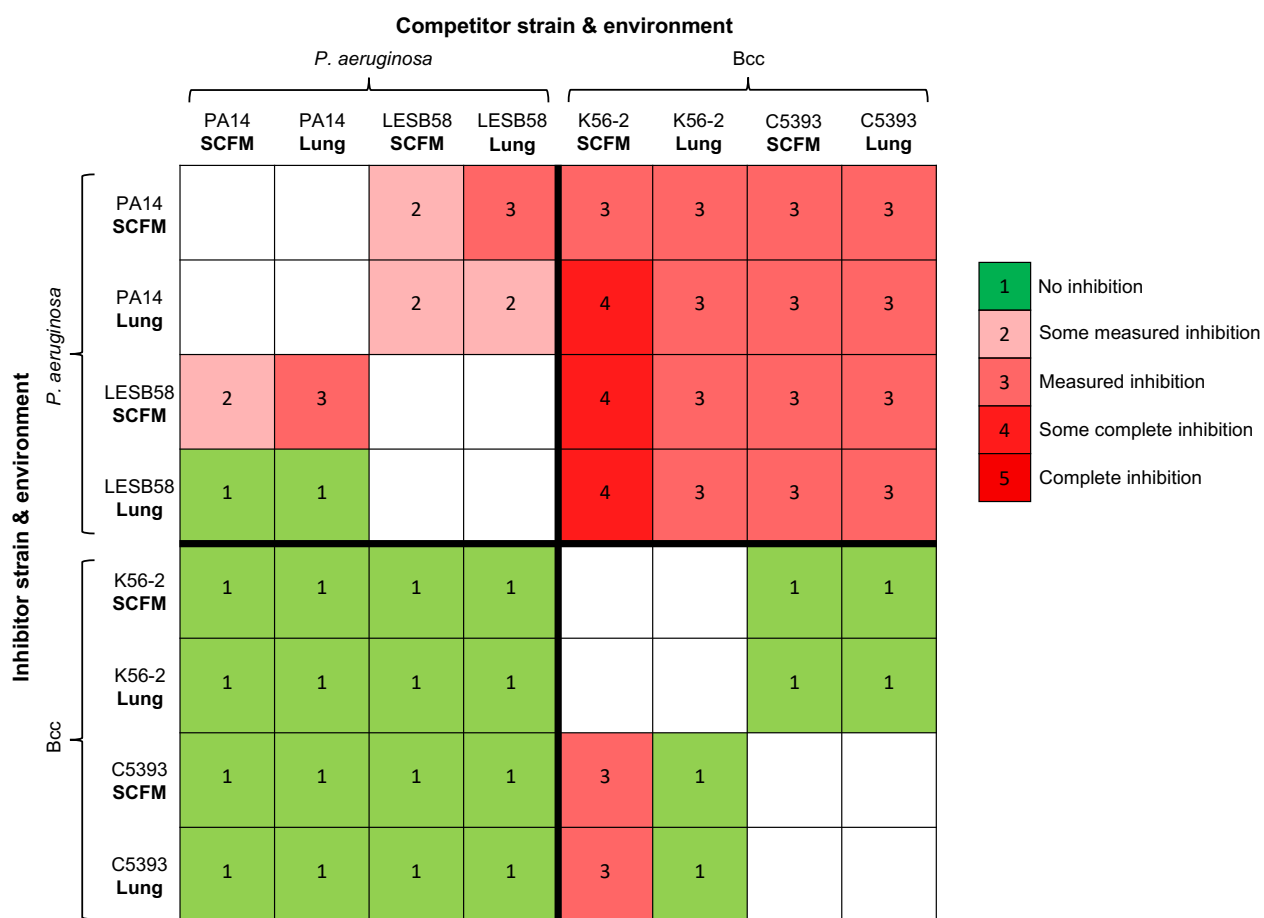
Figure 6.8: **A heatmap summarising the inhibition between *Pseudomonas aeruginosa* PA14, *P. aeruginosa* LESB58, *Burkholderia cenocepacia* K56-2, and *Burkholderia multivorans* C5393 in synthetic cystic fibrosis sputum media (SCFM) and the lung-associated biofilm in the *ex vivo* pig lung (EVPL) model (Lung).** Each strain was grown in either SCFM *in vitro* or the EVPL model for 2 d prior to performing an inhibition assay on Luria-Bertani (LB) agar. The inhibitor strain was initially grown on the LB agar plate overnight at 37 °C, then the competitor strain was added to the plate perpendicular to the inhibitor strain and incubated at 37 °C for a further night. Any inhibition of the competitor strain was measured and classified into one of the categories shown in the key. The two intermediate categories (2 and 4) represent assays where some repeats exhibited the inhibition in the category below and some exhibited inhibition in the category above. The inhibition was determined using three SCFM repeats and three EVPL repeats from each of two independent pig lungs. The colours and numbers represent the category of inhibition caused by the inhibitor strain (left) on the competitor strain (above) from each of the growth environments.

There was a significant reduction in the CFU lung^{-1} of *B. multivorans* C5393 after 3 days in the EVPL model, that was not observed for *P. aeruginosa* PA14 or *B. cenocepacia* K56-2.

P. aeruginosa PA14 infection of the EVPL model over 7 d was studied throughout the previous chapters, however Bcc was not. Therefore, *B. cenocepacia* K56-2 and *B. multivorans* C5393 were first grown individually in the EVPL model for 7 d, and the CFU lung $^{-1}$ was determined every day (Figure 6.9). The aim was to confirm whether the model was able to maintain the Bcc populations for 7 d and thus whether it was a suitable model for the Bcc. *P. aeruginosa* PA14 was also studied as a control and for comparison with mixed infection. Consistent with the results in chapter 3, PA14 was maintained in the EVPL biofilm for 7 d (Figure 6.9A). There was a significant difference in the *P. aeruginosa* PA14 CFU lung^{-1} found over the 7 d (ANOVA: day $F_{6,28}$ = 12.65, *P* < 0.01, lung $F_{1,28}$ = 0.69, *P* = 0.41, interaction $F_{6,28}$ = 2.15, *P* = 0.08). Post hoc Tukey HSD analysis revealed the consecutive days where there was a significant change were 1 d to 2 d (*P* < 0.01), 2 d to 3 d (*P* < 0.01), 5 d to 6 d (*P* = 0.01), and 6 d to 7 d (*P* = 0.01). However, the variation in mean CFU lung^{-1} was between 10^8 and 10^9 over the 7 d (Figure 6.9A), consistent with chapter 3 and the CFU ml^{-1} recovered from people with CF (Palmer et al., 2005).
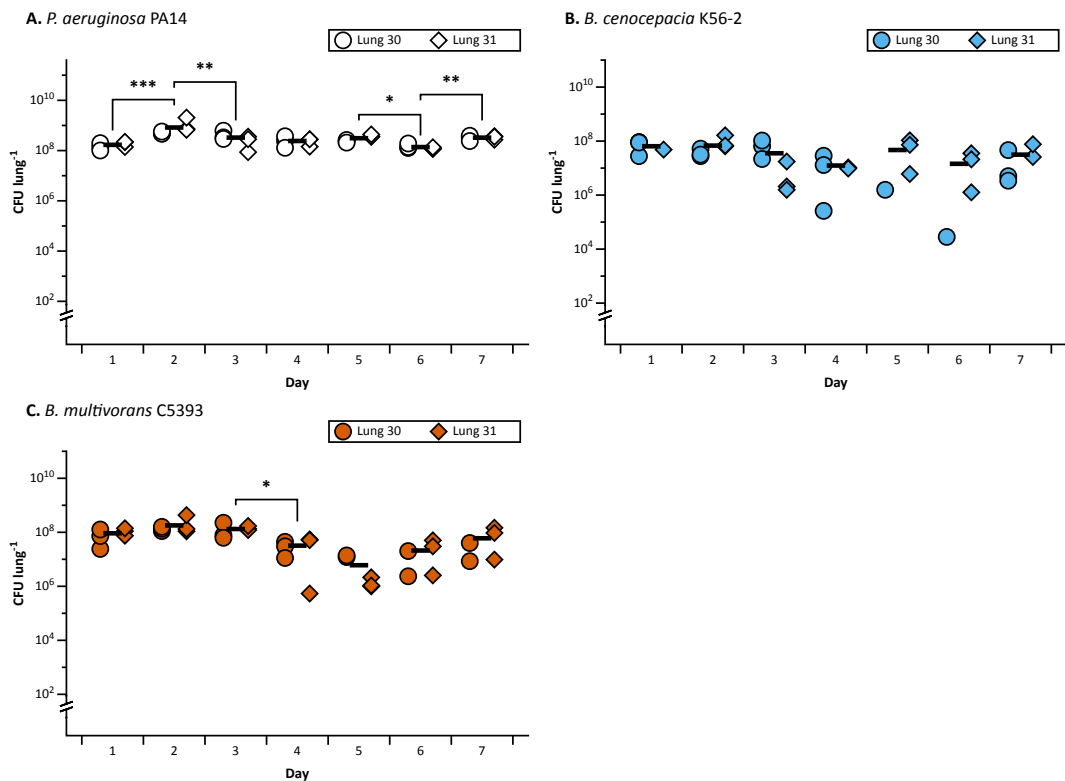
Figure 6.9: **The colony forming units per lung tissue piece (CFU lung^{-1}) of *Pseudomonas aeruginosa* PA14, *Burkholderia cenocepacia* K56-2, and *Burkholderia multivorans* C5393 in the *ex vivo* pig lung (EVPL) model every day for 7 d.** The CFU lung^{-1} was determined from the biofilm recovered from three tissue pieces from each of two independent pig lungs per day, each lung is shown by different shaped data points (lung 30 = circles, lung 31 = diamonds). The mean across both lungs was determined each day, as shown by the horizontal black lines. The significant differences are shown ('***' = P < 0.001, '**' = P < 0.01, '*' = P < 0.05). The y axes are $\log_{10}$ scale. **(A)** The CFU lung^{-1} of *P. aeruginosa* PA14 over 7 d, ANOVA statistical analysis was performed and the results from a post hoc Tukey HSD analysis are shown for consecutive days. **(B)** The CFU lung^{-1} of *B. cenocepacia* K56-2 over 7 d, a non-parametric Kruskal-Wallis test was performed and no significant difference was found. **(C)** The CFU lung^{-1} of *B. multivorans* C5393 over 7 d , a non-parametric Kruskal-Wallis test was performed and a post hoc Dunn's test. The significant differences between consecutive days are shown.

There were endogenous species in lungs 30 and 31 able to grow on the polymyxin B agar used to isolate the Bcc from *P. aeruginosa*, that were indistinguishable from the Bcc strains. This was identified by comparison with uninfected tissue samples, as explained in the introduction. The *B. cenocepacia* K56-2 and *B. multivorans* C5393 infected tissue pieces that had indistinguishable polymyxin B resistant endogenous species growth were removed from the analysis, and are not shown on the graphs in Figure 6.9. As some samples were removed, non-parametric analyses were performed. There was no significant difference in the CFU lung^{-1} of *B. cenocepacia* K56-2 found over 7 d in the EVPL model (Kruskal-Wallis: χ_2 = 10.55, df = 6, P = 0.10). The bacterial load was comparable to *P. aeruginosa* PA14; at 1 d the CFU lung^{-1} was within a 1 $\log_{10}$ range (mean K56-2: 6.4 x 10^7,

PA14: 1.7 x 10^8). However, there was an increase in the variation between samples from individual lungs from 4 d (Figure 6.9B), not observed for PA14. *B. multivorans* C5393 was also found to have a comparable number of CFU lung^{-1} to the other two strains initially (Figure 6.9C). There was however a significant difference in CFU lung^{-1} over 7 d found (Kruskal-Wallis: χ_2 = 25.31, df = 6, P < 0.01). A post hoc Dunn's test showed that there was a significant difference in the CFU lung^{-1} from 3 d to 4 d (P = 0.03). There were no other significant differences found between any other consecutive days. This indicated that there was a reduction in the *B. multivorans* C5393 CFU lung^{-1} after 3 d in the EVPL model (Figure 6.9C).

The CFU lung^{-1} of *B. cenocepacia* K56-2 or *B. multivorans* C5393 during co-infection with *P. aeruginosa* PA14 were reduced over 7 days.

As growth of single strain infections over 7 d in the EVPL model indicated that it was able to maintain the Bcc populations, mixed infections were also performed in the same pig lungs. *P. aeruginosa* PA14 and *B. cenocepacia* K56-2 were co-infected, and *P. aeruginosa* PA14 and *B. multivorans* C5393 were also co-infected, to determine whether the genera could survive together in the EVPL model and if so, for how long. The CFU lung^{-1} was determined using LB agar for *P. aeruginosa* PA14 and LB agar supplemented with 50 µg ml^{-1} polymyxin B for the Bcc, every day for 7 d. Each sample was plated on both agars to determine the bacterial load of both strains during mixed infection. Some samples were removed as performed for single infection, because the polymyxin B resistant endogenous growth was indistinsguishable from the Bcc strains. Non-parametric statistical analyses were then performed where required.

As shown in Figure 6.10A, there was no change in the CFU lung^{-1} of *P. aeruginosa* PA14 over 7 d when it was co-infected with *B. cenocepacia* K56-2 (ANOVA: day $F_{6,28}$ = 1.44, P = 0.24, lung $F_{1,28}$ = 4.56, P = 0.04, interaction $F_{6,28}$ = 1.07, P = 0.40). Although there was a significant difference found between lungs, the interaction with each day was not significant so it was unlikely this affected the CFU lung^{-1}. The mean CFU lung^{-1} values in Figure 6.10B show that there was no clear difference in *P. aeruginosa* PA14 bacterial load in the EVPL model whether it was grown alone, or in co-infection with *B. cenocepacia* K56-2. However, this was not observed for *B. cenocepacia* K56-2; there was a lower CFU lung^{-1} recovered when it was co-infected with *P. aeruginosa* PA14 (Figure 6.10B). There was also a significant difference in CFU lung^{-1} over the 7 d when it was co-infected with

PA14 (Kruskal-Wallis: χ_2 = 16.46, df = 6, P = 0.01). A post hoc Dunn's test showed there were no significant differences in CFU lung^{-1} between consecutive days, indicating that the reduction in *B. cenocepacia* K56-2 was gradual. There was a significant decrease in CFU lung $^{-1}$ from 1 d to 5 d (P = 0.04), and from 2 d to 5 d (P = 0.04). There was no *B. cenocepacia* K56-2 recovered from some tissue pieces during mixed infection from 3 d onwards, and in no samples at 5 d and 6 d (Figure 6.10A). However, when *B. cenocepacia* K56-2 was grown in the EVPL model alone the CFU lung^{-1} did not fall below 9 x 10^6 (at 6 d; Figure 6.10B).

Figure 6.10: **The colony forming units per lung tissue piece (CFU lung^{-1}) for mixed infection with** *Pseudomonas aeruginosa* **PA14 and** *Burkholderia cenocepacia* **K56-2 in the** *ex vivo* **pig lung (EVPL) model every day for 7 d.** The CFU lung^{-1} was determined from three tissue pieces, from each of two independent pig lungs every day for 7 d. The y axes are log$_{10}$ scale. **(A)** The CFU lung^{-1} for *P. aeruginosa* PA14 (white) and *B. cenocepacia* K56-2 (blue) associated with each tissue piece at each day during co-infection, represented by individual data points. There was no significant differences found between consecutive days. The coloured region at the bottom of the graph (below the y axis break) indicates samples where there were no CFU found. **(B)** The mean CFU lung^{-1} for *P. aeruginosa* PA14 (white) and *B. cenocepacia* K56-2 (blue) during co-infection (triangles) and single infection (circles) of the EVPL model. The dashed line represents the detection threshold and data points below were when no CFU was detected for any of the repeats.

Co-infection with *B. multivorans* C5393 also did not appear to affect the *P. aeruginosa* PA14 CFU lung^{-1} (Figure 6.11). There was a significant difference found over 7 d (ANOVA: day $F_{6,28}$ = 4.24, P < 0.01, lung $F_{1,28}$ = 2.30, P = 0.14, interaction $F_{6,28}$ = 1.03, P = 0.43), and post hoc Tukey HSD analysis showed the only significant change between consecutive days was an increase in CFU lung^{-1} from 1 d to 2 d (P < 0.01). The other significant difference found was an increase from 1 d to 7 d (P = 0.03). The PA14 CFU lung^{-1} during co-infection did not appear to differ from single infection in the EVPL model (Figure 6.11B). In contrast, there was a reduction in *B. multivorans* C5393 CFU lung^{-1} during co-infection compared with single infection (Figure 6.11B). At 1 d, there were similar CFU lung^{-1} for *P. aeruginosa* PA14 and *B. multivorans* C5393 during co-infection (mean 1.7 x 10^8 and 1.7 x

10^7 respecitvely). There was also a significant difference in C5393 CFU lung^{-1} over the 7 d (Kruskal-Wallis: χ_2 = 27.63, df = 6, *P* < 0.01). Although a post hoc Dunn's test identified no significant differences between consecutive days, there was a significant reduction in CFU lung^{-1} from 1 d to each of 4 d (*P* = 0.03), 5 d (*P* = 0.03), 6 d (*P* < 0.01), and 7 d (*P* = 0.02). There was also a significant reduction from 2 d to each of 4 d (*P* = 0.03), 5 d (*P* = 0.03), 6 d (*P* < 0.01), and 7 d (*P* = 0.02). Thus indicating that during co-infection there was a reduction in the CFU lung^{-1} of *B. multivorans* C5393 recovered from 4 d (Figure 6.11A), similar to that seen for *B. cenocepacia* K56-2 mixed infection (Figure 6.10A).
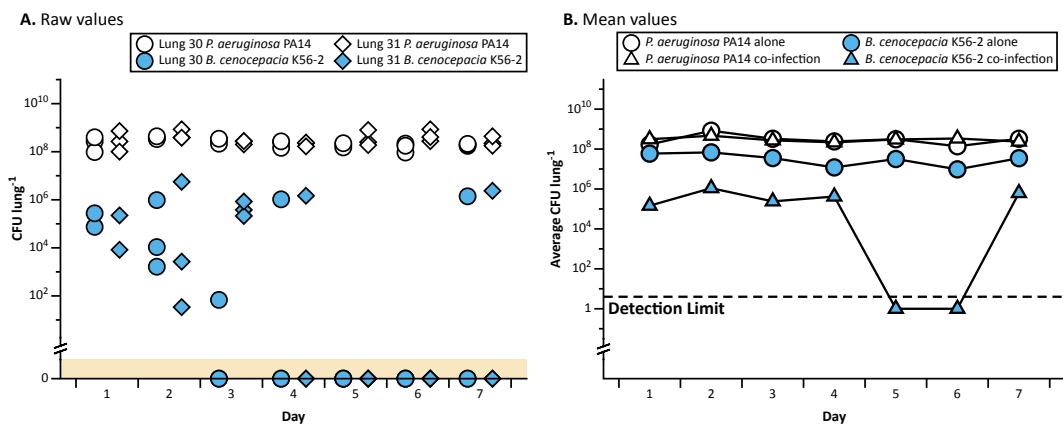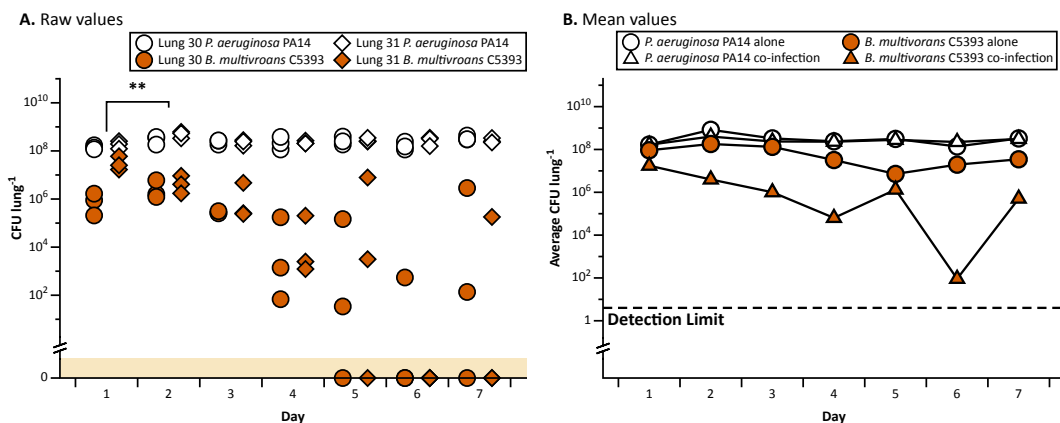

Figure 6.11: **The colony forming units per lung tissue piece (CFU lung^{-1}) for mixed infection with *Pseudomonas aeruginosa* PA14 and *Burkholderia multivorans* C5393 in the *ex vivo* pig lung (EVPL) model every day for 7 d.** The CFU lung^{-1} was determined from three tissue pieces, from each of two independent pig lungs every day for 7 d. The y axes are log$_{10}$ scale. **(A)** The CFU lung^{-1} for *P. aeruginosa* PA14 (white) and *B. multivorans* C5393 (orange) associated with each tissue piece at each da during co-infection, represented by individual data points. The significant difference between consecutive days is shown ('***' = *P* < 0.001, '**' = *P* < 0.01). The coloured region at the bottom of the graph (below the y axis break) indicates samples where there were no CFU found. **(B)** The mean CFU lung^{-1} for *P. aeruginosa* PA14 (white) and *B. multivorans* C5393 (orange1) during co-infection (triangles) and single infection (circles) of the EVPL model. The dashed line represents the detection threshold and data points below were when no CFU was detected for any of the repeats.

6.2.2 Bcc super-infection of *P. aeruginosa* biofilms in the EVPL model

The co-infection experiments showed that each Bcc strain was not consistently recovered from mixed infection with *P. aeruginosa* PA14 in the EVPL model throughout 7 d. As *P. aeruginosa* infection often precedes Bcc infection in the CF lung (Filkins and O'Toole, 2015), super-infection experiments were then performed to determine whether this improved Bcc recovery. *B. cenocepacia* K56-2 and *B. multivorans* C5393 were introduced to a *P. aeruginosa* PA14 biofilm in the EVPL model 1 d or 2 d after initial infection. Co-infection was also performed in tissue samples from the same pig lungs as a control

for comparison. All tissue pieces were incubated for a total of 7 d and the CFU lung^{-1} of each species was then determined using selective agar. There were no polymyxin B resistant lung endogenous species present in the pig lungs used for these experiments. The production of short and long chain AHLs was also measured to determine whether there was a difference in QS signal molecule production during co-infection compared with Bcc super-infection at 1 d, or 2 d, in the EVPL model. The aim was to identify whether there may have been an interaction between the two genera in the EVPL model involving QS signalling, and if it was affected by the infection timeline.

B. multivorans C5393 was more reliably recovered from the EVPL model when it was introduced to a _P. aeruginosa_ PA14 biofilm during super-infection compared with co-infection, this was not seen for _B. cenocepacia_ K56-2.

There was no difference in the _P. aeruginosa_ PA14 CFU lung^{-1} whether it was co-infected in the EVPL model with _B. cenocepacia_ K56-2, or super-infected at 1 d or 2 d (Figure 6.12). This was confirmed with statistical analysis (ANOVA: infection $F_{2,12}$ = 3.05, P = 0.09, lung $F_{1,12}$ = 1.16, P = 0.30, interaction $F_{2,12}$ = 0.25, P = 0.78). There was also no significant difference found in the _B. cenocepacia_ K56-2 CFU lung^{-1} during co-infection with PA14 or super-infection (ANOVA: infection $F_{2,12}$ = 0.50, P = 0.62, lung $F_{1,12}$ = 0.03, P = 0.87, interaction $F_{2,12}$ = 0.71, P = 0.51). However, there were less CFU of _B. cenocepacia_ K56-2 recovered than _P. aeruginosa_ PA14 during each infection, and there were a number of replicates where there was no _B. cenocepacia_ K56-2 recovered (Figure 6.12). Following super-infection of the _P. aeruginosa_ PA14 biofilm at 2 d, there was only one sample where _B. cenocepacia_ K56-2 was recovered.
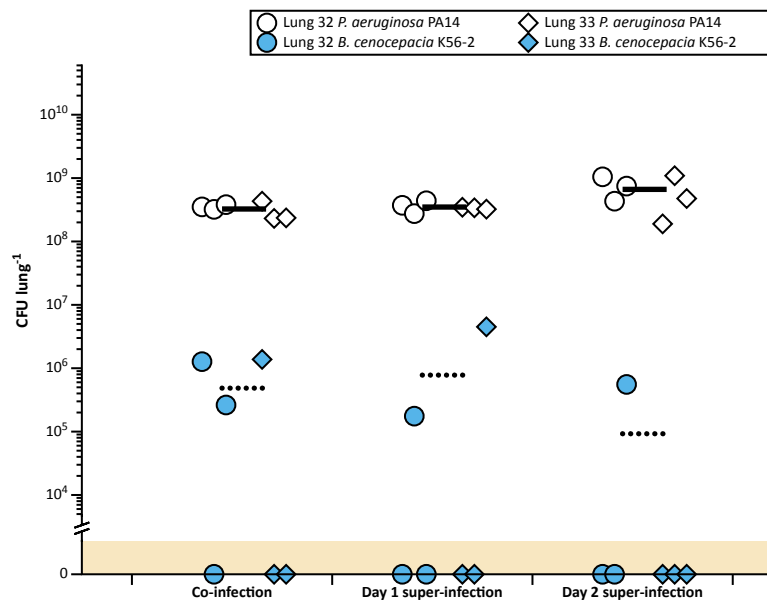
Figure 6.12: **The colony forming units per lung (CFU lung^{-1}) at 7 d for co-infection and super-infection of** ***Pseudomonas aeruginosa*** **PA14 and** ***Burkholderia cenocepacia*** **K56-2 in the** ***ex vivo*** **pig lung (EVPL) model.** Three tissue pieces from each of two independent lungs were used for each infection, shown by individual data points. For co-infection, the EVPL tissue pieces were infected with *P. aeruginosa* PA14 (white) and *B. cenocepacia* K56-2 (blue) following dissection and incubated at 37 °C for 7 d. For super-infection, tissue pieces were infected with *P. aeruginosa* PA14 following dissection then incubated at 37 °C for 7 d. At 1 d or 2 d, the super-infection pieces were infected with *B. cenocepacia* K56-2 then the incubation was continued. The dashed horizontal lines show the mean CFU lung^{-1} for *B. cenocepacia* K56-2 and the solid horizontal lines show the mean for *P. aeruginosa* PA14. The coloured region below the y axes break represents samples where no CFU were detected. The y axis is log$_{10}$ scale.

There was similarly no significant difference in the *P. aeruginosa* PA14 CFU lung^{-1} during co-infection or super-infection with *B. multivorans* C5393 in the EVPL model (ANOVA: infection $F_{2,12} = 1.00$, *P* = 0.40, lung $F_{1,12} = 0.66$, *P* = 0.43, interaction $F_{2,12} = 0.58$, *P* = 0.58). There was also no significant difference in the *B. multivorans* C5393 CFU lung^{-1} (ANOVA: infection $F_{2,12} = 2.09$, *P* = 0.17, lung $F_{1,12} = 5.56$, *P* = 0.04, interaction $F_{2,12} = 0.14$, *P* = 0.87). There was a significant difference found between lungs, however as the interaction with infection type was not significant it was unlikely this affected the CFU lung^{-1}. Although, as shown in Figure 6.13, there were no *B. multivorans* C5393 CFU found for half of the co-infection samples. This was not observed for super-infection; there were *B. multivorans* C5393 CFU recovered from all lung pieces (Figure 6.13).
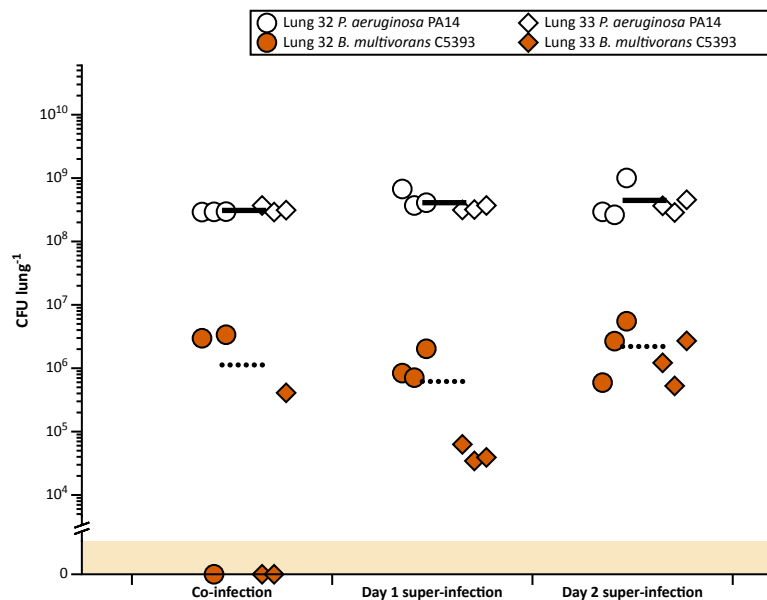
Figure 6.13: **The colony forming units per lung (CFU lung^{-1}) at 7 d for co-infection and super-infection of** ***Pseudomonas aeruginosa* PA14 and *Burkholderia multivorans* C5393 in the *ex vivo* pig lung (EVPL) model.** Three tissue pieces from each of two independent lungs were used for each infection, shown by individual data points. For co-infection, the EVPL tissue pieces were infected with *P. aeruginosa* PA14 (white) and *B. multivorans* C5393 (orange) following dissection and incubated at 37 °C for 7 d. For super-infection, tissue pieces were infected with *P. aeruginosa* PA14 following dissection then incubated at 37 °C for 7 d. At 1 d or 2 d, the super-infection pieces were infected with *B. multivorans* C5393 then the incubation was continued. The dashed horizontal lines show the mean CFU lung^{-1} for *B. multivorans* C5393 and the solid horizontal lines show the mean for *P. aeruginosa* PA14. The coloured region below the y axes break represents samples where no CFU were detected. The y axis is log$_{10}$ scale.

There was a higher concentration of long chain AHLs at 7 days in the EVPL biofilm when *P. aeruginosa* PA14 was super-infected with *B. cenocepacia* K56-2 at 2 days, compared with single infection.

The concentration of long and short chain AHL signal molecules, associated with QS, were then measured in each co-infection and super-infection 7 d sample. The concentration of AHL molecules produced by *P. aeruginosa* PA14, *B. cenocepacia* K56-2, and *B. multivorans* C5393 during single infection at 7 d in the EVPL model were also measured for comparison. The CFU lung^{-1} for the single infections is shown in Appendix C (Figure C.1). The aim was to identify whether there was a change in concentration during mixed infection, and whether this was different following super-infection. As found in chapter 4, the assay for short chain AHL molecules was unable to detect any production in the *P. aeruginosa* PA14 and *B. cenocepacia* K56-2 samples (Figure 6.14), or in the PA14 and *B. multivorans* C5393 samples (Figure 6.15). The concentration measured in each sample was similar to, or less than, the concentration measured in the uninfected EVPL samples.

As the lung tissue did not produce QS signalling molecules, it could not be concluded whether these results showed that there were no short chain AHLs detectable or if there was an issue with the assay.

Figure 6.14: **Concentration of short chain acyl homoserine lactones (AHLs) produced by *Pseudomonas aeruginosa* PA14 and *Burkholderia cenocepacia* K56-2 in the *ex vivo* pig lung model biofilm at 7 d.** The concentration (nM) of short chain AHLs was measured for single infection of each strain, and co-infection where EVPL tissue was infected with *P. aeruginosa* PA14 and *B. cenocepacia* K56-2 following dissection. The short chain AHLs were also measured from *P. aeruginosa* PA14 infected tissue that was infected with *B. cenocepacia* K56-2 1 d after initial infection (Day 1 super-infection) and 2 d after initial infection (Day 2 super-infection). All tissue pieces were incubated at 37 °C and the biofilm recovered at 7 d. Each infection was performed on three replicate tissue pieces from each of two indepent pig lungs, shown by individual data points. The mean is shown by the horizontal lines. The dashed horizontal line shows the mean concentration of short chain AHLs measured in three uninfected EVPL tissue pieces from each lung. The y axis is $\log_{10}$ scale.

Figure 6.15: **Concentration of short chain acyl homoserine lactones (AHLs) produced by *Pseudomonas aeruginosa* PA14 and *Burkholderia multivorans* C5393 in the *ex vivo* pig lung model biofilm at 7 d.** The concentration (nM) of short chain AHLs was measured for single infection of each strain, and co-infection where EVPL tissue was infected with *P. aeruginosa* PA14 and *B. multivorans* C5393 following dissection. The short chain AHLs were also measured from *P. aeruginosa* PA14 infected tissue that was infected with *B. multivorans* C5393 1 d after initial infection (Day 1 super-infection) and 2 d after initial infection (Day 2 super-infection). All tissue pieces were incubated at 37 °C and the biofilm recovered at 7 d. Each infection was performed on three replicate tissue pieces from each of two indepent pig lungs, shown by individual data points. The mean is shown by the horizontal lines. The dashed horizontal line represents the limit of detection, which was the mean concentration of short chain AHLs measured in three uninfected EVPL tissue pieces from each lung. The y axis is $\log_{10}$ scale.

The concentration of long chain AHLs was able to be measured. As shown in Figure 6.16, there were no detectable long chain AHLs in the single infection samples for either *P. aeruginosa* PA14 or *B. cenocepacia* K56-2. All single infection samples were comparable to, or less than, the mean concentration measured in the uninfected EVPL samples. There was an overall significant difference in the concentration of long chain AHLs between PA14 and K56-2 infections (ANOVA: infection $F_{4,20} = 7.07$, $P < 0.01$, lung $F_{1,20} = 7.68$, $P = 0.01$, interaction $F_{4,20} = 1.00$, $P = 0.43$). Although the difference between lungs was significant, the interaction was not significant so it was unlikely this caused the differences in long chain AHL concentration. A post hoc Tukey HSD analysis showed there was a significantly higher concentration in *P. aeruginosa* PA14 samples super-infected with *B. cenocepacia* K56-2 at 2 d compared with single PA14 infection ($P = 0.01$), and K56-2 single infection ($P < 0.01$). Although there were long chain AHLs detected in co-infection samples, the concentration did not significantly differ from single infection (Figure 6.16). There was also no significant difference found between co-infection and super-infection, however

the mean concentration of long chain AHLS was higher for 2 d super-infection than co-infection and 1 d super-infection (Figure 6.16).
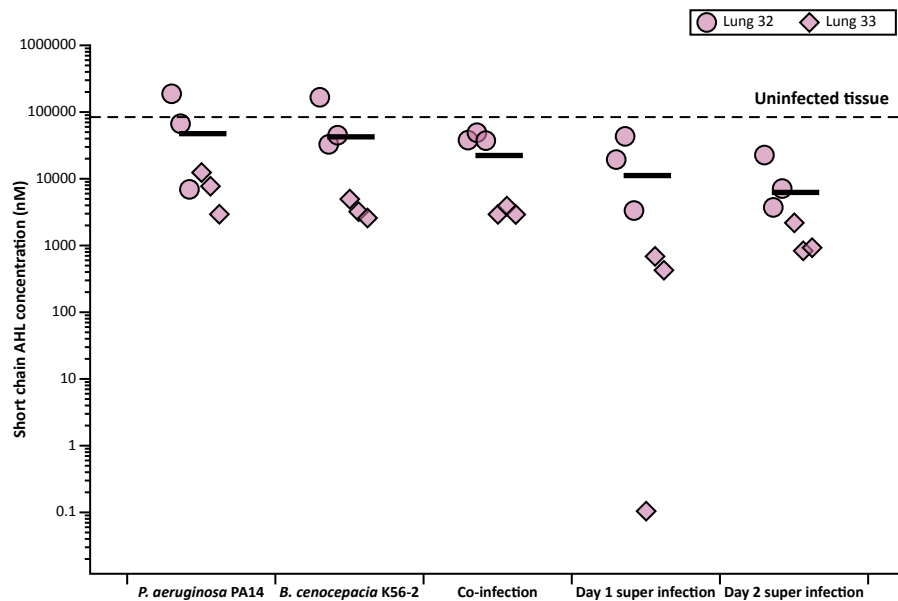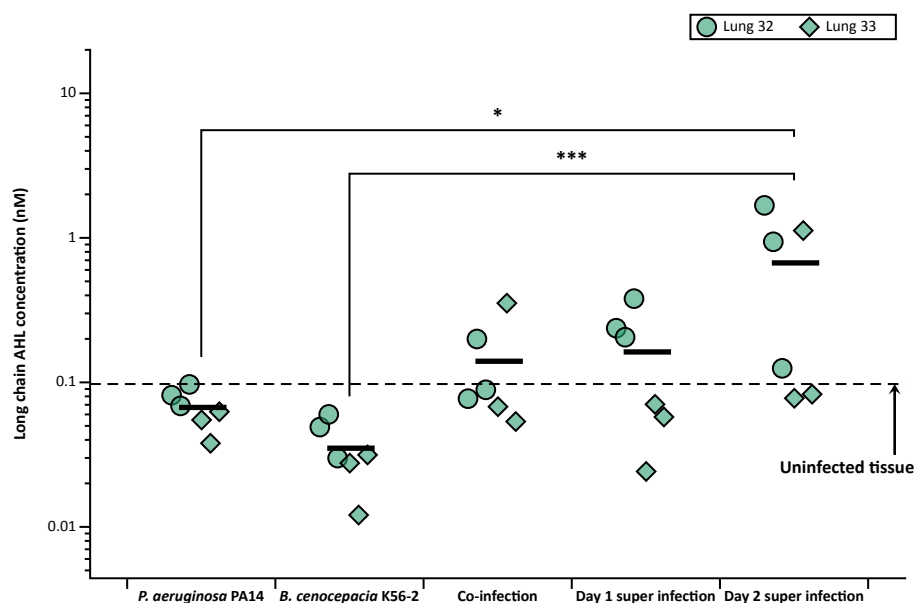

Figure 6.16: **Concentration of long chain acyl homoserine lactones (AHLs) produced by *Pseudomonas aeruginosa* PA14 and *Burkholderia cenocepacia* K56-2 in the *ex vivo* pig lung model biofilm at 7 d.** The concentration (nM) of long chain AHLs was measured for single infection of each strain, and co-infection where EVPL tissue was infected with *P. aeruginosa* PA14 and *B. cenocepacia* K56-2 following dissection. The long chain AHLs were also measured from *P. aeruginosa* PA14 infected tissue that was infected with *B. cenocepacia* K56-2 1 d after initial infection (Day 1 super-infection) and 2 d after initial infection (Day 2 super-infection). All tissue pieces were incubated at 37 °C and the biofilm recovered at 7 d. Each infection was performed on three replicate tissue pieces from each of two indepent pig lungs, shown by individual data points. The mean is shown by the horizontal lines. The dashed horizontal line shows the mean concentration of long chain AHLs measured in three uninfected EVPL tissue pieces from each lung. Any significant differences are shown ('***' = $P < 0.001$, '**' = $P < 0.01$, '*' = $P < 0.05$).The y axis is $\log_{10}$ scale.

The long chain AHL concentration was then measured for *P. aeruginosa* PA14 and *B. multivorans* C5393 samples (Figure 6.17). There was no significant difference found between any of the infection conditions (ANOVA: infection $F_{4, 20}$ = 2.67, P = 0.06, lung $F_{1,20}$ = 5.69, P = 0.03, interaction $F_{4,20}$ = 1.40, P = 0.27). As observed for the *B. cenocepacia* K56-2 mixed infections, the difference between lungs was significant however the interaction was not significant. Hence it was unlikely this caused the differences in long chain AHL concentration. There were no long chain AHLs detected in the *P. aeruginosa* PA14 single infection samples above the concentration measured in uninfected EVPL tissue. They were also only measured in two *B. multivorans* C5393 single infection samples, and one co-infection sample. The two super-infection conditions both had a mean concentration of long chain AHLs above the mean for uninfected EVPL tissue samples (Figure 6.17).
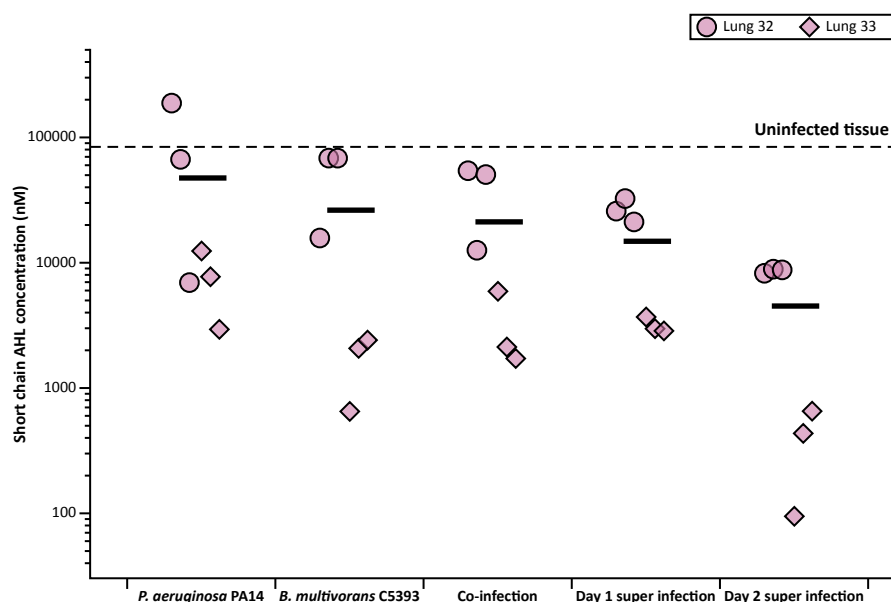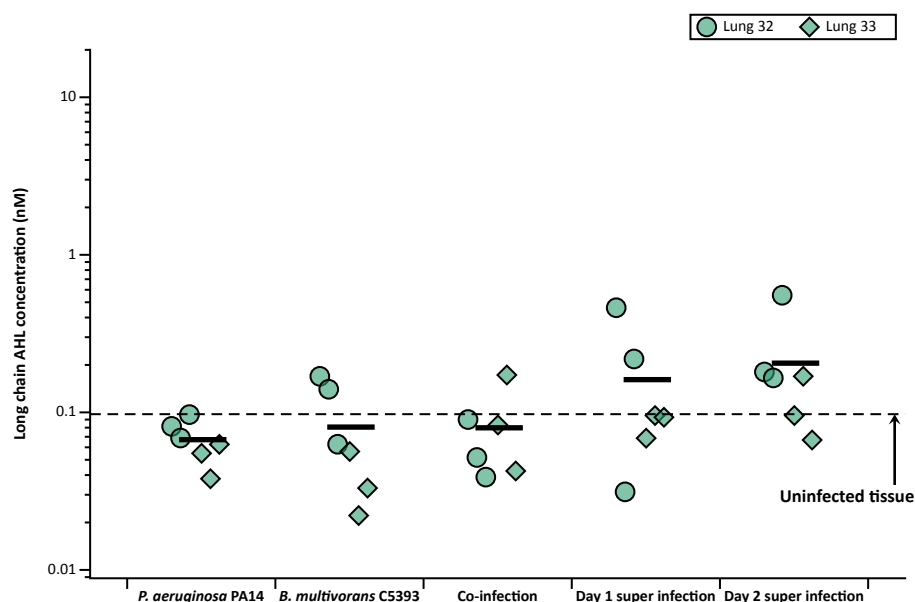
Figure 6.17: **Concentration of long chain acyl homoserine lactones (AHLs) produced by *Pseudomonas aeruginosa* PA14 and *Burkholderia multivorans* C5393 in the *ex vivo* pig lung model biofilm at 7 d.** The concentration (nM) of long chain AHLs was measured for single infection of each strain, and co-infection where EVPL tissue was infected with *P. aeruginosa* PA14 and *B. multivorans* C5393 following dissection. The long chain AHLs were also measured from *P. aeruginosa* PA14 infected tissue that was infected with *B. multivorans* C5393 1 d after initial infection (Day 1 super-infection) and 2 d after initial infection (Day 2 super-infection). All tissue pieces were incubated at 37 °C and the biofilm recovered at 7 d. Each infection was performed on three replicate tissue pieces from each of two indepent pig lungs, shown by individual data points. The mean is shown by the horizontal lines. The dashed horizontal line shows the mean concentration of long chain AHLs measured in three uninfected EVPL tissue pieces from each lung. The y axis is $\log_{10}$ scale.

6.2.3   *P. aeruginosa* clinical isolates and Bcc mixed infection

Following investigation of *P. aeruginosa* PA14 mixed infection with *B. cenocepacia* K56-2 and *B. multivorans* C5393 in the EVPL model, two *P. aeruginosa* CF clinical isolates were introduced. These strains are chronically adapted to the CF lung, so were included to determine whether this had an effect on co-infection with the Bcc strains in the EVPL model. The two clinical isolates: *P. aeruginosa* SED43 and *P. aeruginosa* SED20, were co-infected with each Bcc strain and the CFU lung^{-1} determined at 2 d and 7 d. *P. aeruginosa* PA14 was also included as a control for comparison with the rest of the chapter. The production of two *P. aeruginosa* siderophores: PVD and PCH, were also measured using fluorescence at 2 d, to provide an indication as to whether co-infection had an effect on virulence factor production. All of these experiments were also performed in SCFM *in vitro* to determine whether addition of the lung tissue had an effect, or was comparable to SCFM alone. Single infections of each strain were performed

in all conditions for comparison.

The bacterial load of *B. cenocepacia* K56-2 and *B. multivorans* C5393 was higher during co-infection with *P. aeruginosa* clinical isolates in SCFM and the EVPL model for 2 days than co-infection with *P. aeruginosa* PA14.

As two more *P. aeruginosa* strains were introduced, the CFU lung^{-1} in the EVPL model and CFU ml^{-1} in SCFM were first determined for each strain grown alone. At 2 d, there was an overall significant difference in the CFU ml^{-1} in SCFM (ANOVA: $F_{4,9}$ = 5.55, *P* = 0.02). A post hoc Tukey HSD analysis showed that there was significantly more CFU ml^{-1} of *P. aeruginosa* SED43 compared with *P. aeruginosa* PA14 (*P* = 0.02). There was also significantly higher CFU ml^{-1} of SED43 compared with *B. cenocepacia* K56-2 (*P* = 0.04). However, as shown in Figure 6.18A, the CFU ml^{-1} of each strain grown in SCFM for 2 d were all within a 1 log$_{10}$ range and did not appear to greatly differ. The CFU lung^{-1} in the EVPL model at 2 d were also within a similar range, however the CFU lung^{-1} was more similar between each strain than in SCFM (Figure 6.18B). This was confirmed with statistical analysis, which found no significant difference between strains (ANOVA: infection $F_{4,\,19}$ = 2.05, *P* = 0.13, lung $F_{1,19}$ = 1.87, *P* = 0.19, interaction $F_{4,19}$ = 1.09, *P* = 0.39).

Figure 6.18: **The colony forming units (CFU) ml^{-1} in synthetic cystic fibrosis sputum media (SCFM) and CFU lung^{-1} in the *ex vivo* pig lung (EVPL) model for each strain grown individually for 2 d.** *Pseudomonas aeruginosa* PA14, *P. aeruginosa* SED43, *P. aeruginosa* SED20, *Burkholderia cenocepacia* K56-2, and *Burkholderia multivorans* C5393 were grown in each environment for 2 d at 37 °C, then the CFU was determined. The mean is represented by the horizontal lines. The y axes are log$_{10}$ scale. **(A)** The CFU ml^{-1} in SCFM; three repeats were used for each strain and are represented by individual data points. Any significant differences are shown ('*' = $P < 0.05$). **(B)** The CFU lung^{-1} in the EVPL model; three tissue pieces from each of two independent pig lungs were infected with each strain and are represented by different shaped and coloured data points (see key). Each data point represents an individual sample.

At 7 d the CFU ml^{-1} of each strain in SCFM appeared to be more similar than at 2 d (Figure 6.19A), however there was also a significant difference found (ANOVA: $F_{4,10}$ = 5.46, P = 0.01). Post hoc Tukey HSD analysis showed that there was a significant difference in CFU ml^{-1} between *P. aeruginosa* PA14 and *B. cenocepacia* K56-2 (P = 0.02), and *B. cenocepacia* K56-2 and *B. multivorans* C5393 (P = 0.02). This was unlikely to be of biological importance as the CFU ml^{-1} were all within a 1 log$_{10}$ range (Figure 6.19A). In contrast, there were clear differences in the CFU lung^{-1} in the EVPL model at 7 d (Figure 6.19B), which was not observed at 2 d (Figure 6.18B). There were some *B. cenocepacia* K56-2 and *B. multivorans* C5393 infected tissue pieces where the Bcc colonies were indistinguishable from the endogenous lung species, so they were removed from the data. Hence non-parametric statistical analysis was performed, which found a significant difference in the CFU lung^{-1} between the strains (Kruskal-Wallis: χ_2 = 15.31, df = 4, P

< 0.01). A post hoc Dunn's test showed there was significantly less CFU lung^{-1} of *B. cenocepacia* K56-2 than the two *P. aeruginosa* CF isolates: SED43 (P < 0.01) and SED20 (P = 0.02). The CFU of *B. cenocepacia* K56-2 recovered was less in the EVPL model than SCFM at 7 d (mean 9.0 x 10^6 and 2.2 x 10^8 respectively).

Figure 6.19: **The colony forming units (CFU) ml^{-1} in synthetic cystic fibrosis sputum media (SCFM) and CFU lung^{-1} in the *ex vivo* pig lung (EVPL) model for each strain grown individually for 7 d.** *Pseudomonas aeruginosa* PA14, *P. aeruginosa* SED43, *P. aeruginosa* SED20, *Burkholderia cenocepacia* K56-2, and *Burkholderia multivorans* C5393 were grown in each environment for 7 d at 37 °C, then the CFU was determined. The mean is represented by the horizontal lines. The y axes are log$_{10}$ scale. Any significant differences are shown ('**' = P < 0.01, '*' = P < 0.05). **(A)** The CFU ml^{-1} in SCFM; three repeats were used for each strain and are represented by individual data points. **(B)** The CFU lung^{-1} in the EVPL model; three tissue pieces from each of two independent pig lungs were infected with each strain and are represented by different shaped and coloured data points (see key). Each data point represents an individual sample.

Co-infection of each *P. aeruginosa* strain with *B. cenocepacia* K56-2 was then performed in SCFM and the EVPL model for 2 d and 7 d. There was a difference observed at 2 d in the CFU ml^{-1} of *B. cenocepacia* K56-2 during SCFM co-infection, compared with the CFU lung^{-1} recovered from the EVPL model for co-infection (Figure 6.20). In SCFM, the CFU ml^{-1} of each *P. aeruginosa* strain and *B. cenocepacia* K56-2 was similar during co-infection (Figure 6.20A). However, there were less CFU lung^{-1} of *B. cenocepacia* K56-2 recovered from each co-infection in the EVPL model than the *P. aeruginosa* strains (Figure 6.20B).

There was no significant difference in CFU ml^{-1} found between the *P. aeruginosa* strains in SCFM at 2 d (ANOVA: F$_{2,6}$ = 1.92, *P* = 0.23), however there was a significant difference in *B. cenocepacia* K56-2 CFU ml^{-1} grown with each strain (ANOVA: F$_{2,6}$ = 172.4, *P* < 0.01). The post hoc Tukey HSD analysis found that there was significantly higher CFU ml^{-1} of K56-2 when it was co-infected with *P. aeruginosa* SED43 (*P* < 0.01) and *P. aeruginosa* SED20 (*P* < 0.01), compared with *P. aeruginosa* PA14 in SCFM.
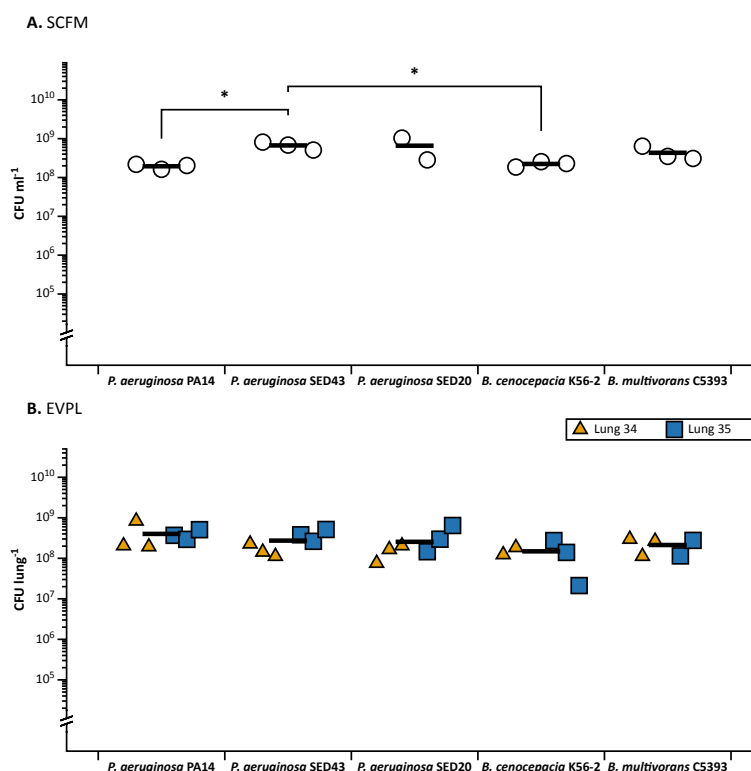

Figure 6.20: **The colony forming units (CFU) ml^{-1} in synthetic cystic fibrosis sputum media (SCFM) and CFU lung^{-1} in the *ex vivo* pig lung (EVPL) model for each *Pseudomonas aeruginosa* strain (white) co-infected with *Burkholderia cenocepacia* K56-2 (blue) for 2 d.** *Pseudomonas aeruginosa* PA14, *P. aeruginosa* SED43, and *P. aeruginosa* SED20 were co-infected with *B. cenocepacia* K56-2 for 2 d at 37 °C, then the CFU was determined. The *P. aeruginosa* mean is represented by the solid horizontal lines and the *B. cenocepacia* mean is shown by the dotted horizontal lines. The y axes are log$_{10}$ scale. Any significant differences are shown ('***' = *P* < 0.001, '**' = *P* < 0.01, '*' = *P* < 0.05). **(A)** The CFU ml^{-1} in SCFM; three repeats were used for each strain and are represented by individual data points. **(B)** The CFU lung^{-1} in the EVPL model; three tissue pieces from each of two independent pig lungs were infected and are represented by different shaped data points (see key). Each data point represents an individual sample.

In the EVPL model at 2 d there was also a significant difference in the *B. cenocepacia* K56-2 CFU lung^{-1} when co-infected with each *P. aeruginosa* strain (ANOVA: infection F$_{2,12}$ = 17.40, *P* < 0.01, lung F$_{1,12}$ = 0.53, *P* = 0.48, interaction F$_{2,12}$ = 1.49, *P* = 0.26). There was significantly more CFU lung^{-1} of K56-2 when it was co-infected with *P. aeruginosa* SED43 (Tukey HSD: *P* < 0.01) and *P. aeruginosa* SED20 (Tukey HSD: *P* < 0.01), compared with *P. aeruginosa* PA14 (Figure 6.20B). This difference was greater than that observed in SCFM (Figure 6.20). There was also a significant difference in *P. aeruginosa* CFU lung^{-1} found (ANOVA: infection F$_{2,12}$ = 9.10, *P* < 0.01, lung F$_{1,12}$ = 10.39, *P* = 0.01, interaction F$_{2,12}$ = 5.06, *P* = 0.03), and post hoc Tukey HSD analysis showed that there was a significant difference between PA14 and SED20 when they were co-infected with *B. cenocepacia* K56-2 (*P* < 0.01). However the interaction between lung and strain was found to be significant, which indicated that this difference was caused by variation between the pig

lungs rather than a difference between the two strains.

The *B. cenocepacia* K56-2 and *P. aeruginosa* co-infections in SCFM and the EVPL model were also performed for 7 d and the CFU determined (Figure 6.21). The bacterial load in SCFM was comparable to 2 d, and there was no significant difference in the CFU ml^{-1} of each *P. aeruginosa* strain (ANOVA: $F_{2,6}$ = 2.16, P = 0.20). There was a significant difference in the *B. cenocepacia* K56-2 CFU ml^{-1} at 7 d (ANOVA: $F_{2,6}$ = 17.82, P < 0.01). As found at 2 d, there was significantly more CFU ml^{-1} of *B. cenocepacia* K56-2 when it was co-infected with *P. aeruginosa* SED43 (Tukey HSD: P < 0.01) and *P. aeruginosa* SED20 (Tukey HSD: P = 0.01), compared with *P. aeruginosa* PA14 co-infection (Figure 6.21A).
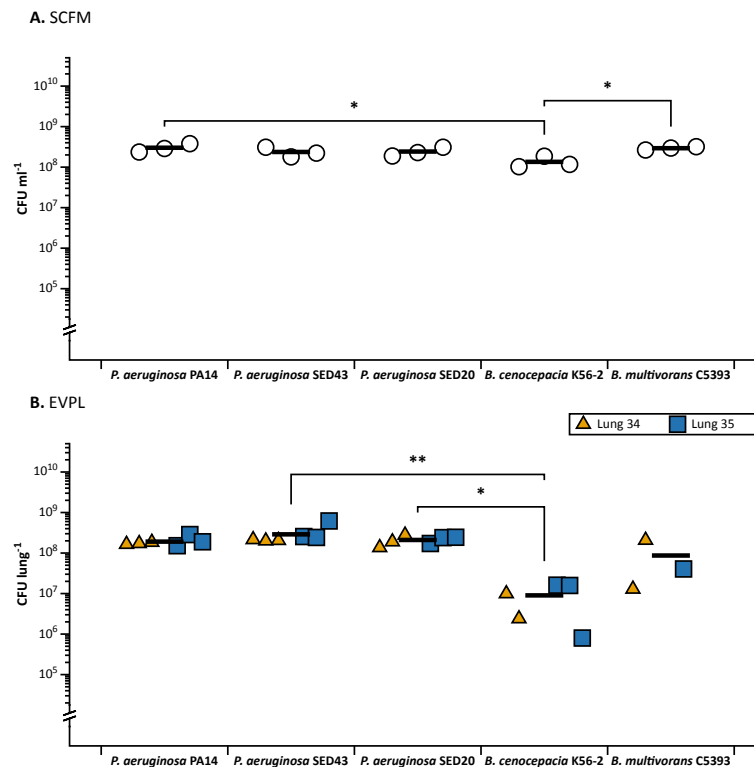

Figure 6.21: **The colony forming units (CFU) ml^{-1} in synthetic cystic fibrosis sputum media (SCFM) and CFU lung^{-1} in the *ex vivo* pig lung (EVPL) model for each *Pseudomonas aeruginosa* strain (white) co-infected with *Burkholderia cenocepacia* K56-2 (blue) for 7 d.** *Pseudomonas aeruginosa* PA14, *P. aeruginosa* SED43, and *P. aeruginosa* SED20 were co-infected with *B. cenocepacia* K56-2 for 7 d at 37 °C, then the CFU was determined. The *P. aeruginosa* mean is represented by the solid horizontal lines and the *B. cenocepacia* mean is shown by the dotted horizontal lines. The y axes are log$_{10}$ scale. Any significant differences are shown ('**' = P < 0.01, '*' = P < 0.05). **(A)** The CFU ml^{-1} in SCFM; three repeats were used for each strain and are represented by individual data points. **(B)** The CFU lung^{-1} in the EVPL model; three tissue pieces from each of two independent pig lungs were infected and are represented by different shaped data points (see key). Each data point represents an individual sample. The coloured region below the y axis break represents samples where no CFU were detected.

In the EVPL model at 7 d *B. cenocepacia* K56-2 was not recovered from all samples during *P. aeruginosa* co-infection (Figure 6.21B). Although there was a significant difference found in K56-2 CFU lung^{-1} for each co-infection (ANOVA: infection $F_{2,12}$ = 11.81, P < 0.01, lung $F_{1,12}$ = 4.39, P = 0.06, interaction $F_{2,12}$ = 15.55, P < 0.01), the interaction with the lung used was found to be significant. Therefore, the significant differences found between co-infection with *P. aeruginosa* PA14 and *P. aeruginosa* SED43 (Tukey HSD: P = 0.01), and PA14 and *P. aeruginosa* SED20 (Tukey HSD: P < 0.01) was likely to have been caused by

differences in the lungs rather than the different *P. aeruginosa* strains. There was also a significant difference in CFU lung^{-1} of each *P. aeruginosa* strain when co-infected with *B. cenocepacia* K56-2 in the EVPL model for 7 d (ANOVA: infection $F_{2,12}$ = 17.39, *P* < 0.01, lung $F_{1,12}$ = 0.53, *P* = 0.48, interaction $F_{2,12}$ = 1.49, *P* = 0.26). Although, the bacterial load was comparable to co-infection at 2 d, and in SCFM at 7 d (Figure 6.21). Post hoc Tukey HSD analysis showed a significant difference between *P. aeruginosa* PA14 and the two clinical *P. aeruginosa* isolates: SED43 (*P* < 0.01) and SED20 (*P* < 0.01). This difference was only small, and the CFU lung^{-1} were all within a $\log_{10}$ range (Figure 6.21B).

P. aeruginosa co-infection with *B. multivorans* C5393 was then studied in SCFM *in vitro* and the EVPL model. At 2 d the CFU were comparable to *B. cenocepacia* K56-2 co-infection, and there was no clear difference between SCFM and EVPL growth (Figure 6.22). There was no significant difference in the CFU of *P. aeruginosa* strains during co-infection with *B. multivorans* C5393 in SCFM (ANOVA: $F_{2,6}$ = 4.87, *P* = 0.06) or in the EVPL model at 2 d (ANOVA: infection $F_{2,12}$ = 0.70, *P* =0.52, lung $F_{1,12}$ = 0.57, *P* = 0.47, interaction $F_{2,12}$ = 0.48, *P* = 0.63). However, there was a significant difference in the CFU ml^{-1} of *B. multivorans* C5393 co-infected with each *P. aeruginosa* strain in SCFM (ANOVA: $F_{2,6}$ = 43.74, *P* < 0.01). There was significantly more CFU ml^{-1} during co-infection with *P. aeruginosa* SED43 and *P. aeruginosa* SED20 than co-infection with *P. aeruginosa* PA14 (Tukey HSD: both *P* < 0.01). The mean CFU ml^{-1} of *B. multivorans* C5393 was higher than the mean CFU of *P. aeruginosa* SED43 and *P. aeruginosa* SED20 when co-infected for 2 d in SCFM (Figure 6.22A). This was not found for *P. aeruginosa* PA14 co-infection (mean C5393: 6.8 x 10^6, PA14: 2.4 x 10^8).

A. SCFM: *B. multivorans* C5393

B. EVPL: *B. multivorans* C5393

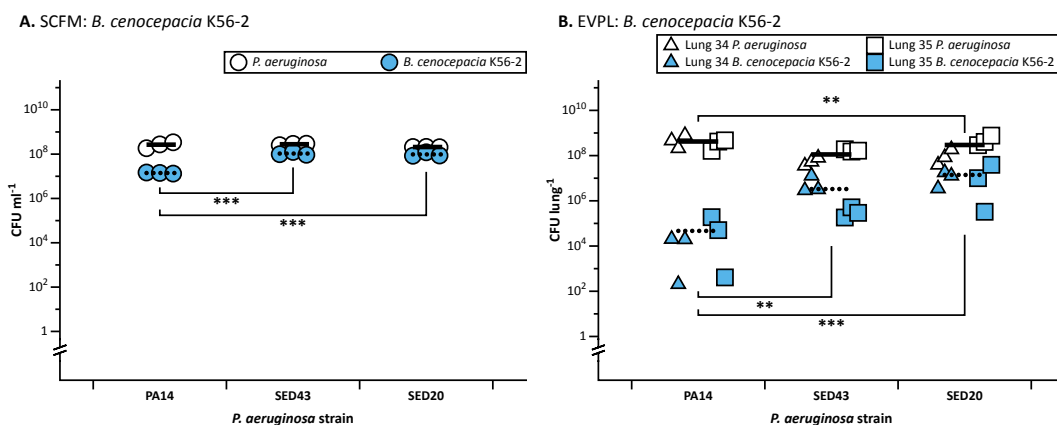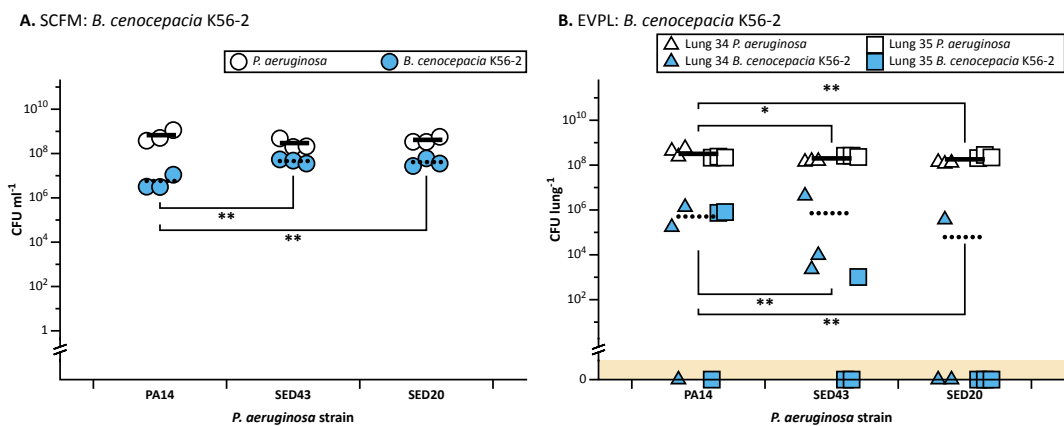Figure 6.22: **The colony forming units (CFU) ml^{-1} in synthetic cystic fibrosis sputum media (SCFM) and CFU lung^{-1} in the *ex vivo* pig lung (EVPL) model for each *Pseudomonas aeruginosa* strain (white) co-infected with *Burkholderia multivorans* C5393 (orange) for 2 d.** *Pseudomonas aeruginosa* PA14, *P. aeruginosa* SED43, and *P. aeruginosa* SED20 were co-infected with *B. multivorans* C5393 for 2 d at 37 °C, then the CFU was determined. The *P. aeruginosa* mean is represented by the solid horizontal lines and the *B. multivorans* mean is shown by the dotted horizontal lines. The y axes are log$_{10}$ scale. Any significant differences are shown ('***' = $P < 0.001$). **(A)** The CFU ml^{-1} in SCFM; three repeats were used for each strain and are represented by individual data points. **(B)** The CFU lung^{-1} in the EVPL model; three tissue pieces from each of two independent pig lungs were infected and are represented by different shaped data points (see key). Each data point represents an individual sample.

As found for SCFM co-infection, there was also a significant difference in *B. multivorans* C5393 CFU lung^{-1} when it was co-infected with each *P. aeruginosa* strain in the EVPL model for 2 d (ANOVA: infection $F_{2,12} = 17.43$, $P < 0.01$, lung $F_{1,12} < 0.01$, $P = 0.95$, interaction $F_{2,12} = 0.09$, $P = 0.91$). Tukey HSD post hoc analysis showed that there was signifcantly more CFU lung^{-1} of C5393 when it was co-infected with *P. aeruginosa* SED43 (Tukey HSD $P < 0.01$) and SED20 (Tukey HSD $P < 0.01$), compared with *P. aeruginosa* PA14. Consistent with the SCFM findings, there were less CFU ml^{-1} of *B. multivorans* C5393 than *P. aeruginosa* PA14 during co-infection in the EVPL model, whereas there was no clear difference during co-infection with *P. aeruginosa* SED43 or *P. aeruginosa* SED20 (Figure 6.22B).

At 7 d in SCFM, the CFU ml^{-1} of each *P. aeruginosa* strain was higher than *B. multivorans* C5393 in all co-infections (Figure 6.23A). However unlike at 2 d, there was no significant difference found between the CFU ml^{-1} of *B. multivorans* C5393 during each co-infection (ANOVA: $F_{2,6} = 1.70$, $P = 0.26$). There was a significant difference in the CFU ml^{-1} of each *P. aeruginosa* strain (ANOVA: $F_{2,6} = 10.55$, $P = 0.01$), and post hoc Tukey HSD analysis found that there was a significant difference between *P. aeruginosa* PA14 and *P. aeruginosa* SED43 ($P = 0.01$). However, the CFU ml^{-1} was within a small range indicating that this

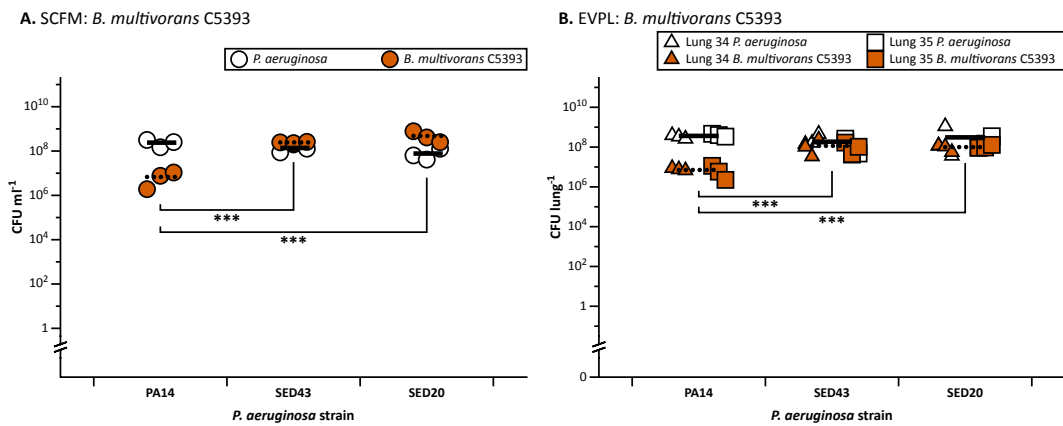difference was not of biological importance (Figure 6.23A).
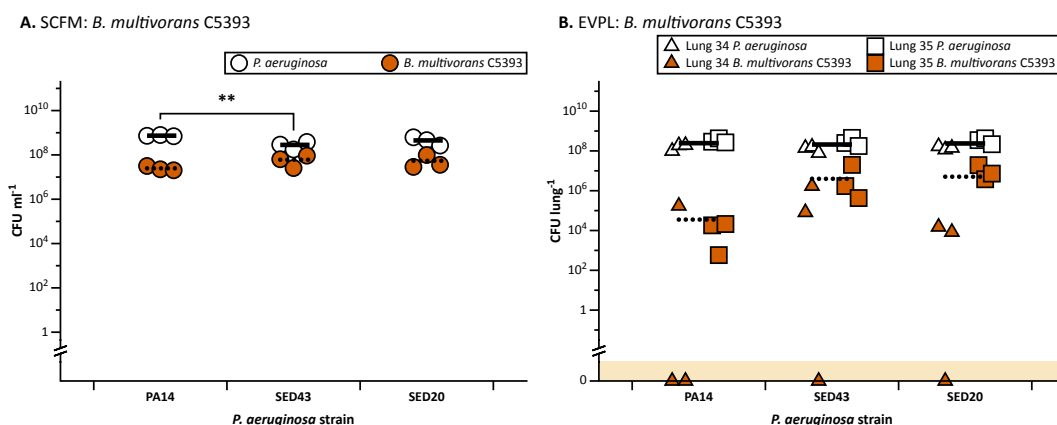
Figure 6.23: **The colony forming units (CFU) ml^{-1} in synthetic cystic fibrosis sputum media (SCFM) and CFU lung^{-1} in the *ex vivo* pig lung (EVPL) model for each *Pseudomonas aeruginosa* strain (white) co-infected with *Burkholderia multivorans* C5393 (orange) for 7 d.** *Pseudomonas aeruginosa* PA14, *P. aeruginosa* SED43, and *P. aeruginosa* SED20 were co-infected with *B. multivorans* C5393 for 7 d at 37 °C, then the CFU was determined. The *P. aeruginosa* mean is represented by the solid horizontal lines and the *B. multivorans* mean is shown by the dotted horizontal lines. The y axes are log$_{10}$ scale. Any significant differences are shown ('**' = $P < 0.01$, '*' = $P < 0.05$). **(A)** The CFU ml^{-1} in SCFM; three repeats were used for each strain and are represented by individual data points. **(B)** The CFU lung^{-1} in the EVPL model; three tissue pieces from each of two independent pig lungs were infected and are represented by different shaped data points (see key). Each data point represents an individual sample. The coloured region below the y axis break represents samples where no CFU were detected.

There was no significant difference found in the CFU lung^{-1} of each *P. aeruginosa* strain during *B. multivorans* C5393 co-infection in the EVPL model for 7 d (ANOVA: infection $F_{2,12} = 0.57$, $P = 0.58$, lung $F_{1,12} == 22.89$, $P < 0.01$, interaction $F_{2,12} = 0.02$, $P = 0.98$). There was also no significant difference in the *B. multivorans* C5393 CFU lung^{-1} found (ANOVA: infection $F_{2,12} = 0.57$, $P = 0.58$, lung $F_{1,12} = 22.89$, $P < 0.01$, interaction $F_{2,12} = 0.02$, $P = 0.98$). However, there was an increase in the mean CFU lung^{-1} when it was co-infected with the two *P. aeruginosa* clinical isolates compared with *P. aeruginosa* PA14 (Figure 6.23B). There were also samples from lung 34 where no *B. multivorans* C5393 was recovered in each co-infection at 7 d.

Siderophore production by *P. aeruginosa* CF clinical isolates SED43 and SED20 was affected by co-infection with *B. cenocepacia* K56-2 and *B. multivorans* C5393.

Production of two *P. aeruginosa* siderophores: PVD and PCH, was then measured using fluorescence, as in chapter 3. This was performed for each co-infection sample from SCFM *in vitro* and the EVPL model at 2 d. To determine whether co-infection with *B. cenocepacia* K56-2 or *B. multivorans* C5393 had an effect on production, this

was compared to PVD and PCH production during *P. aeruginosa* single infection. The corresponding CFU data is shown in Appendix C (Figure C.2). Analysis of the Bcc single infection samples confirmed that there was no detectable signal from these strains that affected the results (Appendix C; Figure C.3).

As shown in Figures 6.24A and 6.24B, there were no significant differences in *P. aeruginosa* PA14 PVD production in SCFM (ANOVA: $F_{2,6}$ = 0.55, *P* = 0.61) or the EVPL model (ANOVA: infection $F_{2,12}$ = 1.44, *P* = 0.27, lung $F_{1,12}$ = 14.61, *P* < 0.01, interaction $F_{2,12}$ = 3.07, *P* = 0.08). However, there was a higher production of PVD when PA14 was grown alone in the EVPL model than in SCFM, consistent with previous work (Harrison and Diggle, 2016). This was also observed when grown with the two Bcc strains. There was less distinction in PVD production between the two environments for the clinical *P. aeruginosa* isolates (Figure 6.24). However production was affected by co-infection with the different *P. aeruginosa* strains. In SCFM, there was a significant difference in *P. aeruginosa* SED43 PVD production (ANOVA: $F_{2,6}$ = 11.84, *P* = 0.01). Tukey HSD post hoc analysis showed that SED43 produced significantly less PVD when co-infected with *B. cenocepacia* K56-2 (*P* = 0.03) and *B. multivorans* C5393 (*P* = 0.01) than during single infection (Figure 6.24C). There was also a significant difference in *P. aeruginosa* SED43 PVD production in the EVPL model (ANOVA: infection $F_{2,12}$ = 3.93, *P* = 0.05, lung $F_{1,12}$ = 3.01, *P* = 0.11, interaction $F_{2,12}$ = 0.49, *P* = 0.62). There was significantly less PVD produced by *P. aeruginosa* SED43 co-infected with *B. multivorans* C5393 than EVPL single infection (Tukey HSD *P* = 0.04). However, there was no significant difference when infected with *B. cenocepacia* K56-2 (Tukey HSD *P* = 0.26), although there was a small reduction (Figure 6.24D).

Figure 6.24: **Pyoverdine (PVD) measured as fluorescence (excitation 400 nm, emission 460 nm) from synthetic cystic fibrosis sputum media (SCFM) and *ex vivo* pig lung (EVPL) model samples following 2 d incubation.** The fluorescence was measured from filter sterilised samples and standardised using the uninfected controls. The SCFM samples **(A,C,E)** included three repeats per infection and the EVPL samples **(B,D,F)** used three repeats from each of two independent pig lungs, shown by different coloured and shaped data points (see keys). The horizontal lines show the mean and any significant differences are shown ('***' = $P < 0.001$, '**' = $P < 0.01$, '*' = $P < 0.05$). The y axes are $\log_{10}$ scale. **(A,B)** PVD measured from *Pseudomonas aeruginosa* PA14 single infection and co-infection with *Burkholderia cenocepacia* K56-2, and *Burkholderia multivorans* C5393. **(C,D)** PVD production by *P. aeruginosa* SED43 during single infection and co-infection with *B. cenocepacia* K56-2, and *B. multivorans* C5393. **(D,E,F)** PVD production by *P. aeruginosa* SED20 during single infection and co-infection with *B. cenocepacia* K56-2, and *B. multivorans* C5393.

Some repeats for *P. aeruginosa* SED20 were contaminated and thus removed from the analysis in both environments. Significant differences in *P. aeruginosa* SED20 PVD

production in SCFM (ANOVA: $F_{2,5}$ = 134.70, $P < 0.01$) and the EVPL model (Kruskal-Wallis: χ_2 = 6.66, df = 2, P = 0.04) were found. There was a significant reduction in PVD production when SED20 was co-infected with *B. multivorans* C5393 compared with single infection in both SCFM (Tukey HSD P = 0.02) and the EVPL model (Dunn's test P = 0.03). There were no other significant changes observed in the EVPL model (Figure 6.24F) . However, *P. aeruginosa* SED20 was also found to produce significantly less PVD when co-infected with *B. cenocepacia* K56-2 in SCFM (Tukey HSD $P < 0.01$). As shown in Figure 6.24, this was the only environment and *P. aeruginosa* strain where there was a significant difference between co-infection with each Bcc strain. There was significantly less PVD measured during SED20 co-infection with *B. multivorans* C5393 compared with *B. cenocepacia* K56-2 co-infection (P = 0.02).

The production of PCH was also measured in the same samples (Figure 6.25). A similar pattern was observed for *P. aeruginosa* PA14 as seen for PVD production; there was no significant difference in PCH production between PA14 single infection and Bcc co-infection in SCFM (ANOVA: $F_{2,6}$ = 1.04, P = 0.41) and the EVPL model (ANOVA: infection $F_{2,12}$ = 0.55, P = 0.59, lung $F_{1,12}$ = 22.74, $P < 0.01$, interaction $F_{2,12}$ = 2.44, P = 0.13). There was also an increase in *P. aeruginosa* PA14 PCH production in the EVPL model (Figure 6.25B) compared with SCFM (Figure 6.25A). As shown in Figure 6.25D, there was no significant difference in *P. aeruginosa* SED43 PCH production between single infection and co-infection in the EVPL model (ANOVA: infection $F_{2,12}$ = 1.98, P = 0.18, lung $F_{1,12}$ = 6.00, P = 0.03, interaction $F_{2,12}$ = 0.14, P = 0.87). However, there was a significant difference found in SCFM (ANOVA: $F_{2,6}$ = 11.68, P = 0.01). Post hoc Tukey HSD analysis showed that there was a significant reduction in *P. aeruginosa* SED43 PCH production when it was co-infected with *B. cenocepacia* K56-2 (P = 0.05) and *B. multivorans* C5393 (P = 0.01), compared with single infection (Figure 6.25C).
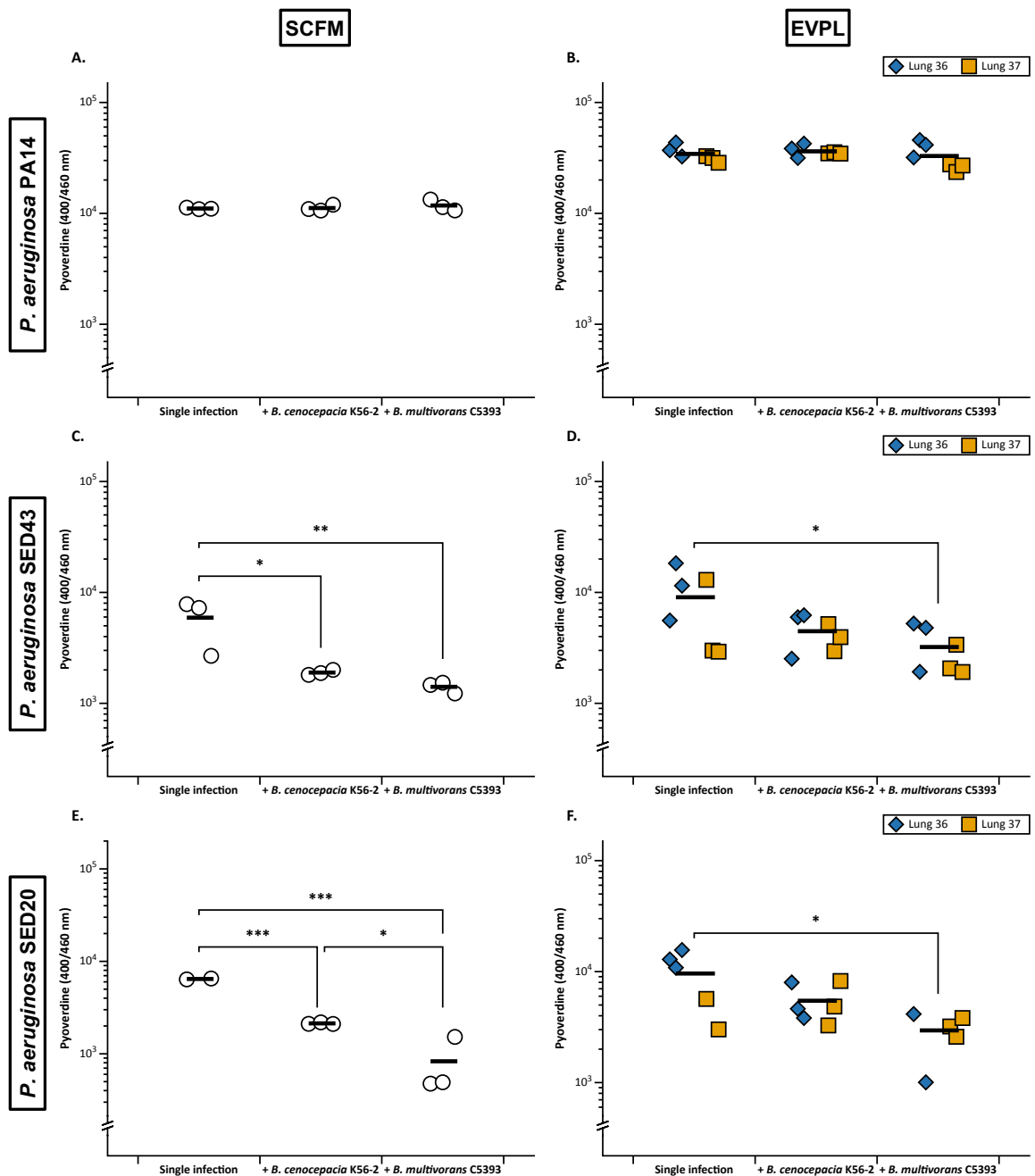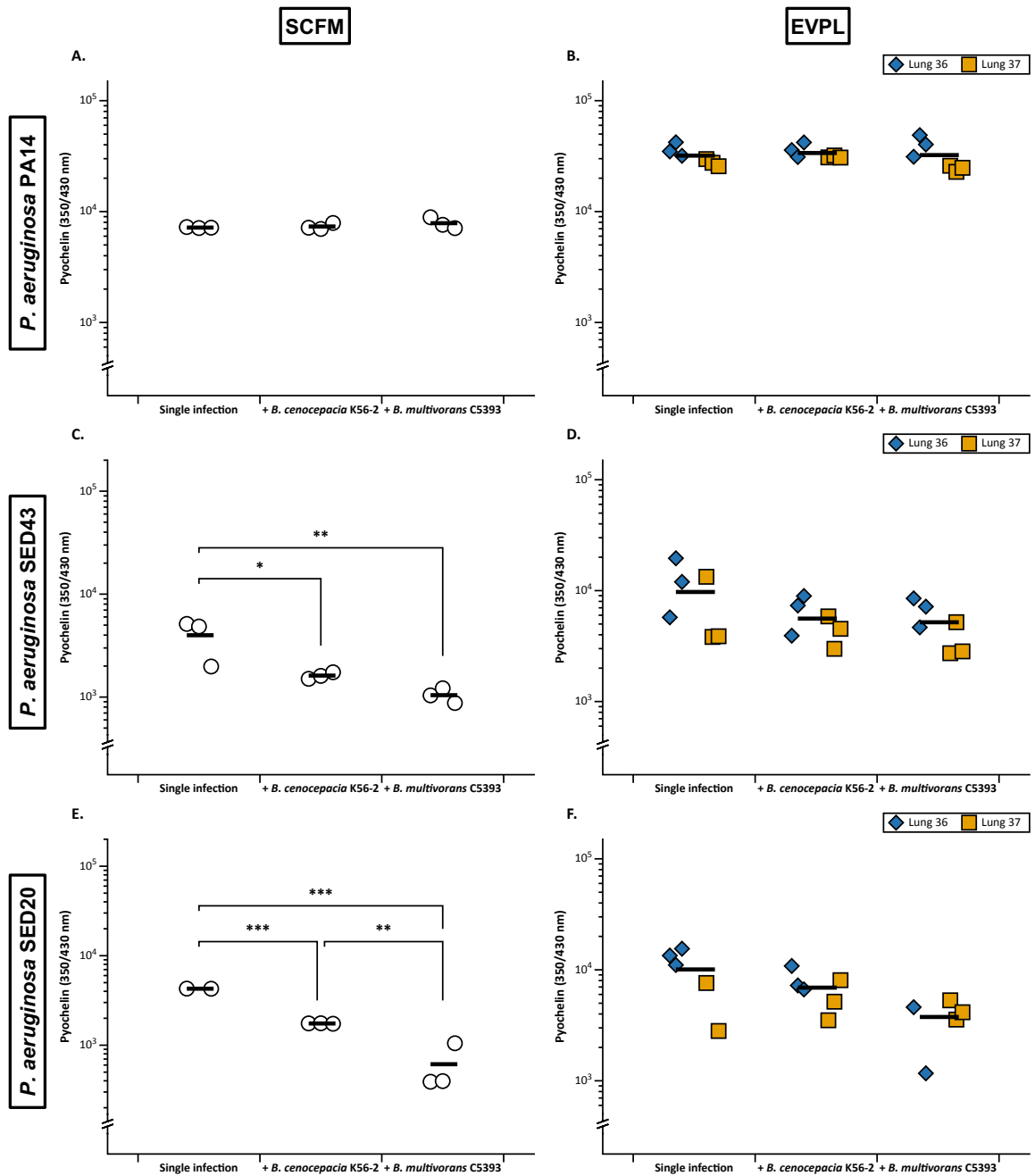
Figure 6.25: **Pyochelin (PCH) measured as fluorescence (excitation 350 nm, emission 430 nm) from synthetic cystic fibrosis sputum media (SCFM) and *ex vivo* pig lung (EVPL) model samples following 2 d incubation.** The fluorescence was measured from filter sterilised samples and standardised using the uninfected controls. The SCFM samples **(A,C,E)** included three repeats per infection and the EVPL samples **(B,D,F)** used three repeats from each of two independent pig lungs, shown by different coloured and shaped data points (see keys). The horizontal lines show the mean and any significant differences are shown ('*****' = $P < 0.001$, '****' = $P < 0.01$, '***' = $P < 0.05$). The y axes are $\log_{10}$ scale. **(A,B)** PCH measured from *Pseudomonas aeruginosa* PA14 single infection and co-infection with *Burkholderia cenocepacia* K56-2, and *Burkholderia multivorans* C5393. **(C,D)** PCH production by *P. aeruginosa* SED43 during single infection and co-infection with *B. cenocepacia* K56-2, and *B. multivorans* C5393. **(D,E,F)** PCH production by *P. aeruginosa* SED20 during single infection and co-infection with *B. cenocepacia* K56-2, and *B. multivorans* C5393.

As shown in Figure 6.25F, there was similarly no significant difference in *P. aeruginosa* SED20 PCH production in the EVPL model (Kruskal-Wallis: χ_2 = 5.21, df = 2, P = 0.07),

although there was a small reduction when co-infected with *B. multivorans* C5393. However, there was a signficant difference in SCFM (ANOVA: $F_{2,5}$ = 141.5, P < 0.01). As shown in Figure 6.25E, there was a significant reduction in *P. aeruginosa* SED20 PCH production when co-infected with *B. cenocepacia* K56-2 compared with single infection (Tukey HSD P < 0.01) and when co-infected with *B. multivorans* C5393 (Tukey HSD P < 0.01). There was also a significant reduction in PCH production when *P. aeruginosa* SED20 was co-infected with *B. multivorans* C5393 compared with *B. cenocepacia* K56-2 co-infection (P = 0.01), as observed for PVD.

6.3 Discussion

Mixed infection of two different species combinations was explored in this chapter: *P. aeruginosa* and *B. cenocepacia*, and *P. aeruginosa* and *B. multivorans*. It has highlighted the importance of using a clinically relevant laboratory model such as the EVPL model to understand multispecies interactions in the CF lung, as well as clinical isolates. The addition of lung tissue to SCFM affected the outcome of co-infection, as did co-infection with *P. aeruginosa* CF clinical isolates compared with PA14. Both Bcc species appeared to better co-exist with the clinical isolates in the EVPL model, particularly *B. multivorans*, indicating that previous chronic adaptations affect interactions in the model. This difference was not observed in SCFM *in vitro*. It is important to have the spatial structure to create the niches in which each species exist, but also to capture the CF lung environment that drives microbial ecological adaptations that influence interactions (Schwab et al., 2014; Perault et al., 2020).

The Bcc strains were introduced following investigation of *P. aeruginosa* PA14 biofilm infection in the EVPL model in earlier chapters, to determine whether it was possible to use the model to study these mixed infections. *B. cenocepacia* K56-2 and *B. multivorans* C5393 survived in the EVPL model over 7 d. Co-infection with *P. aeruginosa* PA14 was also maintained for 3 - 4 d prior to a loss of consistent Bcc recovery. These results demonstrated that the EVPL model is valid for studying this genus and mixed infections. It was found that *P. aeruginosa* virulence factor production may be associated with the Bcc survival during co-infection. A reduction in *P. aeruginosa* CF isolates siderophore production in SCFM correlated with increased Bcc CFU ml^{-1} recovered. It was also shown that when *B. cenocepacia* K56-2 was introduced to a *P. aeruginosa* PA14 biofilm after

2 d in the EVPL model, there was an increase in long chain AHL signal production. This indicated there may have been communication between the two strains and also evidenced the role of infection timing on mixed infection dynamics.

To initially establish mixed infections, the inhibition caused by each strain of the others was investigated; they were grown in the EVPL model and SCFM *in vitro* for 2 d then inhibition assays were performed on LB agar overnight. The *P. aeruginosa* strains were found to inhibit *B. cenocepacia* K56-2 and *B. multivorans* C5393 regardless of the environment they were first grown in. However, the Bcc strains did not inhibit *P. aeruginosa* growth. This was consistent with other studies that have shown during planktonic growth *P. aeruginosa* inhibits *B. cenocepacia* (Bragonzi et al., 2012). It has also been shown that both *P. aeruginosa* and the Bcc have the potential for bacteriocin inhibitory activity in the CF lung. The R-, F-, and S-type pyocins produced by *P. aeruginosa* are involved in the interactions with the Bcc, and can inhibit its growth (Bakkal et al., 2010). Hence, this may have been responsible for the inhibition observed. Future investigation of bacteriocin production would provide more information on potential inhibition. In contrast with these results, *B. cenocepacia* K56-2 and *B. multivorans* C5393 were found to survive during co-infection with *P. aeruginosa* PA14 in the EVPL model and SCFM, for at least 2 d. This indicated that *P. aeruginosa* had less inhibitory activity against the Bcc in these environments than observed following overnight growth on LB agar. The transcriptome analysis in chapter 4 showed that the environmental cues in the EVPL model may have caused *P. aeruginosa* to exhibit chronic-like gene expression, and chapter 3 showed that *P. aeruginosa* PA14 produced low amounts of virulence factors in the EVPL model, which may have facilitated co-existence with the Bcc.

During mixed infection with *P. aeruginosa* PA14 in the EVPL model, there were samples where there was no recovery after 2 d of *B. cenocepacia* K56-2, and after 4 d for *B. multivorans* C5393. This may have been caused by inhibition of the Bcc strain by *P. aeruginosa*, however there are other possible explanations. Although *B. cenocepacia* K56-2 and *B. multivorans* C5393 were able to survive in the EVPL model, there was also a reduction in CFU lung^{-1} over 7 d when grown alone. There was a significant reduction in the bacterial load of *B. multivorans* recovered after 3 d, and the variability in the *B. cenocepacia* bacterial load recovered from the biofilm increased. The Bcc are known to be able to survive intracellularly within neutrophils, macrophages, and human

respiratory epithelial cells (Saldías and Valvano, 2009; Loutet and Valvano, 2010). It has also been suggested that intracellular growth of *B. cenocepacia* in macrophages is a key factor for the worsened disease outcomes observed in CF following infection (Mesureur et al., 2017). It is possible that the EVPL model caused Bcc to enter an intracellular growth lifestyle in pig lung cells, and thus it was no longer recovered from the lung-associated biofilm, accelerated during *P. aeruginosa* co-infection. This would explain why Bcc was recovered at 7 d during co-infection with *P. aeruginosa* in SCFM *in vitro* where there was no tissue, but not the EVPL model.

It should also be considered that the Bcc cells became viable but non-culturable using the current approaches. *B. cepacia* have been shown to enter this state during starvation and become no longer culturable on routine laboratory agars (Lemke and Leff, 2006; Li et al., 2014). *P. aeruginosa* co-infection may have caused increased starvation due to nutrient competition, driving this lifestyle. If this was representative of Bcc adaptation in the CF lung, it may be associated with the relatively low incidence of Bcc in people with CF; it affects ~5% (Leitão et al., 2017). It may indicate that the Bcc is more prevalent than current statistics show, but it becomes non-culturable so is not detected, which is increased when *P. aeruginosa* is present. Microscopy techniques, such as FISH, would provide insight into these hypotheses by visualising the location of Bcc growth and confirming its presence. It would also be of interest to use alveoli in the EVPL model, as performed by Harrison et al. (2014). This would introduce a separate niche in the lower airways for Bcc growth, which may provide insight into its growth lifestyle in different regions of the CF lung and may affect potential interactions with *P. aeruginosa*.

Super-infection of *P. aeruginosa* PA14 biofilms in the EVPL model with *B. cenocepacia* K56-2 and *B. multivorans* C5393 was then performed. It is well known that *P. aeruginosa* is one of the most prevalent pathogens of the CF lung and it increases susceptibility to secondary infections (O'Brien and Fothergill, 2017). Therefore *P. aeruginosa* is typically the first infection, prior to infection with the Bcc (Sajjan et al., 2001). *P. aeruginosa* adapts to the CF lung to form a chronic infection, where virulence is reduced, antibiotic resistance is increased, and a biofilm is formed (Cullen and McClean, 2015; Broder et al., 2016). These changes may affect interactions with the Bcc compared to simultaneous co-infection prior to *P. aeruginosa* lung adaptation. Hence, *B. cenocepacia* K56-2 and *B. multivorans* C5393 were introduced to a *P. aeruginosa* PA14 biofilm associated with

the surface of the EVPL tissue 1 d and 2 d after initial infection. The analysis in chapter 5 demonstrated that by 2 d, *P. aeruginosa* gene expression became reminiscent of chronic infection in contrast with 1 d, including genes involved in biofilm formation and metabolism. Therefore these two time points were selected to identify whether there were differences in Bcc survival when introduced as the *P. aeruginosa* biofilm was establishing (1 d), and when it was likely established (2 d).

Initially, the CFU lung^{-1} recovered at 7 d following each super-infection was determined and compared with co-infection. *B. multivorans* C5393 was recovered from all lung tissue pieces that were super-infected at 1 d and 2 d, alongside *P. aeruginosa* PA14, which was not observed for co-infection. In contrast, there did not appear to be a difference in the *B. cenocepacia* K56-2 bacterial load recovered from super-infection compared to co-infection with PA14. This may demonstrate that *B. multivorans* C5393 was better able to infect the EVPL model when a *P. aeruginosa* biofilm was established, although there was no difference in the two super-infection time points. If this is the case in the CF lung, it may in part explain how *B. multivorans* has become the most prevalent CF Bcc pathogen over *B. cenocepacia* (Kenna et al., 2017). Conversely, it must be considered that the *B. multivorans* strain studied in the EVPL model is a CF clinical isolate, whereas *B. cenocepacia* K56-2 is a laboratory strain. Therefore, the differences in recovery following super-infection of the *P. aeruginosa* PA14 biofilm may have been due to previous adaptations to the CF lung or interactions with *P. aeruginosa*.

Production of the QS AHL signal molecules was also investigated for super-infection and co-infection in the EVPL model. Both *P. aeruginosa* and the Bcc produce AHL signal molecules, and *B. cepacia* is able to respond to *P. aeruginosa* AHL signals (Riedel et al., 2001). As discussed in previous chapters, *P. aeruginosa* possesses two QS systems (*las* and *rhl*) that utilise the AHL signals 3-oxo-C12-HSL and C4-HSL. These systems regulate many infection characteristics including biofilm formation and virulence factor production (Williams and Cámara, 2009). It is believed that all members of the Bcc also use an AHL-dependent QS system, CepIR, which involves N-octanoyl homoserine lactone (C8-HSL) and N-hexanoyl homoserine lactone (C6-HSL) (Gotschlich et al., 2001; Schmid et al., 2012). This system, alongside the diffusible signal factor cis-2-dodecenoic acid (often referred to as BDSF) QS system, has been shown to be essential for Bcc production of proteases and biofilm formation (Schmid et al., 2012).

The concentration of AHL molecules in each EVPL super-infection and co-infection sample was measured and compared with single infection, to determine whether it was affected by the different mixed infections. As in chapter 4, short chain AHLs could not be detected. As this was consistent across multiple experiments it is likely that the bioreporter *E. coli* strain used was unable to detect short chain AHLS in the EVPL samples. This requires future optimisation as there may be interactions with tissue or SCFM components present in each sample, or the time for the assay may need to be increased from the standard protocol. Alternatively, there are other methods for detecting AHLs, such as high-performance liquid chromatography-mass spectrometry (HPLC-MS) approaches that can quantify AHLS (Dal Bello et al., 2021).

The concentration of long chain AHLs was able to be measured. There was a significant increase in the concentration at 7 d in the EVPL model when *P. aeruginosa* PA14 was super-infected with *B. cenocepacia* K56-2 at 2 d, compared with single infection of each strain. This indicated that when *B. cenocepacia* was introduced to an established *P. aeruginosa* biofilm there may have been changes in QS-regulated pathways in one, or both, strains. This was not observed for *B. multivorans*, which was more consistently recovered following super-infection than *B. cenocepacia*. Hence, this may suggest that the increase in long chain AHLs resulted in increased *P. aeruginosa* virulence that inhibited *B. cenocepacia*. Future investigation of virulence factor production of all strains during mixed infection would provide more insight into this potential interaction.

P. aeruginosa clinical CF isolates were then used in co-infection with *B. cenocepacia* K56-2 and *B. multivorans* C5393 in the EVPL model and SCFM, to further explore the implications of *P. aeruginosa* chronic adaptations to the CF lung on mixed infection. For both *B. cenocepacia* and *B. multivorans*, significantly more CFU lung^{-1} were recovered when co-infected with the *P. aeruginosa* clinical isolates compared with *P. aeruginosa* PA14 at 2 d. However at 7 d there were tissue pieces where no Bcc could be recovered from co-infection with any of the *P. aeruginosa* strains. This was not observed in SCFM; there was similar bacterial load recovered of all *P. aeruginosa* and Bcc strains at 2 d and 7 d during co-infection. This may have been associated with the Bcc lifestyle in the EVPL model, as discussed, or *P. aeruginosa* siderophore production. Through use of a *P. aeruginosa* mutant library, it has previously been shown that PVD biosynthesis

is involved in the inhibition of *B. cenocepacia*. The same study also demonstrated that pure PVD was able to inhibit both *B. cenocepacia* and *B. multivorans*, and it was concluded that the production of PVD by *P. aeruginosa* is likely to contribute to its inhibitory action against late-colonizing pathogens in the CF lung (Costello et al., 2014).

There was a significant reduction in PVD production by the *P. aeruginosa* clinical isolates compared with single infection for all SCFM co-infections and *B. multivorans* C5393 co-infection in the EVPL model at 2 d. This reduction was not observed for *B. cenocepacia* K56-2 co-infection with the clinical isolates in the EVPL, or any of the *P. aeruginosa* PA14 co-infections in either environment. The PVD reduction may have led to the increased Bcc survival observed at 7 d in SCFM during co-infection with the clinical *P. aeruginosa* isolates, and for co-infection with *B. multivorans* C5393 in the EVPL model at 7 d. Hence, the lack of recovery of any *B. cenocepacia* K56-2 CFU from co-infected tissue pieces at 7 d may have been caused by no reduction in PVD production by *P. aeruginosa*. A similar pattern was observed for PCH production and *B. cenocepacia* K56-2 recovery. Hence, it was hypothesised that increased Bcc recovery from co-infection with the clinical CF *P. aeruginosa* isolates may have been associated with reduced siderophore production. Other virulence factors should now be studied to determine if there is a similar effect in the EVPL model, and thus indicate whether the reduction in *P. aeruginosa* virulence during chronic adaptation to the CF lung facilitates Bcc super-infection. This could be utilised as a novel target to prevent Bcc infection, which often has fatal outcomes.

To build upon this work in the future, further investigation of these complex interactions in the EVPL model is required. Initially microscopy should be performed to visualise the location of each species in the EVPL model, and to determine whether they form a mixed biofilm or occupy different niches. The preliminary results indicate that *P. aeruginosa* and the Bcc do interact in the EVPL model. Antibiotic treatments could also be introduced to determine how resistance is affected by interactions, and if this can be utilised to combat infections. The production of different virulence factors by both species should also now be measured, as it is likely they have a role in the dynamics of co-infection. More specifically, it was shown that an increase in long chain AHL production was associated with a reduction in Bcc CFU lung^{-1}; when *P. aeruginosa* PA14 was super-infected with *B. cenocepacia* K56-2 at 2 d. As hypothesised above this may have been due to an increase in PA14 virulence driven by the increase in long chain

AHLs. If time had allowed, it would have been of interest to co-infect each Bcc strain with a *P. aeruginosa* mutant for the quorum sensing signal receptor gene *lasR* in the EVPL model. This regulator depends on the long chain AHL 3-oxo-C12-HSL to co-ordinate virulence factor gene expression (Kiratisin et al., 2002). Hence, if there was better Bcc survival with the LasR mutant it would suggest that this an important interaction for their co-existence. It would also explain why co-infection occurs *in vivo* but *P. aeruginosa* often inhibits Bcc *in vitro*, as LasR mutants are a common adaptation during chronic infection of the CF lung (LaFayette et al., 2015).

This work has also shown the importance of optimising infection timelines in the EVPL model for studying multiple species, as super-infection had an effect on the infection characteristics. Therefore, each experiment using the EVPL model for mixed infection should be specifically designed depending on the species and research questions addressed.

6.4   Conclusion

I have performed the preliminary experiments to establish Bcc species *B. cenocepacia* and *B. multivorans* in the EVPL model, and co-infection with *P. aeruginosa*. I have shown that the Bcc and *P. aeruginosa* can co-exist in the model for at least 2 d, and there appears to be an interaction involving QS and virulence factor production. My results also indicate the study of clinical CF isolates of both *P. aeruginosa* and the Bcc may be more appropriate for investigating these interactions and better understanding the complex dynamics in the CF lung. This chapter has build upon the work in the previous chapters, investigating *P. aeruginosa* biofilm infection in the EVPL model, to incorporate another factor of CF lung infection: multispecies interactions. The results have indicated key research questions that should now be addressed using the EVPL model to better understand these mixed species infections to potentially prevent or treat them:

1. Do *P. aeruginosa* and the Bcc form a mixed biofilm?

2. Does the Bcc grow intracellularly or become non-culturable during infection in the EVPL model?

3. What is the role of virulence factors in *P. aeruginosa* and Bcc interactions during mixed infection?

Chapter 7

Discussion

The research in this thesis aimed to establish the EVPL model, composed of pig lung bronchiolar tissue and SCFM, for *P. aeruginosa* biofilm infection of the CF lung. Harrison and Diggle (2016) first published the use of bronchiolar tissue in the EVPL model in 2016, and showed that *P. aeruginosa* formed a biofilm associated with the tissue. This thesis has built upon, and extended, their findings by investigating the phenotypic and transcriptomic characteristics of *P. aeruginosa* biofilm infection in the EVPL model. Preliminary results from mixed infection of *P. aeruginosa* with species of the Bcc have also been reported. The *P. aeruginosa* biofilm associated with the EVPL tissue was shown to be comparable to chronic infection *in vivo*, and key infection traits not observed in current laboratory models were found.

PA14 was the *P. aeruginosa* strain used for all of the work in this thesis, with the exception of one experiment in chapter 6, as it is a well studied laboratory strain. This was important as prior to this project, knowledge of how *P. aeruginosa* behaved in the EVPL model was limited. Therefore, to determine the effects of using the model and its validity as a platform to study CF lung infections, it was important to ensure that any findings were not caused by unique characteristics of individual CF isolates. There was also a reliable *P. aeruginosa* PA14 genome assembly and annotation available for transcriptomic analyses. *P. aeruginosa* PA14 was used over the other most commonly used laboratory strain, *P. aeruginosa* PAO1, as there was access to a PA14 transposon mutant library to investigate the role of different genes in the phenotypes observed in the model. Following on from this thesis, future experiments using the EVPL model should include CF *P. aeruginosa* clinical isolates that have adapted to the CF lung environment as they are likely to be more representative of *in vivo* infection. This

can only be performed now the EVPL model is better understood from using a well characterised strain.

Initially *P. aeruginosa* phenotypes in the EVPL model were investigated. As shown in chapter 3, there was a low level of production of key virulence factors by 48 h infection. At 7 d, the WT *P. aeruginosa* PA14 biofilm associated with the lung tissue had an architecture comparable to patient biopsies from the lungs of people with CF and a chronic *P. aeruginosa* infection (Figure 3.14 and Figure 3.15). The EVPL *P. aeruginosa* biofilm population was also found to be resistant to meropenem. A reduction in virulence factor production, biofilm formation, and increased antibiotic resistance are all key characteristics of chronic *P. aeruginosa* infection in the CF lung (Winstanley et al., 2016). Thus, these findings indicated that the EVPL model was driving *P. aeruginosa* into a chronic-like state of infection. Chronic *P. aeruginosa* infections have traditionally been difficult to replicate in the laboratory, and one of the main focuses in the field of CF lung infection research is the development of more clinically representative models (Cornforth et al., 2020; O'Toole et al., 2021). Hence, these results suggested that the EVPL model may be able to address the current gap in research.

This was further supported by the results described in chapter 4. *P. aeruginosa* PA14 RNA-seq analysis was performed for the EVPL-associated biofilm population and surrounding SCFM, compared with *in vitro* SCFM, at 24 h and 48 h. There were a number of key differences in *P. aeruginosa* gene expression found in the EVPL model compared with *in vitro* SCFM growth, particularly in the lung-associated biofilm. These included differential expression of genes encoding efflux pumps and individual AMR genes. There was also significant differential expression of QS genes, which is an integral part of *in vivo* infection not accurately replicated by the current *in vitro* models. In particular, most of the genes in a conserved set of *las*-regulated genes were significantly underexpressed in the lung-associated biofilm compared with *in vitro* SCFM at 48 h, similarly observed for comparison of gene expression in CF sputum with *in vitro* models (Cornforth et al., 2018). This indicated that *P. aeruginosa* expression of QS genes in the EVPL model may be more representative of human infection than SCFM, which is frequently used in research; the adapted SCFM2 has been identified as one of the optimal models for *P. aeruginosa* CF lung infection (Cornforth et al., 2020). This further highlighted the potential of the EVPL model to recapitulate the chronic infection characteristics missing

from the current models, which has hindered research progress and the development of new treatments.

Cornforth et al. (2018) showed that overall, expression of QS genes in *in vitro P. aeruginosa* biofilms from a range of conditions was distinct from CF sputum. QS genes were expressed at higher levels *in vitro* than in CF, as observed in chapter 4 for *P. aeruginosa* PA14 grown in SCFM compared with the EVPL biofilm. QS may not be as important during chronic biofilm infection as it is during initial infection in the CF lung; it has been suggested that QS may actually negatively affect fitness in the long term, due to the associated metabolic cost (Heurlier et al., 2006). There is an accumulation of QS-associated mutants, predominently of the key QS regulatory gene *lasR* over time in CF (Winstanley and Fothergill, 2009). LasR mutants are present in over a third of people with CF with a chronic *P. aeruginosa* infection. They have been linked to accelerated lung damage and subsequent functional decline, caused by amplification of the host inflammatory response (LaFayette et al., 2015). This is in contrast with the attenuation observed for *lasR* mutants during acute infection (LaFayette et al., 2015); a rat model of acute pneumonia was used to show that a *P. aeruginosa* PAO1 *lasR* deletion mutant was avirulent compared with the WT (Lesprit et al., 2003). Thus the reduction in QS in the CF lung is likely a characteristic of chronic infection in this environment.

The incidence of *lasR* mutants has also been associated with the reduction in virulence factor production seen following initial infection. LasR regulates expression of a number of virulence genes including those that encode exoproteases such as LasA and LasB (Hennemann and Nguyen, 2021), driving a loss of production when *lasR* mutants arise in chronic infection. This is consistent with the low amounts of proteases measured in the EVPL model in chapter 3, supported by earlier work using alveolar tissue in the EVPL model. This study showed reduced *P. aeruginosa* protease production, but also investigated *lasR* mutants in the model to show that this mutation is likely an adaptation to the CF lung (Harrison et al., 2014). Thus, reduced QS gene expression and the high incidence of mutations is likely a key characteristic of *P. aeruginosa* adaptation to the CF lung to form chronic infections. It has been shown that *lasR* mutants have a growth advantage in certain nutrient availability conditions, such as the CF lung. D'Argenio et al. (2007) showed that *P. aeruginosa lasR* mutants from the early stages of CF chronic infection were able to utilise carbon sources, including amino acids, to confer a growth

advantage associated with upregulation of catabolic pathways. This may explain the increased selection for these mutations during chronic infection.

As shown by the work in this thesis, the EVPL model is able to recaptitulate key characteristics of *P. aeruginosa* chronic CF lung infection that have not been observed in other models, such as the mature biofilm architecture. The transcriptome analysis in chapter 4 revealed that the key difference in *P. aeruginosa* expression between the laboratory media SCFM and the EVPL biofilm was overexpression of QS genes in SCFM. This has been highlighted as one of the main *P. aeruginosa* systems that is overexpressed in *in vitro* biofilms compared with human infection (Cornforth et al., 2018). This indicates that the chronic-like *P. aeruginosa* biofilm infection in the EVPL model may be better replicating characteristics of *in vivo* infection as it is able to more accurately capture QS gene expression, associated with a reduction in virulence factor production. Not only does this show that the EVPL model is a good model for these infections, it has also highlights the area of focus for optimising other laboratory models. By more accurately capturing *P. aeruginosa* QS expression in chronic infection, the EVPL model has been able to recapitulate a chronic-like infection not seen in other models. Thus, optimisation of other models should focus on *P. aeruginosa* QS gene expression that replicates human infection. It also shows that the EVPL may be the optimal model for investigating the clinical implications of QS, and to develop and test therapies that target QS, as it appears to more accurately recapitulate these systems.

The work in chapters 3 and 4 demonstrated that the EVPL model was valid for studying *P. aeruginosa* biofilm infection in the CF lung, and may potentially be better than other laboratory models. Following this, the work in chapters 5 and 6 was more hypothesis based to explore *P. aeruginosa* growth in the EVPL model, and better understand chronic CF lung infection. In chapter 5, *P. aeruginosa* PA14 gene expression over time at 24 h, 48 h, and 7 d in the EVPL biofilm was investigated. The transcriptome analysis performed in this chapter, and chapter 4, was followed by phenotypic validation. This included measurement of production of QS signalling molecules and MIC tests. Traditionally, RNA-seq has been validated using quantitative real time PCR (qPCR). However, as next-generation sequencing techniques have become established there has been much debate as to whether this is necessary. As outlined by Coenye (2021), this is based on the previous requirement to validate microarray data, and RNA-seq data is more

reliable. Provided that the experimental design includes enough repeats, and the research question is not based around the expression of a small number of genes, then qPCR is widely no longer considered a necessary validation step. As the RNA-seq analyses performed in this thesis investigated the expression of all *P. aeruginosa* genes and found a wide range of differences, it was considered unnecessary to perform qPCR validation. The use of phenotypic validations instead not only showed that the differential expression found in the RNA-seq data was true, but also that it conferred a change in phenotype. This included underexpression of *arnA* in the lung-associated biofilm from 24 h to 48 h, which is associated with CAMP resistance as discussed in chapter 5. This was consistent with the reduced MIC of the CAMP polymyxin B for *P. aeruginosa* biofilm cells from the EVPL model from 24 h to 48 h. Hence the RNA-seq analysis performed was validated, but it also showed that the differential expression conferred phenotypic changes in the EVPL model, which is not possible with qPCR.

As well as differential expression of AMR genes, there were changes in expression of genes associated with metabolism and biofilm formation in the EVPL biofilm found in chapter 5. The results showed that 48 h was when a chronic-like *P. aeruginosa* infection becomes established in the model. Therefore, future research of the *P. aeruginosa* EVPL biofilm should be performed at 48 h to best represent chronic CF lung infection. The results in this chapter also highlighted aspects of the model that may need to be optimised in the future for its use as a more long term model. These included determination of oxygen avilability to best capture the anoxic regions of the CF lung infections (Worlitzsch et al., 2002; Filkins and O'Toole, 2015), and nutrient availability. This will be key to using the model to perform long term evolution experiments.

P. aeruginosa chronic infection involves adaptation to the CF lung conditions over time, as discussed throughout this thesis. The reduction of virulence factor production, increased antibiotic resistance, and biofilm formation discussed thus far are not the only adaptations to the CF lung. There has also been a high incidence of phenotypic diversity observed in chronic *P. aeruginosa* biofilm populations that is, in part, caused by the spatial structure of the CF lung (Winstanley et al., 2016). If the EVPL model is developed in the future to be viable for longer periods of time than the 7 d studied, it may be possible to maintain a *P. aeruginosa* biofilm population long term. Whole genome sequencing of these populations would show whether the EVPL model can

drive the incidence of *P. aeruginosa* sub-populations seen *in vivo* caused by mutations. This may facilitate better understanding of how to prevent these changes, particularly those that increase AMR. It may also indicate what drives the changes in infection over time that lead to periods of acute exacerbation. This is when worsened disease symtoms, increased mortality, and increased *P. aeruginosa* virulence is observed (Langan et al., 2015). Exacerbations are not associated with newly infecting strains, but with the adaptation of the current infection population (Aaron et al., 2003). If the EVPL model was adapted for long term study, it may be possible to model an acute exacerbation and thus potentially determine how to prevent them. This could reduce the associated mortalities and improve quality of life for those with CF.

There are a number of considerations for developing the model for long term evolution experiments, such as the viability of tissue. Determination of how long the lung tissue can be used for is essential, and optimisation of how to transfer the *P. aeruginosa* biofilm from one tissue piece to another. The effect of using tissue pieces from different pig lungs must also be considered. It is not feasible to store pig lung tissue over time and maintain the structure, therefore biofilm transfer would use tissue pieces from fresh lungs. Another consideration is the supplementation of SCFM, the results in chapter 5 indicated that nutrient availability is likely to become an issue following 7 d infection. A method for continuous flow of SCFM incorporated in the EVPL model would likely be required for long term evolution experiments.

Infections of the CF lung are not only caused by *P. aeruginosa*, it is now established that the CF lung is complex and polymicrobial (Filkins and O'Toole, 2015). Increasing the length of time *P. aeruginosa* infection, and potentially a range of different bacterial species, can be maintained in the EVPL model may allow for investigation of the effect of invading species. This includes introducing a pathogen to a microbiota community or adding a new species to an established infection. The work in chapter 6 began to look at this, introducing *B. cenocepacia* and *B. multivorans* to *P. aeruginosa* in the EVPL model after 48 h. This was shown to result in an increase in long-chain AHL molecule production at 7 d, when *B. cenocepacia* K56-2 was introduced at 48 h. This was not observed for co-infection, which indicated that there is an effect of introducing species at different times. This may also better reflect the timeline of infection that occurs *in vivo* (Figure 1.1).

The work on mixed infection of *P. aeruginosa* and the Bcc in chapter 6 also showed that the EVPL model can be used to study co-infections. This is one of the main targets for current model development for CF lung infections (O'Toole et al., 2021). Hence, the EVPL model has potential to be used in the future to study mixed infections, and thus provide information for the development of treatments. More specifically, the preliminary data in chapter 6 showed that future work on mixed *P. aeruginosa* and Bcc infections in the EVPL model would benefit from using clinical CF isolates that are adapted to the CF lung to best understand, and establish, co-infections. It also raised key research questions for further work, as outlined in the chapter discussion. In particular, visualisation of the mixed infection is an important next step that would have been performed if there had been more time. Preliminary work has begun using fluorescence *in situ* hybridisation (FISH) and confocal microscopy to look at *P. aeruginosa* PA14 and *B. multivorans* C5393 co-infection in the EVPL model (Figure 7.1). Further in-depth investigation is required to determine whether it is likely the two genera are interacting in a close proximity, potentially as a mixed biofilm, and to determine the lifestyle of Bcc in the model. As discussed in chapter 6, the Bcc has the ability to survive intracellulary in the CF lung. Microscopy focusing on Bcc interaction with the lung tissue would show whether this occurs in the model and if it is affected by co-infection with *P. aeruginosa*. This would also show more possibilities for the EVPL model to study different infection lifestyles.
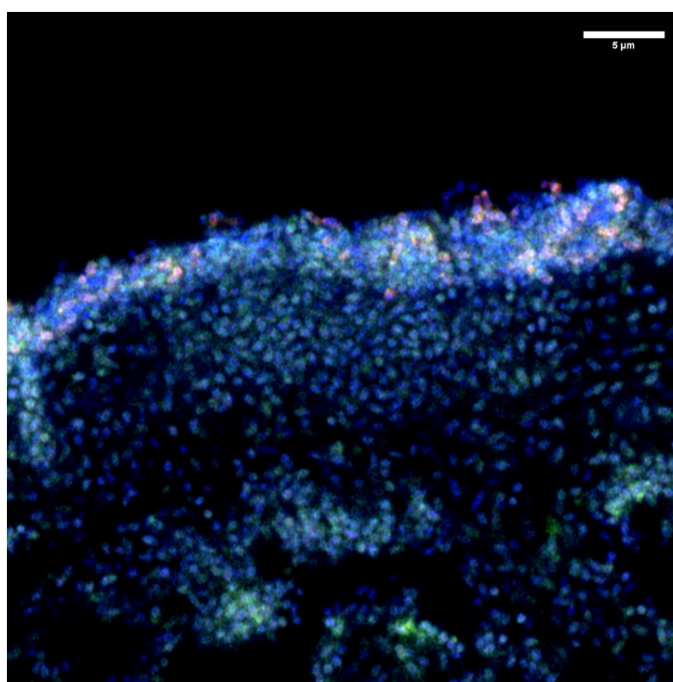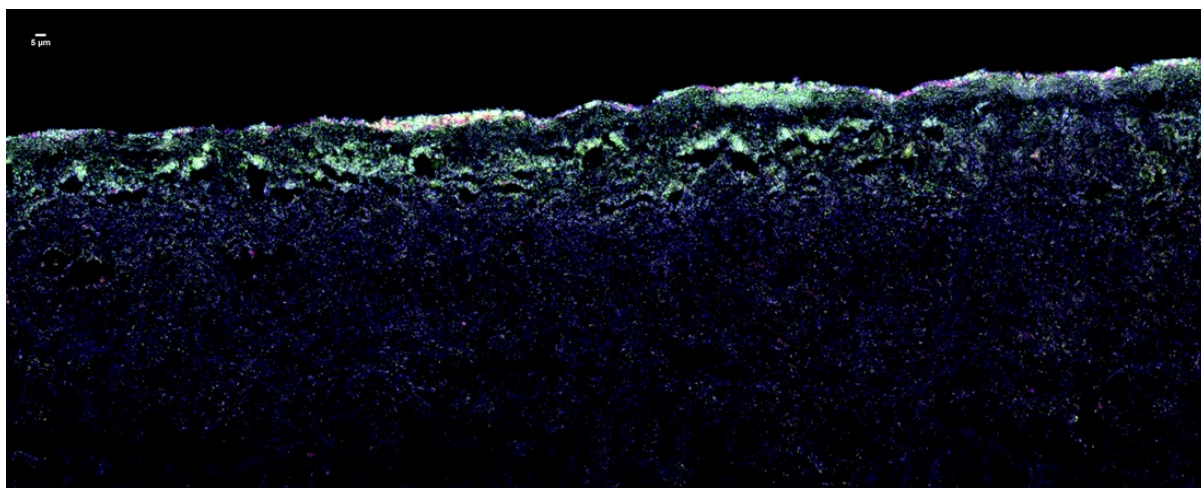
Figure 7.1: ***Pseudomonas aeruginosa* PA14 (green) and *Burkholderia multivorans* C5393 (red) in the *ex vivo* pig lung (EVPL) model at 48 h.** Fluorescence *in situ* hybridisation was performed and each strain is stained a different colour, as described. The DNA was stained blue. Images were taken using Zeiss LSM 880 confocal laser scanning microscope and x100 magnification. The top image was stitched in FIJI with the Grid/Collection Stitching Plugin (Preibisch et al., 2009; Schindelin et al., 2012). The bottom image was additionally images using the AiryScan module in Superresolution mode. The scale bars are shown. Following dissection and infection, the sample preparation, staining, imaging and image processing was performed by Dr. John MJ Lapage.

Additionally, the work on *P. aeruginosa* and Bcc mixed infections showed that *B. cenocepacia* and *B. multivorans* are able to grow and survive in the EVPL model. This demonstrated that the model is suitable for studying Bcc species as well as *P. aeruginosa*. Bcc infections in the CF lung, particularly *B. cenocepacia*, are associated with poor clinical outcomes following lung transplantation (Yeung et al., 2020). There has been some debate as to whether lung transplants should be an option for people with CF who are

infected with *B. cenocepacia* as it is a considerable risk factor for transplantation (Olland et al., 2011). To better understand these infections to treat them, or ideally prevent them, would not only improve transplant outcomes but also prevent the highly fatal, resultant cepacia syndrome (Sousa et al., 2010). Thus, the indication that the EVPL model is a clinically relevant platform to study these infections may facilitate this research.

The Bcc and *P. aeruginosa* are pathogens of the CF lung; it would also be of interest to study non-pathogenic microbial species in the EVPL model. This could include co-infection with pathogens such as *P. aeruginosa*, which has been extensively studied in this thesis, to investigate any interactions. It would also be interesting to establish a microbial community in the EVPL model to replicate the lung microbiota then introduce *P. aeruginosa* and other pathogens, to determine the effect this has on pathogenesis. Bacteria are also not the only microbes present in the CF lung. Viruses, including bacteriophages, and fungi have traditionally been overlooked, however it has been hypothesised that they may have a key role in the pathogenesis of CF lung disease (Jean-Pierre et al., 2021). Lung tissue from the EVPL model has previously been incorporated in a continuous flow model to grow *P. aeruginosa* and *S. aureus* co-infections with the fungus *Candida albicans* (O'Brien et al., 2021). Therefore, there is potential to broaden the research use of the EVPL model for different CF lung infections.

Overall this thesis has demonstrated that the EVPL model replicates key phenotypes and gene expression patterns of *P. aeruginosa* chronic infection in the CF lung, not observed in other laboratory models. It can now be used to study a number of key aspects of CF lung disease, including mixed species infections involving *P. aeruginosa*. There are also other aspects of *P. aeruginosa* infection to be explored such as metabolomic analysis to reveal more about growth in the EVPL model. This project has addressed the current research gap for a clinically relevant laboratory model for *P. aeruginosa* chronic biofilm infection. Despite this being an extensive field of research, further understanding is now limited by the model systems available, which the EVPL model has shown the potential to solve. As the model uses pig lung tissue that is a waste product from the meat industry there are no ethical concerns. Therefore, as well being more clinically relevant than other models it also reduces the need for live animal models. Additionally, validation of the EVPL model has importance for clinical work.

The EVPL model has potential as a diagnostic platform and to be used to develop novel treatments. *P. aeruginosa* has been shown to be highly resistant to antibiotics in the model in this thesis, and in the work by Hassan et al. (2020) and Sweeney et al. (2020b). Therefore, it may be used to more accurately determine the antibiotic susceptibility profile of *P. aeruginosa* isolates from patient samples. This could improve treatment outcomes by more reliably determining whether an antibiotic will be effective *in vivo*, thus reducing the cost associated with prescribing ineffective antibiotics. This would also improve quality of life of individuals with CF by hopefully limiting the rigourous antibiotic treatments to only those that will be effective. The lungs used in this model are often sourced for free, or at a low cost, from a local butcher, which makes it financially viable as a diagnostic platform. The EVPL model could also be used to develop, and test, new antimicrobials and potential prevention methods. In fact, during this project we have worked in collaboration with Perfectus Biomed group , who have gained UKAS accreditation (The United Kingdom Accreditation Service) to ISO 17025 for the EVPL model as a biofilm testing method for new treatments. I trained their staff members to use the model, and it has since been used to test candidate therapeutics developed by their clients for CF lung infections. Thus, the work in this thesis has contributed to better validation and understanding of the EVPL model for the CF lung, specifically *P. aeruginosa* biofilm infections, that addresses key research questions but also has clinical implications to improve outcomes for people with CF.

Bibliography

Aali, M., Caldwell, A., House, K., Zhou, J., Chappe, V., and Lehmann, C. (2017). Iron chelation as novel treatment for lung inflammation in cystic fibrosis. *Medical Hypotheses*, 104:86–88.

Aaron, S. D., Ramotar, K., Ferris, W., Vandemheen, K., Saginur, R., Tullis, E., Haase, D., Kottachchi, D., St. Denis, M., and Chan, F. (2003). Adult Cystic Fibrosis Exacerbations and New Strains of Pseudomonas aeruginosa. *https://doi.org/10.1164/rccm.200309-1306OC*, 169(7):811–815.

Adalsteinsson, D. and Schultz, P. (2020). The DataGraph Manual. *https://www.visualdatatools.com/DataGraph/*, (Accessed 27 January 2022).

Adam, D., Roux-Delrieu, J., Luczka, E., Bonnomet, A., Lesage, J., Mérol, J.-C., Polette, M., Abély, M., and Coraux, C. (2015). Cystic fibrosis airway epithelium remodelling: involvement of inflammation. *The Journal of Pathology*, 235(3):408–419.

Aendekerk, S., Diggle, S. P., Song, Z., Høiby, N., Cornelis, P., Williams, P., and Cámara, M. (2005). The MexGHI-OpmD multidrug efflux pump controls growth, antibiotic susceptibility and virulence in Pseudomonas aeruginosa via 4-quinolone-dependent cell-to-cell communication. *Microbiology*, 151(4):1113–1125.

Alcock, B. P., Raphenya, A. R., Lau, T. T., Tsang, K. K., Bouchard, M., Edalatmand, A., Huynh, W., Nguyen, A. L. V., Cheng, A. A., Liu, S., Min, S. Y., Miroshnichenko, A., Tran, H. K., Werfalli, R. E., Nasir, J. A., Oloni, M., Speicher, D. J., Florescu, A., Singh, B., Faltyn, M., Hernandez-Koutoucheva, A., Sharma, A. N., Bordeleau, E., Pawlowski, A. C., Zubyk, H. L., Dooley, D., Griffiths, E., Maguire, F., Winsor, G. L., Beiko, R. G., Brinkman, F. S., Hsiao, W. W., Domselaar, G. V., and McArthur, A. G. (2020). CARD 2020: Antibiotic resistome surveillance with the comprehensive antibiotic resistance database. *Nucleic Acids Research*, 48(D1):D517–D525.

Alexa, A. and Rahnenfuhrer, J. (2019). topGO: Enrichment Analysis for Gene Ontology. *https://bioconductor.org/packages/release/bioc/html/topGO.html*, (Accessed 12 May 2021).

Allegretta, G., Maurer, C. K., Eberhard, J., Maura, D., Hartmann, R. W., Rahme, L., and Empting, M. (2017). In-depth Profiling of MvfR-Regulated Small Molecules in Pseudomonas aeruginosa after Quorum Sensing Inhibitor Treatment. *Frontiers in Microbiology*, 8(MAY).

Almblad, H., Rybtke, M., Hendiani, S., Bo Andersen, J., Givskov, M., and Tolker-Nielsen, T. (2019). High levels of cAMP inhibit Pseudomonas aeruginosa biofilm formation through reduction of the c-di-GMP content. *Microbiology*, 165(3).

Alvarez-Ortega, C. and Harwood, C. S. (2007). Responses of Pseudomonas aeruginosa to low oxygen indicate that growth in the cystic fibrosis lung is by aerobic respiration. *Molecular microbiology*, 65(1):153.

Andrews, S. (2018). FastQC: a quality control tool for high throughput sequence data. *https://www.bioinformatics.babraham.ac.uk/projects/fastqc/*, (Accessed 12 May 2021).

Bains, M., Fernández, L., and Hancock, R. E. (2012). Phosphate starvation promotes swarming motility and cytotoxicity of Pseudomonas aeruginosa. *Applied and Environmental Microbiology*, 78(18):6762–6768.

Bakkal, S., Robinson, S. M., Ordonez, C. L., Waltz, D. A., and Riley, M. A. (2010). Role of bacteriocins in mediating interactions of bacterial isolates taken from cystic fibrosis patients. *Microbiology*, 156(Pt 7):2058.

Baltimore, R. S., Christie, C. D., and Walker Smith, G. J. (1989). Immunohistopathologic localization of Pseudomonas aeruginosa in lungs from patients with cystic fibrosis. Implications for the pathogenesis of progressive lung deterioration. *American Review of Respiratory Disease*, 140(6):1650–1661.

Barraza, J. P. and Whiteley, M. (2021). A pseudomonas aeruginosa antimicrobial affects the biogeography but not fitness of staphylococcus aureus during coculture. *mBio*, 12(2).

Bayes, H. K., Ritchie, N., Irvine, S., and Evans, T. J. (2016). A murine model of early Pseudomonas aeruginosa lung disease with transition to chronic infection. *Scientific Reports*, 6(1):35838.

Benahmed, M. A., Elbayed, K., Daubeuf, F., Santelmo, N., Frossard, N., and Namer, I. J. (2014). NMR HRMAS spectroscopy of lung biopsy samples: Comparison study between human, pig, rat, and mouse metabolomics. *Magnetic Resonance in Medicine*, 71(1):35–43.

Berube, B. J., Rangel, S. M., and Hauser, A. R. (2016). Pseudomonas aeruginosa: breaking down barriers. *Current Genetics*, 62(1):109–113.

Bhagirath, A. Y., Li, Y., Somayajula, D., Dadashi, M., Badr, S., and Duan, K. (2016). Cystic fibrosis lung environment and Pseudomonas aeruginosa infection. *BMC Pulmonary Medicine*, 16(1):1–22.

Bjarnsholt, T., Østrup Jensen, P., Fiandaca, M. J., Pedersen, J., Rønne Hansen, C., Bøgelund Andersen, C., Pressler, T., Givskov, M., and Høiby, N. (2009). Pseudomonas aeruginosa Biofilms in the Respiratory Tract of Cystic Fibrosis Patients. *Pediatric Pulmonology*, 44:547–558.

Bolger, A. M., Lohse, M., and Usadel, B. (2014). Trimmomatic: A flexible trimmer for Illumina sequence data. *Bioinformatics*, 30(15):2114–2120.

Bonfield, T., Panuska, J., Konstan, M., Hilliard, K., Hilliard, J., Ghnaim, H., and Berger, M. (1995). Inflammatory cytokines in cystic fibrosis lungs. *American journal of respiratory and critical care medicine*, 152(6 Pt 1):2111–2118.

Bottery, M. J., Matthews, J. L., Wood, A. J., Johansen, H. K., Pitchford, J. W., and Friman, V. P. (2021). Inter-species interactions alter antibiotic efficacy in bacterial communities. *The ISME Journal 2021*, pages 1–10.

Boucher, R. C. (2007). Airway Surface Dehydration in Cystic Fibrosis: Pathogenesis and Therapy. *The Annual Review of Medicine*, 58:157–170.

Bouillet, S., Ba, M., Houot, L., Iobbi-Nivol, C., and Bordi, C. (2019). Connected partner-switches control the life style of Pseudomonas aeruginosa through RpoS regulation. *Scientific Reports*, 9(1):6496.

Bragonzi, A., Farulla, I., Paroni, M., Twomey, K. B., Pirone, L., Lorè, N. I., Bianconi, I., Dalmastri, C., Ryan, R. P., and Bevivino, A. (2012). Modelling Co-Infection of the Cystic Fibrosis Lung by Pseudomonas aeruginosa and Burkholderia cenocepacia Reveals Influences on Biofilm Formation and Host Response. *PLoS ONE*, 7(12):e52330.

Bragonzi, A., Horati, H., Kerrigan, L., Lorè, N. I., Scholte, B. J., and Weldon, S. (2018). Inflammation and host-pathogen interaction: Cause and consequence in cystic fibrosis lung disease. *Journal of Cystic Fibrosis*, 17(2):S40–S45.

Bragonzi, A., Paroni, M., Nonis, A., Cramer, N., Montanari, S., Rejman, J., Di Serio, C., Döring, G., and Tümmler, B. (2009). Pseudomonas aeruginosa Microevolution during Cystic Fibrosis Lung Infection Establishes Clones with Adapted Virulence. *American Journal of Respiratory and Critical Care Medicine*, 180(2):138–145.

Broder, U. N., Jaeger, T., and Jenal, U. (2016). LadS is a calcium-responsive kinase that induces acute-to-chronic virulence switch in Pseudomonas aeruginosa. *Nature Microbiology*, 2(1):1–11.

Burden, N., Chapman, K., Sewell, F., and Robinson, V. (2015). Pioneering Better Science through the 3Rs: An Introduction to the National Centre for the Replacement, Refinement, and Reduction of Animals in Research (NC3Rs). *Journal of the American Association for Laboratory Animal Science*, 54(2):198–208.

Buxton, J. (2021). National life tables - life expectancy in the UK: 2018 to 2020. *https://www.ons.gov.uk*, (Accessed 10 January 2022).

Charman, S., Connon, R., Cosgriff, R., Lee, A., Carr, S., Ainsley, C., Gunn, E., and Earlam, K. (2018). UK Cystic Fibrosis Registry Annual Data Report 2017. Technical report, Cystic Fibrosis Trust.

Chávez-Jacobo, V. M., Hernández-Ramírez, K. C., Romo-Rodríguez, P., Pérez-Gallardo, R. V., Campos-García, J., Félix Gutiérrez-Corona, J., García-Merinos, J. P., Meza-Carmen, V., Silva-Sánchez, J., and Ramírez-Díaz, M. I. (2018). CrpP is a novel ciprofloxacin-modifying enzyme encoded by the pseudomonas aeruginosa pUM505 plasmid. *Antimicrobial Agents and Chemotherapy*, 62(6).

Chen, H. (2021). VennDiagram: Generate High-Resolution Venn and Euler Plots. R package version 1.7.0. *https://CRAN.R-project.org/package=VennDiagram*, (Accessed 12 June 2020).

Cheng, P. W., Boat, T. F., Cranfill, K., Yankaskas, J. R., and Boucher, R. C. (1989). Increased sulfation of glycoconjugates by cultured nasal epithelial cells from patients with cystic fibrosis. *The Journal of Clinical Investigation*, 84(1):68–72.

Chevaleyre, C., Riou, M., Bréa, D., Vandebrouck, C., Barc, C., Pezant, J., Melo, S., Olivier, M., Delaunay, R., Boulesteix, O., Berthon, P., Rossignol, C., Gaillard, J. B., Becq, F., Gauthier, F., Si-Tahar, M., Meurens, F., Berri, M., Caballero-Posadas, I., and Attucci, S. (2016). The Pig: A Relevant Model for Evaluating the Neutrophil Serine Protease Activities during Acute Pseudomonas aeruginosa Lung Infection. *PLOS ONE*, 11(12):e0168577.

Chevalier, S., Bouffartigues, E., Bodilis, J., Maillot, O., Lesouhaitier, O., Feuilloley, M. G., Orange, N., Dufour, A., and Cornelis, P. (2017). Structure, function and regulation of Pseudomonas aeruginosa porins. *FEMS Microbiology Reviews*, 41(5):698–722.

Chuanchuen, R., Narasaki, C. T., and Schweizer, H. P. (2002). The MexJK efflux pump of Pseudomonas aeruginosa requires OprM for antibiotic efflux but not for efflux of triclosan. *Journal of Bacteriology*, 184(18):5036–5044.

Chugani, S., Kim, B. S., Phattarasukol, S., Brittnacher, M. J., Choi, S. H., Harwood, C. S., and Greenberg, E. P. (2012). Strain-dependent diversity in the Pseudomonas aeruginosa quorum-sensing regulon. *Proceedings of the National Academy of Sciences of the United States of America*, 109(41):E2823–E2831.

Clunes, M. T. and Boucher, R. C. (2007). Cystic Fibrosis: The Mechanisms of Pathogenesis of an Inherited Lung Disorder. *Drug discovery today. Disease mechanisms*, 4(2):63.

Coenye, T. (2021). Do results obtained with RNA-sequencing require independent verification? *Biofilm*, 3:100043.

Colvin, K. M., Gordon, V. D., Murakami, K., Borlee, B. R., Wozniak, D. J., Wong, G. C. L., and Parsek, M. R. (2011). The Pel Polysaccharide Can Serve a Structural and Protective Role in the Biofilm Matrix of Pseudomonas aeruginosa. *PLoS Pathogens*, 7(1):e1001264.

Conibear, T. C., Collins, S. L., and Webb, J. S. (2009). Role of Mutation in Pseudomonas aeruginosa Biofilm Development. *PLOS ONE*, 4(7):e6289.

Cornelis, P. and Dingemans, J. (2013). Pseudomonas aeruginosa adapts its iron uptake

strategies in function of the type of infections. *Frontiers in Cellular and Infection Microbiology*, 3.

Cornforth, D. M., Dees, J. L., Ibberson, C. B., Huse, H. K., Mathiesen, I. H., Kirketerp-Møller, K., Wolcott, R. D., Rumbaugh, K. P., Bjarnsholt, T., and Whiteley, M. (2018). Pseudomonas aeruginosa Transcriptome during Human Infection. *Proceedings of the National Academy of Sciences of the United States of America*, 115(22):E5125–E5134.

Cornforth, D. M., Diggle, F. L., Melvin, J. A., Bomberger, J. M., and Whiteley, M. (2020). Quantitative framework for model evaluation in microbiology research using Pseudomonas aeruginosa and cystic fibrosis infection as a test case. *mBio*, 11(1).

Costaglioli, P., Barthe, C., Claverol, S., Brözel, V. S., Perrot, M., Crouzet, M., Bonneu, M., Garbay, B., and Vilain, S. (2012). Evidence for the involvement of the anthranilate degradation pathway in Pseudomonas aeruginosa biofilm formation. *MicrobiologyOpen*, 1(3):326.

Costello, A., Reen, F. J., O'Gara, F., Callaghan, M., and McClean, S. (2014). Inhibition of co-colonizing cystic fibrosis-associated pathogens by Pseudomonas aeruginosa and Burkholderia multivorans. *Microbiology (United Kingdom)*, 160(PART 7):1474–1487.

Cullen, L. and McClean, S. (2015). Bacterial Adaptation during Chronic Respiratory Infections. *Pathogens 2015, Vol. 4, Pages 66-89*, 4(1):66–89.

Cuthbertson, L., Walker, A. W., Oliver, A. E., Rogers, G. B., Rivett, D. W., Hampton, T. H., Ashare, A., Elborn, J. S., De Soyza, A., Carroll, M. P., Hoffman, L. R., Lanyon, C., Moskowitz, S. M., O'Toole, G. A., Parkhill, J., Planet, P. J., Teneback, C. C., Tunney, M. M., Zuckerman, J. B., Bruce, K. D., and Van Der Gast, C. J. (2020). Lung function and microbiota diversity in cystic fibrosis. *Microbiome*, 8(1):1–13.

Cutting, G. R. (2015). Cystic fibrosis genetics: from molecular understanding to clinical application. *Nature Reviews Genetics*, 16:45–56.

Cypel, M., Yeung, J. C., Liu, M., Anraku, M., Chen, F., Karolak, W., Sato, M., Laratta, J., Azad, S., Madonik, M., Chow, C.-W., Chaparro, C., Hutcheon, M., Singer, L. G., Slutsky, A. S., Yasufuku, K., de Perrot, M., Pierre, A. F., Waddell, T. K., and Keshavjee, S. (2011). Normothermic Ex Vivo Lung Perfusion in Clinical Lung Transplantation. *The New England journal of medicine*, 364(15):1431–1440.

Dal Bello, F., Zorzi, M., Aigotti, R., Medica, D., Fanelli, V., Cantaluppi, V., Amante, E., Orlandi, V. T., and Medana, C. (2021). Targeted and untargeted quantification of quorum sensing signalling molecules in bacterial cultures and biological samples via HPLC-TQ MS techniques. *Analytical and Bioanalytical Chemistry*, 413(3):853–864.

Darch, S. E., McNally, A., Harrison, F., Corander, J., Barr, H. L., Paszkiewicz, K., Holden, S., Fogarty, A., Crusz, S. A., and Diggle, S. P. (2015). Recombination is a key driver of genomic and phenotypic diversity in a Pseudomonas aeruginosa population during cystic fibrosis infection. *Scientific reports*, 5:7649.

D'Argenio, D. A., Wu, M., Hoffman, L. R., Kulasekara, H. D., Déziel, E., Smith, E. E., Nguyen, H., Ernst, R. K., Larson Freeman, T. J., Spencer, D. H., Brittnacher, M., Hayden, H. S., Selgrade, S., Klausen, M., Goodlett, D. R., Burns, J. L., Ramsey, B. W., and Miller, S. I. (2007). Growth phenotypes of Pseudomonas aeruginosa lasR mutants adapted to the airways of cystic fibrosis patients. *Molecular Microbiology*, 64(2):512–533.

Davidson, D. J. and Rolfe, M. (2001). Mouse models of cystic fibrosis. *Trends in Genetics*, 17(10):S29–S37.

Davies, D. G., Parsek, M. R., Pearson, J. P., Iglewski, B. H., Costerton, J. W., and Greenberg, E. P. (1998). The involvement of cell-to-cell signals in the development of a bacterial biofilm. *Science*, 280(5361):295–298.

Davis, P. B. (2012). Cystic Fibrosis Since 1938. *American Journal of Respiratory and Critical Care Medicine*, 173(5):475–482.

De Kievit, T. R., Parkins, M. D., Gillis, R. J., Srikumar, R., Ceri, H., Poole, K., Iglewski, B. H., and Storey, D. G. (2001). Multidrug efflux pumps: Expression patterns and contribution to antibiotic resistance in Pseudomonas aeruginosa biofilms. *Antimicrobial Agents and Chemotherapy*, 45(6):1761–1770.

De Oliveira, D. M., Forde, B. M., Kidd, T. J., Harris, P. N., Schembri, M. A., Beatson, S. A., Paterson, D. L., and Walker, M. J. (2020). Antimicrobial resistance in ESKAPE pathogens. *Clinical Microbiology Reviews*, 33(3).

DeBritto, S., Gajbar, T. D., Satapute, P., Sundaram, L., Lakshmikantha, R. Y., Jogaiah, S., and Ito, S.-i. (2020). Isolation and characterization of nutrient dependent pyocyanin from Pseudomonas aeruginosa and its dye and agrochemical properties. *Scientific Reports 2020 10:1*, 10(1):1–12.

Defoirdt, T. (2018). Quorum-Sensing Systems as Targets for Antivirulence Therapy. *Trends in Microbiology*, 26(4):313–328.

Depluverez, S., Devos, S., and Devreese, B. (2016). The Role of Bacterial Secretion Systems in the Virulence of Gram-Negative Airway Pathogens Associated with Cystic Fibrosis. *Frontiers in Microbiology*, 7(AUG):1336.

Dettman, J. R. and Kassen, R. (2021). Evolutionary Genomics of Niche-Specific Adaptation to the Cystic Fibrosis Lung in Pseudomonas aeruginosa. *Molecular Biology and Evolution*, 38(2):663–675.

Dietrich, L. E., Price-Whelan, A., Petersen, A., Whiteley, M., and Newman, D. K. (2006). The phenazine pyocyanin is a terminal signalling factor in the quorum sensing network of Pseudomonas aeruginosa. *Molecular Microbiology*, 61(5):1308–1321.

Diggle, S. P., Griffin, A. S., Campbell, G. S., and West, S. A. (2007). Cooperation and conflict in quorum-sensing bacterial populations. *Nature 2007 450:7168*, 450(7168):411–414.

Diggle, S. P., Stacey, R. E., Dodd, C., Cámara, M., Williams, P., and Winzer, K. (2006). The galactophilic lectin, LecA, contributes to biofilm development in Pseudomonas aeruginosa. *Environmental Microbiology*, 8(6):1095–1104.

Diggle, S. P. and Whiteley, M. (2020). Microbe profile: Pseudomonas aeruginosa: Opportunistic pathogen and lab rat. *Microbiology (United Kingdom)*, 166(1):30–33.

Dötsch, A., Becker, T., Pommerenke, C., Magnowska, Z., Jänsch, L., and Häussler, S. (2009). Genomewide identification of genetic determinants of antimicrobial drug resistance in Pseudomonas aeruginosa. *Antimicrobial Agents and Chemotherapy*, 53(6):2522–2531.

Dumas, Z., Ross-Gillespie, A., and Kümmerli, R. (2013). Switching between apparently redundant iron-uptake mechanisms benefits bacteria in changeable environments. *Proceedings of the Royal Society B: Biological Sciences*, 280(1764).

Elborn, J. S. (2016). Cystic fibrosis. *The Lancet*, 388(10059):2519–2531.

Faure, E., Kwong, K., and Nguyen, D. (2018). Pseudomonas aeruginosa in Chronic Lung Infections: How to Adapt Within the Host? *Frontiers in Immunology*, 9:2416.

Filkins, L. M. and O'Toole, G. A. (2015). Cystic Fibrosis Lung Infections: Polymicrobial, Complex, and Hard to Treat. *PLOS Pathogens*, 11(12):e1005258.

Flemming, H. C. and Wingender, J. (2010). The biofilm matrix. *Nature Reviews Microbiology*, 8(9):623–633.

Flemming, H.-C., Wingender, J., Szewzyk, U., Steinberg, P., Rice, S. A., and Kjelleberg, S. (2016). Biofilms: an emergent form of bacterial life. *Nature Publishing Group*.

Folkesson, A., Jelsbak, L., Yang, L., Johansen, H. K., Ciofu, O., Høiby, N., and Molin, S. (2012). Adaptation of Pseudomonas aeruginosa to the cystic fibrosis airway: an evolutionary perspective. *Nature Reviews Microbiology 2012 10:12*, 10(12):841–851.

Fonseca, E. L., Marin, M. A., Encinas, F., and Vicente, A. C. P. (2015). Full characterization of the integrative and conjugative element carrying the metallo-β-lactamase blaSPM-1 and bicyclomycin bcr1 resistance genes found in the pandemic Pseudomonas aeruginosa clone SP/ST277. *Journal of Antimicrobial Chemotherapy*, 70(9):2547–2550.

Fothergill, J. L., Panagea, S., Hart, C. A., Walshaw, M. J., Pitt, T. L., and Winstanley, C. (2007). Widespread pyocyanin over-production among isolates of a cystic fibrosis epidemic strain. *BMC Microbiology*, 7(1):1–10.

Francis, V. I., Stevenson, E. C., and Porter, S. L. (2017). Two-component systems required for virulence in Pseudomonas aeruginosa. *FEMS Microbiology Letters*, 364(11):104.

Friedman, L. and Kolter, R. (2004). Genes involved in matrix formation in Pseudomonas aeruginosa PA14 biofilms. *Molecular Microbiology*, 51(3):675–690.

Fuchs, E. L., Brutinel, E. D., Klem, E. R., Fehr, A. R., Yahr, T. L., and Wolfgang, M. C. (2010). In vitro and in vivo characterization of the Pseudomonas aeruginosa cyclic AMP (cAMP) phosphodiesterase CpdA, required for cAMP homeostasis and virulence factor regulation. *Journal of Bacteriology*, 192(11):2779–2790.

Gao, B., Gallagher, T., Zhang, Y., Elbadawi-Sidhu, M., Lai, Z., Fiehn, O., and Whiteson, K. L. (2018). Tracking Polymicrobial Metabolism in Cystic Fibrosis Airways: Pseudomonas aeruginosa Metabolism and Physiology Are Influenced by Rothia mucilaginosa-Derived Metabolites. *mSphere*, 3(2).

Ghafoor, A., Hay, I. D., and Rehm, B. H. (2011). Role of exopolysaccharides in Pseudomonas aeruginosa biofilm formation and architecture. *Applied and Environmental Microbiology*, 77(15):5238–5246.

Ghani, M. and Soothill, J. S. (1997). Ceftazidime, gentamicin, and rifampicin, in combination, kill biofilms of mucoid Pseudomonas aeruginosa. *https://doi.org/10.1139/m97-144*, 43(11):999–1004.

Gi, M., Lee, K.-M., Kim, S. C., Yoon, J.-H., Yoon, S. S., and Choi, J. Y. (2015). A novel siderophore system is essential for the growth of Pseudomonas aeruginosa in airway mucus. *Scientific Reports 2015 5:1*, 5(1):1–15.

Gomez, N. O., Tetard, A., Ouerdane, L., Laffont, C., Brutesco, C., Ball, G., Lobinski, R., Denis, Y., Plésiat, P., Llanes, C., Arnoux, P., and Voulhoux, R. (2021). Involvement of the Pseudomonas aeruginosa MexAB–OprM efflux pump in the secretion of the metallophore pseudopaline. *Molecular Microbiology*, 115(1):84–98.

Gooderham, W. J. and Hancock, R. E. W. (2009). Regulation of virulence and antibiotic resistance by two-component regulatory systems in Pseudomonas aeruginosa. *FEMS Microbiology Reviews*, 33(2):279–294.

Goodman, A. L., Kulasekara, B., Rietsch, A., Boyd, D., Smith, R. S., and Lory, S. (2004). A Signaling Network Reciprocally Regulates Genes Associated with Acute Infection and Chronic Persistence in Pseudomonas aeruginosa. *Developmental Cell*, 7(5):745–754.

Görisch, H. (2003). The ethanol oxidation system and its regulation in Pseudomonas aeruginosa. *Biochimica et Biophysica Acta (BBA) - Proteins and Proteomics*, 1647(1-2):98–102.

Goss, C. H. and Burns, J. L. (2007). Exacerbations in cystic fibrosis · 1: Epidemiology and pathogenesis. *Thorax*, 62(4):360.

Gotschlich, A., Huber, B., Geisenberger, O., Togl, A., Steidle, A., Riedel, K., Hill, P., Tümmler, B., Vandamme, P., Middleton, B., Camara, M., Williams, P., Hardman, A., and Eberl, L. (2001). Synthesis of Multiple N-Acylhomoserine Lactones is Wide-spread Among the Members of the Burkholderia cepacia Complex. *Systematic and Applied Microbiology*, 24(1):1–14.

Grandclément, C., Tannières, M., Moréra, S., Dessaux, Y., and Faure, D. (2016). Quorum quenching: role in nature and applied developments. *FEMS Microbiology Reviews*, 40(1):86–116.

GraphPad (2021). GraphPad Software. *www.graphpad.com*, (Accessed 10 April 2021).

Gu, Z., Eils, R., and Schlesner, M. (2016). Complex heatmaps reveal patterns and correlations in multidimensional genomic data. *Bioinformatics*, 32(18):2847–2849.

Gutu, A. D., Rodgers, N. S., Park, J., and Moskowitz, S. M. (2015). Pseudomonas aeruginosa high-level resistance to polymyxins and other antimicrobial peptides requires cprA, a gene that is disrupted in the PAO1 strain. *Antimicrobial Agents and Chemotherapy*, 59(9):5377–5387.

Gyaneshwar, P., Paliy, O., McAuliffe, J., Popham, D. L., Jordan, M. I., and Kustu, S. (2005). Sulfur and nitrogen limitation in Escherichia coli K-12: Specific homeostatic responses. *Journal of Bacteriology*, 187(3):1074–1090.

Harrington, N. E., Littler, J. L., and Harrison, F. (2021a). Transcriptome analysis of Pseudomonas aeruginosa biofilm infection in an ex vivo pig model of the cystic fibrosis lung. *Applied and Environmental Microbiology*, In Press.

Harrington, N. E., Sweeney, E., Alav, I., Allen, F., Moat, J., and Harrison, F. (2021b). Antibiotic Efficacy Testing in an Ex vivo Model of Pseudomonas aeruginosa and Staphylococcus aureus Biofilms in the Cystic Fibrosis Lung. *Journal of Visualized Experiments*, (167):62187.

Harrington, N. E., Sweeney, E., and Harrison, F. (2020). Building a better biofilm - Formation of in vivo-like biofilm structures by Pseudomonas aeruginosa in a porcine model of cystic fibrosis lung infection. *Biofilm*, 2:100024.

Harrison, F. and Diggle, S. P. (2016). An ex vivo lung model to study bronchioles infected with Pseudomonas aeruginosa biofilms. *Microbiology*, 162:1755–1760.

Harrison, F., McNally, A., da Silva, A. C., Heeb, S., and Diggle, S. P. (2017). Optimised chronic infection models demonstrate that siderophore 'cheating' in Pseudomonas aeruginosa is context specific. *The ISME Journal*, 11(11):2492–2509.

Harrison, F., Muruli, A., Higgins, S., and Diggle, S. P. (2014). Development of an Ex Vivo Porcine Lung Model for Studying Growth, Virulence, and Signaling of Pseudomonas aeruginosa. *Infection and Immunity*, 82(8):3312–3323.

Hassan, M. M., Harrington, N. E., Sweeney, E., and Harrison, F. (2020). Predicting Antibiotic-Associated Virulence of Pseudomonas aeruginosa Using an ex vivo Lung Biofilm Model. *Frontiers in Microbiology*, 11:2175.

Heijerman, H. (2005). Infection and inflammation in cystic fibrosis: A short review. *Journal of Cystic Fibrosis*, 4:3–5.

Henderson, A. G., Ehre, C., Button, B., Abdullah, L. H., Cai, L.-H., Leigh, M. W., DeMaria, G. C., Matsui, H., Donaldson, S. H., Davis, C. W., Sheehan, J. K., Boucher, R. C., and Kesimer, M. (2014). Cystic fibrosis airway secretions exhibit mucin hyperconcentration and increased osmotic pressure. *The Journal of clinical investigation*, 124(7):3047–60.

Hennemann, L. C. and Nguyen, D. (2021). LasR-regulated proteases in acute vs. chronic lung infection: a double-edged sword. *Microbial Cell*, 8(7):161.

Hermansen, G., Hansen, M., Khademi, S., and Jelsback, L. (2018). Intergenic evolution during host adaptation increases expression of the metallophore pseudopaline in Pseudomonas aeruginosa. *Microbiology*, 164(8).

Heurlier, K., Dénervaud, V., and Haas, D. (2006). Impact of quorum sensing on fitness of Pseudomonas aeruginosa. *International Journal of Medical Microbiology*, 296(2-3):93–102.

Heurlier, K., Williams, F., Heeb, S., Dormond, C., Pessi, G., Singer, D., Cámara, M., Williams, P., and Haas, D. (2004). Positive Control of Swarming, Rhamnolipid Synthesis, and Lipase Production by the Posttranscriptional RsmA/RsmZ System in Pseudomonas aeruginosa PAO1. *Journal of Bacteriology*, 186(10):2936.

Higgins, S., Heeb, S., Rampioni, G., Fletcher, M. P., Williams, P., and Cámara, M. (2018). Differential regulation of the phenazine biosynthetic operons by quorum sensing in Pseudomonas aeruginosa PAO1-N. *Frontiers in Cellular and Infection Microbiology*, 8(JUL):252.

Hine, C., Nagakumar, P., and Desai, M. (2020). Small molecule drugs in cystic fibrosis. *Arch Dis Child Educ Pract Ed*, 0:1–4.

Hochstim, C. J., Choi, J. Y., Lowe, D., Masood, R., and Rice, D. H. (2010). Biofilm detection with hematoxylin-eosin staining. *Archives of Otolaryngology - Head and Neck Surgery*, 136(5):453–456.

Hogardt, M. and Heesemann, J. (2010). Adaptation of Pseudomonas aeruginosa during persistence in the cystic fibrosis lung. *International Journal of Medical Microbiology*, 300(8):557–562.

Hogardt, M. and Heesemann, J. (2011). Microevolution of Pseudomonas aeruginosa to a Chronic Pathogen of the Cystic Fibrosis Lung. *Current Topics in Microbiology and Immunology*, 358:91–118.

Høiby, N., Bjarnsholt, T., Givskov, M., Molin, S., and Ciofu, O. (2010). Antibiotic resistance of bacterial biofilms. *International Journal of Antimicrobial Agents*, 35(4):322–332.

Høiby, N., Bjarnsholt, T., Moser, C., Jensen, P. Ø., Kolpen, M., Qvist, T., Aanæs, K., Pressler, T., Skov, M., and Ciofu, O. (2017). Diagnosis of biofilm infections in cystic fibrosis patients. *APMIS*, 125(4):339–343.

Hong, S. D., Dhong, H.-J., Chung, S.-K., Kim, H. Y., Park, J., and Ha, S. Y. (2014). Hematoxylin and Eosin Staining for Detecting Biofilms: Practical and Cost-Effective Methods for Predicting Worse Outcomes after Endoscopic Sinus Surgery. *Clinical and experimental otorhinolaryngology*, 7(3):193–7.

Hothorn, T., Bretz, F., and Westfall, P. (2008). Simultaneous Inference in General Parametric Models. *Biometrical Journal*, 50(3):346–363.

Hotterbeekx, A., Kumar-Singh, S., Goossens, H., and Malhotra-Kumar, S. (2017). In vivo and In vitro interactions between Pseudomonas aeruginosa and Staphylococcus spp. *Frontiers in Cellular and Infection Microbiology*, 7(APR):106.

Hurley, M. N., Ariff, A. H. A., Bertenshaw, C., Bhatt, J., and Smyth, A. R. (2012). Results of antibiotic susceptibility testing do not influence clinical outcome in children with cystic fibrosis. *Journal of cystic fibrosis : official journal of the European Cystic Fibrosis Society*, 11(4):288–92.

Isles, A., Maclusky, I., Corey, M., Gold, R., Prober, C., Fleming, P., and Levison, H. (1984). Pseudomonas cepacia infection in cystic fibrosis: An emerging problem. *The Journal of Pediatrics*, 104(2):206–210.

Janssen, K. H., Corley, J. M., Djapgne, L., Cribbs, J. T., Voelker, D., Slusher, Z., Nordell, R., Regulski, E. E., Kazmierczak, B. I., McMackin, E. W., and Yahr, T. L. (2020). Hfq and sRNA 179 inhibit expression of the pseudomonas aeruginosa cAMP-Vfr and type III secretion regulons. *mBio*, 11(3):1–15.

Jean-Pierre, F., Vyas, A., Hampton, T. H., Henson, M. A., and O'toole, G. A. (2021). One versus many: Polymicrobial communities and the cystic fibrosis airway. *mBio*, 12(2):1–7.

Jennings, L. K., Storek, K. M., Ledvina, H. E., Coulon, C., Marmont, L. S., Sadovskaya, I., Secor, P. R., Tseng, B. S., Scian, M., Filloux, A., Wozniak, D. J., Howell, P. L., and Parsek, M. R. (2015). Pel is a cationic exopolysaccharide that cross-links extracellular DNA in the Pseudomonas aeruginosa biofilm matrix. *Proceedings of the National Academy of Sciences of the United States of America*, 112(36):11353–11358.

Jimenez, P. N., Koch, G., Thompson, J. A., Xavier, K. B., Cool, R. H., and Quax, W. J. (2012). The multiple signaling systems regulating virulence in Pseudomonas aeruginosa. *Microbiology and molecular biology reviews : MMBR*, 76(1):46–65.

Jiricny, N., Molin, S., Foster, K., Diggle, S. P., Scanlan, P. D., Ghoul, M., Johansen, H. K., Santorelli, L. A., Popat, R., West, S. A., and Griffin, A. S. (2014). Loss of Social Behaviours in Populations of Pseudomonas aeruginosa Infecting Lungs of Patients with Cystic Fibrosis. *PLOS ONE*, 9(1):e83124.

Jones, A. K., Fulcher, N. B., Balzer, G. J., Urbanowski, M. L., Pritchett, C. L., Schurr, M. J., Yahr, T. L., and Wolfgang, M. C. (2010). Activation of the Pseudomonas aeruginosa AlgU Regulon through mucA Mutation Inhibits Cyclic AMP/Vfr Signaling. *Journal of Bacteriology*, 192(21):5709–5717.

Jones, R. A., Shropshire, H., Zhao, C., Murphy, A., Lidbury, I., Wei, T., Scanlan, D. J., and Chen, Y. (2021). Phosphorus stress induces the synthesis of novel glycolipids in Pseudomonas aeruginosa that confer protection against a last-resort antibiotic. *The ISME Journal 2021 15:11*, 15(11):3303–3314.

Jurado-Martín, I., Sainz-Mejías, M., and McClean, S. (2021). Pseudomonas aeruginosa: An Audacious Pathogen with an Adaptable Arsenal of Virulence Factors. *International Journal of Molecular Sciences 2021, Vol. 22, Page 3128*, 22(6):3128.

Kanehisa, M. (2019). Toward understanding the origin and evolution of cellular organisms. *Protein science : a publication of the Protein Society*, 28(11):1947–1951.

Kanehisa, M., Furumichi, M., Sato, Y., Ishiguro-Watanabe, M., and Tanabe, M. (2021). KEGG: integrating viruses and cellular organisms. *Nucleic acids research*, 49(D1):D545–D551.

Kanehisa, M. and Goto, S. (2000). KEGG: kyoto encyclopedia of genes and genomes. *Nucleic acids research*, 28(1):27–30.

Kang, D. and Kirienko, N. V. (2018). Interdependence between iron acquisition and biofilm formation in Pseudomonas aeruginosa. *Journal of Microbiology*, 56(7):449–457.

Kassambara, A. (2020). ggpubr: 'ggplot2' Based Publication Ready Plots. R package version 0.4.0. *https://github.com/kassambara/ggpubr*, (Accessed 21 September 2021).

Kawasaki, S., Arai, H., Kodama, T., and Igarashi, Y. (1997). Gene cluster for dissimilatory nitrite reductase (nir) from Pseudomonas aeruginosa: Sequencing and identification of a locus for heme d1 biosynthesis. *Journal of Bacteriology*, 179(1):235–242.

Kenna, D., Lilley, D., Coward, A., Martin, K., Perry, C., Pike, R., Hill, R., and Turton, J. (2017). Prevalence of Burkholderia species, including members of Burkholderia cepacia complex, among UK cystic and non-cystic fibrosis patients. *Journal of Medical Microbiology*, 66:490–501.

Kidd, T. J. (2017). Pseudomonas aeruginosa infection after CFTR restoration: One step back, one step forward. *American Journal of Respiratory and Critical Care Medicine*, 195(12):1550–1552.

Kim, D., Paggi, J. M., Park, C., Bennett, C., and Salzberg, S. L. (2019). Graph-based genome alignment and genotyping with HISAT2 and HISAT-genotype. *Nature Biotechnology*, 37(8):907–915.

Kiratisin, P., Tucker, K. D., and Passador, L. (2002). LasR, a transcriptional activator of Pseudomonas aeruginosa virulence genes, functions as a multimer. *Journal of Bacteriology*, 184(17):4912–4919.

Kolpen, M., Appeldorff, C. F., Brandt, S., Mousavi, N., Kragh, K. N., Aydogan, S., Uppal, H. A., Bjarnsholt, T., Ciofu, O., Høiby, N., and Jensen, P. (2016). Increased bactericidal activity of colistin on Pseudomonas aeruginosa biofilms in anaerobic conditions. *Pathogens and Disease*, 74(1):86.

Konings, A. F., Martin, L. W., Sharples, K. J., Roddam, L. F., Latham, R., Reid, D. W., and Lamont, I. L. (2013). Pseudomonas aeruginosa uses multiple pathways to acquire iron during chronic infection in cystic fibrosis lungs. *Infection and Immunity*, 81(8):2697–2704.

Konstan, M. W., Morgan, W. J., Butler, S. M., Pasta, D. J., Craib, M. L., Silva, S. J., Stokes, D. C., Wohl, M. E. B., Wagener, J. S., Regelmann, W. E., and Johnson, C. A. (2007). Risk Factors For Rate of Decline in Forced Expiratory Volume in One Second in Children and Adolescents with Cystic Fibrosis. *The Journal of Pediatrics*, 151(2):134–139.e1.

Kopylova, E., Noé, L., and Touzet, H. (2012). SortMeRNA: Fast and accurate filtering of ribosomal RNAs in metatranscriptomic data. *Bioinformatics*, 28(24):3211–3217.

Kordes, A., Preusse, M., Willger, S. D., Braubach, P., Jonigk, D., Haverich, A., Warnecke, G., and Häussler, S. (2019). Genetically diverse Pseudomonas aeruginosa populations display similar transcriptomic profiles in a cystic fibrosis explanted lung. *Nature Communications*, 10(1):1–10.

Kostylev, M., Kim, D. Y., Smalley, N. E., Salukhe, I., Greenberg, E. P., and Dandekar, A. A. (2019). Evolution of the Pseudomonas aeruginosa quorum-sensing hierarchy. *Proceedings of the National Academy of Sciences*, 116(14):7027–7032.

Kragh, K. N., Alhede, M., Kvich, L., and Bjarnsholt, T. (2019). Into the well—A close look at the complex structures of a microtiter biofilm and the crystal violet assay. *Biofilm*, 1:100006.

LaFayette, S. L., Houle, D., Beaudoin, T., Wojewodka, G., Radzioch, D., Hoffman, L. R., Burns, J. L., Dandekar, A. A., Smalley, N. E., Chandler, J. R., Zlosnik, J. E., Speert, D. P., Bernier, J., Matouk, E., Brochiero, E., Rousseau, S., and Nguyen, D. (2015). Cystic fibrosis–adapted Pseudomonas aeruginosa quorum sensing lasR mutants cause hyperinflammatory responses. *Science Advances*, 1(6).

Lamblin, G., Degroote, S., Perini, J. M., Delmotte, P., Scharfman, A., Davril, M., Lo-Guidice, J. M., Houdret, N., Dumur, V., Klein, A., and Roussel, P. (2001). Human airway mucin glycosylation: a combinatory of carbohydrate determinants which vary in cystic fibrosis. *Glycoconjugate journal*, 18(9):661–684.

Lamont, I. L., Beare, P. A., Ochsner, U., Vasil, A. I., and Vasil, M. L. (2002). Siderophore-mediated signaling regulates virulence factor production in Pseudomonas aeruginosa. *Proceedings of the National Academy of Sciences*, 99(10):7072–7077.

Langan, K. M., Kotsimbos, T., and Peleg, A. Y. (2015). Managing Pseudomonas aeruginosa respiratory infections in cystic fibrosis. *Current Opinion in Infectious Diseases*, 28(6):547–556.

Laselva, O., Guerra, L., Castellani, S., Favia, M., Di Gioia, S., and Conese, M. (2021). Small-molecule drugs for cystic fibrosis: Where are we now? *Pulmonary Pharmacology & Therapeutics*, page 102098.

Lee, J. and Zhang, L. (2015). The hierarchy quorum sensing network in Pseudomonas aeruginosa. *Protein and Cell*, 6(1):26–41.

Leitão, J., Feliciano, J., Sousa, S., Pita, T., and Guerreiro, S. (2017). Burkholderia cepacia complex infections among cystic fibrosis patients: perspectives and challenges. In Sriramulu, D., editor, *Progress in Understanding Cystic Fibrosis*, pages 74–99. IntechOpen Limited., London, UK.

Lemke, M. J. and Leff, L. G. (2006). Microbial Ecology Culturability of Stream Bacteria Assessed at the Assemblage and Population Levels. *Microbial Ecology*, 51:365–374.

Lesprit, P., Faurisson, F., Join-Lambert, O., Roudot-Thoraval, F., Foglino, M., Vissuzaine, C., and Carbon, C. (2003). Role of the Quorum-sensing System in Experimental Pneumonia due to Pseudomonas aeruginosa in Rats. *American Journal of Respiratory and Critical Care Medicine*, 167(11):1478–1482.

Lhospice, S., Gomez, N. O., Ouerdane, L., Brutesco, C., Ghssein, G., Hajjar, C., Liratni, A., Wang, S., Richaud, P., Bleves, S., Ball, G., Borezée-Durant, E., Lobinski, R., Pignol, D., Arnoux, P., and Voulhoux, R. (2017). Pseudomonas aeruginosa zinc uptake in chelating environment is primarily mediated by the metallophore pseudopaline. *Scientific Reports*, 7(1).

Li, H. (2013). Aligning sequence reads, clone sequences and assembly contigs with BWA-MEM. *arXiv:1303.3997v2 [q-bio.GN]*.

Li, H. (2015). A toolkit for processing sequences in FASTA/Q formats. *https://github.com/lh3/seqtk*, (Accessed 21 April 2020).

Li, L., Mendis, N., Trigui, H., Oliver, J. D., and Faucher, S. P. (2014). The importance of the viable but non-culturable state in human bacterial pathogens. *Frontiers in Microbiology*, 5.

Liao, Y., Smyth, G. K., and Shi, W. (2019). The R package Rsubread is easier, faster, cheaper and better for alignment and quantification of RNA sequencing reads. *Nucleic Acids Research*, 47(8):e47–e47.

Liberati, N. T., Urbach, J. M., Miyata, S., Lee, D. G., Drenkard, E., Wu, G., Villanueva, J., Wei, T., and Ausubel, F. M. (2006a). An ordered, nonredundant library of Pseudomonas aeruginosa strain PA14 transposon insertion mutants. *PNAS*, 103(8):2833–2838.

Liberati, N. T., Urbach, J. M., Miyata, S., Lee, D. G., Drenkard, E., Wu, G., Wei, T., Villanueva, J., and Ausubel, F. M. (2006b). PA14 Transposon Insertion Mutant Library. *http://pa14.mgh.harvard.edu/cgi-bin/pa14/home.cgi*, (Accessed 11 May 2018).

Lim, Y. W., Schmieder, R., Haynes, M., Furlan, M., Matthews, T. D., Whiteson, K., Poole, S. J., Hayes, C. S., Low, D. A., Maughan, H., Edwards, R., Conrad, D., and Rohwer, F. (2013). Mechanistic Model of Rothia mucilaginosa Adaptation toward Persistence in the CF Lung, Based on a Genome Reconstructed from Metagenomic Data. *PLOS ONE*, 8(5):e64285.

Limoli, D. H., Warren, E. A., Yarrington, K. D., Donegan, N. P., Cheung, A. L., and O'Toole, G. A. (2019). Interspecies interactions induce exploratory motility in pseudomonas aeruginosa. *eLife*, 8.

Limoli, D. H., Whitfield, G. B., Kitao, T., Ivey, M. L., Davis, M. R., Grahl, N., Hogan, D. A., Rahme, L. G., Howell, P. L., O'Toole, G. A., and Goldberg, J. B. (2017). Pseudomonas aeruginosa Alginate Overproduction Promotes Coexistence with Staphylococcus aureus in a Model of Cystic Fibrosis Respiratory Infection. *mBio*, 8(2):e00186–17.

Line, L., Alhede, M., Kolpen, M., Kühl, M., Ciofu, O., Bjarnsholt, T., Moser, C., Toyofuku, M., Nomura, N., Høiby, N., and Jensen, P. Ø. (2014). Physiological levels of nitrate support anoxic growth by denitrification of Pseudomonas aeruginosa at growth rates reported in cystic fibrosis lungs and sputum. *Frontiers in Microbiology*, 5(OCT):554.

Lood, C., Peeters, C., Lamy-Besnier, Q., Wagemans, J., De Vos, D., Proesmans, M., Pirnay, J. P., Echahidi, F., Piérard, D., Thimmesch, M., Boeras, A., Lagrou, K., De Canck, E.,

De Wachter, E., van Noort, V., Lavigne, R., and Vandamme, P. (2021). Genomics of an endemic cystic fibrosis Burkholderia multivorans strain reveals low within-patient evolution but high between-patient diversity. *PLOS Pathogens*, 17(3):e1009418.

Loutet, S. A. and Valvano, M. A. (2010). A decade of Burkholderia cenocepacia virulence determinant research. *Infection and Immunity*, 78(10):4088–4100.

Love, M. I., Huber, W., and Anders, S. (2014). Moderated estimation of fold change and dispersion for RNA-seq data with DESeq2. *Genome Biology*, 15(12):550.

Luna, C. M., Sibila, O., Agusti, C., and Torres, A. (2009). Animal models of ventilator-associated pneumonia. *European Respiratory Journal*, 33(1):182–188.

Lund-Palau, H., Turnbull, A. R., Bush, A., Bardin, E., Cameron, L., Soren, O., Wierre-Gore, N., Alton, E. W. F. W., Bundy, J. G., Connett, G., Faust, S. N., Filloux, A., Freemont, P., Jones, A., Khoo, V., Morales, S., Murphy, R., Pabary, R., Simbo, A., Schelenz, S., Takats, Z., Webb, J., Williams, H. D., and Davies, J. C. (2016). Pseudomonas aeruginosa infection in cystic fibrosis: pathophysiological mechanisms and therapeutic approaches. *Expert Review of Respiratory Medicine*, 10(6):685–697.

Luo, Y., Zhao, K., Baker, A. E., Kuchma, S. L., Coggan, K. A., Wolfgang, M. C., Wong, G. C., and O'Toole, G. A. (2015). A hierarchical cascade of second messengers regulates Pseudomonas aeruginosa Surface Behaviors. *mBio*, 6(1).

Mah, T. F. C. and O'Toole, G. A. (2001). Mechanisms of biofilm resistance to antimicrobial agents. *Trends in Microbiology*, 9(1):34–39.

Mahenthiralingam, E., Coenye, T., Chung, J. W., Speert, D. P., Govan, J. R. W., Taylor, P., and Vandamme, P. (2000). Diagnostically and Experimentally Useful Panel of Strains from the Burkholderia cepacia Complex. *Journal of Clinical Microbiology*, 38(2):910.

Mann, E. E. and Wozniak, D. J. (2012). Pseudomonas biofilm matrix composition and niche biology. *FEMS Microbiology Reviews*, 36(4):893–916.

Marmont, L. S., Whitfield, G. B., Rich, J. D., Yip, P., Giesbrecht, L. B., Stremick, C. A., Whitney, J. C., Parsek, M. R., Harrison, J. J., Lynne Howell, P., and Whitfield, C. (2017). PelA and PelB proteins form a modification and secretion complex essential for Pel polysaccharide-dependent biofilm formation in Pseudomonas aeruginosa. *J. Biol. Chem.*, 292(47):19411–19422.

Maura, D., Hazan, R., Kitao, T., Ballok, A. E., and Rahme, L. G. (2016). Evidence for Direct Control of Virulence and Defense Gene Circuits by the Pseudomonas aeruginosa Quorum Sensing Regulator, MvfR. *Scientific Reports 2016 6:1*, 6(1):1–14.

McBennett, K. A., Davis, P. B., and Konstan, M. W. (2021). Increasing life expectancy in cystic fibrosis: Advances and challenges. *Pediatric Pulmonology*, pages 1–8.

McCaslin, C. A., Petrusca, D. N., Poirier, C., Serban, K. A., Anderson, G. G., and Petrache, I. (2015). Impact of alginate-producing Pseudomonas aeruginosa on alveolar macrophage apoptotic cell clearance. *Journal of Cystic Fibrosis*, 14(1):70–77.

Mern, D., Ha, S., Khodaverdi, V., Gliese, N., and Görisch, H. (2010). A complex regulatory network controls aerobic ethanol oxidation in Pseudomonas aeruginosa: indication of four levels of sensor kinases and response regulators. *Microbiology*, 156(5).

Mesureur, J., Feliciano, J. R., Wagner, N., Gomes, M. C., Zhang, L., Blanco-Gonzalez, M., van der Vaart, M., O'Callaghan, D., Meijer, A. H., and Vergunst, A. C. (2017). Macrophages, but not neutrophils, are critical for proliferation of Burkholderia cenocepacia and ensuing host-damaging inflammation. *PLOS Pathogens*, 13(6):e1006437.

Meurens, F., Summerfield, A., Nauwynck, H., Saif, L., and Gerdts, V. (2012). The pig: a model for human infectious diseases. *Trends in Microbiology*, 20(1):50–57.

Meyer, J. M., Neely, A., Stintzi, A., Georges, C., and Holder, I. A. (1996). Pyoverdin is essential for virulence of Pseudomonas aeruginosa. *Infection and Immunity*, 64(2):518–523.

Mikkelsen, H., Sivaneson, M., and Filloux, A. (2011). Key two-component regulatory systems that control biofilm formation in Pseudomonas aeruginosa. *Environmental Microbiology*, 13(7):1666–1681.

Minandri, F., Imperi, F., Frangipani, E., Bonchi, C., Visaggio, D., Facchini, M., Pasquali, P., Bragonzi, A., and Visca, P. (2016). Role of Iron Uptake Systems in Pseudomonas aeruginosa Virulence and Airway Infection. *Infection and Immunity*, 84(8):2324.

Moore, J. E. and Mastoridis, P. (2017). Clinical implications of Pseudomonas aeruginosa location in the lungs of patients with cystic fibrosis. *Journal of Clinical Pharmacy and Therapeutics*, 42(3):259–267.

Mukherjee, S., Moustafa, D., Smith, C. D., Goldberg, J. B., and Bassler, B. L. (2017). The RhlR quorum-sensing receptor controls Pseudomonas aeruginosa pathogenesis and biofilm development independently of its canonical homoserine lactone autoinducer. *PLOS Pathogens*, 13(7):e1006504.

Mulcahy, L. R., Burns, J. L., Lory, S., and Lewis, K. (2010). Emergence of Pseudomonas aeruginosa strains producing high levels of persister cells in patients with cystic fibrosis. *Journal of Bacteriology*, 192(23):6191–6199.

Müsken, M., Klimmek, K., Sauer-Heilborn, A., Donnert, M., Sedlacek, L., Suerbaum, S., and Häussler, S. (2017). Towards individualized diagnostics of biofilm-associated infections: a case study. *npj Biofilms and Microbiomes*, 3(1):22.

Nelson, C. E., Huang, W., Brewer, L. K., Nguyen, A. T., Kane, M. A., Wilks, A., and Oglesby-Sherrouse, A. G. (2019). Proteomic Analysis of the Pseudomonas aeruginosa Iron Starvation Response Reveals PrrF Small Regulatory RNA-Dependent Iron Regulation of Twitching Motility, Amino Acid Metabolism, and Zinc Homeostasis Proteins. *Journal of Bacteriology*, 201(12).

Neve, R. L., Carrillo, B. D., and Phelan, V. V. (2021). Impact of artificial sputum medium formulation on pseudomonas aeruginosa secondary metabolite production. *Journal of Bacteriology*, 203(21).

Nguyen, A. T., O'Neill, M. J., Watts, A. M., Robson, C. L., Lamont, I. L., Wilks, A., and Oglesby-Sherrouse, A. G. (2014). Adaptation of Iron Homeostasis Pathways by a Pseudomonas aeruginosa Pyoverdine Mutant in the Cystic Fibrosis Lung. *Journal of Bacteriology*, 196(12):2265.

Nixon, G. M., Armstrong, D. S., Carzino, R., Carlin, J. B., Olinsky, A., Robertson, C. F., and Grimwood, K. (2001). Clinical outcome after early Pseudomonas aeruginosa infection in cystic fibrosis. *The Journal of Pediatrics*, 138(5):699–704.

O'Brien, S. and Fothergill, J. L. (2017). The role of multispecies social interactions in shaping Pseudomonas aeruginosa pathogenicity in the cystic fibrosis lung. *FEMS Microbiology Letters*, 364(15):128.

O'Brien, S., Williams, D., Fothergill, J. L., Paterson, S., Winstanley, C., and Brockhurst, M. A. (2017). High virulence sub-populations in Pseudomonas aeruginosa long-term cystic fibrosis airway infections. *BMC Microbiology 2017 17:1*, 17(1):1–8.

O'Brien, T. J., Hassan, M. M., Harrison, F., and Welch, M. (2021). An in vitro model for the cultivation of polymicrobial biofilms under continuous-flow conditions. *F1000Research 2021 10:801*, 10:801.

Olland, A., Falcoz, P. E., Kessler, R., and Massard, G. (2011). Should cystic fibrosis patients infected with Burkholderia cepacia complex be listed for lung transplantation? *Interactive CardioVascular and Thoracic Surgery*, 13(6):631–634.

O'Toole, G. A., Crabbé, A., Kümmerli, R., LiPuma, J. J., Bomberger, J. M., Davies, J. C., Limoli, D., Phelan, V. V., Bliska, J. B., DePas, W. H., Dietrich, L. E., Hampton, T. H., Hunter, R., Khursigara, C. M., Price-Whelan, A., Ashare, A., Cramer, R. A., Goldberg, J. B., Harrison, F., Hogan, D. A., Henson, M. A., Madden, D. R., Mayers, J. R., Nadell, C., Newman, D., Prince, A., Rivett, D. W., Schwartzman, J. D., Schultz, D., Sheppard, D. C., Smyth, A. R., Spero, M. A., Stanton, B. A., Turner, P. E., van der Gast, C., Whelan, F. J., Whitaker, R., and Whiteson, K. (2021). Model Systems to Study the Chronic, Polymicrobial Infections in Cystic Fibrosis: Current Approaches and Exploring Future Directions. *mBio*, 12(5).

Palmer, K. L., Aye, L. M., and Whiteley, M. (2007). Nutritional cues control Pseudomonas aeruginosa multicellular behavior in cystic fibrosis sputum. *Journal of Bacteriology*, 189(22):8079–87.

Palmer, K. L., Mashburn, L. M., Singh, P. K., and Whiteley, M. (2005). Cystic fibrosis sputum supports growth and cues key aspects of Pseudomonas aeruginosa physiology. *Journal of bacteriology*, 187(15):5267–77.

Pamp, S. J., Gjermansen, M., Johansen, H. K., and Tolker-Nielsen, T. (2008). Tolerance to the antimicrobial peptide colistin in Pseudomonas aeruginosa biofilms is linked to metabolically active cells, and depends on the pmr and mexAB-oprM genes. *Molecular Microbiology*, 68(1):223–240.

Pan, Y. p., hong Xu, Y., xin Wang, Z., ping Fang, Y., and lu Shen, J. (2016). Overexpression of MexAB-OprM efflux pump in carbapenem-resistant Pseudomonas aeruginosa. *Archives of Microbiology*, 198(6):565–571.

Pang, Z., Raudonis, R., Glick, B. R., Lin, T. J., and Cheng, Z. (2019). Antibiotic resistance in Pseudomonas aeruginosa: mechanisms and alternative therapeutic strategies. *Biotechnology Advances*, 37(1):177–192.

Parkins, M. D., Ceri, H., and Storey, D. G. (2001). Pseudomonas aeruginosa GacA, a factor in multihost virulence, is also essential for biofilm formation. *Molecular Microbiology*, 40(5):1215–1226.

Passos da Silva, D., Matwichuk, M. L., Townsend, D. O., Reichhardt, C., Lamba, D., Wozniak, D. J., and Parsek, M. R. (2019). The Pseudomonas aeruginosa lectin LecB binds to the exopolysaccharide Psl and stabilizes the biofilm matrix. *Nature Communications 2019 10:1*, 10(1):1–11.

Perault, A. I., Chandler, C. E., Rasko, D. A., Ernst, R. K., Wolfgang, M. C., and Cotter, P. A. (2020). Host Adaptation Predisposes Pseudomonas aeruginosa to Type VI Secretion System-Mediated Predation by the Burkholderia cepacia Complex. *Cell Host and Microbe*, 28(4):534–547.e3.

Poole, K. (2009). Efflux pumps as antimicrobial resistance mechanisms. *Annals of Medicine*, 39(3):162–176.

Preibisch, S., Saalfeld, S., and Tomancak, P. (2009). Globally optimal stitching of tiled 3D microscopic image acquisitions. *Bioinformatics*, 25(11):1463.

Ramos, I., Dietrich, L. E., Price-Whelan, A., and Newman, D. K. (2010). Phenazines affect biofilm formation by Pseudomonas aeruginosa in similar ways at various scales. *Research in Microbiology*, 161(3):187–191.

Reid, D. W., Carroll, V., O'may, C., Champion, A., and Kirov, S. M. (2007). Increased airway iron as a potential factor in the persistence of Pseudomonas aeruginosa infection in cystic fibrosis. *European Respiratory Journal*, 30:286–292.

Reimmann, C., Beyeler, M., Latifi, A., Winteler, H., Foglino, M., Lazdunski, A., and Haas, D. (1997). The global activator GacA of Pseudomonas aeruginosa PAO positively controls the production of the autoinducer N-butyryl-homoserine lactone and the formation of the virulence factors pyocyanin, cyanide, and lipase. *Molecular Microbiology*, 24(2):309–319.

Rhodes, K. A. and Schweizer, H. P. (2016). Antibiotic resistance in Burkholderia species. *Drug Resistance Updates*, 28:82–90.

Ridley, K. and Condren, M. (2020). Elexacaftor-Tezacaftor-Ivacaftor: The First

Triple-Combination Cystic Fibrosis Transmembrane Conductance Regulator Modulating Therapy. *The Journal of Pediatric Pharmacology and Therapeutics : JPPT*, 25(3):192.

Riedel, K., Hentzer, M., Geisenberger, O., Huber, B., Steidle, A., Wu, H., Høiby, N., Givskov, M., Molin, S., and Eberl, L. (2001). N-acylhomoserine-lactone-mediated communication between Pseudomonas aeruginosa and Burkholderia cepacia in mixed biofilms. *Microbiology*, 147(12):3249–3262.

Rimessi, A., Bezzerri, V., Salvatori, F., Tamanini, A., Nigro, F., Dechecchi, M. C., Santangelo, A., Prandini, P., Munari, S., Provezza, L., de Loubresse, N. G., Muller, J., Ribeiro, C. M. P., Lippi, G., Gambari, R., Pinton, P., and Cabrini, G. (2018). PLCB3 Loss of Function Reduces Pseudomonas aeruginosa–Dependent IL-8 Release in Cystic Fibrosis. *American Journal of Respiratory Cell and Molecular Biology*, 59(4):428–436.

Riordan, J., Rommens, J., Kerem, B., Alon, N., Rozmahel, R., Grzelczak, Z., Zielenski, J., Lok, S., Plavsic, N., and Chou, J. (1986). Identification of the cystic fibrosis gene: cloning and characterization of complementary DNA. *Science*, 232(4758):1648–1650.

Roberts, A. E., Kragh, K. N., Bjarnsholt, T., and Diggle, S. P. (2015). The Limitations of in Vitro Experimentation in Understanding Biofilms and Chronic Infection. *Journal of Molecular Biology*, 427(23):3646–3661.

Roberts, A. E., Powell, L. C., Pritchard, M. F., Thomas, D. W., and Jenkins, R. E. (2019). Anti-pseudomonad activity of manuka honey and antibiotics in a specialized ex vivo model simulating cystic fibrosis lung infection. *Frontiers in Microbiology*, 10:869.

Robinson, C. V., Elkins, M. R., Bialkowski, K. M., Thornton, D. J., and Kertesz, M. A. (2012). Desulfurization of mucin by Pseudomonas aeruginosa: Influence of sulfate in the lungs of cystic fibrosis patients. *Journal of Medical Microbiology*, 61(PART12):1644–1653.

Rogers, G. B., Carroll, M. P., Serisier, D. J., Hockey, P. M., Jones, G., and Bruce, K. D. (2004). Characterization of bacterial community diversity in cystic fibrosis lung infections by use of 16S ribosomal DNA terminal restriction fragment length polymorphism profiling. *Journal of Clinical Microbiology*, 42(11):5176–5183.

Rossi, E., Falcone, M., Molin, S., and Krogh Johansen, H. (2018). High-resolution in situ transcriptomics of Pseudomonas aeruginosa unveils genotype independent patho-phenotypes in cystic fibrosis lungs. *Nature Communications*, 9(1):3459.

Rossi, E., La Rosa, R., Bartell, J. A., Marvig, R. L., Haagensen, J. A., Sommer, L. M., Molin, S., and Johansen, H. K. (2020). Pseudomonas aeruginosa adaptation and evolution in patients with cystic fibrosis. *Nature Reviews Microbiology 2020 19:5*, 19(5):331–342.

Sajjan, U., Thanassoulis, G., Cherapanov, V., Lu, A., Sjolin, C., Steer, B., Wu, Y. J., Rotstein, O. D., Kent, G., McKerlie, C., Forstner, J., and Downey, G. P. (2001). Enhanced susceptibility to pulmonary infection with Burkholderia cepacia in Cftr-/-mice. *Infection and Immunity*, 69(8):5138–5150.

Saldías, M. S. and Valvano, M. A. (2009). Interactions of Burkholderia cenocepacia and other Burkholderia cepacia complex bacteria with epithelial and phagocytic cells. *Microbiology*, 155:2809–2817.

Sanders, D. B. and Fink, A. K. (2016). Background and Epidemiology. *Pediatric clinics of North America*, 63(4):567–84.

Sandri, A., Ortombina, A., Boschi, F., Cremonini, E., Boaretti, M., Sorio, C., Melotti, P., Bergamini, G., and Lleo, M. (2018). Inhibition of pseudomonas aeruginosa secreted virulence factors reduces lung inflammation in CF mice. *Virulence*, 9(1):1008–1018.

Schiessl, K. T., Hu, F., Jo, J., Nazia, S. Z., Wang, B., Price-Whelan, A., Min, W., and Dietrich, L. E. (2019). Phenazine production promotes antibiotic tolerance and metabolic heterogeneity in Pseudomonas aeruginosa biofilms. *Nature Communications*, 10(1):1–10.

Schindelin, J., Arganda-Carreras, I., Frise, E., Kaynig, V., Longair, M., Pietzsch, T., Preibisch, S., Rueden, C., Saalfeld, S., Schmid, B., Tinevez, J. Y., White, D. J., Hartenstein, V., Eliceiri, K., Tomancak, P., and Cardona, A. (2012). Fiji: an open-source platform for biological-image analysis. *Nature Methods 2012 9:7*, 9(7):676–682.

Schmid, N., Pessi, G., Deng, Y., Aguilar, C., Carlier, A. L., Grunau, A., Omasits, U., Zhang, L. H., Ahrens, C. H., and Eberl, L. (2012). The AHL- and BDSF-Dependent Quorum Sensing Systems Control Specific and Overlapping Sets of Genes in Burkholderia cenocepacia H111. *PLoS ONE*, 7(11):49966.

Schobert, M. and Jahn, D. (2010). Anaerobic physiology of Pseudomonas aeruginosa in the cystic fibrosis lung. *International Journal of Medical Microbiology*, 300(8):549–556.

Schreiber, K., Boes, N., Eschbach, M., Jaensch, L., Wehland, J., Bjarnsholt, T., Givskov, M., Hentzer, M., and Schobert, M. (2006). Anaerobic Survival of Pseudomonas aeruginosa by Pyruvate Fermentation Requires an Usp-Type Stress Protein. *Journal of Bacteriology*, 188(2):659.

Schwab, U., Abdullah, L. H., Perlmutt, O. S., Albert, D., Davis, C. W., Arnold, R. R., Yankaskas, J. R., Gilligan, P., Neubauer, H., Randell, S. H., and Boucher, R. C. (2014). Localization of Burkholderia cepacia Complex Bacteria in Cystic Fibrosis Lungs and Interactions with Pseudomonas aeruginosa in Hypoxic Mucus. *Infection and Immunity*, 82(11):4729–4745.

Scoffone, V. C., Chiarelli, L. R., Trespidi, G., Mentasti, M., Riccardi, G., and Buroni, S. (2017). Burkholderia cenocepacia Infections in Cystic Fibrosis Patients: Drug Resistance and Therapeutic Approaches. *Frontiers in Microbiology*, 8:1592.

Scoffone, V. C., Trespidi, G., Chiarelli, L. R., Barbieri, G., and Buroni, S. (2019). Quorum sensing as antivirulence target in cystic fibrosis pathogens. *International Journal of Molecular Sciences*, 20(8).

Semaniakou, A., Croll, R. P., and Chappe, V. (2018). Animal Models in the Pathophysiology of Cystic Fibrosis. *Frontiers in Pharmacology*, 9.

Shropshire, H., Jones, R. A., Aguilo-Ferretjans, M. M., Scanlan, D. J., and Chen, Y. (2021). Proteomics insights into the Burkholderia cenocepacia phosphorus stress response. *Environmental Microbiology*, 23(9):5069–5086.

Sievert, C. (2020). *Interactive Web-Based Data Visualization with R, plotly, and shiny*. Chapman and Hall/CRC.

Smith, A. L., Fiel, S. B., Mayer-Hamblett, N., Ramsey, B., and Burns, J. L. (2003). Susceptibility Testing of Pseudomonas aeruginosa Isolates and Clinical Response to Parenteral Antibiotic Administration. *Chest*, 123(5):1495–1502.

Smith, E. E., Buckley, D. G., Wu, Z., Saenphimmachak, C., Hoffman, L. R., D'Argenio, D. A., Miller, S. I., Ramsey, B. W., Speert, D. P., Moskowitz, S. M., Burns, J. L., Kaul, R., and Olson, M. V. (2006). Genetic adaptation by Pseudomonas aeruginosa to the airways of cystic fibrosis patients. *Proceedings of the National Academy of Sciences*, 103(22):8487–8492.

Smith, S., Waters, V., Jahnke, N., and Ratjen, F. (2020). Standard versus biofilm antimicrobial susceptibility testing to guide antibiotic therapy in cystic fibrosis. *The Cochrane Database of Systematic Reviews*, 2020(6).

Sosnay, P. R., Siklosi, K. R., Van Goor, F., Kaniecki, K., Yu, H., Sharma, N., Ramalho, A. S., Amaral, M. D., Dorfman, R., Zielenski, J., Masica, D. L., Karchin, R., Millen, L., Thomas, P. J., Patrinos, G. P., Corey, M., Lewis, M. H., Rommens, J. M., Castellani, C., Penland, C. M., and Cutting, G. R. (2013). Defining the disease liability of variants in the cystic fibrosis transmembrane conductance regulator gene. *Nature Genetics 2013 45:10*, 45(10):1160–1167.

Sousa, S. A., Ramos, C. G., and Leitão, J. H. (2010). Burkholderia cepacia Complex: Emerging Multihost Pathogens Equipped with a Wide Range of Virulence Factors and Determinants. *International journal of microbiology*, 2011.

Stick, S., Tiddens, H., Aurora, P., Gustafsson, P., Ranganathan, S., Robinson, P., Rosenfeld, M., Sly, P., and Ratjen, F. (2013). Early intervention studies in infants and preschool children with cystic fibrosis: are we ready? *European Respiratory Journal*, 42(2):527–538.

Stites, S. W., Walters, B., O'Brien-Ladner, A. R., Bailey, K., and Wesselius, L. J. (1998). Increased Iron and Ferritin Content of Sputum From Patients With Cystic Fibrosis or Chronic Bronchitis. *Chest*, 114(3):814–819.

Stoltz, D. A., Meyerholz, D. K., and Welsh, M. J. (2015). Origins of cystic fibrosis lung disease. *The New England journal of medicine*, 372(4):351–62.

Surette, M. G. (2014). The Cystic Fibrosis Lung Microbiome. *Annals of the American Thoracic Society*, 11(Supplement 1):S61–S65.

Sweeney, E., Harrington, N. E., Harley Henriques, A. G., Hassan, M. M., Crealock-Ashurst, B., Smyth, A. R., Hurley, M. N., Tormo-Mas, M. Á., and Harrison, F. (2020a). An ex vivo cystic fibrosis model recapitulates key clinical aspects of chronic staphylococcus aureus infection. *Microbiology*, 167(1):1–15.

Sweeney, E., Sabnis, A., Edwards, A. M., and Harrison, F. (2020b). Effect of host-mimicking medium and biofilm growth on the ability of colistin to kill Pseudomonas aeruginosa. *Microbiology*, 166(12):1171–1180.

Swift, S., Karlyshev, A. V., Fish, L., Durant, E. L., Winson, M. K., Chhabra, S. R., Williams, P., Macintyre, S., and Stewart, G. S. (1997). Quorum sensing in Aeromonas hydrophila and Aeromonas salmonicida: identification of the LuxRI homologs AhyRI and AsaRI and their cognate N-acylhomoserine lactone signal molecules. *Journal of Bacteriology*, 179(17):5271–5281.

Tata, M., Wolfinger, M. T., Amman, F., Roschanski, N., Dötsch, A., Sonnleitner, E., Häussler, S., and Bläsi, U. (2016). RNASeq Based Transcriptional Profiling of Pseudomonas aeruginosa PA14 after Short- and Long-Term Anoxic Cultivation in Synthetic Cystic Fibrosis Sputum Medium. *PLOS ONE*, 11(1):e0147811.

The European Committee on Antimicrobial Susceptibility Testing (2021). Breakpoint tables for interpretation of MICs and zone diameters. Version 11.0.

Tóth, L., Csomor, P., Sziklai, I., and Karosi, T. (2011). Biofilm detection in chronic rhinosinusitis by combined application of hematoxylin-eosin and gram staining. *European Archives of Oto-Rhino-Laryngology*, 268(10):1455–1462.

Toyofuku, M., Nomura, N., Kuno, E., Tashiro, Y., Nakajima, T., and Uchiyama, H. (2008). Influence of the Pseudomonas quinolone signal on denitrification in Pseudomonas aeruginosa. *Journal of Bacteriology*, 190(24):7947–7956.

Tralau, T., Vuilleumier, S., Thibault, C., Campbell, B. J., Hart, C. A., and Kertesz, M. A. (2007). Transcriptomic Analysis of the Sulfate Starvation Response of Pseudomonas aeruginosa. *Journal of Bacteriology*, 189(19):6743.

Trunk, K., Benkert, B., Quäck, N., Münch, R., Scheer, M., Garbe, J., Jänsch, L., Trost, M., Wehland, J., Buer, J., Jahn, M., Schobert, M., and Jahn, D. (2010). Anaerobic adaptation in Pseudomonas aeruginosa: definition of the Anr and Dnr regulons. *Environmental Microbiology*, 12(6):1719–1733.

Turner, K. H., Wessel, A. K., Palmer, G. C., Murray, J. L., and Whiteley, M. (2015). Essential genome of Pseudomonas aeruginosa in cystic fibrosis sputum. *Proceedings of the National Academy of Sciences of the United States of America*, 112(13):4110–5.

Van den Bossche, S., De Broe, E., Coenye, T., Van Braeckel, E., and Crabbé, A. (2021). The cystic fibrosis lung microenvironment alters antibiotic activity: causes and effects. *European Respiratory Review*, 30(161).

Varadarajan, A. R., Allan, R. N., Valentin, J. D., Castañeda Ocampo, O. E., Somerville, V., Pietsch, F., Buhmann, M. T., West, J., Skipp, P. J., van der Mei, H. C., Ren, Q., Schreiber, F., Webb, J. S., and Ahrens, C. H. (2020). An integrated model system to gain mechanistic insights into biofilm-associated antimicrobial resistance in Pseudomonas aeruginosa MPAO1. *npj Biofilms and Microbiomes 2020 6:1*, 6(1):1–17.

Wardell, S. J. T., Gauthier, J., Martin, L. W., Potvin, M., Brockway, B., Levesque, R. C., and Lamont, I. L. (2021). Genome evolution drives transcriptomic and phenotypic adaptation in Pseudomonas aeruginosa during 20 years of infection. *Microbial Genomics*, 7:681.

Weaver, V. B. and Kolter, R. (2004). Burkholderia spp. alter Pseudomonas aeruginosa physiology through iron sequestration. *Journal of bacteriology*, 186(8):2376–84.

Welsh, M., Ramsey, B., Accurso, F., and Cutting, G. (2001). *Cystic Fibrosis*. McGraw-Hill, New York, 8 edition.

Wickham, H. (2016). *ggplot2: Elegant Graphics for Data Analysis*. Springer-Verlag New York.

Wiegand, I., Hilpert, K., and Hancock, R. (2008). Agar and broth dilution methods to determine the minimal inhibitory concentration (MIC) of antimicrobial substances. *Nature protocols*, 3(2):163–175.

Williams, P. and Cámara, M. (2009). Quorum sensing and environmental adaptation in Pseudomonas aeruginosa: a tale of regulatory networks and multifunctional signal molecules. *Current Opinion in Microbiology*, 12(2):182–191.

Wilton, M., Charron-Mazenod, L., Moore, R., and Lewenza, S. (2016). Extracellular DNA acidifies biofilms and induces aminoglycoside resistance in Pseudomonas aeruginosa. *Antimicrobial Agents and Chemotherapy*, 60(1):544–553.

Winson, M. K., Swift, S., Fish, L., Throup, J. P., Jørgensen, F., Chhabra, S. R., Bycroft, B. W., Williams, P., and Stewart, G. S. (1998). Construction and analysis of luxCDABE-based plasmid sensors for investigating N-acyl homoserine lactone-mediated quorum sensing. *FEMS Microbiology Letters*, 163(2):185–192.

Winsor, G. L., Griffiths, E. J., Lo, R., Dhillon, B. K., Shay, J. A., and Brinkman, F. S. (2016). Enhanced annotations and features for comparing thousands of

Pseudomonasgenomes in the Pseudomonas genome database. *Nucleic Acids Research*, 44(D1):D646–D653.

Winstanley, C. and Fothergill, J. L. (2009). The role of quorum sensing in chronic cystic fibrosis Pseudomonas aeruginosa infections. *FEMS Microbiology Letters*, 290(1):1–9.

Winstanley, C., O'Brien, S., and Brockhurst, M. A. (2016). Pseudomonas aeruginosa Evolutionary Adaptation and Diversification in Cystic Fibrosis Chronic Lung Infections. *Trends in Microbiology*, 24(5):327–337.

Wolloscheck, D., Krishnamoorthy, G., Nguyen, J., and Zgurskaya, H. I. (2018). Kinetic control of quorum sensing in Pseudomonas aeruginosa by multidrug efflux pumps. *ACS infectious diseases*, 4(2):185.

Worlitzsch, D., Tarran, R., Ulrich, M., Schwab, U., Cekici, A., Meyer, K. C., Birrer, P., Bellon, G., Berger, J., Weiss, T., Botzenhart, K., Yankaskas, J. R., Randell, S., Boucher, R. C., and Döring, G. (2002). Effects of reduced mucus oxygen concentration in airway Pseudomonas infections of cystic fibrosis patients. *The Journal of Clinical Investigation*, 109(3):317–325.

Wozniak, D. J., Wyckoff, T. J. O., Starkey, M., Keyser, R., Azadi, P., O'Toole, G. A., and Parsek, M. R. (2003). Alginate is not a Significant Component of the Extracellular Polysaccharide Matrix of PA14 and PAO1 Pseudomonas aeruginosa Biofilms. *Proceedings of the National Academy of Sciences of the United States of America*, 100(13):7907–12.

Xia, B., Royall, J. A., Damera, G., Sachdev, G. P., and Cummings, R. D. (2005). Altered O-glycosylation and sulfation of airway mucins associated with cystic fibrosis. *Glycobiology*, 15(8):747–775.

Xu, B., Soukup, R. J., Jones, C. J., Fishel, R., and Wozniak, D. J. (2016). Pseudomonas aeruginosa AmrZ Binds to Four Sites in the algD Promoter, Inducing DNA-AmrZ Complex Formation and Transcriptional Activation. *Journal of bacteriology*, 198(19):2673–81.

Yabuuchi, E., Kosako, Y., Oyaizu, H., Yano, I., Hotta, H., Hashimoto, Y., Ezaki, T., and Arakawa, M. (1992). Proposal of Burkholderia gen. nov. and Transfer of Seven Species of the Genus Pseudomonas Homology Group II to the New Genus, with the Type Species Burkholderia cepacia (Palleroni and Holmes 1981) comb. nov. *Microbiology and Immunology*, 36(12):1251–1275.

Yang, B., Liu, C., Pan, X., Fu, W., Fan, Z., Jin, Y., Bai, F., Cheng, Z., and Wu, W. (2021). Identification of Novel phoP-phoQ Regulated Genes that Contribute to Polymyxin B Tolerance in Pseudomonas aeruginosa. *Microorganisms*, 9(2):1–22.

Yeung, J. C., Machuca, T. N., Chaparro, C., Cypel, M., Stephenson, A. L., Solomon, M., Saito, T., Binnie, M., Chow, C.-W., Grasemann, H., Pierre, A. F., Yasufuku, K., De Perrot, M., Donahoe, L. L., Tikkanen, J., Martinu, T., Waddell, T. K., Tullis, E., Singer, L. G., and Keshavjee, S. (2020). Lung transplantation for cystic fibrosis. *J Heart Lung Transplant*, 39:553–560.

Yu, G., Wang, L. G., Han, Y., and He, Q. Y. (2012). ClusterProfiler: An R package for comparing biological themes among gene clusters. *OMICS A Journal of Integrative Biology*, 16(5):284–287.

Zahedi bialvaei, A., Rahbar, M., Hamidi-Farahani, R., Asgari, A., Esmailkhani, A., Mardani dashti, Y., and Soleiman-Meigooni, S. (2021). Expression of RND efflux pumps mediated antibiotic resistance in Pseudomonas aeruginosa clinical strains. *Microbial Pathogenesis*, 153:104789.

Zhang, Y., Doranz, B., Yankaskas, J. R., and Engelhardt, J. F. (1995). Genotypic analysis of respiratory mucous sulfation defects in cystic fibrosis. *The Journal of Clinical Investigation*, 96(6):2997–3004.

Appendix A: Chapter 4

Table A.1. Sequencing statistics for all *Pseudomonas aeruginosa* PA14 RNA sequencing samples analysed in chapter 4 (also used in chapter 5). Sequencing was perfomed by Genewiz using an Illumina NovaSeq. 150 bp paired-end run. The growth environments include the two environments of the *ex vivo* pig lung model: the lung tissue and surrounding synthetic cystic fibrosis sputum media (SCFM), and *in vitro* SCFM.

Environment	Time	Repeat	Number of reads	Mean quality score
SCFM	24 h	A	10649610	35.08
SCFM	24 h	B	11413366	35.38
SCFM	24 h	C	10965928	35.65
Lung 20	24 h	A	36321837	35.07
Lung 20	24 h	B	10865462	35.58
Lung 20	24 h	C	10125663	35.38
Lung 21	24 h	A	11303435	35.54
Lung 21	24 h	B	10050709	35.30
Lung 21	24 h	C	10774082	35.42
Surrounding SCFM (Lung 20)	24 h	A	10061428	35.24
Surrounding SCFM (Lung 20)	24 h	B	16414826	34.81
Surrounding SCFM (Lung 20)	24 h	C	10655125	35.08
Surrounding SCFM (Lung 21)	24 h	A	9836111	35.15
Surrounding SCFM (Lung 21)	24 h	B	12279023	35.28
Surrounding SCFM (Lung 21)	24 h	C	10584839	34.21
SCFM	48 h	A	9882957	35.56
SCFM	48 h	B	11007267	35.44
SCFM	48 h	C	9343806	35.27
Lung 20	48 h	A	9527826	35.39
Lung 20	48 h	B	9644072	35.45
Lung 20	48 h	C	10129355	35.45
Lung 21	48 h	A	10450696	35.40
Lung 21	48 h	B	10506314	35.47
Lung 21	48 h	C	10208278	35.51
Surrounding SCFM (Lung 20)	48 h	A	10527053	35.50
Surrounding SCFM (Lung 20)	48 h	B	11269187	35.26
Surrounding SCFM (Lung 20)	48 h	C	11511624	35.48

Table 7.1 – continued from previous page

Environment	Time	Repeat	Number of reads	Mean quality score
Surrounding SCFM (Lung 21)	48 h	A	9805761	35.24
Surrounding SCFM (Lung 21)	48 h	B	11170009	35.36
Surrounding SCFM (Lung 21)	48 h	C	11408201	35.43
Lung 20	7 d	A	10854512	35.60
Lung 20	7 d	B	11655497	35.51
Lung 20	7 d	C	9290038	35.40
Lung 21	7 d	A	10203463	35.34
Lung 21	7 d	B	9796687	35.56
Lung 21	7 d	C	11144505	35.33

A. Lung vs SCFM (24 h)

B. Surrounding SCFM vs SCFM (24 h)

C. Lung vs SCFM (48 h)

D. Surrounding SCFM vs SCFM (48 h)
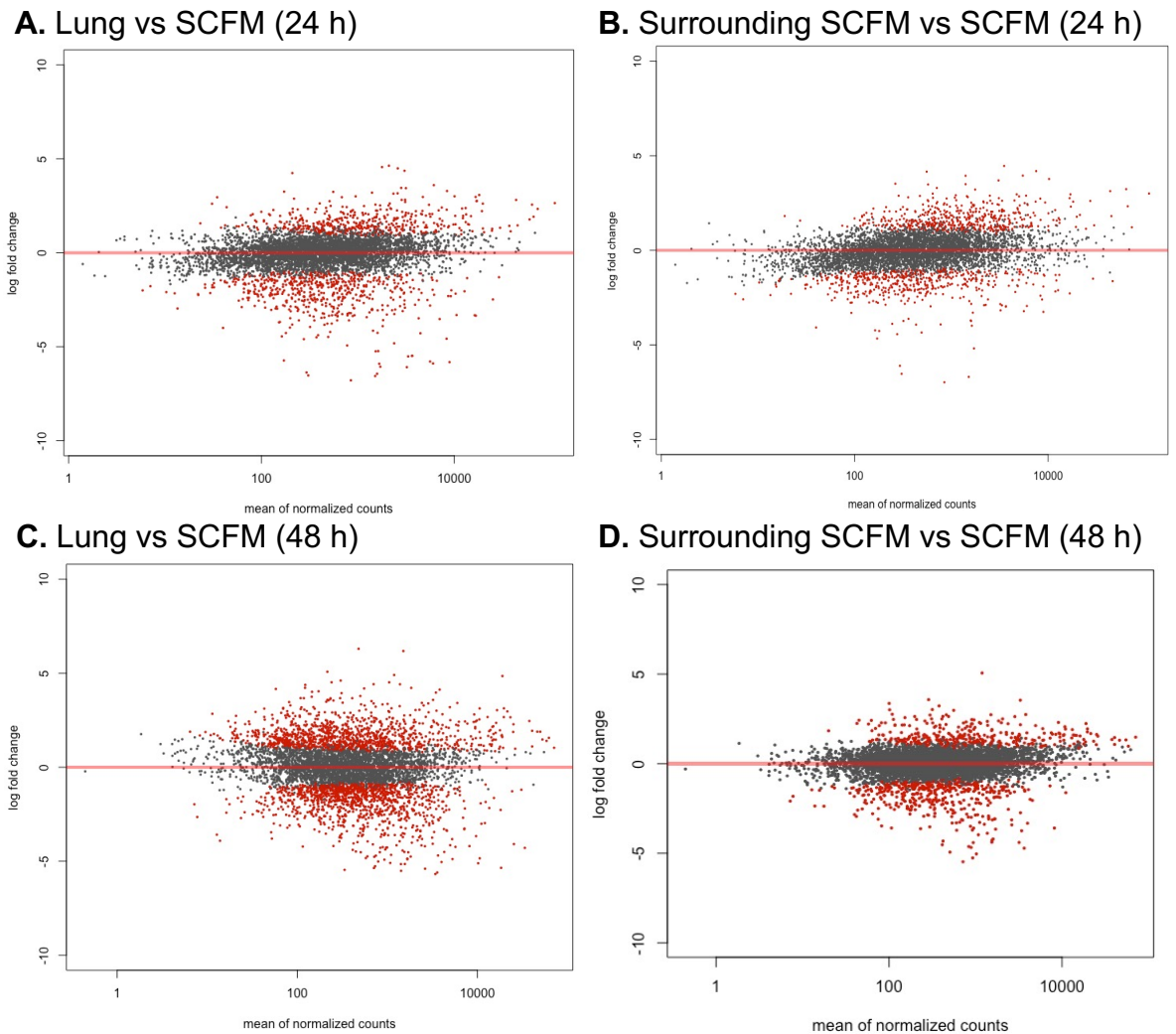
Figure A.1. MA plots for each *Pseudomonas aeruginosa* PA14 RNA sequencing contrast investigated in chapter 4: **(A)** The *ex vivo* pig lung (EVPL)-associated biofilm compared with *in vitro* synthetic cystic fibrosis sputum media (SCFM) at 24 h. **(B)** The EVPL surrounding SCFM compared with *in vitro* SCFM (SCFM) at 24 h. **(C)** The EVPL-associated biofilm compared with *in vitro* SCFM at 48 h. **(D)** The EVPL surrounding SCFM compared with *in vitro* SCFM (SCFM) at 48 h. Each gene is represented by an individual data point, the y axis is the $\log_2$ fold change in expression compared with *in vitro* SCFM, and the mean normalized counts on the x axis. The red data points are genes significantly differentially expressed: $\log_2$ fold change $\geq$ |1.5|, *P* < 0.05. An example of quality control steps performed to ensure the significant genes are across the full range of expression levels, as shown.

A. Lung vs SCFM (24 h)
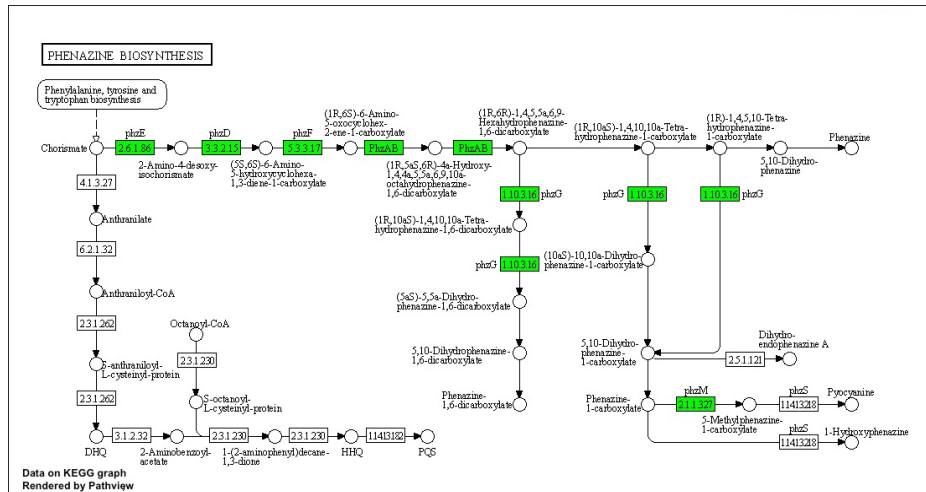
B. Surrounding SCFM vs SCFM (24 h)
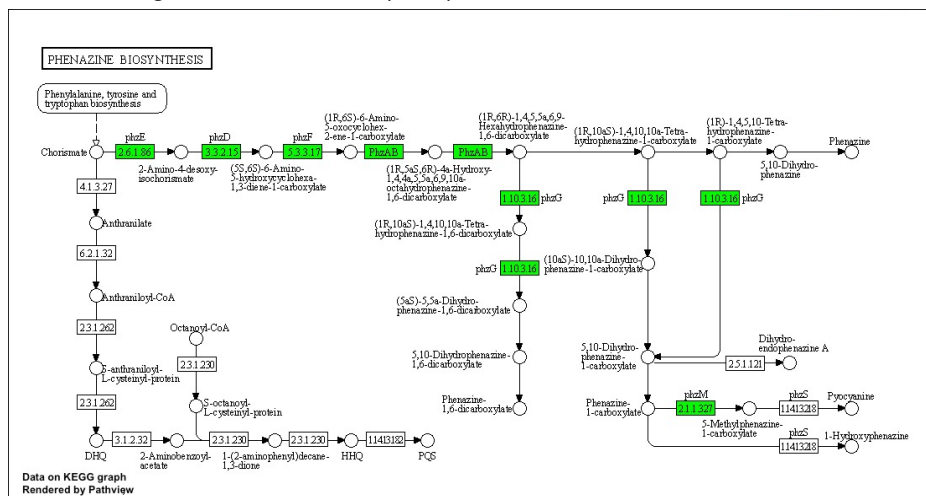
C. Surrounding SCFM vs SCFM (48 h)
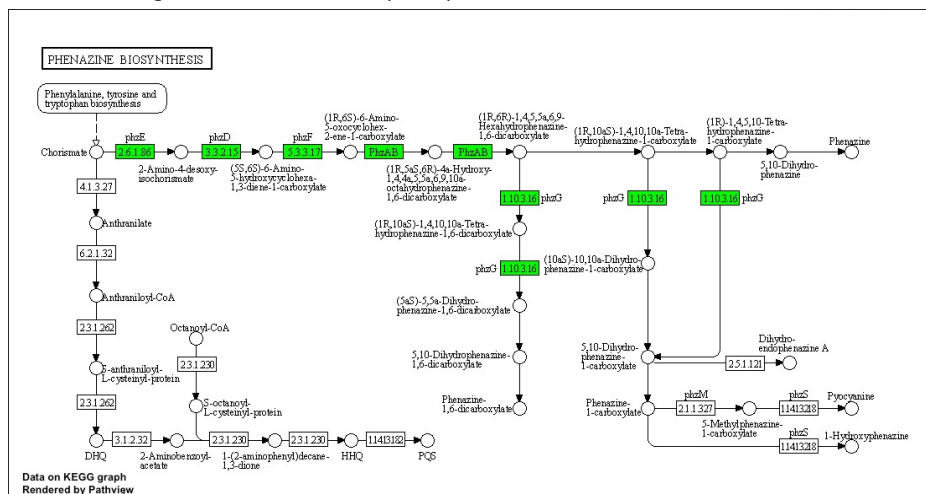
Figure A.2. The Kyoto encyclopedia of genes and genomes (KEGG) *Pseudomonas aeruginosa* PA14 phenazine biosynthesis pathway. Genes that were significantly underexpressed in each contrast (log2 fold change $\leq$ |-1.5|, P < 0.05) are highlighted in green. No genes in the pathway were found to be significantly overexpressed in any of the contrasts. **(A, B, C)** Each pathway map shows the results from each contrast as specified.

Table A.2. All *Pseudomonas aeruginosa* PA14 genes in the quorum sensing Kyoto encyclopedia of genes and genomes (KEGG) pathway. Genes were considered significant if the $\log_2$ fold change was $\leq$ -1.5 or $\geq$ 1.5 compared with *in vitro* synthetic cystic fibrosis sputum media (SCFM) and *P* < 0.05, in the *ex vivo* pig lung-associated biofilm (Lung) and surrounding SCFM at 24 h and 48 h. The $\log_2$ fold change values are shown in the table. This is the full gene list used for Table 4.4 in chapter 4.

Locus tag	Gene name	Gene product	24 h Lung	48 h Lung	24 h Surrounding SCFM	48 h Surrounding SCFM
PA14_02720			-1.16	0.87	-1.51	0.12
PA14_04900	*ftsY*	Signal recognition particle receptor FtsY	0.93	0.50	0.00	0.48
PA14_05550	*oprM*	Major intrinsic multiple antibiotic resistance efflux outer membrane protein OprM precursor	1.00	-0.33	0.87	0.57
PA14_07850		ABC transporter substrate-binding protein	0.71	0.91	0.43	0.14
PA14_07860		ABC transporter ATP-binding protein	1.09	-0.11	1.40	-0.51
PA14_07870		ABC transporter substrate-binding protein	0.38	-1.27	1.41	-0.96
PA14_07890		ABC transporter permease	-0.33	-0.80	0.73	-0.97
PA14_07900		ABC transporter permease	-0.29	-0.64	0.55	-0.86
PA14_07940	*trpE*	Anthranilate synthase component I	0.62	0.47	0.22	-0.09
PA14_08340	*trpG*	Anthranilate synthase component II	0.64	0.39	0.26	0.08
PA14_08370	*vfr*	cAMP-regulatory protein	1.25	0.70	0.79	0.62
PA14_08695	*secE*	Preprotein translocase subunit SecE	-0.83	0.55	-1.31	-0.14
PA14_09050	*secY*	Preprotein translocase subunit SecY	0.75	1.94	-0.32	1.07
PA14_09410	*hfq*	RNA-binding protein Hfq	-3.90	-4.38	-1.97	-2.55

Continued on next page

Table 7.2 – continued from previous page

Locus tag	Gene name	Gene product	24 h Lung	48 h Lung	24 h Surrounding SCFM	48 h Surrounding SCFM
PA14_09420	*phzF1*	Phenazine biosynthesis protein	-5.48	-4.90	-2.98	-3.07
PA14_09440	*phzE1*	Phenazine biosynthesis protein PhzE	-5.82	-5.04	-3.26	-3.33
PA14_09450	*phzD1*	Phenazine biosynthesis protein PhzD	-6.09	-5.51	-3.17	-3.09
PA14_09460	*phzC1*	Phenazine biosynthesis protein PhzC	-4.82	-5.15	-1.79	-2.92
PA14_09470	*phzB1*	Phenazine biosynthesis protein	-4.50	-4.19	-	-2.93
PA14_09480	*phzA1*	Phenazine biosynthesis protein	-3.68	-2.61	-2.68	-2.30
PA14_09520	*mexI*	RND efflux transporter	-1.97	-2.83	-1.73	-1.53
PA14_09530	*mexH*	RND efflux membrane fusion protein	-0.85	-2.74	-0.37	-0.93
PA14_11400	*ribD*	Riboflavin-specific deaminase/reductase	1.01	-0.72	0.58	0.09
PA14_11510	*ribA*	GTP cyclohydrolase II	0.54	0.05	0.08	0.27
PA14_14610	*yajC*	Preprotein translocase subunit YajC	0.95	0.45	0.59	1.05
PA14_15520	*trbJ*	Conjugal transfer protein TrbJ	0.64	0.76	0.28	-0.11
PA14_15540		Mating pair formation protein TrbL	0.30	0.15	0.10	-0.33
PA14_15960	*ffh*	Signal recognition particle protein Ffh	0.01	0.49	-0.79	0.16
PA14_16250	*lasB*	Elastase LasB	-3.35	-3.01	-2.28	-1.62
PA14_17140		Membrane-associated zinc metalloprotease	1.08	1.94	-0.44	0.69
PA14_19100	*rhlA*	Rhamnosyltransferase chain A	-1.21	-0.35	-1.17	-0.49
PA14_19110	*rhlB*	Rhamnosyltransferase chain B	-1.79	-1.33	-1.08	-0.90
PA14_19120	*rhlR*	Transcriptional regulator RhlR	-0.77	-1.23	-0.06	-0.70

Table 7.2 – continued from previous page

Locus tag	Gene name	Gene product	24 h Lung	48 h Lung	24 h Surrounding SCFM	48 h Surrounding SCFM
PA14_19130	*rhlI*	Autoinducer synthesis protein RhlI	-0.27	0.17	-0.90	-0.55
PA14_20580	*amiC*	Aliphatic amidase expression-regulating protein	-0.47	0.90	-0.63	-0.02
PA14_20610	*lecB*	Fucose-binding lectin PA-IIL	-3.43	-2.90	-2.52	-1.95
PA14_21090			-2.20	0.16	-1.07	0.48
PA14_21110	*plcN*	Non-hemolytic phospholipase C	-0.86	1.16	-1.07	0.05
PA14_21340	*fadD2*	Long-chain-fatty-acid-CoA ligase	-0.14	-0.19	0.16	-0.25
PA14_21370	*fadD1*	Long-chain-fatty-acid-CoA ligase	0.30	-0.20	-0.97	-0.47
PA14_21910		ABC transporter ATP-binding protein	-0.06	-0.74	0.31	-0.59
PA14_21920		ABC transporter permease	0.23	0.07	0.28	-0.62
PA14_21930		ABC transporter permease	-0.07	0.80	-0.15	-0.47
PA14_21960			0.25	-0.74	0.41	-0.35
PA14_25980	*aroF*	Phospho-2-dehydro-3-deoxyheptonate aldolase	0.61	0.14	0.03	0.57
PA14_27330			0.13	-3.18	0.52	-2.06
PA14_30630	*pqsH*	FAD-dependent monooxygenase	-0.58	-1.31	0.38	-0.43
PA14_30850		TrbI-like protein	0.50	1.81	-1.77	0.16
PA14_30860		TrbG-like protein	-0.04	1.72	-0.40	-0.66
PA14_30870		Conjugal transfer proten TrbF	-0.52	-0.31	0.04	-0.80
PA14_30880		Conjugal transfer protein TrbL	-0.90	1.31	-1.15	-0.31
PA14_30900		Conjugal transfer protein TrbJ	-1.14	-0.18	-0.72	-1.49
PA14_30910		Conjugal transfer ATPase TrbE	-1.02	0.36	-0.97	-0.52

Table 7.2 – continued from previous page

Locus tag	Gene name	Gene product	24 h Lung	48 h Lung	24 h Surrounding SCFM	48 h Surrounding SCFM
PA14_30930		TrbC-like protein	-0.80	1.38	-1.39	-0.97
PA14_30940		Conjugal transfer protein	-1.04	0.66	-1.35	-0.53
PA14_31290	*pa1L*	PA-I galactophilic lectin	-3.94	1.52	-3.73	0.04
PA14_31300			-1.34	0.03	-0.11	-0.04
PA14_39880	*phzG2*	Pyridoxamine 5'-phosphate oxidase	-5.51	-5.15	-2.91	-3.14
PA14_39890	*phzF2*	Phenazine biosynthesis protein	-5.48	-4.86	-2.96	-3.09
PA14_39910	*phzE2*	Phenazine biosynthesis protein PhzE	-5.78	-5.40	-3.22	-3.42
PA14_39925	*phzD2*	Phenazine biosynthesis protein PhzD	-5.91	-5.36	-3.30	-3.16
PA14_39945	*phzC2*	Phenazine biosynthesis protein PhzC	-5.89	-5.68	-2.95	-3.75
PA14_39960	*phzB2*	Phenazine biosynthesis protein	-5.24	-5.09	-2.68	-3.97
PA14_39970	*phzA2*	Phenazine biosynthesis protein	-4.93	-4.40	-3.92	-4.52
PA14_40260			-2.17	-3.26	-0.17	-0.88
PA14_40290	*lasA*	LasA protease	-2.09	-2.22	-1.36	-1.53
PA14_41920	*aroF-1*	Phospho-2-dehydro-3-deoxyheptonate aldolase	-0.26	-0.15	-0.48	-0.43
PA14_43340	*kdpE*	Two-component response regulator KdpE	-0.34	-1.26	-0.12	-0.56
PA14_45940	*lasI*	Autoinducer synthesis protein LasI	-0.10	-0.57	0.94	-1.10
PA14_45960	*lasR*	Transcriptional regulator LasR	0.03	-0.53	0.82	0.03
PA14_47370		Signal peptidase	0.62	0.73	0.34	0.60
PA14_49760	*rhlC*	Rhamnosyltransferase 2	-1.72	-1.61	-0.96	-1.01
PA14_50520	*braC*	Branched-chain amino acid transport protein BraC	0.70	-0.68	1.01	-0.69
PA14_50530	*braD*	Branched-chain amino acid transport protein BraD	0.19	-0.56	-0.04	-1.16

Table 7.2 – continued from previous page

Locus tag	Gene name	Gene product	24 h Lung	48 h Lung	24 h Surrounding SCFM	48 h Surrounding SCFM
PA14_50540	*livM*	Leucine/isoleucine/valine transporter permease subunit	0.07	-1.26	-0.19	-1.65
PA14_50550	*livG*	Leucine/isoleucine/valine transporter ATP-binding subunit	-0.37	-1.37	-0.23	-1.65
PA14_50560	*braG*	Branched-chain amino acid transport protein BraG	-0.39	-1.24	-0.45	-1.90
PA14_51340	*mvfR*	Transcriptional regulator MvfR	-0.44	-0.09	-0.83	-0.22
PA14_51350	*phnB*	Anthranilate synthase component II	-0.56	-1.36	-0.75	-0.30
PA14_51360	*phnA*	Anthranilate synthase component I	-0.78	-1.20	-1.07	-0.31
PA14_51380	*pqsE*	Quinolone signal response protein	-0.82	-0.57	-1.29	0.12
PA14_51390	*pqsD*	3-oxoacyl-ACP synthase	-0.99	-1.83	-0.97	-0.47
PA14_51410	*pqsC*	PqsC	-1.32	-1.87	-0.89	-0.55
PA14_51420	*pqsB*	PqsB	-1.02	-0.86	-0.96	0.18
PA14_51430	*pqsA*	PqsA	-1.06	-0.97	-1.34	-0.20
PA14_53360	*plcH*	Hemolytic phospholipase C	-0.16	1.50	-0.53	0.54
PA14_54350	*lepB*	Signal peptidase I	0.20	0.07	-0.43	0.17
PA14_57220	*secA*	Preprotein translocase subunit SecA	0.38	0.83	0.01	0.52
PA14_58360	*dppA2*	Dipeptide ABC transporter substrate-binding protein DppA2	2.25	2.33	0.80	0.44
PA14_62810	*secG*	Preprotein translocase subunit SecG	0.24	2.50	-0.88	0.76
PA14_63150	*pmrA*	Two-component response regulator	1.51	0.37	0.14	-0.28

Table 7.2 – continued from previous page

| Locus tag	Gene name	Gene product	24 h Lung	48 h Lung	24 h Surrounding SCFM	48 h Surrounding SCFM
PA14_63160	*pmrB*	PmrB: two-component regulator system signal sensor kinase PmrB	1.40	0.10	0.27	-0.35
PA14_63480		Amino acid permease	0.06	1.18	0.06	0.08
PA14_63650			0.63	-0.09	-0.33	0.79
PA14_64860		ABC transporter ATP-binding protein	-2.97	-1.62	-2.12	-0.91
PA14_64870		ABC transporter ATP-binding protein	-2.29	-1.11	-1.71	-0.89
PA14_64880		Branched chain amino acid ABC transporter permease	-2.04	-0.39	-1.82	-0.60
PA14_64890		Branched chain amino acid ABC transporter permease	-0.80	-0.09	-0.28	-0.03
PA14_64900		ABC transporter substrate-binding protein	-0.98	-0.82	0.01	-0.32
PA14_65310		RNA-binding protein Hfq	1.59	0.52	1.87	0.45
PA14_67720	*secB*	Preprotein translocase subunit SecB	-0.10	-1.00	0.40	-0.19
PA14_70200	*dppA5*	Dipeptide ABC transporter substrate-binding protein DppA5	0.38	0.28	0.37	-0.24
PA14_72560	*np20*	Transcriptional regulator np20	-1.32	-2.17	0.14	-0.31
PA14_73410		Inner membrane protein translocase component YidC	0.03	0.75	-1.23	0.40

A. 24 h

B. 48 h
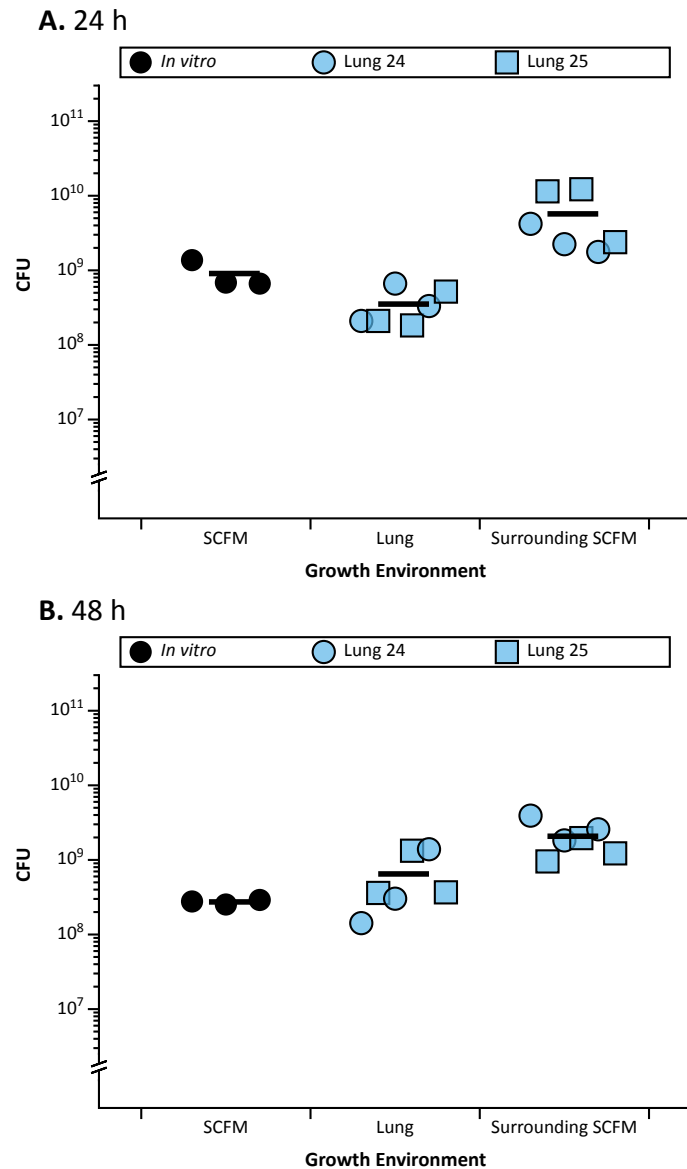
Figure A.3. Colony forming units (CFU) of *Pseudomonas aeruginosa* PA14 in synthetic cystic fibrosis sputum media (SCFM) *in vitro* (SCFM) per ml, and in the two environments of the *ex vivo* pig lung (EVPL) model: the lung-associated biofilm (Lung) per lung piece and SCFM surrounding each tissue piece (Surrounding SCFM) per ml. This data is from the same samples as the acyl homoserine lactones (AHLs) measurements in chapter 4 were taken from (Figure 4.12 and Figure 4.13). The *in vitro* SCFM samples used for this experiment were prepared by, and the CFU ml^{-1} was measured by, Jenny Littler. Each data point represents an individual sample; *in vitro* SCFM cultures were prepared in triplicate per time point and three tissue pieces from each of two independent lungs were prepared for the EVPL model environments. The environments and individual lungs are represented by different shaped and coloured data points (see key). The horizontal, bold lines represent the mean concentration. The y axes are log$_{10}$ scale. The CFU were determined at **(A)** 24 h and **(B)** 48 h.

Table A.3. All 52 genes predicted to be involved in *Pseudomonas aeruginosa* PA14 antimicrobial resistance by the Comprehensive Antibiotic Resistance Database (CARD) (Alcock et al., 2020). PA14 expression in the two locations of the *ex vivo* pig lung model: the lung tissue-associated biofilm (lung) and the synthetic cystic fibrosis sputum media (SCFM) surrounding the lung tissue (surrounding SCFM), was compared with *in vitro* SCFM (SCFM) growth. Samples were compared at 24 h and 48 h post infection. The $\log_2$ fold change (lfc) is shown. The model name detailed by the CARD is also shown alongside the gene locus tag and gene product. This is the full gene list used for Table 4.6 in chapter 4.

Locus tag	Model name	Gene product	24 h Lung	48 h Lung	24 h Surrounding SCFM	48 h Surrounding SCFM
PA14_01940	TriA	RND efflux membrane fusion protein	-0.04	-0.90	0.08	-0.88
PA14_01960	TriB	RND efflux membrane fusion protein	-0.55	-1.72	-0.039	-0.97
PA14_01970	TriC	RND efflux transporter	-0.56	-1.10	-0.24	-0.86
PA14_05520	MexR	Multidrug resistance operon repressor MexR	0.25	0.69	-0.15	0.40
PA14_05530	MexA	RND multidrug efflux membrane fusion protein MexA	0.48	0.66	0.24	0.69
PA14_05540	MexB	RND multidrug efflux transporter MexB	0.95	0.94	0.28	0.99
PA14_05550	OprM	Major intrinsic multiple antibiotic resistance efflux outer membrane protein OprM precursor	1.00	-0.33	0.87	0.57
PA14_09500	OpmD	Outer membrane protein	-2.77	-3.41	-1.87	-1.79
PA14_09520	MexI	RND efflux transporter	-1.97	-2.83	-1.73	-1.53
PA14_09530	MexH	RND efflux membrane fusion protein	-0.85	-2.74	-0.37	-0.93
PA14_09540	MexG	Hypothetical protein	-0.60	-2.32	-0.02	-0.07
PA14_10470	bcr-1	MFS transporter	2.06	-0.03	1.25	-0.12
PA14_10670	APH(3')-IIb	Aminoglycoside 3'-phosphotransferase type IIB	-0.15	0.41	-1.09	0.37
PA14_10790	PDC-9	Beta-lactamase	0.37	0.72	0.53	0.73
PA14_16280	nalC	Transcriptional regulator	-0.86	-0.57	0.88	0.73

Continued on next page

Table 7.3 – continued from previous page

Locus tag	Model name	Gene product	24 h Lung	48 h Lung	24 h Surrounding SCFM	48 h Surrounding SCFM
PA14_16300	ArmR	Hypothetical protein	-1.52	-0.80	1.00	1.16
PA14_16790	MexL	TetR family transcriptional regulator	-0.67	-1.62	0.25	-0.14
PA14_16800	MexJ	Efflux transmembrane protein	0.85	1.31	0.01	0.41
PA14_16820	MexK	Efflux transmembrane protein	1.13	1.29	-0.36	-0.01
PA14_18080	nalD	TetR family transcriptional regulator	1.17	1.45	2.22	2.04
PA14_18350	arnA	Bifunctional UDP-glucuronic acid decarboxylase/UDP-4-amino-4-deoxy-L-arabinose formyltransferase	2.34	1.42	-0.39	0.25
PA14_18760	mexP	RND efflux membrane fusion protein	0.91	1.84	1.14	1.76
PA14_18780	mexQ	RND efflux transporter	0.84	1.44	0.70	1.19
PA14_18790	opmE	Outer membrane efflux protein	0.88	1.27	0.72	1.61
PA14_22760	*Pseudomonas aeruginosa* CpxR	Two-component response regulator	0.68	-0.19	0.29	-0.26
PA14_31870	MuxA	RND efflux membrane fusion protein	1.17	1.67	-0.01	0.43
PA14_31890	MuxB	RND efflux transporter	0.86	0.37	0.02	-0.01
PA14_31900	MuxC	Efflux transporter	1.55	0.84	0.19	0.19
PA14_31920	OpmB	Outer membrane protein	1.68	0.25	0.87	0.29
PA14_32380	OprN	Multidrug efflux outer membrane protein OprN precursor	-0.28	-0.56	-0.53	-0.73
PA14_32390	MexF	RND multidrug efflux transporter MexF	-0.30	0.69	-1.12	-0.23
PA14_32400	MexE	RND multidrug effluc membrane fusion protein MexE	-0.42	0.82	-1.28	0.49

Table 7.3 – continued from previous page

Locus tag	Model name	Gene product	24 h Lung	48 h Lung	24 h Surrounding SCFM	48 h Surrounding SCFM
PA14_32410	MexT	Transcriptional regulator MexT	-0.05	-0.46	-0.04	0.05
PA14_32420	MexS	Oxidoreductase	-0.40	-0.63	-0.30	-0.03
PA14_35170	*Pseudomonas aeruginosa* soxR	Redox-sensing activator of soxS	-1.17	-0.91	-0.31	-0.05
PA14_38380	MexZ	Transcriptional regulator	-1.16	0.10	-0.74	0.48
PA14_45890	MexN	RND efflux transporter	-0.18	0.72	-0.25	0.81
PA14_45910	mexM	RND efflux membrane fusion protein	0.42	1.72	-0.93	0.12
PA14_46680	PmpM	Transporter	0.64	0.87	-0.40	0.29
PA14_49780	FosA	Fosfomycin resistance protein	-1.61	-0.18	-0.88	-0.14
PA14_55170	*Pseudomonas aeruginosa* catB7	Chloramphenicol acetyltransferase	-0.65	-0.09	-1.09	-0.27
PA14_56880	MexV	Membrane fusion protein	0.70	-0.21	0.23	-0.65
PA14_56890	MexW	Multidrug efflux protein	-0.24	-0.29	-0.17	-1.17
PA14_59160	CrpP	CrpP	-0.23	1.68	-0.31	1.18
PA14_60820	OprJ	Outer membrane protein OprJ	0.80	0.31	1.55	1.08
PA14_60830	MexD	Multidrug efflux RND transporter MexD	0.86	1.61	0.25	1.58
PA14_60850	MexC	Multidrug efflux RND membrane fusion protein	0.54	2.09	-0.16	2.25
PA14_60860	Type B NfxB	Transcriptional regulator NfxB	-0.66	-0.33	-0.31	0.44
PA14_63160	basS	PmrB: two-component regulator system signal sensor kinase PmrB	1.40	0.10	0.27	-0.35
PA14_65750	OpmH	Outer membrane efflux protein	0.06	-1.57	0.31	-0.68
PA14_65990	*Pseudomonas aeruginosa* emrE	SMR multidrug efflux transporter	-00.45	1.11	-0.39	0.16

Table 7.3 – continued from previous page

Locus tag	Model name	Gene product	24 h Lung	48 h Lung	24 h Surrounding SCFM	48 h Surrounding SCFM
PA14_72760	OXA-50	Beta-lactamase	-0.30	-0.30	0.15	-0.16

Chapter 5

A. 24 h to 48 h
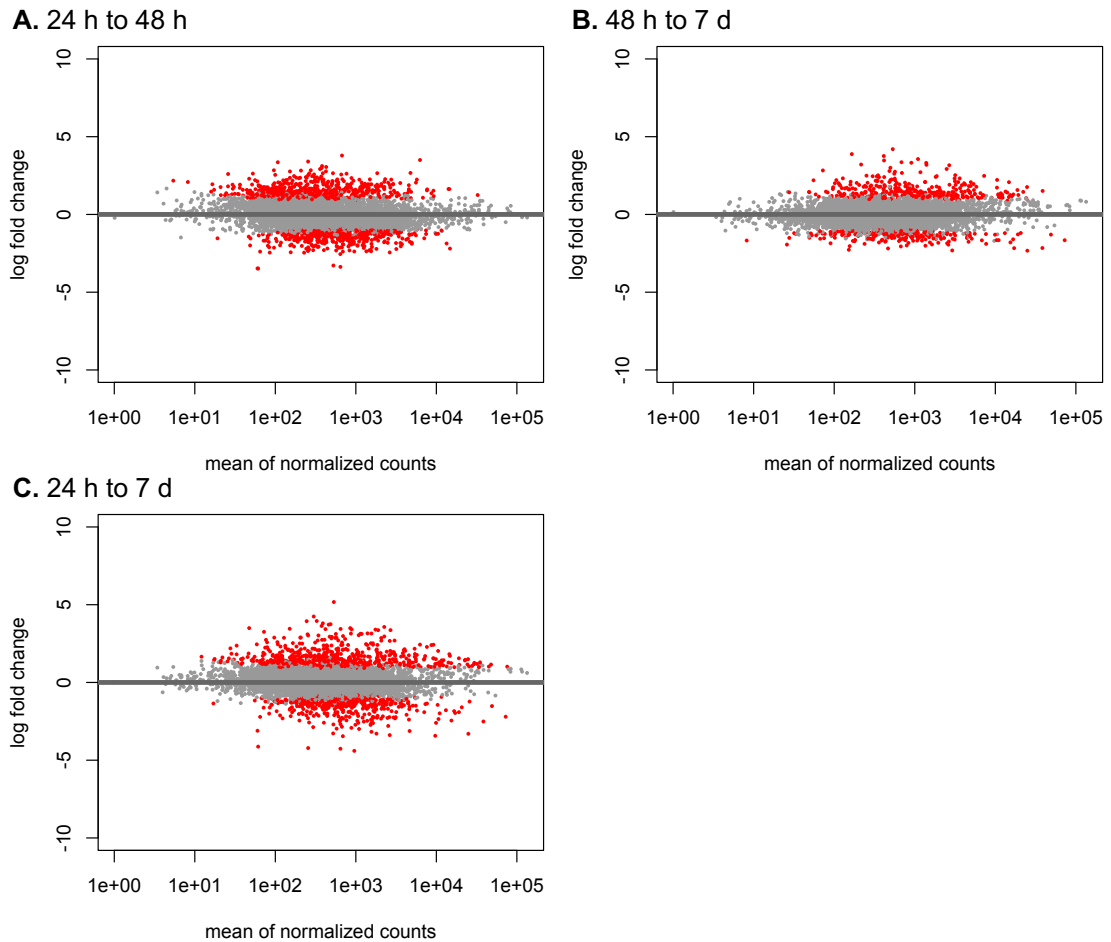
B. 48 h to 7 d

C. 24 h to 7 d

Figure B.1. MA plots for each *Pseudomonas aeruginosa* PA14 RNA sequencing time contrast in the *ex vivo* pig lung biofilm investigated in chapter 5: **(A)** Gene expression at 48 h compared with 24 h, thus showing gene expression changes from 24 h to 48 h. **(B)** Gene expression at 7 d compared with 48 h, thus showing gene expression changes from 48 h to 7 d. **(C)** Gene expression at 7 d compared with 24 h, thus showing gene expression changes from 24 h to 7 d. Each gene is represented by an individual data point; the y axis is the $\log_2$ fold change in expression, and the mean normalized counts on the x axis. The red data points are genes significantly differentially expressed: $\log_2$ fold change $\geq |1.5|$, $P < 0.05$. An example of quality control steps performed to ensure the significant genes are across the full range of expression levels, as shown.

Table B.1. The *Pseudomonas aeruginosa* PA14 genes in the pathway maps in chapter 5, showing the locus tags for each gene that the $\log_2$ fold change values are shown in Figure 5.7, Figure 5.8, andFigure 5.9. The genes are from the Kyoto encyclopedia of genes and genomes (KEGG) biofilm formation and quorum sensing (QS) pathways, and gene product information sourced from Pseudomonas.com (Winsor et al., 2016).

Gene	Gene product	PA14 Locus tag
pqsR	Transcriptional regulator Mvfr (*also referred to as PqsR*)	PA14_51340
rhlI	Autoinducer synthesis protein RhlI	PA14_19130
rhlR	Transcriptional regulator RhlR	PA14_19120
phnA	Anthranilate synthase component I (*also referred to as TrpE*)	PA14_07940
phnB	Anthranilate synthase component II (*also referred to as TrpG*)	PA14_08340
pqsA	PqsA	PA14_51430
pqsB	PqsB	PA14_51420
pqsC	PqsC	PA14_51410
pqsD	3-oxoacyl-ACP synthase	PA14_51390
pqsE	Quinolone signal response protein	PA14_51380
pqsH	FAD-dependent monooxygenase	PA14_30630
lasA	LasA protease	PA14_40290
lasB	Elastase LasB	PA14_16250
lecA	PA-I galactophilic lectin (*also referred to as Pa1L*)	PA14_31290
lecB		PA14_31300
rhlA	Rhamnosyltransferase chain A	PA14_19100
rhlB	Rhamnosyltransferase chain B	PA14_19110
rhlC	Rhamnosyltransferase 2	PA14_49760
lasI	Autoinducer synthesis protein LasI	PA14_45940
lasR	Transcriptional regulator LasR	PA14_45960
sagS	Sensor/response regulator hybrid	PA14_27550
PA1611	Sensor/response regulator hybrid	PA14_43670
PA1976	Two-component sensor	PA14_38970
hptB		PA14_51480
hsbR	Two-component response regulator	PA14_20780
hsbA		PA14_20770
flgM	(Anti-σ)	PA14_20730
fliA	Flagellar biosynthesis sigma factor (σ)	PA14_45630
gacS	Sensor/response regulator hybrid	PA14_52260

Continued on next page

Table 7.4 – continued from previous page

| Gene	Gene product	PA14 Locus tag
gacA	Response regulator GacA	PA14_30650
rsmA	Carbon storage regulator	PA14_52570
retS	RetS - regulator of exopolysaccharide and Type III secretion	PA14_64230
wspB/D		PA14_16440
wspA	Chemotaxis transducer	PA14_16430
wspE	Chemotaxis sensor/effector fusion protein	PA14_16470
wspF	Chemotaxis-specific methylesterase	PA14_16480
wspR	Two-component response regulator	PA14_16500
sadC		PA14_56280
siaD	Diguanylate cyclase	PA14_02110
tpbB	Diguanylate cyclase TpbB	PA14_49890
roeA		PA14_50060
mucR	Membrane sensor domain-containing protein	PA14_42220
bifA	BifA	PA14_56790
fleQ	Transcriptional regulator FleQ	PA14_50220
psl	Mannose-1-phosphate guanylyltransferase (*also referred to as AlgA*)	PA14_18380
pelA		PA14_24480
pelB		PA14_24490
pelC	Lipoprotein	PA14_24500
pelD		PA14_24510
pelE		PA14_24530
pelF		PA14_24550
pelG		PA14_24560
alg44	Alginate biosynthesis protein Alg44	PA14_18550
fimX		PA14_65540
fimW		PA14_65520
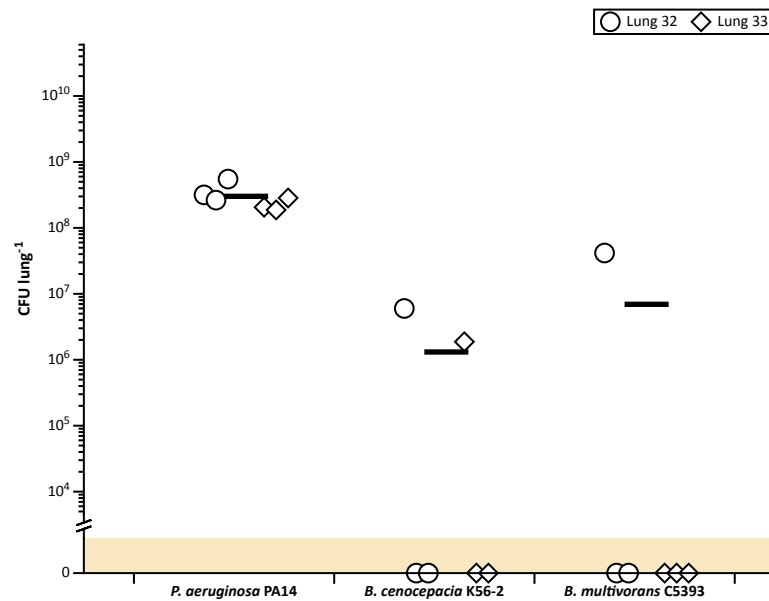
Figure C.1. The colony forming units per lung (CFU lung^{-1}) of *Pseudomonas aeruginosa* PA14, *Burkholderia cenocepacia* K56-2, and *Burkholderia multivorans* C5393 at 7 d in the *ex vivo* pig lung (EVPL) model. Three tissue pieces from each of two independent lungs were infected with each strain, shown by individual data points, and incubated at 37 °C for 7 d. The horizontal lines show the mean CFU lung^{-1}. The coloured region below the y axes break represents samples where no CFU of that strain were detected. The y axis is log$_{10}$ scale. This is the CFU lung^{-1} data for the single infection samples that long chain and short chain AHLs were measured from in chapter 6 (Figure 6.14, Figure 6.15, Figure 6.16, and Figure 6.17).
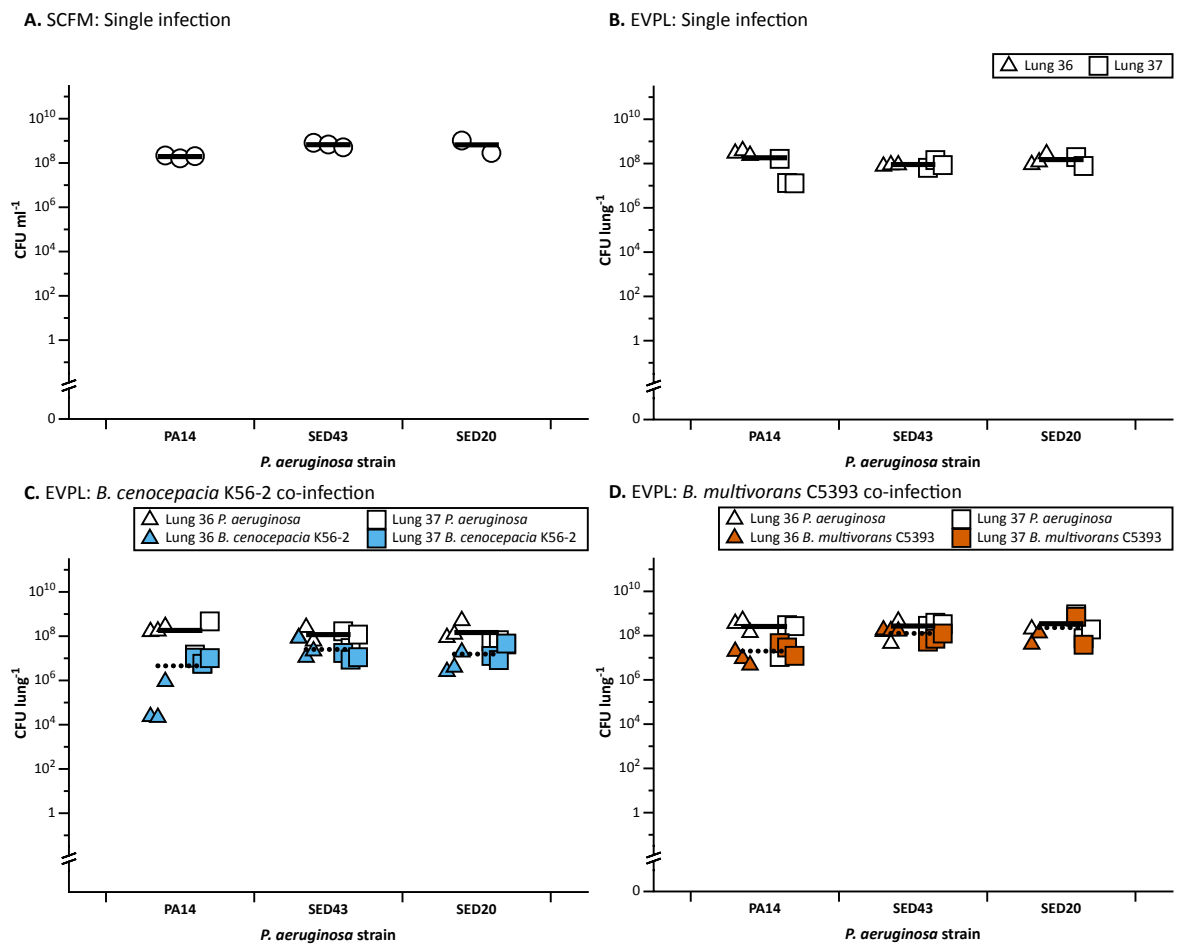
A. SCFM: Single infection

B. EVPL: Single infection

C. EVPL: *B. cenocepacia* K56-2 co-infection

D. EVPL: *B. multivorans* C5393 co-infection

Figure C.2. The colony forming units (CFU) data at 2 d for the synthetic cystic fibrosis sputum media (SCFM) and *ex vivo* pig lung (EVPL) samples that pyoverdine (PVD) and pyochelin (PCH) measurements were taken from in Figure 6.24 and Figure 6.25, in chapter 6. The SCFM mixed infection CFU ml^{-1} is not shown as it is in the main chapter, in Figure 6.20 and Figure 6.22. The y axes are log$_{10}$ scale and the horizontal lines show the mean. Some *P. aeruginosa* SED20 samples were removed due to contamination. **(A)** The CFU ml^{-1} of each *P. aeruginosa* strain in monoculture (single infection) in SCFM *in vitro*. Three repeats were used per strain, represented by individual data points. **(B)** The CFU lung^{-1} of each *P. aeruginosa* strain when single infected in the EVPL model. Three repeats from each of two independent pig lungs are shown as individual data points, and each lung is represented by different shaped data points (see key). **(C,D)** The CFU lung^{-1} of *P. aeruginosa* and each *Burkholderia cepacia* complex strain: *Burkholderia cenocepacia* K56-2 and *Burkholderia multivorans* C5393 in the EVPL model, as labelled. Three repeats from each of two independent pig lungs are shown as individual data points, and each lung is represented by different shaped data points (see key). The *P. aeruginosa* CFU is shown by white data points and the Bcc CFU by the corresponding colours shown in the keys.
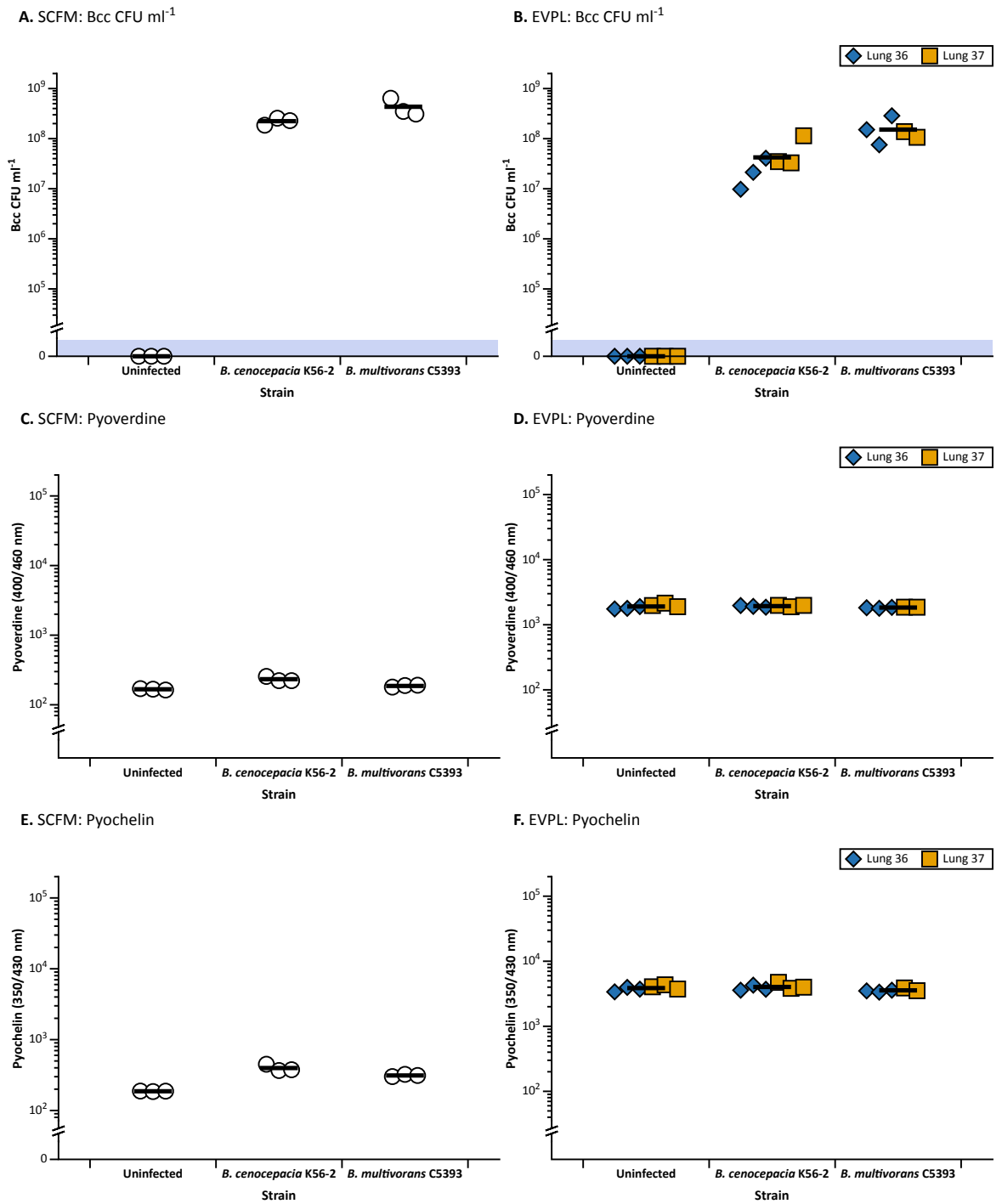
Figure C.3. The colony forming units (CFU), pyoverdine, and pyochelin measurements for *Burkholderia cepacia* complex (Bcc) single infection and uninfected samples from the same experiments as Figure 6.24 and 6.25 in chapter 6. All data is from 2 d. The y axes are $\log_{10}$ scale and the horizontal lines show the mean. **(A)** CFU ml^{-1} of Bcc strains in synthetic cystic fibrosis sputum media (SCFM); the uninfected SCFM samples had no Bcc growth. The CFU ml^{-1} was measured for *Burkholderia cenocepacia* K56-2 and *Burkholderia multivorans* C5393 from single infection. Three repeats were performed per infection, represented by individual data points. The coloured region below the y axis break represents no Bcc CFU detected. **(B)** CFU lung^{-1} of Bcc strains in

the *ex vivo* pig lung model (EVPL); the uninfected tissue had no Bcc growth. The CFU lung^{-1} was measured for *Burkholderia cenocepacia* K56-2 and *Burkholderia multivorans* C5393 from single infection. Three repeats from each of two independent pig lungs were studied, and are represented by different shaped and coloured data points (see key). The coloured region below the y axis break represents no Bcc CFU detected. **(C,E)** The pyoverdine and pyochelin fluorescence measurements for the SCFM samples that the CFU ml^{-1} is shown in A. **(D,F)** The pyoverdine and pyochelin fluorescence measurements for the EPVL samples that the CFU lung^{-1} is shown in B.